Macromolecules Containing Metal and Metal-Like Elements

Volume 7

Nanoscale Interactions of Metal-Containing Polymers

Edited by

Alaa S. Abd-El-Aziz
Department of Chemistry, The University of Winnipeg, Winnipeg, Manitoba, Canada

Charles E. Carraher Jr.
Department of Chemistry and Biochemistry, Florida Atlantic University, Boca Raton, Florida, and Florida Center for Environmental Studies, Palm Beach Gardens, Florida

Charles U. Pittman Jr.
Department of Chemistry, Mississippi State University, Mississippi State, Mississippi

Martel Zeldin
Department of Chemistry, University of Richmond, Richmond, Virginia

WILEY-INTERSCIENCE
A John Wiley & Sons, Inc., Publication

Macromolecules Containing Metal and Metal-Like Elements

Volume 7

Macromolecules Containing Metal and Metal-Like Elements

Volume 7

Nanoscale Interactions of Metal-Containing Polymers

Edited by

Alaa S. Abd-El-Aziz
Department of Chemistry, The University of Winnipeg, Winnipeg, Manitoba, Canada

Charles E. Carraher Jr.
Department of Chemistry and Biochemistry, Florida Atlantic University, Boca Raton, Florida, and Florida Center for Environmental Studies, Palm Beach Gardens, Florida

Charles U. Pittman Jr.
Department of Chemistry, Mississippi State University, Mississippi State, Mississippi

Martel Zeldin
Department of Chemistry, University of Richmond, Richmond, Virginia

WILEY-INTERSCIENCE
A John Wiley & Sons, Inc., Publication

Published by John Wiley & Sons, Inc., Hoboken, New Jersey
Published simultaneously in Canada

Library of Congress Cataloging-in-Publication Data:

ISBN-13 978-0-471-68440-4
ISBN-10 0-471-68440-6
ISSN 1545-438X

Printed in the United States of America

10 9 8 7 6 5 4 3 2 1

Contributors

Laurence Belfiore, Department of Chemical and Bioresource Engineering, Colorado State University, Ft. Collins, CO 80523

Charles Carraher, Department of Chemistry, Florida Atlantic University, Boca Raton, FL 33431 and Florida Center for Environmental Studies, Palm Beach Gardens, FL 33410

A.D. Pomogailo, Institute of Problems of Chemical Physics, Russian Academy of Sciences, Chernogolovka, Moscow Region 142432, RUSSIA

Ulrich Schubert, Institute of Materials Chemistry, Vienna University of Technology, Getreidemarkt 9, A-1060 Wien, AUSTRIA

Contents

Preface

Nanostructured materials have appeared in nature since the beginning of time. The driving force toward the use of nanomaterials is that they offer new properties or enhanced properties that are unobtainable with traditional bulk materials. Along with lightweight, high strength-to-weight features and small size, new properties are emerging because of the very high surface area-to-mass ratios present. These ratios determine where surface atomic and molecular interactions become critical. A definition of nanomaterials is when at least one phase dimension is on the order of 1 to 100 nm. Single linear polymer molecules are nanomaterials since the diameter of a single chain is within this range. Thus, efforts are underway to synthesize single-chain molecular conductors of electrons, light and self-assembled catalysts, and nanocomposites. Metal-containing polymers are at the heart of many of these efforts. The current volume reviews several important areas involved in the nanorevolution.

Series Preface

Most traditional macromolecules are composed of less than 10 elements (mainly C, H, N, O, S, P, C1, F), whereas metal and semi-metal-containing polymers allow properties that can be gained through the inclusion of nearly 100 additional elements. Macromolecules containing metal and metal-like elements are widespread in nature with metalloenzymes supplying a number of essential physiological functions including respiration, photosynthesis, energy transfer, and metal ion storage.

Polysiloxanes (silicones) are one of the most studied classes of polymers. They exhibit a variety of useful properties not common to non-metal-containing macromolecules. They are characterized by combinations of chemical, mechanical, electrical, and other properties that, when taken together, are not found in any other commercially available class of materials. The initial footprints on the moon were made by polysiloxanes. Polysiloxanes are currently sold as high-performance caulks, lubricants, antifoaming agents, window gaskets, O-rings, contact lens, and numerous and variable human biological implants and prosthetics, to mention just a few of their applications.

The variety of macromolecules containing metal and metal-like elements is extremely large, not only because of the large number of metallic and metalloid elements, but also because of the diversity of available oxidation states, the use of combinations of different metals, the ability to include a plethora of organic moieties, and so on. The appearance of new macromolecules containing metal and metal-like elements has been enormous since the early 1950s, with the number increasing explosively since the early 1990s. These new macromolecules represent marriages among many disciplines, including chemistry, biochemistry, materials science, engineering, biomedical science, and physics. These materials also form bridges between ceramics, organic, inorganic, natural and synthetic, alloys, and metallic materials. As a result, new materials with specially designated properties have been made as composites, single- and multiple-site catalysts, biologically active/inert materials, smart materials, nanomaterials, and materials with superior conducting, nonlinear optical, tensile strength, flame retardant, chemical inertness, superior solvent resistance, thermal stability, solvent resistant, and other properties.

There also exist a variety of syntheses, stabilities, and characteristics, which are unique to each particular material. Further, macromolecules containing metal and metal-like elements can be produced in a variety of geometries, including linear, two-dimensional, three-dimensional, dendritic, and star arrays.

In this book series, macromolecules containing metal and metal-like elements will be defined as large structures where the metal and metalloid atoms are (largely) covalently bonded into the macromolecular network within or pendant to the polymer

backbone. This includes various coordination polymers where combinations of ionic, sigma-, and pi-bonding interactions are present. Organometallic macromolecules are materials that contain both organic and metal components. For the purposes of this series, we will define metal-like elements to include both the metalloids as well as materials that are metal-like in at least one important physical characteristic such as electrical conductance. Thus the term includes macromolecules containing boron, silicon, germanium, arsenic, and antimony as well as materials such as poly(sulfur nitride), conducting carbon nanotubes, polyphosphazenes, and polyacetylenes.

The metal and metalloid-containing macromolecules that are covered in this series will be essential materials for the twenty-first century. The first volume is an overview of the discovery and development of these substances. Succeeding volumes will focus on thematic reviews of areas included within the scope of metallic and metalloid-containing macromolecules.

Alaa S. Abd-El-Aziz
Charles E. Carraher Jr.
Charles U. Pittman Jr.
Martel Zeldin

CHAPTER 1

Nanocluster Assemblies and Molecular Orbital Interactions in Macromolecule-Metal Complexes

Laurence A. Belfiore and Sarah E. Fenton

Colorado State University, Department of Chemical Engineering, Polymer Physics and Engineering Laboratory, Ft. Collins, Colorado

CONTENTS

Macromolecules Containing Metal and Metal-Like Elements, Volume 7: Nanoscale Interactions of Metal-Containing Polymers, edited by Alaa S. Abd-El-Aziz, Charles E. Carraher Jr., Charles U. Pittman Jr., and Martel Zeldin.

I. INTRODUCTION

When transition metal cations from the d-block of the Periodic Table coordinate to ligands in the sidegroup of a polymer and modify the thermal response of a macromolecular complex, the enhancement in the glass-transition temperature (T_g) can be explained by focusing on ligand field stabilization[1] of the metal d-electrons. The methodology to identify attractive coordination complexes and predict relative

increases in T_g is described in terms of the local symmetry of the complex, molecular orbital energies, and the d-electron configuration.[2] Interelectronic repulsion is considered for pseudo-octahedral d^6 and d^7 complexes in the glassy state when there is ambiguity in the order in which the d-orbitals are populated. Ligand field stabilization energies are calculated for simple octahedral geometries and 5-coordinate complexes with reduced symmetry, such as square pyramidal, trigonal bipyramidal, and pentagonal planar, in molybdenum hexacarbonyl complexes with poly(vinylamine) above and below the glass-transition temperature. If pseudo-octahedral transition metal complexes bridge two different macromolecules in the glassy state via coordination crosslinks, then 5-coordinate complexes with one surviving metal–polymer bond above T_g represent reasonable geometries in the molten state. This model of thermochemical synergy in macromolecule–metal complexes with no adjustable parameters considers the glass transition as an endothermic process in which sufficient thermal energy must be supplied to dissociate intermolecular bridges or coordination crosslinks and produce coordinatively unsaturated molten state complexes. The enhancement in T_g correlates well with the difference between ligand field stabilization energies in the glassy and molten states for Ru^{2+} (d^6), Co^{2+} (d^7), and Ni^{2+} (d^8) complexes with either poly(4-vinylpyridine) or poly(L-histidine).[2] Larger relative increases in T_g are measured in complexes with the synthetic poly(α-amino acid) relative to those with poly(4-vinylpyridine). Poly(vinylamine) complexes with cobalt chloride hexahydrate[3] and several lanthanide trichloride hydrates[4,5] exhibit some of the largest increases in the glass-transition temperature that have been measured to date.

II. METHODOLOGY OF TRANSITION METAL COORDINATION IN POLYMERIC COMPLEXES

A. Polymeric Coordination Complexes with d-Block Salts that Exhibit an Increase in T_g

It is well known that organic plasticizers decrease a polymer's glass-transition temperature,[6] as described by previous researchers via entropy continuity, volume continuity, free volume concepts,[7] and the conformational entropy description[8] of T_g when flexible diluents are employed. The glass-transition temperature is depressed more at higher diluent concentrations until phase separation occurs. Hence inexpensive brittle polymers can be used in applications that require more flexible and compliant materials if miscible plasticizers are available to lower the glass-transition temperature. When additives *increase* a polymer's T_g, explanations are based on the existence of specific interactions and the formation of molecular complexes or nanoclusters, because one does not typically employ diluents with glass-transition temperatures that are higher than that of the undiluted polymer. Complexation between amorphous polymers and transition metal salts are operative in organic–inorganic hybrids that exhibit enhanced glass-transition temperatures relative to T_g of the undiluted polymer.[9] Chain mobility is hindered when transition metals coordinate to favorable ligands in the polymer's sidegroup via acid–base interactions. Coordination pendant

groups form when p-orbitals of the ligand with comparable energy and the same symmetry properties as d-orbitals of the metal form σ-bonds. If one functional sidegroup in the polymer occupies a vacant site in the first-shell coordination sphere of the metal center, then T_g increases by 10–30°C relative to the undiluted polymer.[10] This occurs, for example, in poly(4-vinylpyridine) complexes with zinc acetate dihydrate.[10,11] Coordination crosslinks occur when the transition metal forms σ-bonds with at least *two* functional sidegroups on different polymer chains.[3] These interactions should produce mobility restricting nanoclusters in the polymeric matrix. Figure 1 illustrates two modes of complexation between macromolecules and metal cations, denoted by *M*; intrachain coordination (upper left) vs. interchain coordination (lower left). Mixed-mode coordination is illustrated on the right side of the figure.

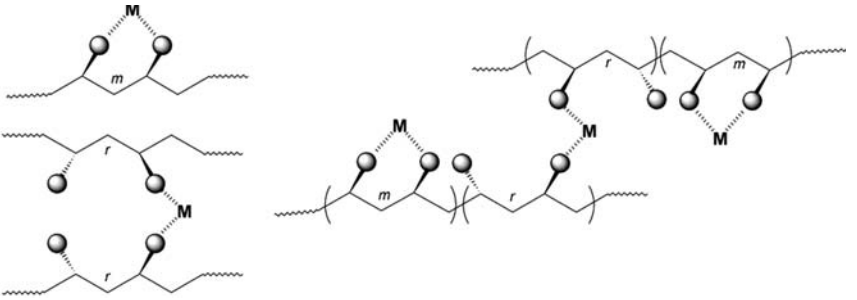

Figure 1 Intrachain vs. interchain coordination of metal centers to functional sidegroups in linear polymers.

It seems reasonable that the glass-transition temperature should experience larger enhancements when a single metal center coordinates to more functional sidegroups in several different polymer chains,[3] analogous to multifunctional crosslinking agents. The overall objectives of this chapter are to estimate differences between electronic energies of d^n configurations for macromolecule–metal complexes in the glassy and molten states, and correlate these d-electron energy differences with enhancements in the glass-transition temperature.

B. Chemical Bonding, Coordination, and Transition Metal Compatibilization

Divalent late transition metals like cobalt (d^7), nickel (d^8), and copper (d^9) in the first row of the d-block can use five 3d orbitals, one 4s orbital, and three 4p orbitals to form 4-, 5-, or 6-coordinate complexes.[12] As a general rule, if there are N ligands in the first-shell coordination sphere of a transition metal complex, then there should be N bonding molecular orbitals, N anti-bonding molecular orbitals, and 9-N nonbonding molecular orbitals.[12] Exceptions to this rule occur in some square–planar complexes in which three orbitals with the same symmetry properties overlap and form chemical bonds.[13] Usually, some coordination sites in the first-shell of the

metal center are occupied by neutral ligands such as waters of hydration, acetonitrile, benzonitrile, or carbon monoxide (i.e., C≡O). Anionic ligands in rather close proximity to the metal cation are required for charge neutrality. Pyridine ligands in poly(4-vinylpyridine), and copolymers that contain 4-vinylpyridine repeat units, coordinate to divalent zinc, copper, nickel, cobalt, and ruthenium.[9,11] Alkene ligands in the mainchain or sidegroup of diene polymers, such as polybutadiene and polyisoprene, coordinate to palladium(II) and platinum(II), but not nickel(II).[14–17] The imidazole ring in the histidine sidegroup of the synthetic poly(α-amino acid), poly(L-histidine), coordinates to divalent cobalt, nickel, copper, ruthenium, and palladium.[18,19] One of the most attractive applications of this technology is transition metal compatibilization of polymers that are immiscible in the absence of the inorganic component. Complexation will induce miscibility if the transition metal center acts as a bridge between two dissimilar chains by coordinating to appropriate ligands in the sidegroup of both polymers. This has been demonstrated for copolymer blends[9,11] of styrene/4-vinylpyridine and 4-vinylpyridine/butylmethacrylate. The proposed structure of this miscible ternary system is illustrated in Figure 2. Nickel acetate tetrahydrate and cobalt chloride hexahydrate function as transition metal compatibilizers and produce miscible 4-vinylpyridine copolymer blends. Dichlorobis(acetonitrile) palladium(II) compatibilizes diene polymer blends, such as atactic 1,2-polybutadiene with atactic 3,4-polyisoprene[15] and 1,2-polybutadiene with cis-polybutadiene[20] via high-temperature palladium-catalyzed chemical crosslinking. Palladium(II) also compatibilizes 3,4-polyisoprene and (1) lightly sulfonated polystyrene, with or without Zn^{2+} neutralization of the sulfonic acid groups;[21] and (2) random copolymers of ethylene and methacrylic acid.[21] Tetrakis(triphenylphosphine)palladium(0) compatibilizes 1,2-polybutadiene with poly(4-bromostyrene)[22] via a macromolecular analog of the Heck reaction (e.g., oxidative addition followed by olefin coordination, migratory insertion, and β-hydrogen elimination).[23]

i. Ligand Field Stabilization Energy Description of the Enhancement in T_g for Polymeric Complexes with Transition Metals

When transition metals coordinate to ligands in the mainchain or sidegroup of amorphous polymers and modify the thermal response of a macromolecular complex, the enhancement in T_g is based on the well-known correlation of lattice enthalpies of hexa–aqua transition metal complexes from the first row of the d-block with octahedral ligand field stabilization energies if these complexes exhibit high-spin, weak-field electronic configurations.[12,24] In complexes with octahedral or tetrahedral symmetry, if the energy difference between two nondegenerate metal-based d-orbitals is smaller than the repulsive energy that electrons experience when they are paired with opposite spin in the same orbital, then the electronic configuration is described as high-spin in a weak ligand field.[12] If one considers the increasingly exothermic enthalpy of formation[12,24] of divalent hexa–aqua transition metal complexes (i.e., $M^{2+}(H_2O)_6$) as a function of the number of d-electrons from calcium (d^0) to zinc (d^{10}), then the additional exothermic effect relative to linear trends from Ca^{2+} to Mn^{2+} and Mn^{2+} to Zn^{2+} (Fig. 3) correlates with the stabilization of metal d-electrons for octahedral complexes in the first row of the d-block that exhibit weak-field

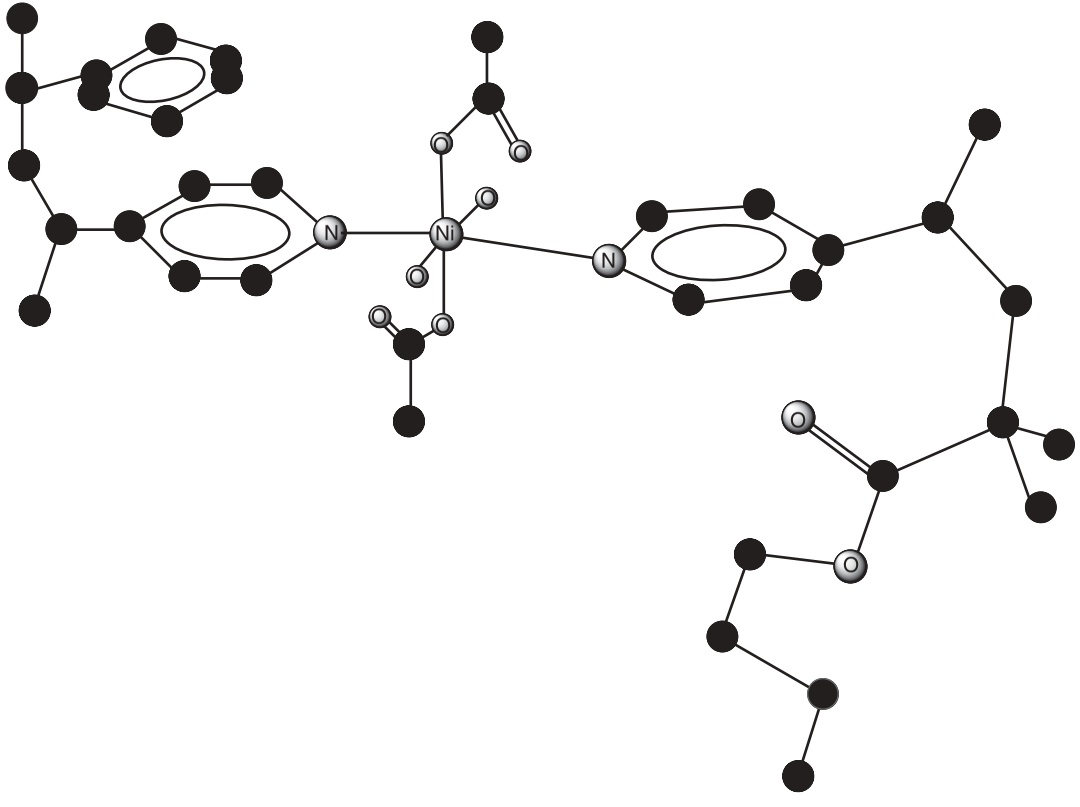

Figure 2 Molecular model showing the concept of transition metal compatibilization of two immiscible vinylpyridine copolymers. The octahedral bonding characteristics of nickel acetate tetrahydrate, together with its previously published crystal structure,[37,38] are used to postulate the structure of the amorphous polymeric coordination complex. It is proposed that the divalent metal salt sheds two hard-base waters of hydration and coordinates to pyridine sidegroups in copolymers of styrene with 4-vinylpyridine (i.e., on the left) and butylmethacrylate with 4-vinylpyridine (i.e., on the right).

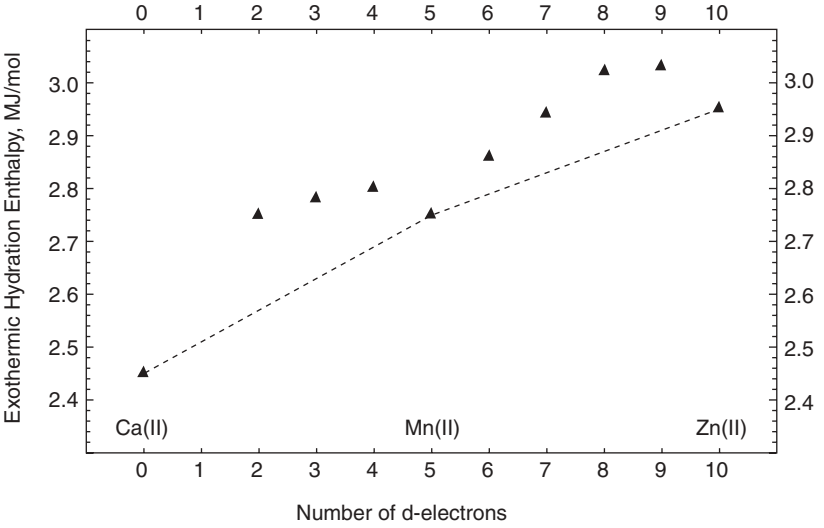

Figure 3 Hydration enthalpies of divalent hexa–aqua metal complexes from the first row of the d-block[12] as a function of the number of d-electrons from Ca^{2+} to Zn^{2+}. Both *dashed lines* illustrate linear trends when weak-field ligand field stabilization energies are subtracted from the experimental hydration enthalpies.

electronic configurations. These empirical correlations between thermodynamic properties and d-electron energies of octahedral complexes provide support for analyzing T_g enhancements in macromolecule–metal complexes via ligand field–induced stabilization of metal d-electrons. Furthermore, this stabilization must be larger for complexes in the glassy state relative to the corresponding molten state complexes to realize metal-induced increases in the glass-transition temperature with respect to T_g of the undiluted polymer.[1,9] The approach described below deviates considerably from well-known free-volume and conformational entropy models of the glass transition. Energetic stabilization of metal d-electrons due to the presence of the ligands is invoked to explain relative increases in T_g when transition metal complexes coordinate to polar sidegroups in amorphous polymers. The absolute magnitude of T_g and the discontinuity in specific heat ΔC_p at the glass-transition temperature are not predicted by these energetic ligand field stabilization models.

ii. Energetic Ligand Field Models and the Methodology of Transition Metal Coordination

The methodology to identify attractive coordination complexes and predict increases in T_g is described in terms of the local symmetry of the complex, energies of the five metal-based atomic d-orbitals when ligands surround the metal center, and the d-electron configuration. The glass transition occurs when sufficient thermal energy is supplied to dissociate a coordination crosslink or bridge between two different polymer chains. If nearby low-molecular-weight neutral ligands, such as

Table 1 Summary of Molecular Point Groups and Coordination Numbers for Transition Metal Complexes

Coordination Number	Point Group Symmetry (structural formula; acronym)
3, ML_3	facial trivacant (C_{3v}), trigonal planar (D_{3h}), T-shaped (C_{2v})
4, ML_4 or MX_2L_2	tetrahedral (ML_4; T_d), trigonal pyramid (ML_4; C_{3v}), square planar (ML_4; C_{4v}), *trans*-square-planar (MX_2L_2; D_{2h}), *cis*-square-planar (MX_2L_2; C_{2v})
5, ML_5	square pyramid (C_{4v}), trigonal bipyramid (D_{3h}), pentagonal planar (D_{5h})
6, ML_6	octahedral (O_h), hexagonal planar (D_{6h}), pentagonal pyramid (C_{5v})
7, ML_7	heptagonal planar (D_{7h}), pentagonal bipyramid (D_{5h}), hexagonal pyramid (C_{6v})
8, ML_8	cubic (O_h), square antiprism (D_{4d}), octagonal planar (D_{8h}), hexagonal bipyramid (D_{6h})
10, ML_{10}	pentagonal antiprism (D_{5d})
12, ML_{12}	icosahedral (I_h)

M, metal; *L*, ligand; *X*, anionic ligand.

waters of hydration (i.e., lattice waters), acetonitrile, benzonitrile, or carbon monoxide, do not occupy the vacant site in the coordination sphere of the transition metal when a polar sidegroup in the polymer is removed from the first shell, then the molten state complex exhibits reduced symmetry relative to the complex below T_g. Detailed calculations are considered for octahedral complexes in the glassy state and 5-coordinate complexes in the molten state. Differences between electronic energies of a d^n configuration for polymeric complexes in the glassy and molten states are used to predict relative increases in T_g. Then these predictions based on ligand field stabilization energies are compared with experimental results in an attempt to establish universal trends. In general, one associates the following coordination numbers to complexes which exhibit point group symmetries that are summarized in Table 1.

C. Well-Defined Low-Molecular-Weight Transition Metal Complexes that Increase T_g

The x-ray crystallography literature is useful to locate previously published crystal structures of attractive low-molecular-weight d-block metal complexes. Information about coordination numbers and the molecular point groups, summarized in Table 2, is useful (1) to postulate possible ligand substitution schemes that involve weakly bound lattice waters, acetonitrile, or carbon monoxide; (2) to adopt the same symmetry for the complex that forms between polymer and metal center in the glassy state; and (3) to calculate ligand field splittings and the corresponding ligand field stabilization energies. Table 2 summarizes molecular point groups, coordination numbers, and the number of weakly bound neutral ligands that can be displaced for several late transition metal complexes on the right side of the d-block.

Table 2 Transition Metal Complexes that Increase the Glass-Transition Temperature of Functional Polymers

Metal Complex	Structural Formula (including neutral ligands in the first shell)	Molecular Point Group (pseudo)	Coordination Number	Number of weakly bound neutral ligands
Cobalt chloride	$CoCl_2(H_2O)_6$	octahedral	6	4
Nickel chloride	$NiCl_2(H_2O)_6$	octahedral	6	4
Copper chloride	$CuCl_2(H_2O)_2$	tetrahedral	4	2
Zinc chloride	$ZnCl_2$	polymeric		
Nickel acetate	$Ni(OOCH_3)_2(H_2O)_4$	octahedral	6	4
Zinc acetate	$Zn(OOCH_3)_2(H_2O)_2$	tetrahedral	4	2
Dichlorotricarbonyl-ruthenium(II)	$[RuCl_2(CO)_3]_2$	octahedral	6	3 and a vacant site
Dichlorobis(aceto-nitrile)palladium(II)	$PdCl_2(CH_3CN)_2$	square planar	4	2
Dichlorobis(benzo-nitrile)platinum(II)	$PtCl_2(C_6H_5CN)_2$	square planar	4	2

D. Attractive Polymeric Ligands

Polymers with functional groups that coordinate to transition metal complexes represent an important design criterion for glass-transition temperature enhancement. Reactive blending is based on the fact that selected functional groups in the main-chain or sidegroup of the polymer are stronger bases than the original weakly bound neutral ligands in the coordination sphere of the transition metal. Hence, these ligands in the polymer will displace neutral ligands such as waters of hydration, carbonyls (i.e., C≡O), acetonitriles, and benzonitriles. In most cases, weak-base neutral ligands are displaced by strong-base polymeric ligands that are also neutral. In less frequent situations, polymeric ligands cleave the dihalide bridge in a dimeric transition metal complex[25] and coordinate to the vacant site after cleavage. The hard and soft acid–base theory[26,27] is useful for selecting proper combinations of polymeric ligands and transition metals that have an affinity for each other.

E. Identifying Attractive Interactions via Hard and Soft Acids and Bases

One possible set of guidelines for acid–base interactions follows concepts from hard and soft acid–base theory to identify the hardness of the metal center as an acid and the hardness of the ligands, including important functional groups in the polymer, as bases. Frontier orbital energy differences between the highest occupied and lowest unoccupied molecular orbitals are small and perturbations in the electronic distribution occur rather easily, yielding covalent bonds for soft acid–base pairs.[12] In

contrast, when the frontier molecular orbital energy differences are large, it is difficult to perturb the electronic distribution, and ionic bonding dominates in hard acid–base pairs.[12] There is an affinity between acids and bases with the same classification.[26,27] If there is a mismatch in hardness between the metal center and a neutral ligand, then this metal–ligand bond should be the focus of a potential displacement reaction. Basic functional groups in the polymer with the same hardness classification as the metal could displace a ligand of dissimilar hardness. Waters of hydration (i.e., lattice waters) are neutral hard bases. Hence if the low-molecular-weight metal complex contains lattice waters in the first-shell coordination sphere of a soft or borderline acidic metal center, then soft or borderline basic ligands in the sidegroup of the polymer might displace these hard bases. Hardness classifications for various acids and bases[12,26,27] are summarized in Table 3.

F. Displacement of Weak Neutral Bases in the First-Shell Coordination Sphere by Stronger Bases

One should consider all of the basic ligands in the coordination sphere of the low-molecular-weight metal complex, as well as potential basic ligands in the main-chain or sidegroup of the polymer, and rank the strengths of these bases using the pK_A/pK_B scale. The pK_A scale, which summarizes the strengths of acids and bases, is completely independent of the hardness classification discussed in the previous section (Table 3). At 25°C, the equilibrium constant for the following reaction;

$$HA(\text{aqueous}) + H_2O(\text{liquid}) \Leftrightarrow H_3O^+ + A^-$$

is defined by K_A;

$$K_A = \frac{[H_3O^+][A^-]}{[HA][H_2O]}$$

and $pK_A = -\log K_A = \log\{K_A^{-1}\}$. Stronger acids HA have a greater tendency to donate H^+ to H_2O and generate H_3O^+ and A^-; and they exhibit larger values of K_A, smaller values of K_A^{-1}, and smaller values of pK_A. The acidity constant for H_2O is

Table 3 Hard, Soft, and Borderline Classifications for Acids and Bases[12,26,27]

	Acids
Hard	H^+, Li^+, Na^+, K^+, Mg^{2+}, Ca^{2+}, Mn^{2+}, Cr^{3+}, Fe^{3+}, Co^{3+}
Borderline	Fe^{2+}, Co^{2+}, Ni^{2+}, Cu^{2+}, Zn^{2+}, Rh^{3+}, Ir^{3+}, Ru^{2+}, Os^{2+}
Soft	Cu^+, Ag^+, Au^+, Pd^{2+}, Cd^{2+}, Pt^{2+}, zero-valent metal atoms
	Bases
Hard	F^-, Cl^-, OH^-, H_2O, NH_3, RNH_2, NO_3^-, O^{2-}
Borderline	NO_2^-, Br^-, N_2, C_5H_5N, $C_6H_5NH_2$
Soft	H^-, I^-, CN^-, $C{\equiv}O$, C_6H_6, PR_3, $P(OR)_3$
	R represents an alkyl group, like CH_3 or C_2H_5

10^{-14} at 25°C,[12] which corresponds to the equilibrium constant for the previous reaction when HA(aqueous) is replaced by H_2O. Hence

$$H_2O(\text{aqueous}) + H_2O(\text{liquid}) \Leftrightarrow H_3O^+ + OH^-$$

with

$$K_A = K_W = \frac{[H_3O^+][OH^-]}{[H_2O]^2} = 10^{-14}$$

If one adds the previous two reactions, in which reactants and products in the first reaction are reversed, then

$$H_3O^+ + A^- \Leftrightarrow HA(\text{aqueous}) + H_2O(\text{liquid})$$

with

$$\frac{1}{K_A} = \frac{[HA][H_2O]}{[H_3O^+][A^-]}$$

The net reaction is

$$H_2O(\text{liquid}) + A^- \Leftrightarrow HA\,(\text{aqueous}) + OH^-$$

where the equilibrium constant for this reaction is defined by K_B, and $pK_B = -\log K_B$. Hence

$$K_B = \frac{[HA][OH^-]}{[H_2O][A^-]} = \frac{[HA][H_2O]}{[H_3O^+][A^-]}\,\frac{[H_3O^+][OH^-]}{[H_2O]^2} = \frac{10^{-14}}{K_A}$$

Stronger bases A^- can extract H^+ from H_2O more readily to generate HA and OH^-; and they exhibit larger values of K_B, smaller values of K_B^{-1}, and smaller values of pK_B. Furthermore

$$\log K_B = -14 - \log K_A$$

or

$$pK_A + pK_B = 14$$

The pK_A of water as an acid is 14, and its conjugate base (the hydroxyl anion, OH^-) has a pK_B of 0.[12] The pK_B of water as a base is 14, and its conjugate acid (the hydronium cation, H_3O^+) has a pK_A of 0.[12] pK_A and pK_B sum to 14 for an acid/conjugate-base pair. Acidity and basicity increase, respectively, when pK_A and pK_B decrease. When an acid is stronger than the hydronium cation, pK_A is negative. When a base is stronger than the hydroxyl anion, pK_B is negative. Acidity constants for several acid/conjugate-base pairs in aqueous solution at 25°C are provided in Table 4.[12,28]

If the polymer contains functional groups that are stronger bases than some of the neutral ligands chemically bound to the metal center, then these weak basic ligands

Table 4 Acidity Constants for Acid (HA) / Conjugate-Base (A^-) Pairs in Aqueous Solution at 25°C[12,28]

Acid	HA	A^-	pK_A
Hydriodic	HI	I^-	−11
Hydrobromic	HBr	Br^-	−9
Hydrochloric	HCl	Cl^-	−7
Phenol super-acid	$C_6H_5OH_2^+$	C_6H_5OH	−6.4
Ether super-acids	$R_1R_2OH^+$	R_1OR_2	−3.5
Hydronium	H_3O^+	H_2O	0
Hydrofluoric	HF	F^-	3.45
Carboxylic	RCOOH	$RCOO^-$	4–5
Pyridinium	$C_6H_5N^+H$	C_6H_5N	5.25
Cyanide	HCN	CN^-	9.3
Ammonium	N^+H_4	NH_3	9.25
Tertiary ammonium	R_3N^+H	NR_3	10–11
Secondary ammonium	$R_2N^+H_2$	R_2NH	11
Primary ammonium	RN^+H_3	RNH_2	10–11

that occupy sites in the coordination sphere are susceptible to displacement reactions. When weak bases are displaced by stronger bases, the metal–ligand σ-bonds that form are stronger than those that are dissociated, and this type of ligand exchange corresponds to an exothermic reaction. Consequently, some of the ligand-based bonding molecular orbitals are stabilized (i.e., lowered in energy) after ligand displacement occurs, and the metal–ligand σ-antibonding e_g orbitals are destabilized[12] in systems with local octahedral symmetry. This increases the ligand field splitting.

i. Anionic Ligands Are the Last Ones that Should Be Displaced to the Second Shell

Weak basic neutral ligands with a different hardness classification than the metal center are most susceptible to displacement reactions. If all of the lattice waters (i.e., hard bases) and some of the weak base chloride anions (i.e., hard bases) in a divalent metal chloride hydrate are displaced by strong-base polymeric ligands, then the following ligand exchange reaction is possible

$$M^{2+}Cl_2(H_2O)_4 + (4 + y)[\text{Polymer}] \Rightarrow M^{2+}Cl_{2-y}[\text{Polymer}]_{4+y} + (y)Cl^- + 4H_2O$$

where $0 < y \leq 2$, and the displaced anionic ligands reside in the second shell. One should not propose a scheme that displaces anionic ligands in the coordination sphere of a cationic metal center unless all of the neutral basic ligands have already been displaced and the displacing ligand in the polymer is a strong base. If anionic ligands are displaced, then they must reside in the second shell. For example, cobalt chloride hexahydrate, $CoCl_2(H_2O)_6$, forms complexes with poly(vinylamine) when the lone pair of electrons on the amino nitrogen displaces all four waters of hydration in the first shell.[3,29] It is also possible that amino nitrogens displace one or both of the anionic chlorides to the second shell.[30–32] Hence, cobalt(II) acts as a multifunctional bridge between several amino sidegroups. This structure, which forms via self-assembly, is

postulated to explain the unusually large increase in T_g for these cobalt(II) complexes (i.e., 45°C per mol% salt, up to 3 mol% Co^{2+}) relative to the undiluted polymer.[3,5,29] Contrary to some of the results discussed in Section VI for complexes with poly(4-vinylpyridine) and poly(L-histidine), which are much weaker bases (i.e., by four or five orders of magnitude since pK_A is a *logarithmic* scale) than poly(vinylamine), Co^{2+} performs exceptionally well with poly(vinylamine) due to its ability to coordinate several amino groups, as described by the previous ligand substitution reaction. This is not possible for dichlorotricarbonylruthenium(II), $\{RuCl_2(C{\equiv}O)_3\}_2$, because it is increasingly difficult for amino sidegroups in poly(vinylamine) to displace more than one carbonyl ligand in the ruthenium complex after cleaving the dichloride bridge.[25,33] Hence, $CoCl_2(H_2O)_6$ is superior to $\{RuCl_2(C{\equiv}O)_3\}_2$ from the viewpoint of enhancing the glass-transition temperature of poly(vinylamine),[5,29] based on a reduction in chain mobility and the formation of nanoscale clusters when NH_2 sidegroups occupy sites in the coordination sphere of Co^{2+} vs. Ru^{2+}, where Co^{2+} contains weak-base lattice waters and Ru^{2+} contains C≡O ligands.

G. Complexes with the Same Local Symmetry Above and Below the Glass Transition

If T_g of the polymeric complex is higher than T_g of the undiluted polymer, then one postulates that the glass transition occurs when sufficient thermal energy is provided to remove N or N−1 ligands in the sidegroup of the polymer from the first-shell coordination sphere of the transition metal center.[3] Hence one ligand in the polymer could survive this dissociation process if only N−1 ligands are removed. Now, the transition metal complex represents a bulky coordination pendant group. The N−1 vacant sites in the coordination sphere of the metal could be occupied by neutral basic ligands that were displaced originally by polymeric ligands, if this process seems reasonable. In other words, displaced C≡O ligands that bubble out of solution or sublime should not be used to fill vacant sites, but waters of hydration that have not volatilized are available.

i. Complexes with Reduced Symmetry Above T_g

The displacement reaction on the previous page simulates the glass transition process by preserving ligand arrangements and geometries of macromolecule-metal complexes above and below the second-order phase transition. If ligands that were displaced originally are not available to occupy vacant sites when metal–polymer σ-bonds are dissociated, then it might seem reasonable to postulate a decrease in coordination number for coordinatively unsaturated complexes[2] that survive above T_g. This approach is adopted for zero-valent molybdenum hexacarbonyl complexes as described below, because displaced C≡O ligands are not available to occupy vacant sites above T_g. When geometric perturbations occur, as macromolecule–metal complexes transform from glasses to highly viscous liquids, ligand field stabilization energies (LFSEs) for the state of lower symmetry above the glass-transition temperature require more complex methods of analysis in comparison with LFSE calculations for octahedral and tetrahedral geometries. LFSE calculations for 5-coordinate

transition metal complexes in the molten state are discussed below in significant detail. All of the possible five-coordinate geometries in Table 1 should be considered if the glass transition corresponds to the dissociation of one polymeric sidegroup from the coordination sphere of a macromolecule–metal complex with pseudo-octahedral symmetry in the glassy state. Similarly, all possible three-coordinate geometries should be considered when pseudo-tetrahedral macromolecule–metal complexes are heated into the molten state, and T_g is described by the formation of a three-coordinate complex as one ligand in the sidegroup of a functional polymer is removed from the coordination sphere of the metal center. When the geometry of the complex is not pseudo-octahedral or pseudo-tetrahedral, the five d-orbitals of the metal do not split into a triply degenerate set denoted by t_{2g} and a doubly degenerate set denoted by e_g, based on the symmetry properties of these d-orbitals.[34] Hence the ligand field splitting does not represent the energy difference between any two orbitals at different energy. If $\Delta_0 = 10$ Dq represents the octahedral ligand field splitting, or the energy difference between e_g and t_{2g} metal-based molecular orbitals in complexes with local octahedral symmetry,[12] then there are several examples where the energy difference between two adjacent nondegenerate d-orbitals in ML_5 complexes is much less than 10 Dq. Consequently, it is not uncommon for the pairing energy that characterizes interelectronic repulsion to be larger than the energy difference between two adjacent nondegenerate d-orbitals. This scenario produces the so-called high-spin population of metal d-orbitals, because electrons would rather populate vacant orbitals at slightly higher energy instead of occupying orbitals at lower energy that already contain one electron.

H. Consideration of Interelectronic Repulsion and Ligand Field Splitting When There is Ambiguity in the d-Electron Configuration

Quantum-chemical group contribution methods and tabulated parameters are available to estimate the ligand field splitting (i.e., Δ_0 or Δ_T) for transition metal complexes with local octahedral O_h or tetrahedral T_d symmetry.[24,34,35] Detailed calculations of the energy difference between metal-based molecular orbitals for ML_6 and ML_4 complexes are summarized below. It is also possible to estimate the Racah interelectronic repulsion energy, $B = B_0(1 - hk)$, in the presence of an octahedral arrangement of ligands if B_0 is known for the free metal ion (i.e., see Table 5). The parameters h and k are characteristic of the ligand and metal, respectively. The Racah interelectronic repulsion energy B is inversely proportional to the effective radius of the d-electron cloud on the metal. When ligands interact with the metal and form a complex, expansion of the d-electron cloud occurs, which is known as the nephelauxetic (i.e., cloud expansion) effect.[12] As a consequence of the delocalization of metal d-electrons over the ligands, interelectronic repulsion is weaker and the Racah B parameter is reduced in magnitude relative to the free metal ion. These considerations are important when there is ambiguity in the electronic configuration and the ligand field stabilization energy for d^n complexes. For example, octahedral d^7 complexes exhibit a low-spin $\{t_{2g}\}^6\{e_g\}^1$ ground state (Table 13), with six paired

electrons occupying the triply degenerate t_{2g} orbitals at lower energy and one electron occupying a higher energy doubly degenerate e_g orbital, when[12]

$$\Delta_0/B > \{\Delta_0/B\}_{critical}$$

A high-spin $\{t_{2g}\}^5\{e_g\}^2$ ground state is preferred (Table 13), with five electrons occupying the triply degenerate orbitals at lower energy and two unpaired electrons occupying the doubly degenerate higher energy orbitals, when[12]

$$\Delta_0/B < \{\Delta_0/B\}_{critical}$$

In other words, in the presence of ligands that are classified as strong bases with large pK_As or small pK_Bs, and strong π-acceptors at the top of the spectrochemical series, heavy-metal octahedral complexes exhibit large energy differences between t_{2g} and e_g metal-based molecular orbitals. Hence the ligand field splitting is large, metal d-electron density is delocalized significantly over these basic ligands such that the Racah interelectronic repulsion energy is reduced, and the low-spin electronic configuration is favored, especially for complexes with heavy-metal centers from the second and third rows of the d-block that contain C≡O ligands. For transition metal complexes with tetrahedral symmetry, the five degenerate d-orbitals of the metal split into a doubly degenerate set with e-symmetry at lower energy and a triply degenerate set with t_2-symmetry at higher energy.[12] The energy difference between these electronic orbitals is approximately twofold smaller for tetrahedral complexes relative to octahedral complexes. Now, for d^7 complexes with 7 d-electrons and tetrahedral symmetry, there is no ambiguity in the electronic configuration because four paired electrons populate the doubly degenerate e-orbitals at lower energy and three unpaired electrons populate the triply degenerate t_2 orbitals at higher energy, $\{e\}^4\{t_2\}^3$, irrespective of the ligand field strength. For octahedral complexes, one should use Jørgensen's "group contribution" methodology[24,34,35] to estimate the ratio of the ligand field splitting Δ_0 (i.e., the energy difference between e_g and t_{2g} metal-based molecular orbitals) to the reduced Racah interelectronic repulsion energy B, as discussed below, and inspect the appropriate Tanabe-Sugano diagram,[12] which summarizes electronic states and d-d transitions for d^n complexes with octahedral symmetry. A summary of the critical values of Δ_0/B on the horizontal axes of the Tanabe-Sugano diagrams for d^n complexes is provided below, where $n = 4, 5, 6, 7$. A crossover occurs in the electronic ground state from high-spin to low-spin when the ligand field splitting Δ_0 matches and, subsequently, exceeds the pairing energy for interelectronic repulsion. The pairing energy is defined by $B\{\Delta_0/B\}_{critical}$ when two d-electrons with opposite spin occupy the same molecular orbital.

Number of d-Electrons	$\{\Delta_0/B\}_{critical}$
4	27
5	28
6	20
7	22

As mentioned earlier in this chapter, pseudo-octahedral d^7 cobalt(II) chloride complexes with poly(vinylamine) induce significant increases in the polymer's glass-transition temperature.[3,5] Quantum-chemical group contribution predictions for six-coordinate Co^{2+} complexes with anionic chloride ligands, lattice waters, and methyl amine as a model ligand for the amino sidegroup of poly(vinylamine) yield estimates[3] of Δ_0/B between 11 and 14. Hence the d-electron configuration in these pseudo-octahedral d^7 complexes is $\{t_{2g}\}^5\{e_g\}^2$ for a weak ligand field because Δ_0/B is less than the critical value of 22, as expected for complexes from the first row of the d-block that do not contain C≡O ligands. If a complex exhibits tetrahedral symmetry, one should proceed with calculations based on tabulated parameters for octahedral geometries and reduce the octahedral ligand field splitting, Δ_0, by a factor of $\frac{4}{9}$ (i.e., $\Delta_T \approx 0.45\ \Delta_0$).[12,35] It seems reasonable that tetrahedral complexes with four ligands in the first-shell coordination sphere of the transition metal will not expand the d-electron cloud as much as six ligands with octahedral symmetry. Consequently, tetrahedral complexes should experience a smaller reduction in the Racah interelectronic repulsion energy B from its value for the free transition metal ion. For example, divalent cobalt tetrachloride $[CoCl_4]^{2-}$ exhibits an experimental Racah parameter $B = 730\,cm^{-1}$, based on an analysis of its electronic spectrum.[35] Quantum-chemical group contribution predictions of the corresponding octahedral complex $[CoCl_6]^{4-}$ suggest that $B \approx 580\,cm^{-1}$. Since the free-ion interelectronic repulsion energy[35] B_0 for Co^{2+} is $1120\,cm^{-1}$, $B = 730\,cm^{-1}$ for the tetrahedral complex $[CoCl_4]^{2-}$ represents a 72% reduction in B_0 relative to the octahedral complex. In general, estimates of B in the presence of ligands for complexes with T_d symmetry are not as straightforward as estimates of the tetrahedral ligand field splitting (i.e., the energy difference between t_2 and e metal-based molecular orbitals)

$$\Delta_T = (4/9)\ \Delta_0$$

The Tanabe-Sugano diagram for a d^n complex with tetrahedral symmetry is equivalent to the Tanabe-Sugano diagram for a d^{10-n} complex with octahedral symmetry. The important questions that must be considered are: (i) What molecular orbital does the fourth metal d-electron populate in complexes with octahedral symmetry?; and (ii) What orbital does the third metal d-electron populate in complexes with tetrahedral symmetry? The answers are: (i) the d-orbital at lower energy is populated and electron pairing occurs when

$$\Delta_0/B > \{\Delta_0/B\}_{critical}$$

which corresponds to the strong-field, low-spin situation; and (ii) the d-orbital at higher energy is populated, with spin-correlation for all of these unpaired electrons, when

$$\Delta_0/B < \{\Delta_0/B\}_{critical}$$

which corresponds to the weak-field, high-spin case.

III. JØRGENSEN'S PARAMETRIC REPRESENTATION OF LIGAND FIELD SPLITTING AND INTERELECTRONIC REPULSION

For several ML_6 complexes with true octahedral symmetry, it is possible to estimate electronic properties empirically that agree quite well with data from electronic spectroscopy, based on the information in Table 5.[24,34,45] For example, one predicts the octahedral ligand field splitting (i.e., $\Delta_0 = 10\,Dq$), or the energy difference between the triply degenerate t_{2g} metal-based molecular orbitals at lower energy and the higher energy doubly degenerate e_g antibonding metal-based molecular orbitals, and the Racah interelectronic repulsion energy B, for ML_6 complexes with six identical monodentate ligands as follows [24,34,35]

$$\Delta_0 = 10\,Dq = fg\ [10^3\,cm^{-1}]$$

$$B = B_0(1 - hk)$$

where *g* and *k* are characteristic of the metal, *f* and *h* are unique to the six ligands, and B_0 describes the interelectronic repulsion energy of the free metal ion in the absence of the ligand field. The metal-based g-factor provides the strongest influence on Δ_0.

As described below, the *rule of average environments* is invoked to predict electronic properties of mixed-ligand complexes with pseudo-octahedral symmetry.[24,35] The concept of the magnitude of a cubic ligand field is appropriate for complexes that exhibit approximate cubic symmetry.[35] For example, if χ_k represents a normalized

Table 5 Jørgensen's Parameters for Ligand Field Splittings and Interelectronic Repulsion in Octahedral ML_6 Complexes[24,34,35]

Metal Ion	*g*	*k*	B_0 (cm^{-1})	Ligands	*f*	h
Mn^{2+}	8.0–8.5	0.07	960	Br^-	0.72–0.76	2.3
Ni^{2+}	8.7–8.9	0.12	1080	Cl^-	0.78–0.80	2.0
Co^{2+}	9.0–9.3	0.24	1120	F^-	0.90	0.8
Fe^{2+}	10.0		1060	$(NH_2)_2CO$	0.91–0.92	1.2
Cu^{2+}	12.0		1240	CH_3COO^-	0.94–0.96	
Fe^{3+}	14.0	0.24		H_2O	1.00	1.0
Cr^{3+}	17.0–17.4	0.21	1030	CH_3NH_2	1.17	
Co^{3+}	18.2–19.0	0.35		CH_3CN	1.22	
Ru^{2+}	20		620	C_5H_5N	1.23–1.25	
Ti^{3+}	20.3			NH_3	1.25	1.4
Mn^{3+}	21		1140	Histidine	1.32	
				CN^-	1.7	2.0
Mn^{4+}	23	0.5		C≡O	5–8	
Mo^{3+}	24.0–24.6	0.15				
Rh^{3+}	27.0	0.3				
Ir^{3+}	32	0.3				
Pt^{4+}	36	0.5				

weighting factor for the fraction of L_k-type ligands in a pseudo-octahedral complex, then the octahedral ligand field splitting of these mixed-ligand complexes is predicted as follows;

$$\Delta_0 (ML_AL_BL_C) = \sum_{k=A,B,C} \chi_k \Delta_0(ML_6)_k$$

where $\Delta_0(ML_6)_k$ represents the octahedral ligand field splitting of an ML_6 complex, with six identical monodentate L_k-type ligands that can be predicted using the parameters in Table 5. For mixed-ligand complexes with pseudo-tetrahedral symmetry, one can (1) predict octahedral ligand field splittings for ML_6 complexes with six identical L_k-type ligands using parameters in Table 5, (2) scale each of these predictions for $\Delta_0(ML_6)_k$ by 0.45 to obtain $\Delta_T(ML_4)_k$ for complexes with true tetrahedral symmetry, and (3) use the following equation to predict pseudo-tetrahedral ligand field splittings for mixed-ligand complexes.

$$\Delta_T(ML_AL_BL_C) = \frac{4}{9} \sum_{n=A,B,C} \chi_n \Delta_0(ML_6)_n$$

where χ_n represents a normalized weighting factor for the fraction of L_n-type ligands in these pseudo-tetrahedral complexes.

A. Polymeric Complexes with Enhanced Glass-Transition Temperatures

Inorganic models of the glass-transition process, based on a consideration of ligand field splittings and LFSEs for d^n complexes with specific geometries and coordination numbers, predict an increase in T_g if metal d-electrons are stabilized when complexes form in solution and persist in the glassy state. If there is no change in local symmetry of metal complexes in the glassy and molten states, simply a change in ligand environment when ligand exchange occurs to simulate the glass-transition process, then metal d-electrons experience destabilization when N or N−1 polymeric ligands are removed from the coordination sphere of the transition metal via thermal energy and the original ligands of weaker basicity occupy these vacant sites in the first shell. Hence these ligand displacement reactions that simulate the glass-transition process are endothermic because stronger metal-ligand σ-bonds are dissociated and weaker ones reform. If the molten state is described better by a reduction in symmetry of the metal complex relative to the glassy state, then dissociation of at least one ligand in the sidegroup of the polymer from the first-shell coordination sphere of the metal center is also an endothermic process, based on metal-ligand bond energies or destabilization of metal d-electrons in the molten state complex of reduced symmetry. All of these models, described qualitatively above and investigated quantitatively below, are consistent with the fact that T_g is enhanced by most transition metal salts investigated to date.

B. Polymeric Complexes with Reduced Glass-Transition Temperatures

Ligand field models predict a decrease in T_g if metal d-electrons are stabilized when N or N-1 polymeric ligands of similar hardness are removed from the coordination sphere of the transition metal via the addition of thermal energy and the original ligands of stronger basicity, but different hardness, occupy these vacant sites in the molten state. Under these conditions, ligand displacement reactions that simulate the glass transition process are "exothermic" because weaker metal-ligand σ-bonds are dissociated and stronger ones reform. Transition metal salts can decrease the glass-transition temperature, and stabilization of metal d-electrons in the molten state provides an energetic explanation for this phenomenon, even though the glass transition process is generically endothermic. For example, Co^{2+}, Ni^{2+}, Cu^{2+} and Zn^{2+} chlorides decrease the glass-transition temperature of poly(L-lysine)hydrobromide,[19,36] because the presence of bromide counterions that neutralize quaternary lysine sidegroups [i.e., $(CH_2)_4N^+H_3$] at neutral pHs precludes any complexation between these divalent metal cations and the amino nitrogen lone pair.

C. Other Considerations

It is helpful to use the 18-electron rule[23] as a standard for estimating the rates of ligand substitution reactions in organometallic complexes with carbon-containing ligands, like C≡O, acetate, acetonitrile, etc. Complexes that are coordinatively saturated with a total of 18 metal d-electrons and ligand electrons in the frontier orbitals usually follow a dissociative mechanism of ligand exchange that is inherently slow.[23] Transition states are described by lower coordination number,[12] relative to reactants or products, when substitution proceeds by a dissociative mechanism. Coordinatively *un*saturated complexes with less than 18 electrons are labile, and the associative mechanism of ligand substitution is much faster, relative to the dissociative mechanism of ligand exchange. Transition states are described by higher coordination numbers, relative to reactants or products, when substitution proceeds by an associative mechanism.[12,23]

IV. PSEUDO-OCTAHEDRAL d^8 NICKEL COMPLEXES WITH POLY(4-VINYLPYRIDINE)

A. Ligand Field Stabilization Energies

Nickel acetate tetrahydrate forms coordination complexes with poly(4-vinylpyridine) (P4VP) and increases the glass-transition temperature of this amorphous polymer by 102°C when the Ni^{2+} concentration is ≈36 mol%. The complete concentration dependence of the effect of Ni^{2+} on P4VP's T_g is summarized in Table 6.[1]

Table 6 Effect of Nickel Acetate Tetrahydrate on the Glass Transition Temperature of Poly(4-vinylpyridine)

Mole Fraction Nickel Acetate	Glass-Transition Temperature (°C)	$T_{g,complex} - T_{g,P4VP}$ (°C)
0.000	149	0
0.055	175	26
0.110	201	52
0.219	227	78
0.359	251	102
0.528	189	40
0.771	171	22

The formalism outlined above is employed to analyze T_g enhancement when the local symmetry about Ni^{2+} does not change as complexes are heated through the second-order phase transition. The energy difference between the t_{2g} and e_g metal-based molecular orbitals in octahedral ML_6 complexes with six identical monodentate ligands can be predicted via Jørgensen's parameters,[34,35] listed in Table 5. Pyridine is a physically realistic model that captures the electronic characteristics of pyridine sidegroups in the polymer, but it cannot reproduce the correct steric hindrance due to the chain backbone. Analysis of T_g enhancement based on structurally simple model compounds is consistent with the energetic description of the glass-transition process in this chapter, whereas an entropic model of T_g modification that does not consider steric hindrance as ligands in the polymer's sidegroup coordinate to the metal center is not acceptable. One predicts ligand field splittings for the 6-coordinate nickel acetate anion $[Ni(CH_3COO)_6]^{4-}$, the hexa-aqua nickel cation $[Ni(H_2O)_6]^{2+}$, and the 6-coordinate nickel pyridine cation $[Ni(C_5H_5N)_6]^{2+}$, some of which agree with spectroscopic data.

Ni^{2+} Complex	**Ligand Field Splitting (cm^{-1})**
$[Ni(CH_3COO)_6]^{4-}$	8,544
$[Ni(H_2O)_6]^{2+}$	8,900
$[Ni(C_5H_5N)_6]^{2+}$	11,125

The rule of average environments[24,35] is subsequently invoked, which states that "when all ligands coordinate to a metal center in monodentate fashion, the ligand field splitting for a pseudo-octahedral mixed-ligand complex is obtained from a weighted average of the splittings calculated for each of the mono-ligand 6-coordinate complexes separately." Hence, group-contribution quantum-chemical empiricism is employed to predict the octahedral ligand field splitting for nickel acetate tetrahydrate, nickel acetate trihydrate coordinated to one pyridine sidegroup, and nickel acetate dihydrate coordinated to two pyridine sidegroups. The latter complex [i.e., $Ni(CH_3 \cdot COO)_2(H_2O)_2(C_5H_5N)_2$] represents a "coordination crosslink" where

nickel acetate forms metal-ligand σ-bonds with pyridine sidegroups on two different macromolecular chains. One estimates the pseudo-octahedral ligand field splitting Δ_0 for these three mixed-ligand complexes via the parameters in Table 5:

Ni^{2+} Complex	**Ligand Field Splitting (cm^{-1})**
$Ni(CH_3COO)_2(H_2O)_4$	8781
$Ni(CH_3COO)_2(H_2O)_3(C_5H_5N)$	9152
$Ni(CH_3COO)_2(H_2O)_2(C_5H_5N)_2$	9523

LFSEs are based on the electronic energy level separation between the t_{2g} and e_g metal-based molecular orbitals and the d-electron configuration of a transition metal complex. When metal d-electrons are influenced by the Coulombic ligand-field potential appropriate to an octahedral distribution of electron donors around the metal center,[24,35] the five metal d-orbitals split into a triply degenerate set of molecular orbitals, denoted by d_{xy}, d_{yz}, and d_{zx} with t_{2g} symmetry, that are at lower energy relative to the doubly degenerate pair denoted by $d_{x^2-y^2}$ and d_{z^2} with e_g symmetry. These molecular orbitals with e_g symmetry have lobes that are directed along the metal-ligand bond axis and are of the correct symmetry to participate in metal–ligand σ-bonding. The three degenerate orbitals with t_{2g} symmetry at lower energy have lobes that are directed to each side of the metal-ligand bond axis, and are of the correct symmetry to participate in metal–ligand π-bonds. The ground state electronic configuration of a d^8 octahedral complex is $\{t_{2g}\}^6\{e_g\}^2$, which does not depend on the strength of the ligand field or the ratio of the ligand field splitting Δ_0 to the Racah interelectronic repulsion energy. Quantum mechanical calculations based on zero-order perturbation theory allow one to determine the energies of the t_{2g} and e_g metal-based molecular orbitals. Relative to the five degenerate atomic d-orbitals of the free metal cation, the t_{2g} orbitals are $0.4\Delta_0$ lower in energy, and the e_g orbitals are $0.6\Delta_0$ higher in energy.[12,35] Hence the ligand field stabilization energy is 120% of Δ_0 when six metal d-electrons are spin-paired in the t_{2g} molecular orbitals and the remaining two unpaired electrons populate the e_g orbitals for an octahedral d^8 complex that does not distort to tetragonal or square-planar geometries. Since $1\,cm^{-1}$ (i.e., wavenumber) corresponds to 11.963 J/mol, calculations of the ligand field splittings given above yield an LFSE for $Ni(CH_3COO)_2 \cdot (H_2O)_2(C_5H_5N)_2$ that is 5.3 kJ/mol larger than the LFSE of $Ni(CH_3COO)_2(H_2O)_3 \cdot (C_5H_5N)$.

B. Coordination Crosslinks vs. Coordination Pendant Groups

Empirical quantum-chemical predictions summarized above from classic inorganic chemistry and ligand field theory are correlated with macroscopic enhancements in the glass-transition temperature for Ni(II) complexes with poly(4-vinylpyridine). The 102°C enhancement in T_g of P4VP occurs when the metal/pyridine-ligand concentration ratio is approximately 1:2 on a molar basis. It is postulated that thermal

synergy (i.e., the enhancement in T_g) is a consequence of coordination crosslinking where the nickel cation forms metal–ligand bonds with two pyridine nitrogen lone pairs on different macromolecular chains.[1] This coordination complex is modeled by $Ni(CH_3COO)_2(H_2O)_2(C_5H_5N)_2$ and the proposed molecular structure is illustrated in Figure 4, based on the following facts:

1. The crystal structure of undiluted nickel acetate tetrahydrate is pseudo-octahedral.[37,38]
2. Six-coordinate d^8 nickel complexes are strongly favored from an equilibrium viewpoint when good donor ligands such as pyridine are present,[39] even though the macromolecule–metal complex is completely amorphous.
3. Nickel(II) and pyridine are classified as a borderline acid–base pair, whereas lattice waters in the first shell of nickel acetate tetrahydrate are hard bases.
4. Stronger metal-ligand σ-bonding occurs when pyridines replace weak-base waters of hydration in the coordination sphere of Ni(II).
5. Coordination crosslinks were proposed, but not necessarily defined, by Agnew [40,41] in the 1970s for transition metal complexes of nickel(II) chloride with poly(4-vinylpyridine).

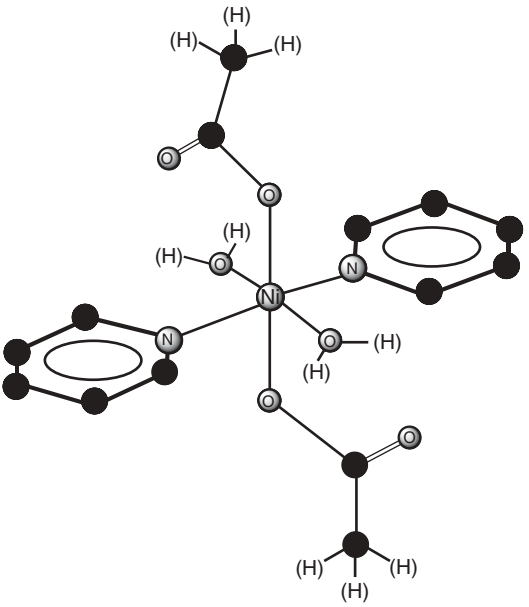

Figure 4 Molecular model of nickel acetate dihydrate coordinated to two pyridine sidegroups in P4VP illustrating the concept of *coordination crosslinks.* This model is adopted from the geometry of nickel acetate tetrahydrate, based on its crystal structure.[37,38] It is proposed that pyridine sidegroups in the polymer displace weak-base waters of hydration in the coordination sphere of the divalent nickel cation.

The onset of translational and rotational motion of the chain backbone in P4VP is severely restricted until enough thermal energy is supplied to dissociate one nickel-pyridine bond for each metal center that is coordinated to two pyridine ligands from different macromolecular chains and induce the glass–rubber transition. The structure of the proposed pseudo-octahedral model compound in the molten state is $Ni(CH_3COO)_2(H_2O)_3(C_5H_5N)$, because coordination of each metal center to one pyridine nitrogen lone pair only increases the size of the sidegroup in P4VP, similar to a para-substituent on the phenyl ring of polystyrene. It is interesting that a *t*-butyl [$-C(CH_3)_3$] sidegroup in the para-position of the styrene ring increases the glass-transition temperature of polystyrene[42,43] by approximately 30°C. This is comparable to the T_g enhancement of P4VP by nickel acetate for the "equimolar" complex, identified in Table 6 at a Ni^{2+} mole fraction of 0.528, where each nickel cation hypothetically coordinates to one pyridine ligand and the thermal synergy is ≈40°C. On an absolute basis, the thermal energy required to dissociate coordination crosslinks and induce the glass–rubber transition is estimated by $RT_{g,complex}$, where R is the gas constant and $T_{g,complex}$ is concentration dependent. Relative to the undiluted polymer or the polymer attached to a bulky nickel acetate trihydrate pendant group, the thermal energy required to remove one pyridine ligand from the coordination sphere of the nickel cation on a molar basis and disrupt coordination crosslinks is estimated by[1,9,11]

$$R\{T_{g,complex} - T_{g,undiluted\ polymer}\}$$

No effort is made to account for the concentration-dependent effect on the glass-transition temperature of P4VP due to nickel acetate trihydrate pendant groups coordinated to the lone pair of electrons on nitrogen in the pyridine ring. This "bulky sidegroup effect" becomes more important when the nickel concentration exceeds 33 mol% and approaches 50 mol%.

C. Ligand Field Model of the Glass Transition in Macromolecule–Metal Complexes

A simple coordination-interaction model is formulated that accounts for the disruption of coordination crosslinks and includes LFSEs for model complexes in the glassy and molten states. Both metal complexes have the same local symmetry (i.e., pseudo-octahedral) above and below the glass-transition temperature;

$$Ni(CH_3COO)_2(H_2O)_2(C_5H_5N)_2 + H_2O$$
$$\Rightarrow Ni(CH_3COO)_2(H_2O)_3(C_5H_5N) + C_5H_5N$$

The energetics of this ligand substitution scheme are endothermic because pyridine is a stronger base than water by approximately five orders of magnitude (see Table 4), and the metal complex on the left has an estimated LFSE that is 5.3 kJ/mol larger than that for the complex on the right of the above reaction (i.e., $\Delta(LFSE) = LFSE_{glass} - LFSE_{liquid} \approx 5.3$ kJ/mol). Free water and pyridine are included for completeness in the ligand exchange process, but they are excluded from energetic considerations. When

the disruption of metal–ligand bonds, instead of the stabilization of metal d-electrons, is correlated with T_g enhancement, the energetics of each species in the proposed ligand displacement reaction is considered. The endothermic nature of the ligand exchange process, illustrated above, is consistent with the facts that energy must be supplied to disrupt coordination crosslinks and that the glass-transition temperature of P4VP/Ni^{2+} complexes is enhanced relative to T_g of undiluted P4VP. The energy input required to remove a pyridine ligand from the coordination sphere of the nickel cation and achieve the rubbery state is comparable to the enhancement in T_g. Pyridine and P4VP are electronically similar when nickel(II) coordination to the nitrogen lone pair is considered, but there is a significant amount of steric hindrance due to the chain backbone that is not captured by pyridine when coordination occurs. The concentration dependence of the coordination interaction is adopted from the Flory-Huggins lattice theory[44] for nonideal mixing energetics of polymer/small-molecule blends with (1) $RT\chi$ replaced by Δ(LFSE) and (2) the polymer segment (i.e., volume) fraction replaced by the mole fraction of the repeat unit. The difference between the use of mole fraction vs. volume fraction for the concentration dependence of nonideal mixing energetics is equivalent to the difference between the Margules and van Laar models[45,46] for the excess free energy of mixing. In this respect, the proposed model matches the characteristics of the Margules formulation. Hence with the aid of ligand field stabilization, T_g enhancement via metal complexation is estimated from the following energetic equality

$$R\{T_{g,complex} - T_{g,undiluted\ polymer}\} = \beta[\Delta(LFSE)]\zeta(1-\zeta)$$

where ζ represents mole fraction. The empirical parameter β is included in the previous equation to account for at least three possible scenarios that have been overlooked by the simple energetic model:

1. Ligand field splitting calculations appropriate to small-molecule crystalline coordination complexes[34,35] have been adopted to predict stabilization energies for amorphous polymer/metal–salt blends. It is not possible for nickel acetate to coordinate to an amorphous polymer, like P4VP, with long-range crystallographic order and true octahedral symmetry. Distortions to tetragonal and square-planar geometries are not uncommon in d^8 complexes to lower the energy of the electronic configuration.[12] Hence β accounts for amorphous imperfections and the possibility that distortions to lower symmetry might occur.

2. When nickel coordinates to two pyridine ligands, there is no guarantee that these ligands reside on different macromolecular chains, producing effective crosslinks. Intramolecular loops form if both ligands originate from the same chain, and T_g should not increase much, if at all, due to ineffective crosslinks. Hence β accounts for the fraction of *effective inter*molecular coordination crosslinks.

3. Nickel acetate trihydrate pendant groups in the para-position of the pyridine ring could affect the glass transition temperature of P4VP. If this type of coordination occurs for nickel acetate concentrations below 35 mol%, then this effect is contained in the parameter β.

The linear least squares calculation of β is 0.7 for P4VP/Ni^{2+} complexes with pseudo-octahedral symmetry and Δ(LFSE) ≈ 5.3 kJ/mol. This suggests that the experimentally measured enhancement in T_g represents 70% of predictions based on the octahedral ligand field model. If nickel complexes with poly(4-vinylpyridine) exhibit tetrahedral coordination above and below T_g, then the electronic configuration of eight metal d-electrons in the molecular orbitals of the complex[12] is $\{e\}^4\{t_2\}^4$, tetrahedral ligand field splittings are 4/9 as large as the corresponding octahedral ligand field splittings,[12,35] LFSE for the electronic configuration $\{e\}^4\{t_2\}^4$ is 80% of the tetrahedral ligand field splitting,[12] and Δ(LFSE) is 2.4 kJ/mol for the disruption of coordination crosslinks without a reduction in local symmetry[1] above T_g. If tetrahedral parameters for nickel acetate coordinated to either one or two pyridine ligands are employed in the energetic model of T_g enhancement, then the linear least squares calculation[1] of β is 1.6 to generate agreement between prediction and experimental glass-transition temperature data. This is physically unrealistic because crystal field coordination parameters should not *underestimate* bonding in the amorphous phase by approximately 60%.

D. Linear Least Squares Analysis of Δ(LFSE) via the Concentration Dependence of T_g in P4VP/Ni^{2+} Complexes, Subject to the Constraint that $\beta \leq 1$

In light of the glass-transition data for nickel acetate tetrahydrate and P4VP (Table 6), linear least squares analysis of the energetic ligand field model of T_g enhancement provides insight about the required magnitude of the ligand field stabilization energy parameter [i.e., Δ(LFSE)] for macromolecule–metal complexes of arbitrary geometry. Begin by constructing the square of the difference between the actual T_g enhancement data in Table 6 and predictions using the energetic expression on the previous page that includes Δ(LFSE). Using the first five data points in Table 6, one obtains:

$$\text{Minimization function} = \sum_{i=1}^{5} \{R(\Delta T_g)_i - \beta[\Delta(\text{LFSE})]\zeta_i(1-\zeta_i)\}^2$$

Since the maximum glass-transition temperature of P4VP occurs at a nickel acetate mole fraction of ≈0.36, whereas the Margules concentration dependence of T_g in the ligand field model is symmetric and predicts maximum enhancement at $\zeta = 0.50$, the optimum value of β in the previous equation was based on the first five data points in Table 6. Optimization proceeds as follows:

$$\frac{d}{d\beta}(\text{Minimization function}) =$$

$$-2\sum_{i=1}^{5} \{R(\Delta T_g)_i - \beta[\Delta(\text{LFSE})]\zeta_i(1-\zeta_i)\}\,[\Delta(\text{LFSE})]\zeta_i(1-\zeta_i) = 0$$

$$\sum_{i=1}^{5} \{R(\Delta T_g)_i - \beta[\Delta(\text{LFSE})]\zeta_i(1-\zeta_i)\}\zeta_i(1-\zeta_i) = 0$$

When ligand field stabilization energies for glassy and molten state complexes are predicted using the methodologies described in this chapter, one calculates the best value of β to match experimental data.

$$\beta = \frac{\sum_{i=1}^{5} R(\Delta T_g)_i \zeta_i (1-\zeta_i)}{\Delta(\mathrm{LFSE}) \sum_{i=1}^{5} \{\zeta_i (1-\zeta_i)\}^2}$$

As mentioned above, it seems reasonable that β should not exceed unity if crystal field coordination parameters do not *underestimate* metal–ligand bonding in the amorphous phase. This restriction on β allows one to identify the minimum value of Δ(LFSE) for complexes with arbitrary geometry and coordination number. Based solely on experimental data and the proposed concentration dependence of glass transition temperature enhancement,

$$\Delta(\mathrm{LFSE}) \geq \frac{\sum_{i=1}^{5} R(\Delta T_g)_i \zeta_i (1-\zeta_i)}{\sum_{i=1}^{5} \{\zeta_i (1-\zeta_i)\}^2}$$

T_g enhancement data for nickel acetate complexes with P4VP require that ligand field stabilization energy differences above and below T_g, Δ(LFSE), must be greater than 3.8 kJ/mol for physically realistic predictions via the energetic ligand field model. This linear least squares analysis precludes tetrahedral coordination of Ni^{2+} to pyridine sidegroups in P4VP, where Δ(LFSE) was predicted to be 2.4 kJ/mol.

V. d⁶ MOLYBDENUM CARBONYL COMPLEXES WITH POLY(VINYLAMINE) THAT EXHIBIT REDUCED SYMMETRY ABOVE THE GLASS-TRANSITION TEMPERATURE

A. Experimental Results

Chromium ($3d^6$), molybdenum ($4d^6$), and tungsten ($5d^6$) hexacarbonyls form coordination complexes[47–49] with acrylonitrile and poly(acrylonitrile), PAN. The nitrogen lone pair in the acrylonitrile sidegroup (i.e., –C≡N:) displaces a carbonyl ligand[47] and occupies an octahedral site in the coordination sphere of the transition metal. $Metal(C{\equiv}O)_5(CH_2CHC{\equiv}N:)$ and $Metal(C{\equiv}O)_4(CH_2CHC{\equiv}N:)_2$ have been prepared[47] from the corresponding acetonitrile complexes, $Metal(C{\equiv}O)_5(CH_3C{\equiv}N:)$ and $Metal(C{\equiv}O)_4(CH_3C{\equiv}N:)_2$. Formation of these acetonitrile complexes from zero-valent coordinatively saturated d^6 hexacarbonyls was accelerated photochemically (i.e., to eject carbon monoxide ligands) because displacement of C≡O by acetonitrile proceeds via a dissociative mechanism where the intermediate complex

is five-coordinate. In light of these results, the analysis below focuses on poly(vinylamine), PVAm, complexes with d^6 molybdenum hexacarbonyl to stimulate experimental investigations of these materials that have not been prepared in the laboratory to date. If two C≡O ligands are displaced from the coordination sphere of molybdenum and the metal bridges amino sidegroups on two different PVAm chains via the lone pair on nitrogen, then $Mo(C{\equiv}O)_4(PVAm)_2$ represents a coordinatively crosslinked pseudo-octahedral complex with considerably less mobility than the undiluted polymer. This glassy structure is postulated below T_g, and it is analyzed via ligand field models that exhibit reduced symmetry in the molten state.

B. Ligand Field Splitting Parameters for Molybdenum Hexacarbonyl

Low-spin d^6 octahedral complexes of molybdenum exhibit ligand field stabilization energies that are 240% of the corresponding octahedral ligand field splitting.[12] The strong-field nature of heavy-metal centers from the second row of the d-block and π-acceptor carbonyl ligands at the top of the spectrochemical series force all six metal d-electrons to populate the lower energy triply degenerate t_{2g} molecular orbitals in complexes with local octahedral symmetry. The experimental ligand field splitting for molybdenum hexacarbonyl[50,51] is 32,150 cm^{-1}. This data point allows one to bracket an acceptable range of Jørgensen's g-factor for molybdenum in the zero-valent oxidation state, because[34,35]

$$f_{C\equiv O} g_{Mo^{(0)}} = 32.150$$

with units of 10^3 wavenumbers, based on quantum-chemical group contribution estimates of the octahedral ligand field splitting when all six monodentate ligands are identical. Since C≡O is the strongest π-acceptor in the spectrochemical series of ligands, its f-factor must be larger than that for cyanide anions, CN^-, which has a value of 1.7, as listed in Table 5. Hence, the g-factor for $Mo^{(0)}$ is

$$g_{Mo^{(0)}} = \frac{32.150}{f_{C\equiv O}} < 18.9$$

Further consideration of the octahedral ligand field splitting for manganese hexacarbonyl in the +1 oxidation state[50,51] (i.e., $\Delta_0 = 41{,}650\ cm^{-1}$) and Jørgensen's g-factors for Mn^{2+}, Mn^{3+}, and Mn^{4+} (i.e., 8.5, 21, 23, respectively; Table 5) allow one to estimate the f-factor for C≡O between 5 and 8. The g-factor for Mn^{1+} must be less than 8.5, yielding a reasonable estimate of the g-factor for $Mo^{(0)}$ between 4 and 6.5 to reproduce experimental ligand field splittings for $Mo(C{\equiv}O)_6$ and $\{Mn(C{\equiv}O)_6\}^{1+}$. These estimates of ligand field splitting parameters (i.e., f- and g-factors), not included in Jørgensen's database, are consistent with the fact that Δ_0 is smaller when the metal center is in a lower oxidation state and the effective nuclear charge experienced by the ligands (i.e., +Ze) is smaller.

C. Ligand Field Stabilization for Complexes of Molybdenum Hexacarbonyl and Poly(vinylamine) in the Glassy State

Six metal d-electrons in zero-valent molybdenum complexes with local octahedral symmetry adopt a strong-field electronic configuration given by $\{t_{2g}\}^6$. This corresponds to an energetic stabilization[12,35] of $2.4\Delta_0$ because each t_{2g} metal-based molecular orbital is stabilized by $0.4\Delta_0$ relative to the five degenerate d-atomic orbitals of $Mo^{(0)}$. Methylamine, with an f-factor of 1.17 (Table 5), is employed in model calculations as a "small-molecule" analog of the polymer that provides a reasonable estimate of electronic interactions between $Mo^{(0)}$ and poly(vinylamine), but it cannot capture the true steric hindrance imposed by the chain backbone when coordination occurs. Hence one should not replace the polymer by methylamine and expect to interpret T_g enhancement via an entropic model, because entropy, steric hindrance, and the number of amino sidegroups that occupy sites in the first-shell coordination sphere of $Mo^{(0)}$ are strongly coupled. The following complexes are of interest when poly(vinylamine) displaces carbonyl ligands, possibly with photochemical assistance, in the coordination sphere of molybdenum; $Mo(C{\equiv}O)_x(CH_3NH_2)_{6-x}$, where $x \geq 4$. Based on the rule of average environments discussed above,[24,35] the LFSE for pseudo-octahedral complexes with x C≡O ligands and $(6-x)$ methylamine ligands is

$$\mathrm{LFSE}(T < T_g) = 2.4 g_{Mo^{(0)}} \left\{ \frac{x}{6} f_{C\equiv O} + \left[1 - \frac{x}{6} \right] f_{CH_3NH_2} \right\} (11.96) \frac{\mathrm{kJ}}{\mathrm{mol}}$$

D. Quantum Mechanical Model Parameters and Trigonal Bipyramid 5-Coordinate d⁶ Complexes of Molybdenum Hexacarbonyl and Poly(vinylamine) with D_{3h} Symmetry Above T_g

Models are required to estimate the relative energies of the five d-orbitals in the molten state before ligand field stabilizations can be calculated for 5-coordinate complexes. These energies are expressed in terms of the parameters Dq and Cp,[34] where 10 Dq represents the corresponding octahedral ligand field splitting Δ_0. In terms of atomic parameters for octahedral complexes where six point charges, each one of magnitude $-ze$, are placed a distance L from the metal center with effective nuclear charge $+Ze$, Dq and Cp are defined as follows:[34]

$$\mathrm{Dq} = \frac{Zze^2\langle r^4 \rangle}{6L^5} \qquad \frac{7\ \mathrm{Cp}}{12\ \mathrm{Dq}} = \frac{L^2\langle r^2 \rangle}{\langle r^4 \rangle}$$

In these expressions, $\langle \mathrm{r}^n \rangle$ represents the average (i.e., expectation value) of r^n with respect to the radial part of the d-electron wavefunctions, r is the radius of the electron cloud about the metal center, and L is the metal–ligand bond distance. There are five 3d-orbital wavefunctions, and each one exhibits a different spherical harmonic expression in terms of polar angle θ and azimuthal angle φ in spherical coordinates.

However, the radial part of each 3d-orbital wavefunction ρ (r) is the same, as given by[12]

$$\rho(r) = \frac{1}{9\sqrt{30}}\left(\frac{Z}{a_0}\right)^{3/2}\left[\frac{2Zr}{3a_0}\right]^2 \exp\left\{-\frac{Zr}{3a_0}\right\}$$

where $a_0 = 0.529$ Å is the Bohr radius and Z represents the atomic number. The second and fourth moments (i.e., expectation values) of the radial part of the 3d-orbital wavefunctions are defined by

$$\langle r^n \rangle = \frac{\int_{r=0}^{\infty} r^n \{\rho(r)\}^2 r^2 dr}{\int_{r=0}^{\infty} \{\rho(r)\}^2 r^2 dr}$$

with $n = 2,4$. Hence, $\langle r^n \rangle$ increases (i.e., $n > 0$) when the d-electron cloud experiences more delocalization due to the ligands as a consequence of the nephelauxetic effect. A similar conclusion is based on the radial part of the 4d-orbital wavefunctions. The following d-orbital energy levels are available for trigonal bipyramid complexes[34] when 7 Cp/12 Dq = 1:

d-orbital	**Energy (Dq)**
z^2	+6.21
xy	+0.035
$x^2 - y^2$	+0.035
xz	−3.14
yz	−3.14

When six metal d-electrons populate these orbitals, z^2 at highest energy remains vacant because the energy difference between z^2 and xz or yz is greater than 93% of the corresponding octahedral ligand field splitting, which should exceed the pairing energy that characterizes interelectronic repulsion. Hence pairing occurs in xz and yz, while z^2 is unoccupied. This is reasonable for heavy metals like Mo with π-acceptor carbonyl ligands and large Δ_0 that produce a strong-field electronic configuration given by:

$[d^6]$: $\{xz\}^2\{yz\}^2\{xy\}^1\{x^2 - y^2\}^1$ D_{3h} symmetry w/ 7 Cp/12 Dq = 1

Stabilization of the metal d-electrons is predicted to be, LFSE ≈ $1.25\Delta_0$.

The following d-orbital energy levels are available for trigonal bipyramid complexes[34] when 7 Cp/12 Dq = 2, corresponding to less d-electron delocalization by the surrounding ligands.

d-orbital	**Energy (Dq)**
z^2	+7.07
xy	−0.82
$x^2 - y^2$	−0.82
xz	−2.72
yz	−2.72

When six metal d-electrons populate these orbitals, z^2 at highest energy remains vacant because the energy difference between z^2 and xz or yz is greater than 97% of the corresponding octahedral ligand field splitting. Once again, spin-pairing occurs in xz and yz, while z^2 is unoccupied. The strong-field electronic configuration is

$$[d^6]: \quad \{xz\}^2\{yz\}^2\{xy\}^1\{x^2-y^2\}^1 \qquad D_{3h} \text{ symmetry w/ } 7\,Cp/12\,Dq = 2$$

which also corresponds to a stability factor given by LFSE $\approx 1.25\Delta_0$.

E. Square Pyramid 5-Coordinate d⁶ Complexes of Molybdenum Hexacarbonyl and Poly(vinylamine) with C_{4v} Symmetry Above T_g

The methodology of identifying the d-electron configuration and LFSE in the previous section is repeated here for complexes with square pyramid geometry. Now there could be ambiguity in the order that six metal d-electrons populate the molecular orbitals of the complex. Low-spin and high-spin configurations are considered. The following d-orbital energy levels are available[34] when 7 Cp/12 Dq = 1:

d-orbital	Energy (Dq)
x^2-y^2	+7.43
z^2	+2.57
xy	−2.57
xz	−3.715
yz	−3.715

The x^2-y^2 d-orbital at highest energy remains vacant because the energy difference between x^2-y^2 and xz or yz is greater than 110% of the corresponding octahedral ligand field splitting. Hence electrons are spin paired in xz and yz. The energy difference between z^2 and xy is 51% of Δ_0, so z^2 and xy each contain one electron for a high-spin configuration, whereas z^2 is vacant at low-spin. The low-spin electronic configuration is given by:

$$\text{low-spin } [d^6]: \quad \{xz\}^2\{yz\}^2\{xy\}^2 \; C_{4v} \text{ symmetry w/ } 7\,Cp/12\,Dq = 1$$

with LFSE $= 2.0\Delta_0$ If the electronic configuration is high-spin with x^2-y^2 vacant, then one obtains

$$\text{high-spin } [d^6]: \quad \{xz\}^2\{yz\}^2\{xy\}^1\{z^2\}^1 \qquad C_{4v} \text{ symmetry w/ } 7\,Cp/12\,Dq = 1$$

This corresponds to LFSE $= 1.49\Delta_0$.

d-Orbital energy levels are provided below for square pyramid complexes[34] when 7 Cp/12 Dq = 2, which corresponds to less electron delocalization by the surrounding ligands such that the fourth moment of the radial part of the d-electron wavefunctions decreases more rapidly than the second moment.

d-orbital	Energy (Dq)
$x^2 - y^2$	+9.14
z^2	+0.86
xy	−0.86
xz	−4.57
yz	−4.57

Now, the $x^2 - y^2$ d-orbital at highest energy undoubtedly remains vacant because the energy difference between $x^2 - y^2$ and xz or yz is greater than 137% of the corresponding octahedral ligand field splitting. The energy difference between z^2 and xy is less than 20% of Δ_0, so each of these d-orbitals should contain one electron. Hence the electronic configuration is

$$[d^6]: \quad \{xz\}^2\{yz\}^2\{xy\}^1\{z^2\}^1 \quad C_{4v} \text{ symmetry w/ } 7\,Cp/12\,Dq = 2$$

with LFSE = $1.83\Delta_0$.

F. Pentagonal Planar 5-Coordinate d^6 Complexes of Molybdenum Hexacarbonyl and Poly(vinylamine) with D_{5h} Symmetry Above T_g

The third possible 5-coordinate geometry in the molten state is pentagonal planar, and the d-orbital energy levels are provided below[34] when 7 Cp/12 Dq = 1.

d-orbital	Energy (Dq)
$x^2 - y^2$	+4.825
xy	+4.825
z^2	−1.07
xz	−4.29
yz	−4.29

The energy difference between xy or $x^2 - y^2$ and xz or yz is slightly greater than 90% of the corresponding octahedral ligand field splitting, so spin-pairing in xz and yz is considered. Since xy or $x^2 - y^2$ and z^2 are separated by ≈59% of Δ_0, spin-pairing in z^2 is considered, also. The strong-field d-electron configuration is

$$\text{low-spin } [d^6]: \quad \{xz\}^2\{yz\}^2\{z^2\}^2 \quad D_{5h} \text{ symmetry w/ } 7\,Cp/12\,Dq = 1$$

with LFSE = $1.93\Delta_0$.

d-Orbital energy levels are summarized below for pentagonal planar complexes[34] when 7 Cp/12 Dq = 2;

d-orbital	Energy (Dq)
$x^2 - y^2$	+9.10
xy	+9.10
z^2	−5.35
xz	−6.42
yz	−6.42

Once again, spin-pairing should occur in *yz*, *xz*, and z^2. The highest energy d-orbitals (i.e., $x^2 - y^2$ and *xy*) remain vacant because they are $\approx 1.55\Delta_0$ above the lowest energy d-orbitals. Most important, they are $\approx 1.45\Delta_0$ above z^2. The strong-field configuration is

$$\text{low-spin } [d^6]: \quad \{xz\}^2\{yz\}^2\{z^2\}^2 \qquad D_{5h} \text{ symmetry w/ } 7\,Cp/12\,Dq = 2$$

and the largest LFSE of all possible scenarios discussed above is $3.64\Delta_0$.

G. Ligand Field Stabilization of 5-Coordinate d^6 Complexes of Molybdenum Hexacarbonyl and Poly(vinylamine) Above T_g

When sufficient thermal energy is supplied to dissociate at least one metal–nitrogen chemical bond in the glassy complex $Mo(C{\equiv}O)_4(CH_3NH_2)_2$, this coordinatively saturated crosslinked structure reverts to a 5-coordinate complex above the glass-transition temperature. The ligand dissociation reaction is

$$Mo(C{\equiv}O)_4\,(CH_3NH_2)_2 \Rightarrow Mo(C{\equiv}O)_4\,(CH_3NH_2) + CH_3NH_2$$

Force field calculations favor a square pyramid geometry in the molten state, where the lone remaining amino ligand could occupy a site in the equatorial plane or at the apical position of the square pyramid. In either case, the rule of average environments[24,35] is invoked to predict 10 Dq for the 5-coordinate complex above T_g, $Mo(C{\equiv}O)_4(CH_3NH_2)$.

$$\Delta_0 = 10\ \text{Dq} = g_{Mo^{(0)}}\left\{\frac{x}{5}f_{C\equiv O} + \left[1 - \frac{x}{5}\right]f_{CH_3NH_2}\right\}(11.96)\,\frac{\text{kJ}}{\text{mol}}$$

where $x = 4$. The previous three sections summarized d-electron configurations and LFSEs for 5-coordinate heavy-metal d^6 complexes with D_{3h}, C_{4v}, and D_{5h} symmetry. In each case, LFSE is expressed in terms of Dq, and Jørgensen's quantum-chemical group contribution method of estimating this parameter for mixed-ligand complexes is useful. Even though force field calculations favor a square pyramid geometry in the molten state after one amino functional group in the sidechain of poly(vinylamine) is removed from the first shell of molybdenum, LFSE is estimated by considering all possible 5-coordinate geometries and d^6 electronic configurations described above. Equal weighting factors for complexes with different symmetry and spin state are employed to calculate an average LFSE above the glass-transition temperature, as summarized in Table 7.

Table 7 LFSEs for 5-Coordinate d^6 Complexes in the Molten State

5-coordinate geometry	d^6 electronic structure	7 Cp/12 Dq	LFSE
D_{3h}, trigonal bipyramid	$\{xz\}^2\,\{yz\}^2\,\{xy\}^1\,\{x^2-y^2\}^1$	1	$1.25\Delta_0$
D_{3h}, trigonal bipyramid	$\{xz\}^2\,\{yz\}^2\,\{xy\}^1\,\{x^2-y^2\}^1$	2	$1.25\Delta_0$
C_{4v}, square pyramid	low-spin; $\{xz\}^2\,\{yz\}^2\,\{xy\}^2$	1	$2.00\Delta_0$
C_{4v}, square pyramid	high-spin; $\{xz\}^2\,\{yz\}^2\,\{xy\}^1\,\{z^2\}^1$	1	$1.49\Delta_0$
C_{4v}, square pyramid	high-spin; $\{xz\}^2\,\{yz\}^2\,\{xy\}^1\,\{z^2\}^1$	2	$1.83\Delta_0$
D_{5h}, pentagonal planar	low-spin; $\{xz\}^2\,\{yz\}^2\,\{z^2\}^2$	1	$1.93\Delta_0$
D_{5h}, pentagonal planar	low-spin; $\{xz\}^2\,\{yz\}^2\,\{z^2\}^2$	2	$3.64\Delta_0$
		Average LFSE($T > T_g$)	$1.9\Delta_0$

The difference between ligand field stabilization energies above and below the glass-transition temperature, in which coordinatively unsaturated molten state complexes exhibit reduced symmetry relative to 6-coordinate complexes in the glassy state, is calculated as follows:

$$\begin{aligned}\Delta(\mathrm{LFSE}) &= \mathrm{LFSE}(T < T_g) - \mathrm{LFSE}(T > T_g) \\ &= g_{Mo^{(0)}}\left[2.4\left\{\frac{x}{6}f_{C\equiv 0} + \left(1 - \frac{x}{6}\right)f_{CH_3NH_2}\right\}\right. \\ &\quad \left. - 1.9\left\{\frac{x}{5}f_{C\equiv 0} + \left(1 - \frac{x}{5}\right)f_{CH_3NH_2}\right\}\right](11.96)\,\frac{\mathrm{kJ}}{\mathrm{mol}}\end{aligned}$$

with $x = 4$ when zero-valent heavy-metal centers, such as $Mo^{(0)}$ coordinate to four C≡O ligands and two amino sidegroups in poly(vinylamine) below the glass-transition temperature. One predicts that Δ(LFSE) ≈ 58 kJ/mol when the g-factor of $Mo^{(0)}$ is ≈5, and the f-factors for C≡O and CH_3NH_2 are ≈6 and 1.17, respectively. Hence the difference between LFSEs above and below T_g for molybdenum hexacarbonyl complexes with poly(vinylamine) is predicted to be an order of magnitude larger than Δ(LFSE) ≈5.3 kJ/mol for pseudo-octahedral nickel acetate complexes with poly(4-vinylpyridine). Since the stabilization of metal d-electrons for $Mo(C{\equiv}O)_4(CH_3NH_2)_2$ is significantly larger than $Mo(C{\equiv}O)_4(CH_3NH_2)$, this should translate into dramatic enhancements in the glass-transition temperature of heavy-metal carbonyl complexes with amorphous polymers that contain strongly basic functional sidegroups, but experimental data are not available for $Mo(C{\equiv}O)_6$ and poly(vinylamine) to verify these predictions. Experimental results described below for ruthenium carbonyl complexes with either poly(4-vinylpyridine) or poly(L-histidine) are consistent with the proposed ligand field stabilization models with reduced symmetry above the glass-transition temperature.

VI. COBALT, NICKEL, AND RUTHENIUM COMPLEXES WITH POLY(4-VINYLPYRIDINE) AND POLY(L-HISTIDINE) THAT EXHIBIT REDUCED SYMMETRY IN THE MOLTEN STATE

A. Polymeric Coordination Complexes with d-Block Salts

Unlike the well-known phenomenon of plasticization,[6] transition metal salts typically increase the glass-transition temperature of polymers that contain attractive ligands in the sidegroup.[11] A plausible mechanism discussed previously in this chapter involves acid–base interactions between the metal center and appropriate functional groups in the polymer via ligand exchange. Whereas plasticizers interact

weakly with the polymer via van der Waals forces and enhance the fractional free volume of the binary mixture,[7] metal-ligand σ-bonds form between transition metals and favorable functional groups in the macromolecule. Since coordination numbers between four and six are most common in d-block complexes,[39] as summarized in Table 2, opportunities exist for basic ligands in the sidegroup of the polymer to occupy sites in the first-shell coordination sphere of an acidic metal center. The concept of coordination crosslinks is realized when functional groups from more than one chain occupy sites in the first-shell of a single metal center.[1] This type of structure exhibits reduced mobility in the vicinity of these thermoreversible crosslinks, which is consistent with an increase in the glass transition temperature. Multifunctional metal centers that coordinate to basic ligands in several different chains[3] could be responsible for the formation of nanoclusters with significant reduction in chain mobility and dramatic increases in T_g. This has been observed recently in polymeric complexes with several lanthanide trichloride hydrates from lanthanum to lutetium in the first-row of the f-block,[4,5] but ligand field splitting energies of lanthanide complexes (i.e., $\approx 100\,cm^{-1} \approx 1.2\,kJ/mol$)[52] are much too small to provide the dominant contribution to T_g enhancement. In addition to exhibiting increased glass transition temperatures, macromolecule-metal complexes could form gels during preparation in dilute solution.[4,53,54] When gelation occurs in aqueous media, applications for water purification, drug release and artificial muscles become attractive.[55] If gels are sensitive to variations in pH, temperature, or electric field strength, then it might be possible to exploit these molecular gates and use them for controlled release of encapsulated molecules with a specific target. Of particular interest in this chapter, the methodology for producing and analyzing macromolecule-metal complexes with significantly enhanced glass-transition temperatures is under investigation from an energetic viewpoint that considers the stabilization of metal d-electrons[1,9]. A systematic study of T_g enhancement in poly(4-vinylpyridine) and poly(L-histidine) via ruthenium(II), cobalt(II), and nickel(II) is employed to extend the methodology outlined above for molybdenum hexacarbonyl complexes with poly(vinylamine) and to compare predictions with experimental data. Poly(4-vinylpyridine) and poly(L-histidine) contain nitrogen lone pairs in either the pyridine sidegroup[9,10] or the imidazole ring of the histidine sidegroup[18] that form σ-bonds with appropriate d-orbitals of the transition metal cation. Ruthenium(II), cobalt(II), and nickel(II) enhance the glass-transition temperatures of these polymers (Figs. 5 and 6). Following the same theme from previous sections of this chapter, transition metal induced enhancements of T_g in selected amorphous polymers are correlated with LFSE differences between complexes in the glassy and molten states. The ligand field model outlined above for molybdenum hexacarbonyl complexes with poly(vinylamine) considers a reduction in symmetry and a decrease in coordination number of the metal center in the molten state above T_g, due to dissociation of a ligand in the polymer's sidegroup from the first-shell coordination sphere. Since the glassy state is described by complexes with local tetrahedral or octahedral symmetry, geometric distortions of 3-coordinate and 5-coordinate polymer–metal complexes in the molten state are considered in the analyses below.

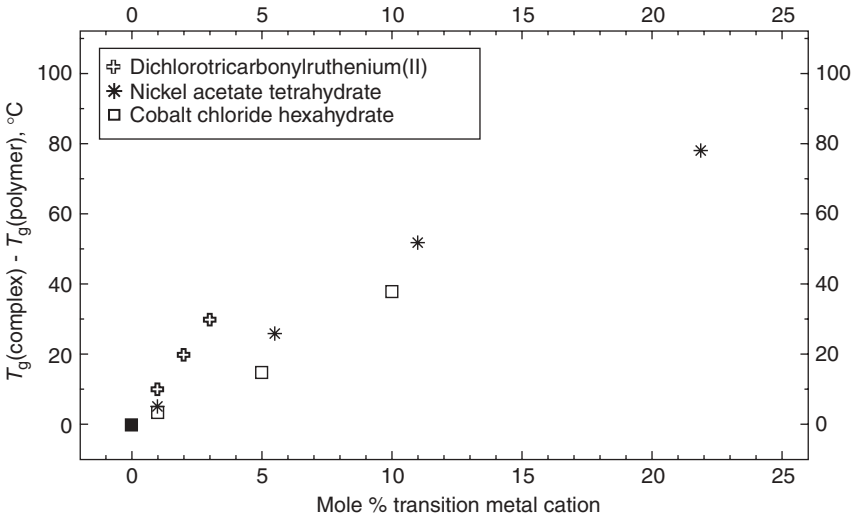

Figure 5 Effect of cobalt chloride hexahydrate, nickel acetate tetrahydrate, and dichlorotricarbonylruthenium(II) on the glass-transition temperature of poly(4-vinylpyridine). The polymer's molecular weight is 2×10^5 daltons.

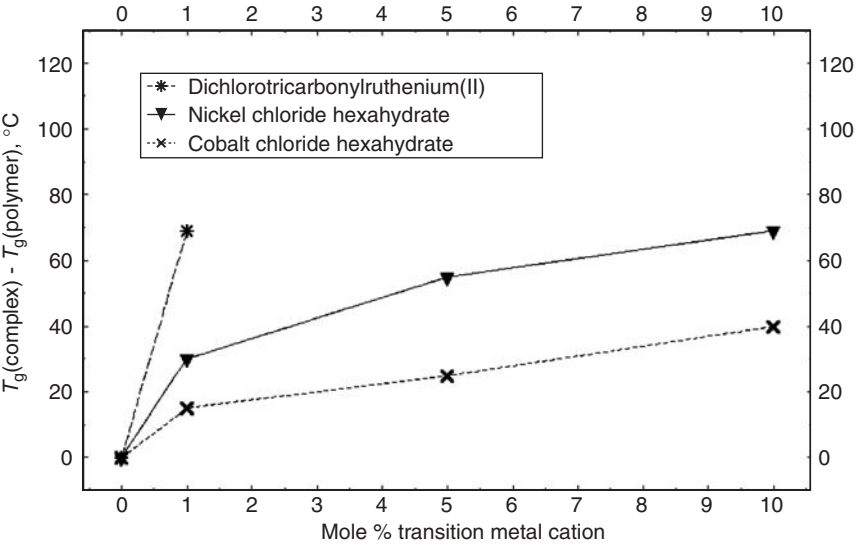

Figure 6 Effect of $CoCl_2(H_2O)_6$, $NiCl_2(H_2O)_6$, and $\{RuCl_2(CO)_3\}_2$ on the glass-transition temperature of poly(L-histidine). The polymer's molecular weight is $1.5–5.0 \times 10^4$ daltons.

B. Ruthenium d^6 Complexes

Ruthenium(II) is an attractive d-block metal cation for T_g enhancement because strong-field low-spin d^6 metal centers with pseudo-octahedral symmetry exhibit large ligand field splittings and stabilization energies.[12] Ru^{2+} is classified as a borderline acid[26,27] which exhibits an affinity for borderline bases, like pyridine ligands in the sidegroup of poly(4-vinylpyridine). Reactions of a particular ruthenium dimer (i.e., $\{RuCl_2(C{\equiv}O)_3\}_2$) with both stoichiometric and excess amounts of pyridine are well documented.[25,33,56] In both cases, the dichloride bridge is cleaved and either one or two pyridine ligands coordinate to each metal center forming complexes with pseudo-octahedral symmetry. The first pyridine ligand occupies the vacant site generated from cleavage of the dichloride bridge. The second pyridine ligand displaces carbon monoxide in the coordination sphere of the metal.[25] Vibrational spectroscopic studies of $[RuCl_2(C{\equiv}O)_3]_2$ in the vicinity of 1900–2200 cm^{-1} fingerprint the infrared absorptions of C≡O that are sensitive to σ-donation and π back-donation.[25,57,58] Electron-rich metal centers backbond to π-acceptor ligands like C≡O and shift the vibrational absorption frequencies of carbon monoxide to lower energy.[12] This process is described by the Dewar-Chatt model of chemical bonding in transition metal complexes,[12] where metal-based t_{2g} molecular orbitals in systems with local octahedral symmetry donate electron density to the antibonding π* orbitals of carbon monoxide. These antibonding orbitals have larger amplitude on the less electronegative atom of C≡O, and this carbon atom participates in σ-bonding with the metal center. Hence the orbital energy levels are similar, proximity is satisfied, and the wave functions of interest have the correct symmetry for t_{2g}-π* molecular orbital overlap to achieve metal-to-ligand flow of electron density into the antibonding orbital of C≡O that weakens its infrared (i.e., triple-bond) stretching frequency.[12] Solid-state carbon-13 NMR spectroscopic data reveal that heteronuclear spin diffusion between ^1H in poly(4-vinylpyridine) and the carbonyl ^{13}C nuclei of $[RuCl_2(C{\equiv}O)_3]_2$ is operative.[9,11] This observation of intermolecular polarization transfer, after the establishment of a magnetization gradient, is consistent with molecular dispersion at the nanoscale level (i.e., dipolar distances between ^1H and ^{13}C that correspond to tenths of a nanometer, or a few angstroms) and subsequent complexation of two dissimilar components.

C. Cobalt d^7 Complexes

Cobalt chloride hexahydrate was used to generate transition metal complexes with amino, pyridine and imidazole ligands in the sidegroup of poly(vinylamine),[3,29] poly(4-vinylpyridine),[9,11] and poly(L-histidine),[18] respectively. Two independent x-ray crystallographic studies[59,60] have deduced a pseudo-octahedral geometry for $CoCl_2 \cdot (H_2O)_6$, with two chloride anions and four equatorial lattice waters in the first-shell coordination sphere of Co^{2+}. The two remaining waters of hydration are free, but they reside near the apical chlorides and form hydrogen bonds with these anions.[61] Several 6-coordinate Co^{2+} complexes with multiple nitrogen-containing ligands have been prepared and characterized.[30–32] These coordination compounds support the concept that multiple

ligands in the sidegroup of nitrogen-containing polymers could displace lattice waters and occupy sites in the coordination sphere of Co^{2+}, which is a borderline acid.[26,27]

D. Nickel d^8 Complexes

Nickel(II) complexes are useful to induce synergistic T_g response in amorphous polymers with nitrogen-containing ligands in the sidegroup. The hexahydrates of nickel chloride and cobalt chloride adopt the same coordination number and ligand arrangement.[62] Nickel acetate tetrahydrate exhibits a pseudo-octahedral geometry in the solid state with four equatorial lattice waters and two apical monodentate acetate ligands.[37,38] In the most favorable situation, pseudo-octahedral Ni^{2+} forms metal-ligand σ-bonds with nitrogen lone pairs in two different macromolecular chains. Six-coordinate d^8 nickel complexes are strongly favored from an equilibrium viewpoint when good donor ligands are present.[39] Five-coordinate square pyramid and trigonal bipyramid complexes, and 4-coordinate tetrahedral and square planar complexes are also common.[39] Physically realistic mechanisms by which nickel acetate tetrahydrate and nickel chloride hexahydrate enhance the glass-transition temperatures of poly(4-vinylpyridine)[1,9,11] and poly(L-histidine),[18] respectively, are discussed below.

E. d-Orbital Energies for Five-Coordinate Complexes above T_g

i. Trigonal Bipyramid d^n Complexes with D_{3h} Symmetry

Electronic energies relative to the five degenerate d-orbitals of the free metal ion, d^n configurations (i.e., $n = 6,7,8$), and ligand field stabilization energies are summarized in Table 8 for trigonal bipyramid complexes when Cp/Dq is either 1.71 or 3.43.[34] If each d-orbital contains one electron, then the total electronic energy is exactly the same as that for the free metal ion, and there is no net stabilization due to the ligand field. One arrives at the same conclusion for d^{10} complexes that contain divalent zinc, because each d-orbital contains a pair of electrons with opposite spin. Stabilization is prevalent when there is a larger population of electrons in lower energy orbitals. In a weak ligand field, electrons occupy vacant orbitals whenever possible, instead of pairing with opposite spin in lower energy orbitals. This produces less ligand field stabilization. In a strong ligand field, it is more probable that two electrons with opposite spin will be paired at lower energy, instead of occupying vacant higher energy orbitals. In general, larger ligand field stabilization energies are possible in a strong ligand field. The z^2 orbital in trigonal bipyramid complexes with 6, 7 or 8 metal d-electrons remains vacant in a strong ligand field because the energy difference between z^2 and xz or yz is 93% (i.e., Cp/Dq = 1.71) to 97% (i.e., Cp/Dq = 3.43) of the octahedral ligand field splitting. Electronic configurations of d^6, d^7, and d^8 complexes are provided in Table 8 for weak and strong ligand fields. Once Dq is measured or predicted, the information in Table 8 is useful to estimate the energetic stabilization of metal d-electrons for coordinatively unsaturated trigonal bipyramid complexes in the molten state.

Table 8 Electronic Energy Calculations for 5-Coordinate Trigonal Bipyramid Complexes with D_{3h} Symmetry[34]

d-Orbital energies (units of Dq)

7 Cp/12 Dq	d_{xz}	d_{yz}	d_{xy}	$d_{x^2-y^2}$	d_{z^2}
1	−3.14	−3.14	+0.035	+0.035	+6.21
2	−2.72	−2.72	−0.815	−0.815	+7.07

d-electron configurations and ligand field stabilization energies

# of d-Electrons	7 Cp/12 Dq	Ligand Field Strength	d-Electron Configuration	LFSE (Dq)
6	1	weak	$\{xz\}^2\ \{yz\}^1\ \{xy\}^1\ \{x^2-y^2\}^1\ \{z^2\}^1$	3.14
6	2	weak	$\{xz\}^2\ \{yz\}^1\ \{xy\}^1\ \{x^2-y^2\}^1\ \{z^2\}^1$	2.72
6	1	strong	$\{xz\}^2\ \{yz\}^2\ \{xy\}^1\ \{x^2-y^2\}^1$	12.51
6	2	strong	$\{xz\}^2\ \{yz\}^2\ \{xy\}^1\ \{x^2-y^2\}^1$	12.51
7	1	weak	$\{xz\}^2\ \{yz\}^2\ \{xy\}^1\ \{x^2-y^2\}^1\ \{z^2\}^1$	6.28
7	2	weak	$\{xz\}^2\ \{yz\}^2\ \{xy\}^1\ \{x^2-y^2\}^1\ \{z^2\}^1$	5.44
7	1	strong	$\{xz\}^2\ \{yz\}^2\ \{xy\}^2\ \{x^2-y^2\}^1$	12.46
7	2	strong	$\{xz\}^2\ \{yz\}^2\ \{xy\}^2\ \{x^2-y^2\}^1$	13.33
8	1	weak	$\{xz\}^2\ \{yz\}^2\ \{xy\}^2\ \{x^2-y^2\}^1\ \{z^2\}^1$	6.25
8	2	weak	$\{xz\}^2\ \{yz\}^2\ \{xy\}^2\ \{x^2-y^2\}^1\ \{z^2\}^1$	6.26
8	1	strong	$\{xz\}^2\ \{yz\}^2\ \{xy\}^2\ \{x^2-y^2\}^2$	12.42
8	2	strong	$\{xz\}^2\ \{yz\}^2\ \{xy\}^2\ \{x^2-y^2\}^2$	14.14

ii. Square Pyramid d^n Complexes with C_{4v} Symmetry

When all bond angles are 90°, energies of the five d-orbitals for square pyramid complexes[34] are summarized in Table 9, where an energy of zero is assigned to the degenerate orbitals of the free metal ion. The x^2-y^2 d-orbital remains vacant for all complexes that contain eight electrons or less, when the ligand field is strong. For d^6 complexes with 7 Cp/12 Dq = 1 in a strong ligand field, z^2 is vacant because the energy difference between z^2 and xy is more than 51% of the octahedral ligand field splitting. The d-electron configurations in Table 9 consider 5-coordinate complexes with 6, 7 or 8 metal d-electrons. LFSE predictions in the far right column of the table are useful for analyzing molten state complexes with reduced symmetry.

iii. Pentagonal Planar d^n Complexes with D_{5h} Symmetry

These 5-coordinate complexes exhibit d-orbital energies[34] summarized in Table 10. In the presence of a strong ligand field, d^6 complexes do not populate xy or x^2-y^2. There is no difference between weak field and strong field d^8 complexes because the two orbitals at highest energy are degenerate. LFSE predictions for these 5-coordinate complexes are summarized in the far right column of Table 10.

Table 9 Electronic Energy Calculations for 5-Coordinate Square Pyramid Complexes with C_{4v} Symmetry[34]

d-Orbital Energies (units of Dq)

7 Cp/12 Dq	d_{xz}	d_{yz}	d_{xy}	d_{z^2}	$d_{x^2-y^2}$
1	−3.715	−3.715	−2.57	+2.57	+7.43
2	−4.57	−4.57	−0.86	+0.86	+9.14

d-Electron Configurations and Ligand Field Stabilization Energies

Number of d-Electrons	7 Cp/12 Dq	Ligand Field Strength	d-Electron Configuration	LFSE (Dq)
6	1	weak	$\{xz\}^2\ \{yz\}^1\ \{xy\}^1\ \{z^2\}^1\ \{x^2-y^2\}^1$	3.72
6	2	weak	$\{xz\}^2\ \{yz\}^1\ \{xy\}^1\ \{z^2\}^1\ \{x^2-y^2\}^1$	4.57
6	1	strong	$\{xz\}^2\ \{yz\}^2\ \{xy\}^2$	20.00
6	2	strong	$\{xz\}^2\ \{yz\}^2\ \{xy\}^1\ \{z^2\}^1$	18.28
7	1	weak	$\{xz\}^2\ \{yz\}^2\ \{xy\}^1\ \{z^2\}^1\ \{x^2-y^2\}^1$	7.43
7	2	weak	$\{xz\}^2\ \{yz\}^2\ \{xy\}^1\ \{z^2\}^1\ \{x^2-y^2\}^1$	9.14
7	1	strong	$\{xz\}^2\ \{yz\}^2\ \{xy\}^2\ \{z^2\}^1$	17.43
7	2	strong	$\{xz\}^2\ \{yz\}^2\ \{xy\}^2\ \{z^2\}^1$	19.14
8	1	weak	$\{xz\}^2\ \{yz\}^2\ \{xy\}^2\ \{z^2\}^1\ \{x^2-y^2\}^1$	10.00
8	2	weak	$\{xz\}^2\ \{yz\}^2\ \{xy\}^2\ \{z^2\}^1\ \{x^2-y^2\}^1$	10.00
8	1	strong	$\{xz\}^2\ \{yz\}^2\ \{xy\}^2\ \{z^2\}^2$	14.86
8	2	strong	$\{xz\}^2\ \{yz\}^2\ \{xy\}^2\ \{z^2\}^2$	18.28

Table 10 Electronic Energy Calculations for 5-Coordinate Pentagonal Planar Complexes with D_{5h} Symmetry[34]

d-Orbital Energies (units of Dq)

7 Cp/12 Dq	d_{xz}	d_{yz}	d_{z^2}	d_{xy}	$d_{x^2-y^2}$
1	−4.29	−4.29	−1.07	+4.825	+4.825
2	−6.42	−6.42	−5.35	+9.10	+9.10

d-electron configurations and ligand field stabilization energies

Number of d-Electrons	7 Cp/12 Dq	Ligand Field Strength	d-Electron Configuration	LFSE (Dq)
6	1	weak	$\{xz\}^2\ \{yz\}^1\ \{z^2\}^1\ \{xy\}^1\ \{x^2-y^2\}^1$	4.29
6	2	weak	$\{xz\}^2\ \{yz\}^1\ \{z^2\}^1\ \{xy\}^1\ \{x^2-y^2\}^1$	6.42
6	1	strong	$\{xz\}^2\ \{yz\}^2\ \{z^2\}^2$	19.30
6	2	strong	$\{xz\}^2\ \{yz\}^2\ \{z^2\}^2$	36.38
7	1	weak	$\{xz\}^2\ \{yz\}^2\ \{z^2\}^1\ \{xy\}^1\ \{x^2-y^2\}^1$	8.58
7	2	weak	$\{xz\}^2\ \{yz\}^2\ \{z^2\}^1\ \{xy\}^1\ \{x^2-y^2\}^1$	12.84
7	1	strong	$\{xz\}^2\ \{yz\}^2\ \{z^2\}^2\ \{xy\}^1$	14.48
7	2	strong	$\{xz\}^2\ \{yz\}^2\ \{z^2\}^2\ \{xy\}^1$	27.28
8	1	weak,strong	$\{xz\}^2\ \{yz\}^2\ \{z^2\}^2\ \{xy\}^1\ \{x^2-y^2\}^1$	9.65
8	2	weak,strong	$\{xz\}^2\ \{yz\}^2\ \{z^2\}^2\ \{xy\}^1\ \{x^2-y^2\}^1$	18.19

F. Summary of LFSE Calculations for 5-Coordinate d^n Complexes

Ligand field stabilization energies for all possible 5-coordinate geometries of a d^n complex in either weak or strong fields are averaged with equal weighting factors. These results are summarized in Table 11. For d^6, d^7, and d^8 complexes, the dependence of LFSE on the number of d-electrons follows opposite trends for weak and strong ligand fields. In other words, LFSE increases from d^6 to d^8 for weak-field configurations, whereas LFSE decreases from d^6 to d^8 for strong-field configurations. All calculations are presented in units of Dq, where the corresponding octahedral ligand field splitting is given by 10Dq. Parametric estimates of Dq are summarized in the following section for pseudo-octahedral mixed ligand complexes with two polymeric ligands in the glassy state, and 5-coordinate mixed ligand complexes with one polymeric ligand in the molten state, above the glass transition temperature.

Table 11 Averaged Ligand Field Stabilization Energies for 5-Coordinate d^n-Complexes

Number of d-electrons	Ligand Field Strength	LFSE (Dq)
d^6	weak	4.14
d^6	strong	19.83
d^7	weak	8.29
d^7	strong	17.35
d^8	weak	10.06
d^8	strong	14.59

G. Stabilization of Metal d-Electrons in Mixed-Ligand Complexes

The following generic ligand dissociation reaction is proposed to analyze the onset of T_g in macromolecule-metal complexes with enhanced glass-transition temperatures relative to the undiluted polymers:

$$M^{2+}(L_A)_2\,(L_B)_2\,(L_C)_2 \Rightarrow M^{2+}(L_A)_2\,(L_B)_2\,L_C + L_C$$

where M^{2+} is either Ru^{2+}, Co^{2+} or Ni^{2+}; L_A is either Cl^- or CH_3COO^-; L_B is either H_2O or C≡O; and L_C is the nitrogen lone pair in the sidegroup of either poly(4-vinylpyridine) or poly(L-histidine). Reactive blending in dilute solution places two sidegroups from these polar polymers in the coordination sphere of a single metal center. After solvent evaporation, 6-coordinate glassy complexes are modeled via the structure on the left side of the previous dissociation reaction. LFSEs, based on the information in Table 11 and Table 13, are computed in Table 12 for the appropriate 6-coordinate and 5-coordinate complexes with 6, 7, or 8 d-electrons that simulate the glassy and molten states. Bold numbers with asterisks in the far right column of Table 12 identify the most probable LFSE, based on strength of the ligand field and the number of d-electrons.

Table 12 Ligand Field Stabilization Energies for Macromolecule–Metal Complexes above (i.e., 5-coordinate) and below (i.e., 6-coordinate) the Glass-Transition Temperature

	10 Dq (kJ/mol)	Ligand field strength	LFSE (kJ/mol)
d^6 complexes			
$RuCl_2(CO)_2[P4VP]_2$	640	weak	4 Dq = 256
		strong	24 Dq = **1536***
$RuCl_2(CO)_2[P4VP]$	709	weak	4.14 Dq = 294
		strong	19.83 Dq = **1406***
$RuCl_2(CO)_2[PHIS]_2$	647	weak	4 Dq = 259
		strong	24 Dq = **1553***
$RuCl_2(CO)_2[PHIS]$	713	weak	4.14 Dq = 295
		strong	19.83 Dq = **1414***
d^7 complexes			
$CoCl_2(H_2O)_2[P4VP]_2$	111	weak	8 Dq = **88.9***
		strong	18 Dq = 200
$CoCl_2(H_2O)_2[P4VP]$	106	weak	8.29 Dq = **88.0***
		strong	17.35 Dq = 184
$CoCl_2(H_2O)_2[PHIS]_2$	114	weak	8 Dq = **91.3***
		strong	18 Dq = 205
$CoCl_2(H_2O)_2[PHIS]$	108	weak	8.29 Dq = **89.4***
		strong	17.35 Dq = 187
d^8 complexes			
$Ni(CH_3COO)_2(H_2O)_2[P4VP]_2$	112	weak	12 Dq = **134***
		strong	12 Dq = 134
$Ni(CH_3COO)_2(H_2O)_2[P4VP]$	108	weak	10.06 Dq = **109***
		strong	14.59 Dq = 158
$NiCl_2(H_2O)_2[PHIS]_2$	109	weak	12 Dq = **131***
		strong	12 Dq = 131
$NiCl_2(H_2O)_2[PHIS]$	103	weak	10.06 Dq = **104***
		strong	14.59 Dq = 150

The rule of average environments[24,35] was invoked to calculate 10 Dq for mixed ligand complexes that are 6-coordinate below T_g and 5-coordinate above T_g. The averaging was performed as follows. For 6-coordinate complexes with three different types of ligands, denoted by $M^{2+}(L_A)_2(L_B)_2(L_C)_2$, one predicts 10 Dq (kJ/mol) via Jørgensen's parameters:[24,34,35]

$$\{10\ \mathrm{Dq}\}_{6-\mathrm{coordinate}} = \frac{11.963}{6} g_{M^{2+}}\{2f(L_A) + 2f(L_B) + 2f(L_C)\}$$

For 5-coordinate complexes with three different types of ligands, denoted by $M^{2+}(L_A)_2(L_B)_2(L_C)$, Jørgensen's prediction of 10 Dq (kJ/mol) is[24,34,35]

$$\{10\ \mathrm{Dq}\}_{5-\mathrm{coordinate}} = \frac{11.963}{5} g_{M^{2+}}\{2f(L_A) + 2f(L_B) + f(L_C)\}$$

where anionic, neutral, and polymeric ligands are denoted by L_A, L_B, and L_C, respectively. An average Jørgensen f-factor of 6.0 was employed for C≡O in $\{RuCl_2(C{\equiv}O)_3\}_2$, which is consistent with the fact that C≡O is the strongest

π-acceptor in the spectrochemical series.[12,35] The f-factor for imidazole in poly(L-histidine) was determined from an empirical correlation between Brønsted ionization equilibrium constants[12,28] (i.e., $pK_B = 14 - pK_A$) and Jørgensen's f-factors[24,34,35] for three anionic ligands (i.e., Br^-, Cl^-, CN^-) and two neutral ligands (i.e., H_2O and C_5H_5N). f-Factors and pK_As for these five ligands are included in Tables 4 and 5. The following third-order polynomial was used to match these five data pairs for f vs. pK_B with a correlation coefficient better than 0.999, and estimate the Jørgensen f-factor for six monodentate imidazole ligands, which is within the range of the dataset.

$$f = 2.61 - 2.51 \times 10^{-1} pK_B + 1.31 \times 10^{-2} pK_B^2 - 2.52 \times 10^{-4} pK_B^3$$

Agreement between this empirical correlation and the five data points for three anionic and two neutral ligands, mentioned above, is shown in Figure 7. Since the Brønsted ionization equilibrium constant for the imidazole ring[63] in histidine is $pK_B = 8.0$, the Jørgensen f-factor for imidazole is estimated to be 1.32.

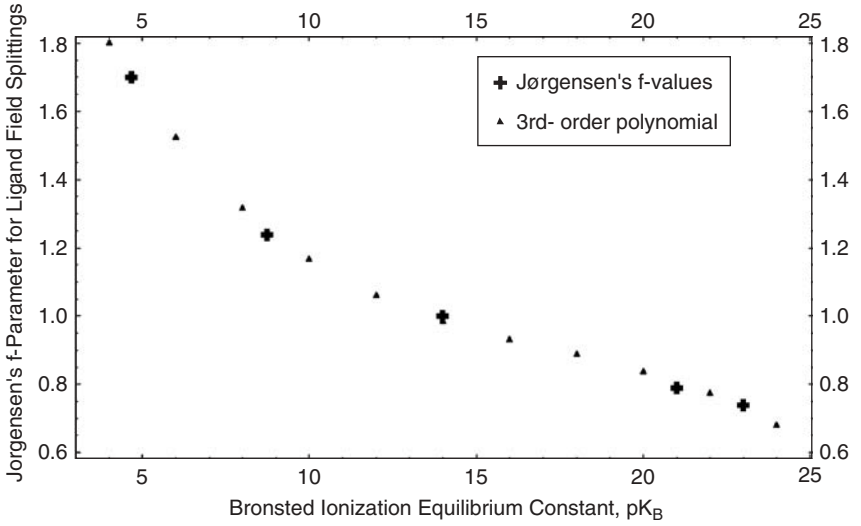

Figure 7 Empirical correlation between Jørgensen f-factors for prediction of octahedral ligand field splittings and Brønsted ionization equilibrium constants (i.e., pK_B) in aqueous solution at 25°C.

H. Consideration of Interelectronic Repulsion and Δ_0 When There is Ambiguity in the d-Electron Configuration for Complexes with Pseudo-Octahedral Symmetry

There is ambiguity in the electronic configuration for d^6 and d^7 octahedral complexes, due to the strength of the ligand field. Table 13 summarizes information

Table 13 Racah Interelectronic Repulsion Energies for Free Metal Cations, Weak- /Strong-Field Crossover Energies, d-Electron Configurations and LFSEs for Pseudo-Octahedral d^n Complexes[a]

	B_0 (cm^{-1})	$\{\Delta_0/B\}$	d-Electron Configuration	LFSE (Dq)
d^6 complexes				
Ru^{2+}	620	<20	$\{t_{2g}\}^4\{e_g\}^2$	4
		>20	$\{t_{2g}\}^6$	24
d^7 complexes				
Co^{2+}	1120	<22	$\{t_{2g}\}^5\{e_g\}^2$	8
		>22	$\{t_{2g}\}^6\{e_g\}^1$	18
d^8 complexes				
Ni^{2+}	1080	—	$\{t_{2g}\}^6\{e_g\}^2$	12

[a] *xy*, *yz*, and *xz* d-orbitals (denoted by t_{2g}) are degenerate at -4 Dq; z^2 and x^2-y^2 d-orbitals (denoted by e_g) are degenerate at $+6$ Dq

about d-orbital energies; B_0 for Ru^{2+}, Co^{2+}, and Ni^{2+}; crossover (i.e., electron pairing) energies for weak and strong ligand fields in terms of $\{\Delta_0/B\}_{\text{critical;}}$ weak-field and strong-field electronic configurations; and the corresponding LFSEs for d^6, d^7, and d^8 complexes with local octahedral symmetry. For Ru^{2+} in the second row of the d-block, the large g-factor (i.e., 20), the extremely large f-factor for C≡O, and the small value of B_0 ($620\,cm^{-1}$)[24,35] suggest that strong field electronic configurations are most probable for these heavy metal d^6 complexes because Δ_0/B is invariably greater than the weak-field/strong-field crossover[12,24] at $\{\Delta_0/B\}_{\text{critical}} \approx 20$. Hence spin pairing occurs in d_{xy}, d_{yz}, and d_{xz}, whereas the z^2 and x^2-y^2 d-orbitals are vacant, corresponding to LFSE = 24 Dq. For Co^{2+} in the first row of the d-block, a much smaller g-factor (i.e., ≈9.2) and a large value of B_0 (i.e., $1120\,cm^{-1}$),[24,35] with no carbonyl ligands, argue in favor of weak-field electronic configurations with Δ_0/B less than the crossover[12,24] at 22. Now, the higher energy d-orbitals (i.e., z^2 and x^2-y^2) contain one electron each, and LFSE is 8 Dq. There is no ambiguity in electronic configuration for d^8 Ni^{2+} complexes with local octahedral symmetry. However, ligand field strength, or Δ_0/B, influences the electronic configuration for 5-coordinate d^8 complexes. Since B_0 and Jørgensen's g-factor for Ni^{2+} are similar to those for Co^{2+} (see Table 5), and no carbonyl ligands occupy sites in the first-shell of Ni^{2+} for the complexes of interest in this chapter, it is reasonable to adopt weak-field electronic configurations for $Ni(CH_3COO)_2(H_2O)_2$[P4VP] and $NiCl_2(H_2O)_2$[PHIS] in the molten state.

I. Correlation Between T_g Enhancement and the Difference Between Ligand Field Stabilization Energies in the Glassy and Molten States

LFSEs are calculated in Table 12 for macromolecule–metal complexes in the glassy and molten states. Based on consideration of interelectronic repulsion in the previous section, asterisks and bold face type in Table 12 identify the most probable LFSEs for 5- and 6-coordinate complexes of Ru^{2+} (strong field), Co^{2+} (weak field), and Ni^{2+} (weak field). When the appropriate ligand field strength is considered in

Table 12, LFSEs are larger for glassy 6-coordinate complexes than they are for 5-coordinate complexes above T_g. More stabilization of metal d-electrons due to geometry and the surrounding ligands in the glassy state is consistent with the fact that these complexes exhibit thermochemical synergy with respect to T_g, upon removal of one ligand in the polymer's sidegroup from the first-shell coordination sphere of the metal center. This is analogous to the fact that larger LFSEs for $\{M(H_2O)_6\}^{2+}$ yield more exothermic hydration enthalpies relative to linear trends from Ca^{2+} to Mn^{2+} to Zn^{2+} for divalent hexa–aqua metal complexes from the first row of the d-block[12,24] (Fig. 3). Furthermore, when one lattice water is removed from these hexa–aqua complexes, the *logarithm* of the kinetic rate constant for this process, or the free energy of activation from the 6-coordinate complex to the transition state, is correlated[34] empirically with the difference between LFSEs (i.e., units of Dq) of octahedral ML_6 and square pyramidal ML_5, without any geometric perturbations of the 5-coordinate complex. In this discussion of T_g enhancement, Dq is estimated for 5- and 6-coordinate mixed-ligand complexes above and below the glass-transition temperature. Then the difference between LFSEs (i.e., ΔLFSE, units of kJ/mol) in the glassy and molten states is correlated with the increase in T_g for poly(4-vinylpyridine) and poly(L-histidine) complexes that contain 1 mol% Ru^{2+}, Co^{2+}, and Ni^{2+}. These results are presented in Figure 8.

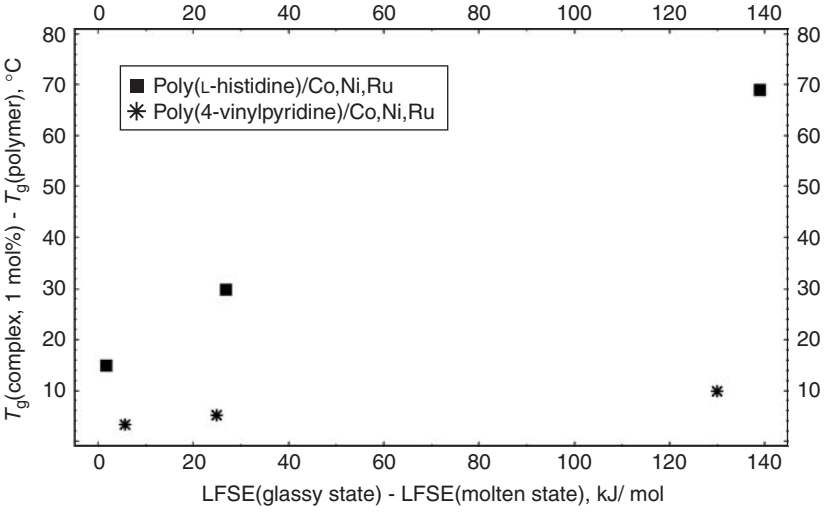

Figure 8 Correlation between T_g enhancement at 1 mol% metal cation and differences between LFSE in the glassy and molten states for Co^{2+}, Ni^{2+}, and Ru^{2+} complexes with poly(4-vinylpyridine) and poly(L-histidine).

The reduction in chain mobility and the increase in T_g is more pronounced when the first trace of metal cation is present. There is further enhancement of T_g at higher concentrations of metal cations, but the relative increase in T_g is not as significant as the initial effect. Most T_g-composition behavior, experimental or theoretical, is nonlinear. Ligand field analysis is correlated with the initial slope of T_g vs. composition,

in the range from 0 to 1 mol% metal cation. Without adjustable parameters that might account for differences in complexation efficiency between pyridine and imidazole, it is not possible to generate a universal correlation for T_g enhancement, based on the six complexes that were analyzed in this section. Nevertheless, a priori calculations of this nature, together with a reasonable model for the onset of T_g, are useful to identify macromolecule–metal complexes that exhibit thermochemical synergy.

J. Tetrahedral Co^{2+} Complexes Below T_g and 3-Coordinate Complexes in the Molten State

An alternate viewpoint of macromolecule–metal complexes with Co^{2+} is presented, in this section, when two ligands in the sidegroup of the polymer occupy sites in the first-shell coordination sphere of the metal center below T_g. $CoCl_2(H_2O)_6$ is pink and the anhydrous salt is blue.[59,61] Cobalt chloride adopts a tetrahedral geometry in ethanol with a characteristic blue color.[61] X-ray diffraction data on dark blue crystals of dichlorobis(4-vinylpyridine)cobalt(II) suggest that the structure of this 4-coordinate pseudo-tetrahedral complex contains two 4-vinylpyridine ligands and no waters of hydration.[64–66] These studies are significant because they demonstrate that the borderline acid Co^{2+} sheds its four hard-base lattice waters in favor of two borderline-base pyridine ligands. Tetrahedral symmetry of the metal center is a common occurrence for d^7 Co^{2+} complexes.[39] If geometric perturbations occur during preparation of complexes with poly(4-vinylpyridine) in ethanol, then octahedral $CoCl_2(H_2O)_6$ might revert to tetrahedral coordination with two pyridine ligands and two anionic chloride ligands. If this 4-coordinate structure persists in the glassy state, then the onset of T_g might occur when one pyridine ligand in the sidegroup of the polymer is removed from the coordination sphere of Co^{2+} due to the addition of thermal energy. Now the coordinatively unsaturated molten state complex above T_g is 3-coordinate, and the possibilities range from facial trivacant (i.e., nonplanar), where all bond angles are 90°, to trigonal planar, where all bond angles are 120° (Table 1). The following scheme represents a model for the glass-transition process in Co^{2+} complexes with poly(4-vinylpyridine) that have been prepared from ethanol:

$$CoCl_2(P4VP)_2 \Rightarrow CoCl_2(P4VP) + P4VP$$

Stabilization energies for metal d-electrons above and below T_g, based on this ligand dissociation reaction are presented in Table 14. Weak-field electronic configurations are favored for 4-coordinate and 3-coordinate d^7 metal complexes from the first-row of the d-block, with no carbonyl ligands. One predicts that LFSE for 4-coordinate tetrahedral Co^{2+} complexes with poly(4-vinylpyridine) below T_g is larger than LFSE for the corresponding 3-coordinate complex in the molten state by 5.8 kJ/mol. Since these complexes were prepared in ethanol, the horizontal coordinate [i.e., Δ(LFSE)] of the empirical correlation for P4VP/Co^{2+} complexes in Figure 8 was changed from 0.9 kJ/mol (Table 12) to 5.8 kJ/mol (Table 14). Previous analysis[9,11] of P4VP/Co^{2+} complexes that were assumed to be pseudo-tetrahedral above and below T_g yielded LFSEs which are 3.7 kJ/mol larger in the glassy state [i.e., $CoCl_2(P4VP)_2$] relative to the molten state [i.e., $CoCl_2(P4VP)(H_2O)$].

Table 14 Electronic Energy Calculations for 3-Coordinate (i.e., C_{3v} & D_{3h}) and 4-Coordinate (i.e., T_d) d^7 Co^{2+} Complexes[34]

d-Orbital energies (Dq) for facial trivacant complexes with C_{3v} symmetry (all bond angles are 90°)

7 Cp/12 Dq	d_{xz}	d_{yz}	d_{xy}	$d_{x^2-y^2}$	d_{z^2}
1,2	−2.00	−2.00	−2.00	+3.00	+3.00

d-Orbital energies (Dq) for trigonal planar complexes with D_{3h} symmetry

7 Cp/12 Dq	d_{xz}	d_{yz}	d_{z^2}	d_{xy}	$d_{x^2-y^2}$
1	−2.57	−2.57	−0.65	+2.895	+2.895
2	−3.85	−3.85	−3.21	+5.46	+5.46

d-Orbital energies (Dq) for tetrahedral complexes with T_d symmetry

7 Cp/12 Dq	$d_{x^2-y^2}$	d_{z^2}	d_{xy}	d_{yz}	d_{xz}
1,2	−2.67	−2.67	+1.78	+1.78	+1.78

LFSEs for 3- and 4-coordinate d^7 complexes

Symmetry	7 Cp/12 Dq	Ligand Field Strength	d-Electron Configuration	LFSE (Dq)
C_{3v}	1,2	weak	$\{xz\}^2\{yz\}^2\{xy\}^1\{x^2-y^2\}^1\{z^2\}^1$	4.00
D_{3h}	1	weak	$\{xz\}^2\{yz\}^2\{z^2\}^1\{xy\}^1\{x^2-y^2\}^1$	5.14
D_{3h}	2	weak	$\{xz\}^2\{yz\}^2\{z^2\}^1\{xy\}^1\{x^2-y^2\}^1$	7.69
			Average LFSE for 3-coordinate complexes	*5.21*
T_d	1,2	weak	$\{x^2-y^2\}^2\ \{z^2\}^2\ \{xy\}^1\ \{yz\}^1\ \{xz\}^1$	5.34

d^7 Complexes	State	10 Dq (kJ/mol)	LFSE (kJ/mol)
$CoCl_2$[P4VP]$_2$	glass	111.7	5.34 Dq = 59.7
$CoCl_2$[P4VP]	molten	103.5	5.21 Dq = 53.9
$CoCl_2$[PHIS]$_2$	glass	116.1	5.34 Dq = 62.0
$CoCl_2$[PHIS]	molten	106.4	5.21 Dq = 55.4

Predictions for Co^{2+} complexes with poly(L-histidine), based on the ligand dissociation reaction in this section, reveal that LFSE for pseudo-tetrahedral complexes in the glassy state is 6.6 kJ/mol larger than that for 3-coordinate complexes in the molten state. However, these poly(L-histidine)/metal complexes were prepared in aqueous solution[18] and lattice waters should be retained in the glassy state structure. Pseudo-octahedral glassy complexes that revert to 5-coordinate complexes via the onset of T_g represent a better model, so Δ(LFSE) of 1.9 kJ/mol from Table 12 is employed on the horizontal axis of Figure 8 for poly(L-histidine)/Co^{2+} instead of 6.6 kJ/mol calculated in Table 14.

VII. TOTAL ENERGETIC REQUIREMENTS TO INDUCE THE GLASS TRANSITION VIA CONSIDERATION OF THE FIRST-SHELL COORDINATION SPHERE IN TRANSITION METAL AND LANTHANIDE COMPLEXES

A. Density Functional Estimates of Metal–Ligand Bond Dissociation Energies

Instead of focusing on the strength of one metal–ligand bond and the corresponding LFSE that represents only a small fraction of the total bond energy, modifications in the glass-transition temperature can be correlated with the difference between the total energetics of all reactants and products in a proposed ligand dissociation scheme. Molecular engineering design focuses on all of the metal–ligand bonds that involve basic functional groups in the polymer, because these weak links determine whether the material can withstand larger forces before failure occurs and higher temperatures before viscous flow or thermal degradation. Density functional methods[67–69] are useful to simulate the energetics of the glass-transition process. Even though most schemes in this chapter focus on the dissociation of one metal–ligand chemical bond, the energetics of all reactants and products consider molecular orbital overlap that is sensitive to coordination number and geometry of the complex. A plausible strategy is described below for zero-valent d^6 transition metal hexacarbonyl complexes [i.e., $M(C{\equiv}O)_6$] with poly(vinylamine), where amino sidegroups in the polymer displace C≡O in the first-shell coordination sphere of the metal via assistance from UV radiation.[47] Heating these hybrid organic–inorganic materials above the glass-transition temperature dissociates metal/polymer–ligand σ-bonds and produces coordinatively unsaturated complexes of lower symmetry in the molten state.

Initially, one estimates the first C≡O single bond dissociation energy for transition-metal hexacarbonyls $M(C{\equiv}O)_6$ with true octahedral symmetry. Since all of the ligands are equivalent, there is no difference between removing equatorial vs. apical ligands, as there is with 5-coordinate square pyramid complexes. One C≡O ligand can be removed from a hexacarbonyl complex by restricting one of the metal–carbon bond distances to be ≈10 Å. The total electronic energy of the original hexacarbonyl complex is compared with that of the distorted complex in which the stretched metal–carbon bond length is ≈10 Å. The difference between the total electronic energy of the original and distorted complexes is the first metal–carbon single bond dissociation energy. Since these calculations force the 5-coordinate (i.e., distorted) complex to be square pyramidal, it should be instructive to compare the total electronic energies of the complexes in 1, 3, and 4 below to establish the best methodology for quantitative predictions of the first metal-C≡O single bond dissociation energy:

1. $M(C{\equiv}O)_6$ vs. square pyramid $M(C{\equiv}O)_5$ with one C≡O ligand occupying the sixth octahedral site at M-C≡O single bond distances of 8, 10, and 12 Å.
2. Square pyramid vs. trigonal bipyramid $M(C{\equiv}O)_5$, for application in 3 and 4, below.

3. $M(C{\equiv}O)_6$ vs. square pyramid $M(C{\equiv}O)_5$ and $C{\equiv}O$, where the energies of $M(C{\equiv}O)_5$ and $C{\equiv}O$ are calculated separately.
4. $M(C{\equiv}O)_6$ vs. trigonal bipyramid $M(C{\equiv}O)_5$ and $C{\equiv}O$, where the energies of $M(C{\equiv}O)_5$ and $C{\equiv}O$ are calculated separately.

Results from 1, 3, and 4 above should be compared with experimental $C{\equiv}O$ single bond dissociation energies for zero-valent d^6 metal hexacarbonyls [i.e., $M(C{\equiv}O)_6$].

Zero-Valent d^6 Hexacarbonyl	**First $C{\equiv}O$ Bond Dissociation Energy**[69]
$Cr(C{\equiv}O)_6$	162 kJ/mol
$Mo(C{\equiv}O)_6$	126 kJ/mol
$W(C{\equiv}O)_6$	166 kJ/mol

The method of choice that provides the best match with experimental data is employed in the following section.

B. The Energetics of Ligand Dissociation Reactions in Model Systems; Comparison with Experimental T_g Enhancements for d-Block and f-Block Complexes

Energy-minimized conformations from molecular mechanics are useful to estimate the energetics of metal–ligand bond dissociation. A plausible thermal dissociation reaction for generic zero-valent metal carbonyl complexes that corresponds to the onset of the glass transition is

$$M(C{\equiv}O)_4\,[\text{Polymer}]_2 \Rightarrow M(C{\equiv}O)_4\,[\text{Polymer}] + \text{Polymer}$$

The complex on the left side of the previous reaction simulates coordination crosslinks, where ligands in the sidegroup of the polymer occupy apical or equatorial sites in the first shell, and the complex on the right side represents a coordination pendant group. Typical models for the polymer in the previous dissociation reaction are as follows

Polymer	**Model compounds**
poly(vinylamine), PVAm	methyl amine, CH_3NH_2
poly(4-vinylpyridine), P4VP	pyridine, C_5H_5N
poly(L-histidine), PHIS	imidazole, $C_3H_4N_2$

These model compounds provide reasonable estimates of the ligands' electronic characteristics, as required for an energetic description of the glass-transition process. At the present time, any connection between the density functional calculations summarized above and experimental T_g-enhancement data is empirical. It is necessary to establish a quantitative link between the formation of mobility-restricting nanoclusters in the coordination sphere of the metal center and the efficiency of T_g enhancement, where the latter is summarized in Table 15 for several polymer/metal–complex combinations.

Table 15 Enhancement in T_g (°C) per mol% Metal Cation (0–1 mol%) for Several Macromolecule–Metal Complexes[a]

d-block complexes	P4VP	PVAm	PHIS	PLYS
$Mg(CH_3COO)_2(H_2O)_4$	0			
$Ca(CH_3COO)_2(H_2O)$	0			
$Ni(CH_3COO)_2(H_2O)_4$	5.2	17		
$Cu(CH_3COO)_2(H_2O)_2$	1.0			
$Zn(CH_3COO)_2(H_2O)_2$	1.3			
$Zn(CH_3[CH_2]_{10}COO)_2$	−6.2*			
$CoCl_2(H_2O)_6$	3.4	45	15	−4.6*
$NiCl_2(H_2O)_6$			30	−5.4*
$CuCl_2(H_2O)_2$			2.8	−1.1*
$ZnCl_2$			3	−6.2*
$\{RuCl_2(C{\equiv}O)_3\}_2$	10	25	69	
$PdCl_2(CH_3C{\equiv}N)_2$			17	

Lanthanide complexes		T_g (@ 0.5 mol% Ln^{3+} w/ PVAm), °C
$LaCl_3(H_2O)_6$	$[Xe]4f^0$	104
$CeCl_3(H_2O)_x$	$[Xe]4f^1$	102
$PrCl_3(H_2O)_7$	$[Xe]4f^2$	102
$NdCl_3(H_2O)_6$	$[Xe]4f^3$	103
$SmCl_3(H_2O)_6$	$[Xe]4f^5$	74
$EuCl_3(H_2O)_6$	$[Xe]4f^6$	79
$GdCl_3(H_2O)_x$	$[Xe]4f^7$	60
$TbCl_3(H_2O)_6$	$[Xe]4f^8$	110
$DyCl_3(H_2O)_6$	$[Xe]4f^9$	107
$HoCl_3(H_2O)_6$	$[Xe]4f^{10}$	105
$ErCl_3(H_2O)_x$	$[Xe]4f^{11}$	74
$TmCl_3(H_2O)_7$	$[Xe]4f^{12}$	112
$YbCl_3(H_2O)_6$	$[Xe]4f^{13}$	106
$LuCl_3(H_2O)_6$	$[Xe]4f^{14}$	112

Polymers	MW (daltons)	T_g (°C), undiluted
poly(4-vinylpyridine), P4VP	2×10^5	145
poly(vinylamine), PVAm	2.3×10^4	57
poly(L-histidine), PHIS	$1.5-5.0 \times 10^4$	169
poly(L-lysine)hydrobromide, PLYS	2×10^5	178

[a] *, polymer/metal–salt mixtures that exhibit a decrease in T_g.

VIII. SUMMARY

Stabilization of metal d-electrons has been employed previously to explain thermodynamic[12,24] and kinetic[34] data for 6-coordinate hexa–aqua divalent transition metal complexes from the first-row of the d-block. Kinetic data[34] for the dissociation of one lattice water from $M^{2+}(H_2O)_6$ were analyzed by postulating a 5-coordinate square pyramidal product [i.e., $M^{2+}(H_2O)_5$] that was not allowed to distort. The

methodology employed herein allows for geometric distortions in the molten state to model the glass-transition process in macromolecule–metal complexes with enhanced T_gs. By focusing on weakly basic ligands with a different hardness classification than the metal center, ligand exchange in the first-shell coordination sphere of d-block cations was invoked to couple at least two different chains via coordination crosslinks. Molybdenum hexacarbonyl complexes with poly(vinylamine) have been analyzed using ligand field models, with the hope that experimental data will follow. For complexes based on dichlorotricarbonylruthenium(II) at low metal cation concentrations, group theory analysis of previous infrared data[70] yields a glassy state structure where two sidegroups from the polymer occupy sites in the first shell of Ru^{2+}. Dissociation of one of these metal–polymer chemical bonds at high temperature produces a 5-coordinate complex with reduced symmetry in the molten state. LFSE differences between 6-coordinate glassy complexes and 5-coordinate molten complexes have been correlated with the enhancement in T_g for Ru^{2+}, Co^{2+}, and Ni^{2+} complexes with poly(L-histidine). For similar complexes with poly(4-vinylpyridine), Ru^{2+} and Ni^{2+} are considered to be pseudo-octahedral below T_g and 5-coordinate above T_g, but the corresponding Co^{2+} complexes prepared from ethanol are considered to be pseudo-tetrahedral below T_g and 3-coordinate above T_g. At 1 mol% of the d-block metal cations, there is much more enhancement in the glass transition of poly(L-histidine), relative to that for poly(4-vinylpyridine). Adjustable parameters were not introduced to develop a correlation between $T_{g,complex} - T_{g,undiluted\ polymer}$, due to self-assembled nanoclusters, and the difference between ligand field stabilization energies below and above T_g. The model predicts thermochemical synergy for six different macromolecule-metal complexes. However, universality of the correlation has not been demonstrated for these six complexes, even though the basicity of the important functional group in the polymer's sidechain influences predictions of LFSEs via Jørgensen's quantum-chemical group contribution method.

IX. ACKNOWLEDGMENTS

The research described herein was supported by the Polymers Program of the National Science Foundation via Grant# DMR-0320980.

X. REFERENCES

1. L. A. Belfiore, H. R. G. Graham, E. Ueda, *Macromolecules*, **25**, 2935 (1992).
2. L. A. Belfiore, M. P. McCurdie, P. K. Das, *Polymer*, **42**, 9995 (2001).
3. L. A. Belfiore, E. M. Indra, P. K. Das, *Macromol. Sympos. Polym. Solvent Complexes*, **114**, 35 (1997).
4. P. K. Das, I. Y. Ruzmaikina, L. A. Belfiore, *J. Polym. Sci. Polym. Phys. Ed.*, **38**, 1931 (2000).

5. L. A. Belfiore, I. Y. Ruzmaikina, P. K. Das, *Polym. Eng. Sci.,* **41**, 1196 (2001).
6. F. N. Kelley, F. Bueche, *J. Polym. Sci.,* **50**, 549 (1961).
7. H. Fujita, A. Kishimoto, *J. Polym. Sci.,* **28**, 547 (1958); *J. Chem. Phys.* **34**, 393 (1961).
8. E. A. DiMarzio, J. H. Gibbs, *J. Polym. Sci. Part A*, **1**, 1417 (1963).
9. L. A. Belfiore, M. P. McCurdie, E. Ueda, *Macromolecules*, **26**, 6908 (1993).
10. L. A. Belfiore, A. T. N. Pires, Y. Wang, H. R. J. Graham, E. Ueda, *Macromolecules*, **25**, 1411 (1992).
11. L. A. Belfiore, M. P. McCurdie, *J. Polym. Sci. Polym. Phys. Ed*., **33**, 105 (1995).
12. D. F. Shriver, P. W. Atkins, C. H. Langford, *Inorganic Chemistry*, Freeman, New York, 1990.
13. L. A. Belfiore, F. Bossé, P. K. Das, *Polym. Int*., **36**, 165 (1995).
14. F. Bossé, P. K. Das, L. A. Belfiore, *Macromolecules*, **28**, 6993 (1995).
15. F. Bossé, P. K. Das, L. A. Belfiore, *J. Polym. Sci. Polym. Phys. Ed.*, **34**, 909 (1996).
16. L. A. Belfiore, P. K. Das, F. Bossé, *J. Polym. Sci. Polym. Phys. Ed.*, **34**, 2675 (1996).
17. L. A. Belfiore, P. K. Das, *J. Polym. Sci. Polym. Phys. Ed.*, **42**, 2270 (2004).
18. M. P. McCurdie, L. A. Belfiore, *J. Polym. Sci. Polym. Phys. Ed.*, **37**, 301 (1999).
19. M. P. McCurdie, PhD thesis, Colorado State University, 1997.
20. L. A. Belfiore, X. Sun, P. K. Das, J. Y. Lee, *Polymer*, **40**, 5583 (1999).
21. P. K. Das, J. K. Lee, I. Y. Ruzmaikina, L. A. Belfiore, *Polymer*, **42**, 8873 (2001).
22. P. K. Das, J. K. Lee, L. A. Belfiore, *J. Polym. Sci. Polym. Phys. Ed.*, **39**, 677 (2001).
23. L. S. Hegedus, *Transition Metals in the Synthesis of Complex Organic Molecules*, 2nd ed., University Science Books, Sausalito, CA, 1999.
24. B. N. Figgis, M. A. Hitchman, *Ligand Field Theory and Its Applications*, Wiley-VCH, New York, 2000.
25. E. Benedetti, G. Braca, G. Sbrana, F. Salvetti, B. Grassi, *J. Organometallic Chem.*, **37**, 361 (1972).
26. R. G. Pearson, in *Survey of Progress in Chemistry*, vol. 6, A. Scott, ed., Academic Press, New York, (1969).
27. R. G. Pearson, ed., *Hard and Soft Acids and Bases, Benchmark Papers in Inorganic Chemistry*; Dowden, Hutchinson, Ross, Stroudsburg, PA, 1973.
28. J. March, *Advanced Organic Chemistry: Reactions, Mechanisms, and Structure*, 3rd ed. Wiley, New York, 1985.
29. L. A. Belfiore, E. M. Indra, *J. Polym. Sci. Polym. Phys. Ed.*, **38**, 552 (2000).
30. A. D. Pomogailo, in *Macromolecule-Metal Complexes*, F. Ciardelli, E. Tsuchida, D. Wöhrle, eds., Springer-Verlag, Berlin, 1996.
31. D. A. House, in *Comprehensive Coordination Chemistry: Synthesis, Reactions, Properties and Applications of Coordination Compounds*, vol. 2, G. Wilkinson, R. D. Gillard, J. A. McCleverty, eds., Pergamon Press, Oxford, UK, 1987.
32. E. C. Constable, *Metals and Ligand Reactivity*, Ellis Horwood, New York, 1990.
33. T. A. Stephenson, G. Wilkinson, *J. Inorganic Nuclear Chem*., **28**, 945 (1966).
34. J. K. Burdett, *Molecular Shapes; Theoretical Models of Inorganic Stereochemistry*, Wiley-Interscience, New York, 1980.
35. B. N. Figgis, *An Introduction to Ligand Fields*, Wiley-Interscience, New York, 1966.
36. L. A. Belfiore, M. P. McCurdie, *Polym. Eng. Sci*., **40**, 738 (2000).
37. J. N. VanNiekerk, F. R. L. Schoening, *Acta Crystallographica*, **6**, 609 (1953).
38. T. C. Downie, W. Harrison, E. S. Raper, M. A. Hepworth, *Acta Crystallographica*, Section B, Structural Science, **B27**, 706 (1971).
39. F. A. Cotton, G. Wilkinson, *Advanced Inorganic Chemistry; A Comprehensive Text*, 3rd ed., Wiley-Interscience, New York, 1972.

40. N. H. Agnew, R. J. Collin, L. F. Larkworthy, *J. Chem. Soc. Dalton Trans*. (3), 272 (1974).
41. N. H. Agnew, *J. Polym. Sci. Polym. Chem. Ed*., **14**, 2819 (1976).
42. J. Brandrup, E. H. Immergut, *Polymer Handbook*, 2nd ed., Wiley-Intersceince, New York, 1975.
43. S. L. Malhotra, P. Lessard, L. P. Blanchard, *J. Macromol. Sci. Chem*., **A15**, 121 **(**1981).
44. P. J. Flory, *Principles of Polymer Chemistry*, Cornell University Press, Ithaca, NY, 1953.
45. J. W. Tester, M. Modell, R. C. Reid, *Thermodynamics and Its Applications*, 3rd ed., Prentice-Hall, Upper Saddle River, NJ, 1997.
46. L. A. Belfiore, *Transport Phenomena for Chemical Reactor Design*, Wiley-Interscience, New York, 2003.
47. B. L. Ross, J. G. Grasselli, W. M. Ritchey, H. D. Kaesz, *Inorganic Chemistry*, **2**, 1023 (1963).
48. T. P. Loginova, L. M. Bronshtein, P. M. Valetskii, M. G. Ezernitskaya, B. V. Lokshin, O. L. Lependina, V. I. Bakhmutov, I. V. Dyumaeva, S. V. Vinogradova, *Organometallic Chem. USSR*, **3**, 87 and 222 (1990).
49. T. P. Loginova, L. M. Bronshtein, E. S. Mirzoeva, M. G. Ezernitskaya, B. V. Lokshin, Y. V. Genin, P. M. Valetskii, *Polym. Sci*., **35**, 21 (1993); Vysokomol. Soed., **35**, 28 (1993).
50. N. A. Beach, H. B. Gray, *J. Am. Chem. Soc.*, **90**, 5713 (1968).
51. F. P. Pruchnik, *Organometallic Chemistry of the Transition Elements*, Plenum Press, New York, 1990.
52. S. J. Ashcroft, C. T. Mortimer, *Thermochemistry of Transition Metal Complexes*, Academic Press, New York, 1970.
53. F. Bossé, P. K. Das, L. A. Belfiore, in *Hybrid Organic-Inorganic Composites*, J. E. Mark, C. Y. C. Lee, P. A. Bianconi, eds., ACS Symp. Ser., **585**, 192 (1995).
54. F. Bossé, P. K. Das, L. A. Belfiore, *Polym. Gels Networks*, **5**, 387 (1997).
55. T. Tanaka, C. Wang, K. King, *Faraday Discussions*, **101**, 201 (1995).
56. S. Merlino, G. Montagnoli, *Atti Soc. Tosc. Scienze Naturali*, **76**, 335 (1970).
57. M. I. Bruce, F. G. A. Stone, *J. Chem. Soc.*, **A**, 1238 (1967).
58. M. J. Cleare, Q. P. Griffith, *J. Chem. Soc.*, **A**, 372 (1969).
59. R. S. Young, ed., *Cobalt: Its Chemistry, Metallurgy, and Uses*, Reinhold Publishing, New York, 1960.
60. J. Mizuno, K. Ukei, T. Sugawara, *J. Phys. Soc. Jpn*., **14**, 383 (1959).
61. D. Nicholls, in: *Comprehensive Inorganic Chemistry*, vol. 3, J. C. Bailar, H. J. Emeléus, R. S. Nyholm, A. F. Trotman-Dickenson, eds., Pergamon Press: Oxford, UK, 1973.
62. A. F. Wells, *Structural Inorganic Chemistry*, 5th ed., Oxford University Press, New York, 1984.
63. R. C. Bohinski, *Modern Concepts in Biochemistry*, 4th ed., Allyn & Bacon, Boston, 1983.
64. L. J. Admiraal, G. Gafner, *Chem. Commun.*, 1221 (1968).
65. N. H. Agnew, L. F. Larkworthy, *J. Chem. Soc.*, 4669 (1965).
66. N. S. Gill, R. S. Nyholm, G. A. Barclay, T. I. Christie, P. J. Pauling, *J. Inorganic Nuclear Chem.*, **18**, 88 (1961).
67. W. J. Hehre, L. Radom, P. R. Schleyer, J. A. Pople, *Ab Initio Molecular Orbital Theory*, Wiley-Interscience, New York, 1986.
68. E. Wimmer, in *Density Functional Methods in Chemistry*, J. K. Labanowski, J. W. Andzelm, eds., Springer-Verlag, Heidelberg, 1991.
69. T. Ziegler, V. Tschinke, in *Density Functional Methods in Chemistry*, J. K. Labanowski, J. W. Andzelm, eds., Springer-Verlag: Heidelberg, 1991.
70. M. P. McCurdie, L. A. Belfiore, *Polymer*, **40**, 2889 (1999).

CHAPTER 2

Metal Oxide Clusters as Building Blocks for Inorganic–Organic Hybrid Polymers

Ulrich Schubert

Institute of Materials Chemistry, Vienna University of Technology, Wien, Austria

CONTENTS

Macromolecules Containing Metal and Metal-Like Elements, Volume 7: Nanoscale Interactions of Metal-Containing Polymers, edited by Alaa S. Abd-El-Aziz, Charles E. Carraher Jr., Charles U. Pittman Jr., and Martel Zeldin.

I. INTRODUCTION

Composite materials are composed of two or more phases of (mostly) different chemical compositions, by which the combination of the two phases and interface phenomena result in new properties of the composite compared to its individual constituents. An example is fiber-reinforced organic polymers. Classical composite materials have distinct phase boundaries between different macroscopic phases.

The basic idea behind the development of inorganic–organic hybrid materials is similar: If the dimensions of the one or both phases making up the composite material are reduced in size down to the nanometer scale or even the molecular level, a synergetic combination of the properties typical of each of the constituents is still expected. It is rather obvious, however, that the materials properties of such "nanocomposites" will be different from that of classical composites, since many properties correlate with the phase dimension. Since molecular building blocks are now used for the construction of the material instead of macroscopic pieces of matter, the interface (or interphase) between the constituents will clearly play a different role.

When organic and inorganic building blocks are combined, so-called inorganic–organic hybrid materials are obtained. Modification of the kind and proportions of their constituents allows, in principle, a deliberate tailoring of properties between purely inorganic and purely organic materials. This contribution focuses on a subclass of nanocomposite materials, in which one phase is an organic polymer and that will, therefore, be named *inorganic–organic hybrid polymers*.

One class of inorganic–organic hybrid materials are those in which the organic component is just entrapped in an inorganic host, or vice versa. Examples include inorganic–organic hybrid polymers with interpenetrating but otherwise nonconnected networks, polymers filled with inorganic particles, or layered inorganic compounds intercalated by organic polymers. In the second class of inorganic–organic hybrid materials, the constituents are connected with each other by strong covalent or ionic bonds. Although the preparation of these materials usually requires some efforts to establish the chemical link, for example, the development of special precursors, the bonding between the two components overcomes problems of macrophase or microphase separation or leaching and allows materials development strategies similar to those for block copolymers in organic polymer chemistry.

The most versatile method for the preparation of the second class of inorganic–organic hybrid *polymers* is sol-gel processing of molecular precursors of the general composition $(RO)_nM–X–A$[1] with a hydrolyzable group $(RO)_nM$, and a polymerizable organic group A connected by some inert spacer *X*. In alkoxysilane chemistry, methacryloxypropyl(trialkoxy)silane, $(RO)_3Si(CH_2)_3OC(O)CMe=CH_2$, or vinyltrimethoxysilane, $(MeO)_3SiCH=CH_2$, are most often used for this purpose, but alkoxysilanes with more than one polymerizable group in the organic substituent were also developed.[2] For the functionalization of metal alkoxides several types of unsaturated organic ligands were used, such as the anions of ß-diketones (allylacetoacetone or 2-(methacryloyloxy)ethyl acetoacetone), carboxylic acids (methacrylic acid, acrylic acid or methacrylamidosalicylic acid), or chelating alcohols (*cis*-but-2-ene-1,4-diol or 3-allyloxypropane-1,2-diol, isoeugenol).[3] The issue of what compositions

and structures these metal derivatives could have will be discussed below. In practice, the functional organic compounds are reacted with the metal alkoxide in situ, and the subsequent reactions are mostly carried out without isolation of the organically substituted metal alkoxide derivative. The precursors are first reacted with water in the presence of the parent alkoxide $M(OR)_{n+1}$ (to achieve a higher inorganic crosslinking density). After sol–gel processing (i.e., formation of the inorganic network) the organic groups A are polymerized or crosslinked to form oligomeric or polymeric organic structures. Organic comonomers may be added to extend the organic structures.

A special challenge of increasing importance is to tailor not only the composition of hybrid materials but also their structural features, especially to control the mutual arrangement of the inorganic and organic building blocks. This goal is more easily reached when the formation of the organic and the inorganic extended structures is done at different times in clearly separated reaction steps. The first option is to use compounds of the type $[(RO)_nM]_xY$, in which Y is a pre-formed organic group or polymer chain linking two ($x = 2$) or more ($x > 2$) metal alkoxide units $[M(OR)_n]$. For example, organic groups of variable length (e.g., saturated or unsaturated hydrocarbon chains, or polyaryls) substituted with $Si(OR)_3$ groups at both ends, or polymers with grafted $Si(OR)_3$ groups were used.[4]

The inorganic counterpart of this method is to use preformed inorganic structures with polymerizable organic groups.[5] Polymer chemists are using inorganic particles for the reinforcement of organic polymers. The dimensions of the filler particles are typically in the upper nanometer to micron range. They may be substituted by reactive organic groups to provide strong chemical interactions with the polymer matrix.[6] As pointed out above, different properties can be expected, when the size of the inorganic particles is reduced to the nanometer scale. Most obviously, the polymers stay transparent because of the small size of the particles. More important, however, is that novel properties can be achieved by using intrinsic physical properties of nanoparticles (e.g., quantum dots or single domain particles) and the high interphase area between the particles and the organic matrix.

The smallest and structurally best defined nanoparticles are molecular inorganic clusters, which have a defined stoichiometry, size, and shape and can be prepared by bottom-up approaches from molecular compounds. The term *cluster* is used in this article for polynuclear metal compounds with a three-dimensional (3D) shape. Molecular clusters need to be stabilized by surface groups, which can be terminal groups (O^-, OH, OR, SR, Cl, etc.) or multidentate organic or inorganic ligands. Since all or nearly all metal atoms of molecular clusters are surface atoms, clusters have the highest possible portion of surface groups. When these groups are provided with some functionality to bind to a polymer matrix, the largest possible interphase region between the inorganic nanoparticles and the organic matrix is achieved.

This concept requires the preparation of molecular clusters covered by reactive organic groups that are capable of binding to organic polymers. The discussion in this article is restricted to metal oxo clusters; however, the concept is rather general.

The only metal oxo cluster type previously investigated in some detail as a constituent of inorganic–organic hybrid polymers are the polyhedral oligomeric

silsesquioxanes, $[RSiO_{3/2}]_n$ (POSS), or spherosilicates, $[ROSiO_{3/2}]_n$,[7] mostly the cubic octamers, $R_8Si_8O_{12}$ or $(RO)_8Si_8O_{12}$. These compounds can be considered the smallest possible piece of silica (eight corner-sharing tetrahedra in the case of the octamers) wrapped by organic groups R. The groups R can be used for crosslinking or polymerization reactions. For example, hybrid polymers were prepared by polymerization of $(RSiMe_2O)_8 \cdot Si_8O_{12}$ or $R_8Si_8O_{12}$ when the organic substituent R contained unsaturated or epoxy groups.[8] It is worth mentioning at this point that such inorganic–organic hybrid polymers have the same overall chemical composition as the corresponding polymers reinforced by glass fibers. It is rather obvious, however, that the nanocomposite has different macroscopic properties from the classical composites.

The crosslinking density in the hybrid polymers based on octa-substituted silicate clusters is high because of the large number of reactive groups on the cluster surface. Recently, a new type of POSS-based hybrid polymers has gained much interest in which POSS molecules are just appended to thermoplastic resins, such as polyolefins, polyepoxides, or polyurethanes.[9,10] The development of these materials was made possible by the straightforward synthesis of monofunctional derivatives of the type $RR'_7Si_8O_{12}$, with only one polymerizable group (R), which are then used as comonomers in polymerization reactions.[7,9]

The interesting properties of POSS-reinforced polymers have widened the view on what is conceivable with other inorganic clusters, considering the wealth of such compounds in terms of composition, structures and properties. Apart of the property enhancements observed for POSS-reinforced polymers, interesting catalytic, magnetic, or electric properties can be *additionally* expected if transition metal based clusters are employed. The development of the corresponding hybrid materials is just beginning. This is mainly due to the lack of suitable organically modified transition metal oxide clusters (OMTOC) as the transition metal equivalents to the POSS. This chapter is aimed at discussion some general concepts, based on our own work, rather being a comprehensive overview on what is known.

II. SYNTHESIS OF ORGANICALLY MODIFIED TRANSITION METAL OXIDE CLUSTERS

A key issue in the preparation of OMTOC is the stable attachment of suitable organic groups to the surface metal atoms of the clusters. Linkage of organic groups via metal–carbon bonds is not possible, because these bonds—unlike silicon–carbon bonds—are not hydrolytically stable. Bonding can be achieved, however, via bidentate or multidentate (chelating or bridging) ligands, such as carboxylates, sulfonates, phosphonates, and ß-diketonates. These groups may carry organic functionalities, such as polymerizable double bonds.[1,11]

OMTOC can be prepared by two strategies. The organic groups can either be grafted to a preformed cluster (postsynthesis modification method) or introduced during the cluster synthesis (in situ method).

A. Postsynthesis Modification of Pre-Formed Metal Oxide Clusters

A huge variety of neutral or, more often, charged metal oxo clusters is known, and there are established routes for their preparation. Therefore, it appears to be an obvious approach to modify the surface groups of available clusters. However, this method is not very general. The reason is that this method requires reactive surface groups, such as O^-, OH, Cl or OR, as well as the simultaneous balancing of charges and co-ordination numbers on substitution of these groups. Substitution can therefore be expected to proceed without major difficulties only if both the number of the occupied coordination sites and the charges of the entering ligands are the same as those of the leaving groups. Alternatively, bridging groups may change their coordination mode (e.g., bridging OR or OH to terminal, μ_3 oxygens to μ_2 oxygens) or metals may change their coordination number to make additional coordination sites available.

For example, when $Ti_{16}O_{16}(OEt)_{32}$ was reacted with small proportions of carboxylic acids, a fraction of the bridging OEt groups was replaced by bridging carboxylate groups; the resulting cluster was not structurally characterized. For higher carboxylate: Ti proportions, the cluster was degraded.[12] However, the presence of bridging alkoxo ligands does not guarantee that substitution by bidentate ligands will take place. Reaction of $Ti_7O_4(OEt)_{20}$ with benzoic acid resulted in the formation of the new cluster $Ti_6O_4(OEt)_{14}(OOCPh)_2$ with concomitant major rearrangement of the cluster core, despite the presence of bridging OR groups in the starting cluster.[13] A rare example in which the general structure of an oxo alkoxo cluster was preserved on substitution of alkoxo ligands by carboxylates was found when $Ti_3O(OPr^i)_{10}$ or $Ti_3O(OPr^i)_9(OMe)$ was converted to $Ti_3O(OPr^i)_8(OOCPh)_2$ by reaction with benzoic acid.[14]

A variation of the postsynthesis modification method makes use of silane coupling agents that are reacted with nucleophilic terminal oxo groups at the cluster surface. There are only few examples because not too many oxometallate clusters have sufficiently nucleophilic oxo groups. The heterotungstate cluster $[SiW_{11}O_{39}]^{8-}$ was derivatized by reaction with various organotrichloro- or organotriethoxysilanes $RSiX_3$ (X = Cl or OR′) with polymerizable groups R.[15] The obtained anionic clusters have the composition $[SiW_{11}O_{35}(O_5Si_2R_2)]^{4-}$. The clusters $[SiW_{10}O_{32}(O_5Si_2R_2)]^{4-}$ and $[SiW_{10}O_{32}(O_8Si_4R_4)]^{4-}$ (R = vinyl or 3-methacryloxypropyl) were similarly prepared from $[SiW_{10}O_{36}]^{8-}$.[16] The unsaturated organic groups were thus attached to the cluster core via W-O-Si-C linkages. In a formal sense, four surface $-O^-$ groups are replaced by the bridging $[R_2Si_2O_5]^{4-}$ or $[R_4Si_4O_8]^{4-}$ units, respectively. Both the overall charge of the ligands and the number of occupied coordination sites are thus preserved, and no rearrangement of the clusters is necessary to accommodate the organosiloxyl groups.

B. In Situ Modification

Carboxylic acids, mainly acetic acid, are used in sol-gel chemistry to moderate the reactivity of metal alkoxides.[17] It was noted rather early that clusters of the

general composition $M_aO_b(OH/OR)_c(OOCR')_d$ may be obtained instead of the anticipated substituted alkoxo derivatives $M(OR)_{x-n}(OOCR')_n$. One of the earliest structurally characterized examples is $Ti_6O_4(OR)_8(OOCMe)_8$, obtained by reaction of $Ti(OR)_4$ with acetic acid.[18] Although the mechanism of the reaction has not been elucidated, the formation of this and related clusters can be explained by the following sequence of reactions. In the first step of the reaction, one or more alkoxide ligands are substituted by carboxylate groups to give $M(OR)_{x-n}(OOCR')_n$ (Eq. 1). The thus liberated alcohol then undergoes an esterification reaction in which water is produced along with the ester (Eq. 2).[19] The in situ generated water serves to hydrolyze all or part of the remaining alkoxide groups and is the source of oxo or hydroxo groups in the clusters (Eq. 3). The slow production of water allows a controlled growth of the carboxylate-substituted oxometallate clusters. The advantage of this process is that the cluster growth is self-limiting because the reaction is based on three interwoven reactions (i.e. two alcohol-producing reactions—equations 1 and 3—and two carboxylic acid-consuming reactions—equations 1 and 2) and because several anionic groups with different charges and coordination possibilities are available to balance the charges and coordination numbers of the metal atoms forming the product cluster.

$$M(OR)_x + nR'COOH \rightarrow M(OR)_{x-n}(OOCR')_n + nROH \quad (1)$$

$$ROH + R'COOH \rightarrow R'COOR + H_2O \quad (2)$$

$$M(OR)_{x-n}(OOCR')_n + H_2O \rightarrow M_aO_b(OR)_c(OOCR')_d + ROH \quad (3)$$

The use of other acids may also result in the formation of oxo-alkoxo clusters by in situ generation of water. For example, the phosphonate and phosphinate-substituted oxotitanium clusters $Ti_4O(O^iPr)_8(O_3PR)_3$ and $Ti_4O_4(O^iPr)_4(O_2PPh_2)_4$ were obtained by reaction of $Ti(OR)_4$ with the corresponding phosphonic or phosphinic acid.[20]

We used this method extensively to prepare oxo-clusters capped by *polymerizable* carboxylate ligands. The prepared clusters include $Ti_4O_2(OR)_6(OMc)_6$[21] (OMc = methacrylate), $Ti_6O_4(OR)_8(OMc)_8$,[3e] $Ti_9O_8(OR)_4(OMc)_{16}$,[22] $M_4O_2(OMc)_{12}$ (M = Zr[23,24], Hf[25]), $M_6(OH)_4O_4(OMc)_{12}$ (M = Zr[23], Hf[25]), $Zr_6O_2(OR)_{10}(OMc)_{10}$, $Zr_6O_2(OR)_6(OMc)_{14}$,[26] and $M_4O_4(OR)_8(OMc)_4$ (M = Nb, Ta)[27,28] as well as the corresponding acrylate derivatives in many cases. A series of methacrylate-substituted Ti/Zr(Hf) or Ti/Y mixed-metal clusters was similarly prepared from $Ti(OR)_4/Zr(OR)_4$ ($Hf(OR)_4$)/methacrylic acid or $Ti(OR)_4/Y(OR)_3$/methacrylic acid mixtures.[25,29] These mixed-metal clusters are particularly interesting because of their rodlike shape of variable length (1.2–1.8 nm [distance between the most distant oxygen atoms], diameters ≈ 0.65 nm).

What the mentioned metal oxo clusters have in common is that their surface is covered by reactive organic groups, which are fully accessible for further reactions. The (meth)acrylate groups chelate or bridge the metal atoms. From a practical point of view, the simplicity of the preparation method is worthy of special mention at this

point. The metal alkoxide(s) and the carboxylic acid are simply mixed together in a certain ratio (see below), and—in most cases—the cluster crystallizes in quantitative yield within a period of a day or so. For example, we prepared about 200 g of $Zr_4O_2(OMc)_{12}$ within a few days.

The size and shape of the clusters can be influenced to a certain degree by the reaction parameters. The most important parameter is the metal alkoxide/carboxylic acid ratio. An example is shown in Figure 1 (for a given ratio, the same cluster is reproducibly obtained).

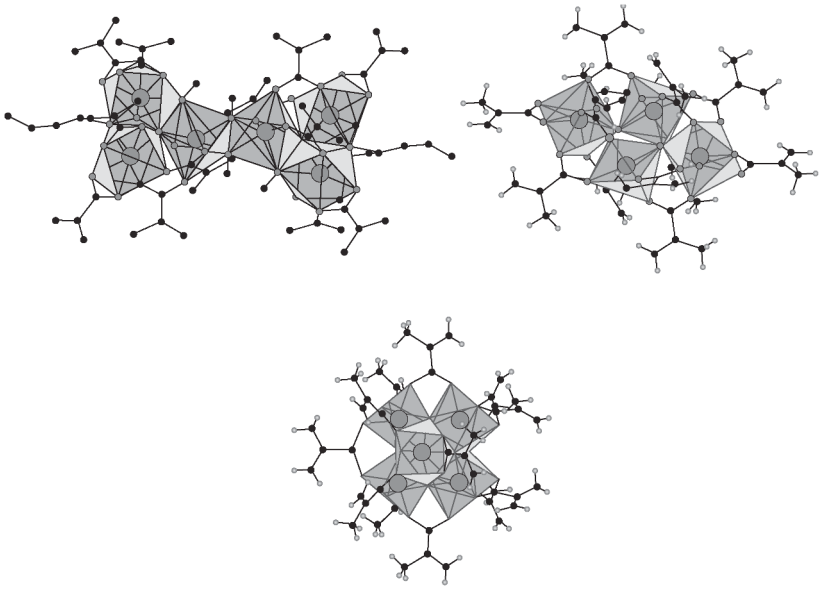

Figure 1 The structures of $Zr_6O_2(OBu)_{10}(OMc)_{10}$ (top left), $Zr_4O_2(OMc)_{12}$ (*top right*) and $Zr_6(OH)_4O_4(OMc)_{12}$ (*bottom*) showing the different condensation of the [ZrO_7] and [ZrO_8] polyhedra. (Reproduced by permission from ref. 11.)

The three oxozirconium clusters $Zr_6O_2(OBu)_{10}(OMc)_{10}$,[26] $Zr_6(OH)_4O_4 \cdot (OMc)_{12}$,[23] and $Zr_4O_2(OMc)_{12}$[23,24] are formed when $Zr(OBu)_4$ is reacted with 1.6, 4, or 7 equivalents of methacrylic acid, respectively. When the metal alkoxide/carboxylic acid ratio is low, most of the carboxylic acid is consumed for the substitution of alkoxide groups; in $Zr_6O_2(OBu)_{10}(OMc)_{10}$ the average degree of substitution of the zirconium atoms by OMc ligands is 1.67. Therefore only a small amount of water is produced. As a consequence, a rather open cluster (low degree of condensation) with a large number of residual alkoxy groups is formed. For a high metal alkoxide/carboxylic acid, a high degree of substitution by methacrylate ligands is achieved

(3.0 in $Zr_4O_2(OMc)_{12}$). Although much more water is produced due to the large excess of carboxylic acid, an open cluster is again formed, because the coordination sites required for a higher degree of condensation are blocked by the OMc ligands. The highest degree of condensation is therefore obtained for a medium metal alkoxide/carboxylic acid ratio. The structure of the cluster core of $Zr_6(OH)_4O_4(OMc)_{12}$ is indeed similar to that of the parent metal oxide. This cluster can be considered to be the smallest possible section of tetragonal zirconia which is covered by organic groups and thus prevented from growing.

A second parameter influencing the kind of formed cluster is the kind of the alkoxide group of the parent alkoxide. For example, when $Ti(OEt)_4$ or $Ti(OPr)_4$ are reacted with two to three equivalents of methacrylic acid, the clusters $Ti_6O_4(OR)_8 \cdot (OMc)_8$ are obtained, while $Ti_4O_2(O^iPr)_6(OMc)_6$ is formed from $Ti(O^iPr)_4$.[3e,21] This can be due to the bulkiness of the alkoxide ligands or to the degree of association of the parent alkoxide ($Ti(OEt)_4$ and $Ti(OPr)_4$ are trimeric in solution, while $Ti(O^iPr)_4$ is monomeric because of its larger alkoxide groups).

In the above-mentioned examples, the water was produced by an in situ reaction. The benefit of this method is its simplicity and that structurally well-defined clusters are formed. However, the method cannot be extended to the synthesis of larger clusters because of the competition of equations 1 and 2. As the portion of surface atoms decreases in larger clusters, a much lower portion of carboxylate ligands is required to substitute the metal atoms at the cluster surface. However, if the metal alkoxide/carboxylic acid ratio is strongly decreased, not enough water would be produced to build up the cluster core. An alternative is to add the water needed for the (partial) hydrolysis of the alkoxo groups externally to a metal alkoxide/carboxylic acid mixture. The disadvantage of this method is that the precise dosage of water for the reproducible synthesis of a certain cluster (particle) size is difficult. However, the synthesis of $Zr_{10}O_6(OH)_4(OPr)_{18}(allylacetoacetate)_6$ by hydrolysis of a solution of $Zr(OPr)_4$ and 0.6 equivalents of allylacetoacetone has shown that this method can be successful.[30] It was also shown that the size of metal oxide particles can be controlled by the metal alkoxide/bidentate ligand ratio. The size of zirconia particles (obtained by hydrolytic condensation) increased from 2 nm to 15 nm when the $Zr(O^iPr)_4$/acetylacetone ratio was increased from 1 to 10.[31] As the portion of surface atoms decreases, a smaller amount of ligands is needed to saturate the surface atoms.

All the clusters discussed so far are substituted with ligands that contain polymerizable double bonds. Clusters with functional groups that allow other polymerization techniques offer additional possibilities for materials syntheses. The first examples are the 2-bromopropionate-substituted metal oxo clusters $Ti_6O_4(O^iPr)_8 \cdot (OOC\text{-}CBrMe_2)_8$, $Zr_5O_4(OPr)_2(OOC\text{-}CBrMe_2)_{10}(PrOH)_4$, and $V_3O_3(OOC\text{-}CBrMe_2R)_6 \cdot ({}^iPrOH)$ employed as macroinitiators for atom-transfer radical polymerizations,[32] and the cluster $Zr_6O_4(OH)_4$ (5-norbornene-2-carboxylate)$_{12}$ used for ring-opening metathesis polymerization (ROMP).[33]

The clusters $M_aO_b(OH/OR)_c(OOCR')_d$ are the transition metal equivalents to the polyhedral oligomeric silsesquioxanes, $[RSiO_{3/2}]_n$, or spherosilicates,

$[ROSiO_{3/2}]_n$, in which each silicon is substituted by a reactive organic group R. When clusters with a large number of unsaturated ligands are copolymerized with organic monomers, the crosslinking density of the obtained hybrid polymers is high (see below). To control the crosslinking density and some polymer properties related to that (flexibility, swelling in organic solvents, thermal degradation, etc.), variation of the number of polymerizable ligands on the surface of a given cluster is desirable (i.e., clusters are needed that contain both nonreactive and polymerizable ligands in an easy-to-adjust ratio). In the extreme, clusters with only one polymerizable ligand would allow the preparation of polymers with the clusters pending on a polymer chain, as for the POSS systems using $RR'_7Si_8O_{12}$ (see above). The transition metal equivalent would be $M_aO_b(OH/OR)_c(OOCR')_d(OOCR'')_e$ substituted by both reactive (OOCR′) and nonreactive (OOCR″) ligands. The preparation of such clusters is still a challenge. We are currently investigating several possibilities:

- In situ synthesis of the clusters in the presence of two different carboxylates (i.e., mixtures of a functional and a nonfunctional carboxylic acid). We obtained a first example, $Zr_6O_4(OH)_4(OMc)_8$ (isobutyrate)$_4$, when $Zr(OBu)_4$ was reacted with a 1 : 1 mixture of methacrylic acid and isobutyric acid.[33]
- Partial exchange of (meth)acrylate ligands by either nonfunctional bidentate ligands (such as acetate or acetylacetonate) or vice versa. When $Zr_4O_2(OMc)_{12}$ was reacted with two equivalents methacrylic acid, an exchange process involving the nonbonded acid molecules was observed by NMR spectroscopy. A rapid exchange was also observed with propionic or isobutyric acid that allowed either complete or partial substitution of the methacrylate ligands.[34,35]
- Partial blocking of polymerizable ligands at the cluster surface by chemical reactions at the double bond.

III. SYNTHESIS AND STRUCTURAL CHARACTERIZATION OF THE CLUSTER-REINFORCED POLYMERS

Inorganic–organic hybrid polymers were obtained by polymerizing $[SiW_{11}O_{34}(O_5Si_2R_2)]^{4-}$ (R = various polymerizable group) in free-radical reactions[15] or by copolymerizing $[SiW_{10}O_{32}(O_5Si_2R_2)]^{4-}$ with ethyl methacrylate[36] or acrylamide[37] in different molar ratios. It was shown in each case that the clusters are retained in the polymers. Polymerization of $[SiW_{11}O_{34}(O_5Si_2R_2)]^{4-}$ gave hybrid polymers with different structures (linear or branched) and spatial repetitions of the clusters, depending on the polymerization conditions. Copolymerization of $[SiW_{10}O_{32}(O_5Si_2R_2)]^{4-}$ with either ethyl methacrylate or acrylamide resulted in swellable gels, where the swelling index increased with an increasing monomer/cluster ratio. This shows that the clusters act as crosslinkers.

In our own work, we investigated radical polymerizations of the clusters $Zr_6(OH)_4O_4(OMc)_{12}$,[35,38,39] $Zr_4O_2(OMc)_{12}$,[39,40] $Ti_4O_2(OPr^i)_6(OMc)_6$, $Ti_6O_4(OEt)_8 \cdot (OMc)_8$,[21,39] or $Ta_4O_4(OEt)_8(OMc)_4$[28] (and some of the corresponding acrylate-substituted clusters)—typically 0.5–2 mol%—with methyl methacrylate (MMA) or methacrylic acid (MA) as comonomers. The materials properties of the resulting hybrid polymers (see below) indicate that the metal oxo clusters crosslink the polymer chains efficiently. Glassy, transparent materials are typically obtained upon copolymerization with MMA in benzene or toluene when the cluster proportion is below 2 mol%. The polymers become opaque or whitish when the cluster proportion is increased. Copolymerization of the clusters with MA results in insoluble powders.

A different type of polymer is obtained when the 2-bromopropionate-substituted titanium zirconium and vanadium oxo clusters mentioned above are employed as macroinitiators for copper-catalyzed atom transfer polymerizations of MMA or styrene. Each carboxylate ligand at the cluster surface acts as an initiator for the growth of a polymer chain from the cluster surface, resulting in core-shell nanoparticles with an inorganic (cluster) core and a polymer shell. These reactions proceed in a controlled manner and rather low polydispersities are achieved.[32]

The interaction between PMMA chains in the hybrid polymer prepared from 2 mol% $Zr_4O_2(OMc)_{12}$ and MMA was investigated by dielectric spectroscopy and a predominant syndiotactic conformation of PMMA chains was found.[41] Comparison with the spectra of syndiotactic and isotactic PMMA clearly indicated that in the hybrid network the macromolecular chains experience a different chemical environment than in cluster-free PMMA. The results suggest that in the hybrid polymer the organic chains are more separated from each other, owing to the cluster crosslinks. This results in less pronounced interchain interactions.

A critical issue is whether the clusters are incorporated into the polymers as such, or whether they are destroyed or rearranged upon reaction with the organic comonomers. An early result was alarming in this respect: The cluster $Zr_4O_2(OMc)_{12}$ was completely degraded by acetylacetone to monomeric $Zr(acac)_2(OMc)_2$.[42] Given the large excess of potentially ligating groups, especially in the reactions of the clusters with methacrylic acid, there was a risk that the clusters would also be degraded. There are no simple straightforward spectroscopic methods that give a "fingerprint" information on the cluster core (especially for the low molar ratios used) by which the clusters can be traced to the final hybrid polymer. However, such information is provided by EXAFS spectroscopy. The two Fourier transforms in Figure 2 are nearly identical, which proves that the cluster core is unchanged in the polymer.[43]

Small-angle x-ray scattering (SAXS) provides valuable information on the distribution of the clusters in the polymers. The SAXS curves for PMMA crosslinked by with various portions of $Zr_6(OH)_4O_4(OMc)_{12}$ are shown in Figure 3.[39] The slope of the linear part at high q-values is compatible with nearly spherical units having a radius of gyration of 0.49 nm. This corresponds well with the radius of the cluster core. The existence of a maximum in the SAXS function indicates some kind of

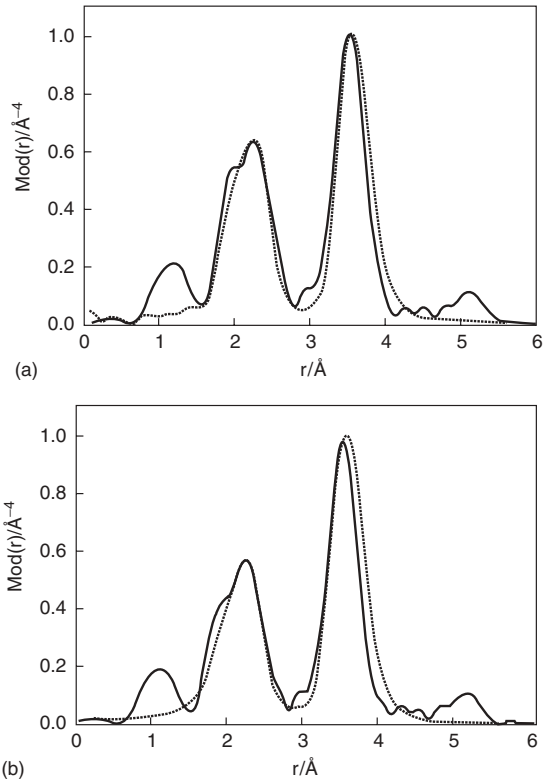

Figure 2 Experimental (*solid line*) and calculated (*dotted line*) Fourier transform of the $k_3\chi(k)$ function of the crystalline $Zr_6(OH)_4O_4(OMc)_{12}$ cluster (right) and $Zr_6(OH)_4O_4(OMc)_{12}$ co-polymerized with MA (left) at the Zr-K edge. (Reproduced by permission from ref. 43).

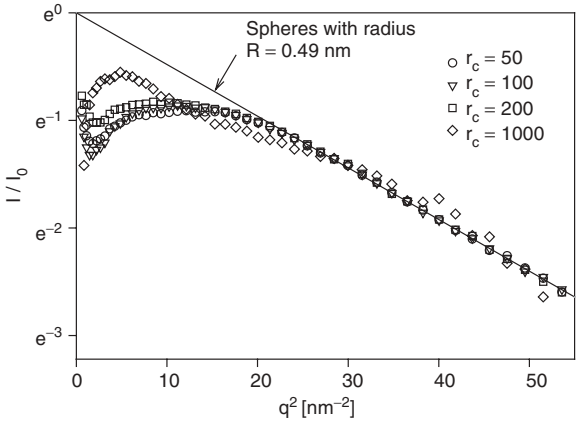

Figure 3 SAXS data of PMMA crosslinked with $Zr_6(OH)_4O_4(OMc)_{12}$. r_c is the MMA/cluster molar ratio in the starting mixture. The *x*-axis corresponds to the square of the scattering vector, q^2, and the *y*-axis to $I(q)/I_0$ on a logarithmic scale (Guinier plot). I(q) is the scattering intensity after subtraction of the signal of cluster-free PMMA and normalization. (Reproduced by permission from ref. 39).

short-range order in the arrangement of the cluster units. The position of the maximum is roughly inversely related to the intercluster distance. As the cluster portion in the polymer decreases, the maximum is shifted to smaller q^2 (i.e., to larger average cluster-cluster distances). The SAXS data therefore show that the microstructure of this particular hybrid polymer can be described by a dispersion of identical (approximately spherical) clusters in the polymer.

Although we found other examples with a roughly statistical distribution of the clusters (e.g., for styrene crosslinked by $Ta_4O_4(OEt)_8(OMc)_4$),[44] we also observed SAXS curves with two maxima instead of one. This indicates a different distribution of the clusters with two different intercluster distances. One possible explanation of the double-maximum is that the anisotropic shape (elongated disks) of some cluster types results in a kind of discotic arrangement. The shorter distance would then correspond to the inter-cluster distances within a pile of disks, and the longer distance to the distance between clusters of neighboring piles (Fig. 4).

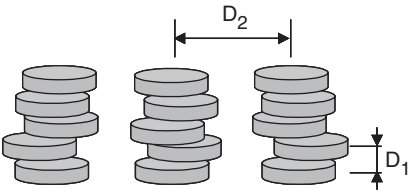

Figure 4 A possible discotic arrangement of flat clusters in the hybrid polymers.

We so far observed three subclasses for this discotic arrangement.

1. The two distances are independent of the cluster concentration. This was, for example, found for $Ti_4O_2(OEt)_6(OMc)_6$ in PMA ($D_1 \approx 1.6$ nm and $D_2 \approx 2.5$ nm)[21] or for $Hf_4O_4(OMc)_{12}$ in PMMA ($D_1 \approx 1.3$ nm and $D_2 \approx 2.1$ nm).[44] This indicates that the clusters aggregate to some extent (clusters of clusters). When a higher proportion of MMA comonomer is employed in the polymerization reactions, the intercluster distance is not increased, but instead the additional organic monomer is apparently incorporated between the cluster aggregates.

2. The shorter distance is independent of the cluster concentration while the larger distance increases when less cluster is incorporated. This behavior was found for $Ti_6O_4(OPr)_8(OAcr)_8$ (OAcr = acrylate) in PMMA ($D_1 \approx 1.3$ nm; $D_2 \approx 2.5$ nm for 2 mol% of cluster and ≈ 3.0 nm for 1 mol% of cluster) or $Ti_4O_2(OEt)_6(OMc)_6$ in PMMA ($D_1 \approx 1.5$ nm; $D_2 \approx 2.3$ nm for 2 mol% of cluster and ≈ 3.1 nm for 0.5 mol% of cluster).[21] This indicates that the intercluster distances within a pile of disks remains constant and additional organic monomer is incorporated between the cluster piles.

3. The longer distance is independent of the cluster concentration while the shorter distance increases when less cluster is incorporated. This behavior was found

for $Ta_4O_4(OEt)_8(OMc)_4$ in PMMA ($D_1 \approx 1.2$ nm for 4 mol% of cluster and ≈ 1.6 nm for 1 mol% of cluster; $D_2 \approx 3.2$ nm).[44] This indicates that the intercluster distances between the piles of disks remains constant and additional organic monomer is incorporated between the clusters of the same pile.

A possible reason for the different aggregation behavior of the clusters may be their shape or the geometrical arrangement of the reactive ligands at the cluster surface. However, we currently do not see an obvious correlation with any structural or kinetic property of the clusters or organic monomers. It must be emphasized again, however, that the clusters of clusters cannot be large or regular, because we do not get any XRD pattern, and the polymers are transparent at the given cluster concentrations.

IV. PROPERTIES OF THE CLUSTER-BASED HYBRID POLYMERS

Investigation of the materials properties of the cluster-based hybrid polymers is in its infancy, and the properties of the new hybrid polymers are far from being exploited. We have seen two clear trends in the materials properties of inorganic–organic hybrid polymers prepared by polymerization of metal oxo clusters with organic comonomers. They depend on the portion of incorporated cluster and, surprisingly, also on the kind of incorporated cluster.[28]

We do not yet understand how the employed cluster can possibly influence the materials properties. Several hypotheses have to be tested:

- The polymerization kinetics of methacrylate ligands bonded to different cluster cores could be different.
- Different clusters could aggregate to different degrees in the hybrid polymer.
- Polymerization from the surface of different clusters could influence the stereoregulatity of the organic polymer chains or the interactions between them.
- The geometrically different arrangement of the unsaturated ligands on the cluster surface could influence the packing of the polymer chains between the clusters.

The properties of the hybrid polymers observed so far are typical of highly crosslinked polymers. Small amounts of the cluster (typically 0.5–2 mol%) are sufficient to achieve drastic property changes compared with the parent polymers.

Cluster-crosslinked PMMA is no longer soluble in organic solvents as the parent polymer but swells. Cluster portions as low as 0.2 mol% (and possibly lower) are sufficient to prevent dissolution of the polymer. For a given cluster type, swelling (i.e., the solvent uptake [g solvent/g polymer]) decreases as the cluster portion is increased. However, swelling, which reflects the structural changes induced by the crosslinking, correlates with neither the number of polymerizable ligands at the cluster surface nor the nuclearity of the cluster. For example, polymers crosslinked by the cluster $Ta_4O_4(OEt)_8(OMc)_4$ swell less than those crosslinked by the same

portion of $Ti_4O_2(OPr^i)_6(OAcr)_6$, although the number of (meth)acrylate ligands is smaller.

Different polymer morphologies can be obtained when the solvent is changed. When MMA was copolymerized with 1 mol% $Zr_6(OH)_4O_4(OMc)_{12}$ or $Ti_6O_4(OEt)_8(OMc)_8$ in the absence of a solvent or in benzene solution, hard transparent glasses were obtained. However, the polymer structure of the two glasses must be somewhat different because the polymer prepared without solvent swells less and takes up only half the amount of ethyl acetate compared to the polymer prepared in benzene solution. Polymerization in a heptane/benzene mixture (1:1) resulted in a colorless powder with a specific surface area of 3.2 m^2/g.[39]

The specific surface areas of the insoluble powders obtained by copolymerization of the (meth)acrylate-substituted clusters with MA also depend on the cluster proportion. For example, the BET surface area of PMA crosslinked by the $Ti_6O_4 \cdot (OEt)_8(OMc)_8$ increased from 12 m^2/g to 200 m^2/g when the cluster proportion was increased from 0.3 to 2 mol%.

All cluster-doped hybrid polymers have a higher thermal stability than the parent polymers.[21,24,39,45] This enhanced stability is again traced back to the crosslinking induced by the cluster. Cluster-free PMMA and PMA depolymerize above 330° and 230°C, respectively. Depolymerization of the polymers is suppressed with 0.5–2 mol% of cluster (depending on the cluster type) and strongly retarded by smaller portions. At higher temperatures, the polymers are oxidatively degraded in air. The amount of inorganic residue obtained after thermolysis depends of course on the employed cluster. For example, PMMA containing 1 mol% of cluster results in 2.9 wt% of inorganic residue for $Ti_4O_2(OPr^i)_6(OAcr)_6$ and 6.3 wt% for $Zr_6O_4(OH)_4 \cdot (OMc)_{12}$.

The glass-transition temperature (T_g) of PMMA (105°C), determined by DMA, increased to 127.5°C when the polymer was crosslinked by 0.3 mol% Ti_6O_4-$(OEt)_8(OMc)_8$.[45] The apparent activation energy E_a of the glass transition is 61.4 kJ/mol for the cluster-crosslinked sample compared with 57.5 kJ/mol for cluster-free PMMA. This again shows that the clusters efficiently crosslink the polymer.

The improvement of mechanical properties by incorporation of clusters was also shown for another polymer. Sol-gel processing of $(EtO)_3Si(CH_2)_3N[CH_2CH_2C(O)OCHMeCH_2OC(O)CMe{=}CH_2]_2$ followed by photochemical polymerization of the organic groups gave a glassy polymer with a flexural strength of 46 MPa and a flexural modulus of 1230 MPa. After storage in water for 7 days these values decreased to 31 and 1000 MPa, respectively. When polymerization was carried out in the presence of 10 wt% of $Zr_4O_2(OMc)_{12}$, the flexural strength was about the same (47 MPa), but the flexural modulus was increased to 1900 MPa. A second major improvement was that the cluster-crosslinked polymers do not loose their flexibility upon water storage. After storage in water for 7 days a flexural strength of 52 MPa and a flexural modulus of 1920 MPa was measured.[46]

The impedance spectra of cluster-doped PMMA classify these hybrid polymers as a good dielectric materials.[28,41,47] For example, a dielectric constant of 1.93 at 25°C and 1 kHz was found for the hybrid polymer prepared from MMA and 2 mol% of $Zr_4O_2(OMc)_{12}$, which is lower than that of cluster-free PMMA (3.0).

Dielectric spectra of the hybrid polymer showed the typical α and ß relaxations that characterize the dielectric response of the high-molecular PMMA materials. The α relaxation is associated to the conformational rearrangements of the polymer chains backbone, while the dielectric ß relaxation peak is generally ascribed to rotations of the $–COOCH_3$ side groups.

While it is rather obvious that the cluster-based hybrid polymers have different materials properties than the cluster-free polymers, a critical attitude toward the discussed hybrid polymers would be that the observed property changes are only due to the high crosslinking density and relate only indirectly to the incorporation of inorganic clusters. This issue is subject to ongoing investigations. An option that has been only scratched so far is to use clusters with interesting intrinsic properties. For example, we have prepared $Mn_{12}O_{12}(acrylate)_{16}$ from $Mn_{12}O_{12}(OOCMe)_{16}$ by exchanging the acetate ligands for acrylate ligands. Manganese oxide clusters of the general composition $Mn_{12}O_{12}(OOCR)_{16}$ have a high total spin and thus interesting magnetic properties. When $Mn_{12}O_{12}(acrylate)_{16}$ was polymerized with MMA, we obtained highly magnetic polymers due to the statistical distribution of the paramagnetic clusters in the polymer.[48]

V. SUMMARY

With the development of preparative methods for metal oxide clusters having reactive organic groups on their surface, the preparation of an interesting new type of inorganic–organic hybrid polymers is possible. A particularly easy preparation method is the hydrolysis of metal alkoxide/carboxylic acid mixtures by in situ generated water. The hybrid polymers are characterized by the presence of metal oxo clusters as structurally well defined nanosized inorganic objects that are incorporated in the organic polymers via covalent bonds. In all cases known until present, the integrity and the typical properties of the clusters are preserved upon copolymerization with organic monomers. Since the clusters are multiply substituted by reactive organic groups, highly crosslinked polymers are obtained.

The development of hybrid materials by this approach is in a rather early stage. However, the currently available results show that there is a high potential for future developments towards novel nanocomposite materials. The prefabrication of the inorganic nano-objects allows the tailoring of specific materials properties.

VI. ACKNOWLEDGMENTS

Our own work was supported by the Fonds zur Förderung der wissenschaftlichen Forschung (FWF), the Jubiläumsfonds of the City of Vienna, and the Air Force Research Office (contract F61775-02-WE037). I am very grateful to a number of excellent Ph.D.

students and postdoctoral fellows; their names are mentioned in the references. This kind of work would not have been possible without the fruitful collaboration with N. Hüsing, G. Kickelbick, H. Peterlik (Vienna, Austria), P. Fratzl (Leoben, Austria), H. Bertagnolli (Stuttgart, Germany), J. Matisons (Mawson Lakes, Australia), N. Mozner (Schaan, Liechtenstein), V. Di Noto (Padova, Italy) and F. Palacio (Zaragoza, Spain), and their coworkers.

VII. REFERENCES

1. U. Schubert, N. Hüsing, A. Lorenz, *Chem. Mater.* **7**, 2010 (1995); U. Schubert, *J. Mater. Chem.* **15** (2005), in press.
2. H. Wolter, W. Glaubitt, K. Rose, *Mat. Res. Soc. Proc.* **271**, 719 (1992); K. Rose, H. Wolter, W. Glaubitt, *Mat. Res. Soc. Proc.* **271**, 731 (1992); H. Wolter, W. Storch, H. Ott, *Mat. Res. Soc. Proc.* **346**, 143 (1994).
3. Selected references: (a) C. Sanchez, in P. Toledano, P. Griesmar, *Mat. Res. Soc. Symp. Proc.* **271**, 669 (1992). (b) R. Di Maggio, L. Fambri, A. Guerriero, *Chem. Mater.* **10**, 1777 (1998). (c) C. Sanchez, *J. Non-Cryst. Solids* **147&148**, 1 (1992). (d) N. Miele-Pajot, L. G. Hubert-Pfalzgraf, R. Papiernik, J. Vaissermann, R. Collier, *J. Mater. Chem.* **9**, 3027 (1999). (e) U. Schubert, E. Arpac, W. Glaubitt, A. Helmerich, C. Chau, *Chem. Mater.* **4**, 291 (1992). (f) C. Barglik-Chory, U. Schubert, *J. Sol-Gel Sci. Technol.* **5**, 135 (1995).
4. C. Sanchez, F. Ribot, *New J. Chem.* **18**, 1007 (1994); D. A. Loy, K. J. Shea, *Chem. Rev.* **95**, 1431 (1995). P. Judeinstein, C. Sanchez, *J. Mater. Chem.* **6**, 511 (1996).
5. F. Ribot, C. Sanchez, *Comments Inorg. Chem.* **20**, 327 (1999); G. Kickelbick, U. Schubert, *Monatsh. Chem.* **132**, 13 (2001); U. Schubert, *Chem. Mater.* **13**, 3487 (2001).
6. For example, R. Laible, K. Hamann, *Angew. Makromol. Chem.* **48**, 97(1975); X. Huang, M. J. Wirth, *Anal. Chem.* **69**, 4477 (1997); O. Prucker, J. Rühe, *Macromolecules* **31**, 602 (1998); T. von Werne, T. E. Patten, *J. Am. Chem. Soc.* **121**, 7409 (1999).
7. P. G. Harrison, *J. Organometal. Chem.* **542**, 141 (1997).
8. For example, A. Sellinger, R. M. Laine, *Macromolecules* **29**, 2327 (1996); A. Sellinger, R. M. Laine, *Chem. Mater.* **8**, 1592 (1996); C. Zhang, R. M. Laine, *J. Organomet. Chem.* **521**, 199 (1996).
9. J. J. Schwab, J. D. Lichtenhan, *Appl. Organomet. Chem.* **12**, 707 (1998).
10. For example, P. Mather, H. G. Jeon, A. Romo-Uribe, T. S. Haddad, J. D. Lichtenhan, *J. Appl. Polym. Sci.* **73**, 1993 (1999); A. Lee, J. D. Lichtenhan, *Macromolecules* **32**, 1194 (1999); J. J. Schwab, J. D. Lichtenhan, K. P. Chaffee, P. Mather, A. Romo-Uribe, *Mat. Res. Soc. Symp. Proc.* **519**, 21 (1998); T. S. Haddad, P. Mather, H. G. Jeon, A. Romo-Uribe, A. R. Farris, J. D. Lichtenhan, *Mat. Res. Soc. Symp. Proc.* **519**, 381 (1998); A. Romo-Uribe, P. T. Mather, T. S. Haddad, J. D. Lichtenhan, *J. Polym. Sci. Part B Polym. Phys.* **36**, 1857 (1998); J. Pyun, K. Matyjaszewski, *Macromolecules* **33**, 217 (2000).
11. U. Schubert, *J. Sol-Gel Sci. Technol*. **26**, 47 (2003).
12. G. J. de A. A. Soler-Illia, L. Rozes, M. K. Boggiano, C. Sanchez, C.-O. Turrin, A.-M. Caminade, J.-P. Majoral, *Angew. Chem. Int. Ed. Engl.* **39**, 4248 (2000); G. J. de A. A. Soler-Illia, E. Scolan, A. Loius, P.-A. Albouy, C. Sanchez, *New J. Chem.* **25**, 156 (2001).
13. I. Mijatovic, G. Kickelbick, U. Schubert, *Eur. J. Chem*. 1933 (2001).
14. I. Mijatovic, G. Kickelbick, M. Puchberger, U. Schubert, *New J. Chem*. **27** (in press).
15. P. Judeinstein, *Chem. Mater.* **4**, 4 (1992); P. Judeinstein, *J. Sol-Gel Sci. Techn.* **2**, 147 (1994).
16. C. R. Mayer, R. Fournier, R. Thouvenot, *Chem. Eur. J.* **6**, 105 (2000).
17. J. Livage, C. Henry, M. Sanchez, *Progr. Solid State Chem.* **18**, 259 (1988).

18. I. Gautier-Luneau, A. Mosset, J. Galy, *Z. Kristallogr*. **180**, 83 (1987). S. Doeuff, Y. Dromzee, F. Taulelle, C. Sanchez, *Inorg. Chem.* **28**, 4439 (1989).
19. G. Kickelbick, M. P. Feth, H. Bertagnolli, M. Puchberger, D. Holzinger, S. Gross, *J. Chem. Soc. Dalton* 3892 (2002).
20. G. Guerrero, M. Mehring, P. H. Mutin, F. Dahan, A. Vioux, *J. Chem. Soc. Dalton* 1537 (1999); M. Mehring, M. Schurmann, P. H. Mutin, A. Vioux, *Z. Kristallogr.* **215**, 591 (2000); M. Mehring, G. Guerro, F. Dahan, P. Mutin, A. Vioux, *Inorg. Chem.* **39**, 3325 (2000); P. H. Mutin, M. Mehring, G. Guerrero, A. Vioux, *Mat. Res. Soc. Symp. Ser.* **628,** CC2.4.1 (2001).
21. B. Moraru, N. Hüsing, G. Kickelbick, U. Schubert, P. Fratzl, H. Peterlik, *Chem. Mater.* **14**, 2732 (2002).
22. G. Kickelbick, U. Schubert, *Eur. J. Inorg. Chem.* 159 (1998).
23. G. Kickelbick, U. Schubert, *Chem. Ber.* **130**, 473 (1997).
24. G. Trimmel, S. Gross, G. Kickelbick, U. Schubert, *Appl. Organomet. Chem.* **15**, 401 (2001).
25. S. Gross, G. Kickelbick, M. Puchberger, U. Schubert, *Monatsh. Chem.* **134**, 1053 (2003).
26. B. Moraru, S. Gross, G. Kickelbick, G. Trimmel, U. Schubert, *Monatsh. Chem.* **132**, 993 (2001).
27. L. G. Hubert-Pfalzgraf, V. Abada, S. Halut, J. Roziere, *Polyhedron* **16**, 581 (1997); N. Stenou, C. Bonhomme, C. Sanchez, J. Vaissermann, L. G. Hubert-Pfalzgraf. *Inorg. Chem.* **37**, 901 (1998).
28. S. Gross, V. DiNoto, G. Kickelbick, U. Schubert, *Mat. Res. Soc. Symp. Proc.* **726**, Q4.1.1 (2002).
29. B. Moraru, G. Kickelbick, U. Schubert, *Eur. J. Inorg. Chem.* 1295 (2001); M. Jupa, G. Kickelbick, U. Schubert, *Eur. J. Inorg. Chem.* 1835 (2004).
30. C. Sanchez, P. Toledano, P. Griesmar, *Mat. Res. Soc. Symp. Proc.* **271**, 669 (1992).
31. M. Chatry, M. Henry, C. Sanchez, J. Livage, *J. Sol-Gel Sci. Technol.* **1**, 233 (1994).
32. G. Kickelbick, D. Holzinger, C. Brick, G. Trimmel, E. Moons, *Chem. Mater.* **14**, 4382 (2002).
33. U. Schubert, Y. Gao, F. R. Kogler, unpublished data.
34. F. R. Kogler, M. Jupa, M. Puchberger, U. Schubert, *J. Mater. Chem.* **14**, 3133 (2004).
35. Y. Gao, D. S. Dragan, M. Jupa, F. R. Kogler, M. Puchberger, U. Schubert, *Mat. Res. Soc. Symp. Proc.* **847** (2005), in press.
36. C. R. Mayer, R. Thouvenot, T. Lalot, *Chem. Mater.* **12**, 257 (2000).
37. C. R. Mayer, V. Cabuil, T. Lalot, R. Thouvenot, *Angew. Chem. Int. Ed. Engl.* **38**, 3672 (1999).
38. G. Trimmel, P. Fratzl, U. Schubert, *Chem. Mater.* **12**, 602 (2000).
39. U. Schubert, G. Trimmel, B. Moraru, W. Tesch, P. Fratzl, S. Gross, G. Kickelbick, N. Hüsing, *Mat. Res. Soc. Symp. Proc*. **628**, CC2.3.1 (2001).
40. G. Trimmel, S. Gross, G. Kickelbick, U. Schubert, *Appl. Organomet. Chem.* **15**, 401 (2001).
41. S. Gross, V. Di Noto, U. Schubert, *J. Non-Cryst. Solids* **322**, 154 (2003).
42. B. Moraru, G. Kickelbick, M. Batistella, U. Schubert, *J. Organomet. Chem.* **636**, 172 (2001).
43. G. Kickelbick, M. P. Feth, H. Bertagnolli, B. Moraru, G. Trimmel, U. Schubert, *Monatsh. Chem.* **133**, 919 (2002).
44. V. Torma, N. Hüsing, H. Peterlik, U. Schubert, *C. R. Chimie* **7**, 495 (2004).
45. Y. Gao, N. R. Choudhury, J. Matisons, U. Schubert, B. Moraru, *Chem. Mater.* **14**, 4522 (2002); Y. Gao, F. R. Kogler, U. Schubert, *J. Polymer Sci. A*, submitted.
46. U. Schubert, T. Völkel, N. Moszner, *Chem. Mater.* **13**, 3811 (2001).
47. G. Trimmel, B. Moraru, S. Gross, V. Di Noto, U. Schubert, *Macromol. Symp.* **175**, 357 (2001); S. Gross, G. Trimmel, U. Schubert, V. Di Noto, *Polym. Adv. Technol*. **13**, 254 (2002).
48. F. Palacio, P. Oliete, U. Schubert, I. Mijatovic, N. Hüsing, H. Peterlik, *J. Mater. Chem.* **14**, 1873 (2004).

CHAPTER 3

Metal-Containing Polydyes

Charles E. Carraher Jr.

Florida Atlantic University, Department of Chemistry and Biochemistry, Boca Raton, Florida and Florida Center for Environmental Studies, Palm Beach Gardens, Florida

CONTENTS

I. INTRODUCTION

This chapter is a review of some of our efforts aimed at incorporation of recognized commercially available dyes into metal-containing polymer backbones. It describes, briefly, our rational for synthesizing these macromolecules and, I hope,

Macromolecules Containing Metal and Metal-Like Elements, Volume 7: Nanoscale Interactions of Metal-Containing Polymers, edited by Alaa S. Abd-El-Aziz, Charles E. Carraher Jr., Charles U. Pittman Jr., and Martel Zeldin.

will create ideas for the reader to expand this potentially exciting area of research. While we have made a number of metal-containing dyes, the present focus is on those containing transition metals. These metal–dye containing macromolecules are given the name *polydyes*.

II. GROUP IVB–CONTAINING POLYDYES

The cyclopentadienyl derivatives of titanium, zirconium, and hafnium were first described by Wilkinson and coworkers in the early 1950s.[1] These compounds have a tetrahedral geometry, possess a high degree of covalent character and behave like organic acid chlorides in condensation polymerization reactions. Group IVB metallocene–containing materials are known to be active catalytic sites and to offer potentially useful photonic and other properties.[2–6]

Overall this project area is aimed at managing light, to either concentrate light or to disperse it. "Normal" and laser light is of interest. One goal is to couple known light-harvesting units in a polymer chain with those that disperse light. Group IVB metallocenes are known to "attract" or harvest light, mainly in the visible and UV regions. They are sometimes referred to as UV "sinks" because of their ability to absorb UV radiation without being degraded. This ability to absorb light and then give it off again has many potential uses, including allowing energy absorbed in a coating to be reemitted at a specific wavelength. This could allow the coating to cure at greater depths and more rapidly. The absorption of light energy by a coating may also be part of an overall effort to harvest radiation to heat and supply energy (including electrical energy) to a dwelling.

A number of dyes were examined.[6–15] Since the usual mode of employed synthesis involves Lewis acid–base reactions, employing solution and interfacial systems, dyes that had two Lewis base sites were generally used. Reaction systems were employed that allowed the rapid room-temperature synthesis of the products while minimizing unwanted rearrangement and degradation.

Another attraction for including dyes into polymers is the (potential) permanent, nonleaching nature of such polymer-containing dyes. This would allow a material that contains a polydye to remain colored for longer times even in solids such as plastics. Migration and loss of colorants occurs even in solids such as plastics. The ability to retain color or other important additive properties is especially important in marine coatings applications, where leaching and subsequent loss is aided by the ever present aqueous environment.

The actual structures of dyes vary with pH. This is shown in scheme 1 for fluorescein.

For dyes with structures similar to fluorescein and sulphonephathalein, two types of reactive sites are present throughout much of the pH range. They can exist as acids or their conjugate bases, the RO^- and $RCOO^-$ (for the fluorescein) or RSO_3^- (for the sulphonephthalein dyes). Since they react similarly, only the fluorescein

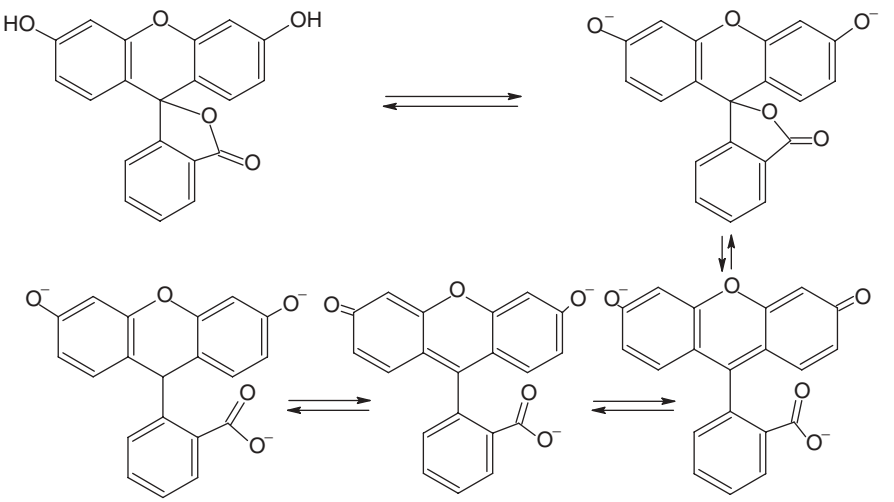

Scheme 1

example will be described here. There are two RO^- groups and one $RCOO^-$. Spectral results are consistent with reaction occurring at one of the RO^- sites and at the $RCOO^-$. It is not clear why this is so but it may involve the fact that once one enol site is reacted, it locks the second site into the nonreactive keto form. Because hydrolysis of organic acid chlorides occurs rapidly, reaction with organic acid chlorides and these dyes results in the production of only the organic acid. (Reaction of similar dyes with organic acid chlorides occurs but not under the conditions employed for the metal-containing polydyes. Here, it is believed that reaction occurs through both RO^- groups and not the $RCOO^-$.[16])

Group IV metallocene dichlorides hydrolyze more slowly than organic acid chlorides. When they hydrolyze they form metallocene aquo derivatives. This aquo form is stable for several hours in the reaction solution. Both the solution and interfacial reactions employed for polydye formation are rapid, occurring within less than a minute, generally within a few second. In fact, because the titanocene dichoride has two color sites—the Ti-Cp yellow and Ti-Cl red—reaction times can be measured by simply noting the time required for color changes to occur. This has been more fully described.[17–24] Thus the reaction with Group IVB metallocene dihalides gives oligomeric to polymeric polydyes by which the dye is incorporated as part of the polymer backbone.

Xanthene dyes have various uses. They are used in the textile field as colorants, as cosmetic colorants, as laser dyes, and in coloring paper. Their good fluorescent behavior make them useful in such specialities as the production of theatrical effects in textiles, in fluorescent sign printing inks, to impart fluorescence

to mineral oils, to locate flaws in metal castings, and to detect water seepage. They are also employed as biological stains, fungicides, and photographic sensitizers. Sulphonephthalein dyes are also widely used and exhibit a relatively high color intensity.

The structure of the polymer produced by reacting titanocene dichloride and phenylsulfonphthalein is given as **1**.

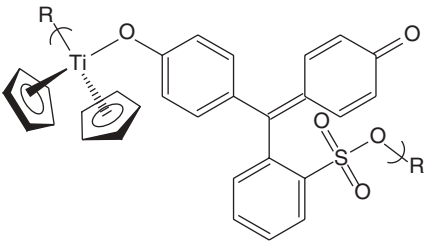

1

The structure of the polymer produced from titanocene dichloride and the xanthene dye Erythrosine B is given as **2**.

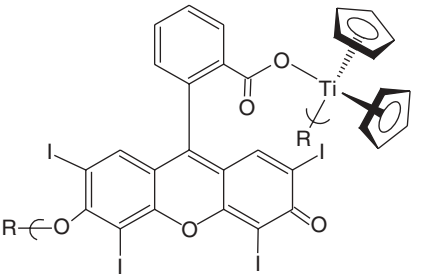

2

Along with the xanthene and sulphonephthalein dyes, a number of other dye types were incorporated into polymeric backbones. These include a number of azo dyes, characterized by the presence of the -N=N- unit. Azo dyes form the largest and most versatile class of commercial dyes. Azo dyes are used in the dyeing of wool, paper, cotton, silk, leather, synthetic fibers such as nylon and viscose rayon; for coloring of plastics, inks, rubber, foods, coatings, drugs, cosmetics, and varnishes. Sample examples are given below to illustrate the wide variety of azo dye structures that can be easily incorporated into polydyes. The polymer from titanocene dichloride and the azo dye Orange B is given as **3**.

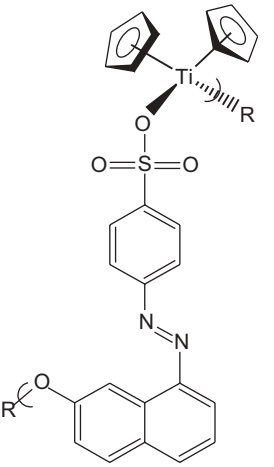

3

The polymer from the azo dye Flavazine L with zirconocene dichloride is given as **4**.

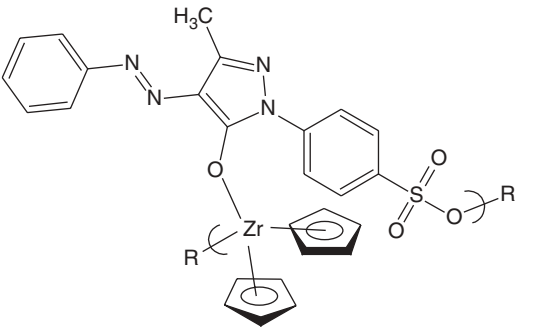

4

The polymer product of hafnocene dichloride and Acid Yellow 33 is given as **5**.

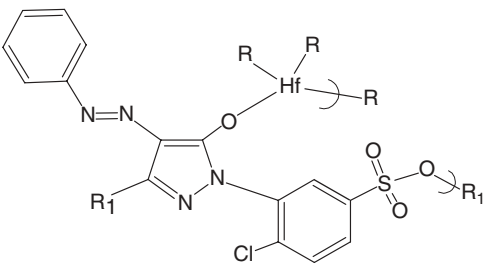

5

Other related dyes were also successfully incorporated as polydyes including nigrosine, **6**.

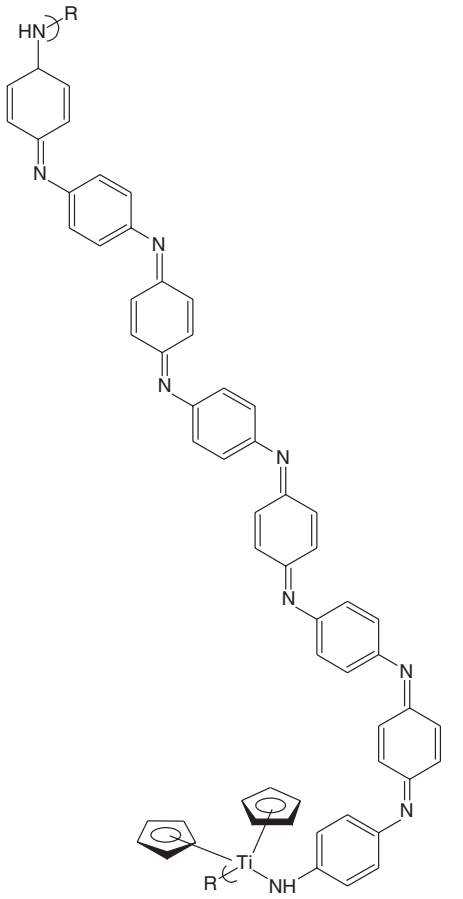

6

Indigo Carmine has also been incorporated as a polydye, **7**.

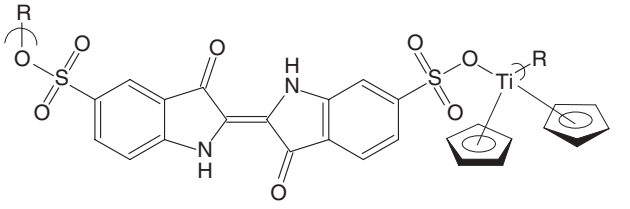

7

The structure of the polydye formed from titanocene dichloride and Eriochrome Black T is given as **8**.

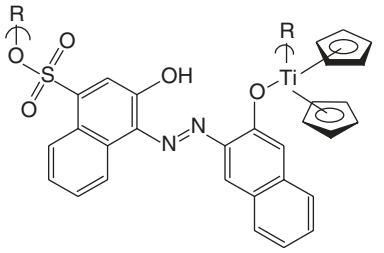

8

Most of these dyes have only two active functional groups that could bind to the metal. However, the Eriochrome Black T has three, two aromatic phenols and a sulfonate grouping. These products probably contain some crosslinking, but they are soluble in DMF, DMSO, and TEP consistent with either a small amount of crosslinking or that the sulfonate to metal bond dissociates reversibly in these polar solvents.

Product yield for a series of Xanthene dyes follows the trend:

$$\text{Erythrosin B} > \text{Eosin Y} > \text{Fluorescein} > \text{Bengal Red B} > \text{Phloxine B}$$

which approximates the order of decreasing nucleophilicy of the reaction sites consistent with a somewhat straightforward S_n2 or associative reaction scheme.

The polydyes were generally soluble in dipolar aprotic liquids such as HMPA, DMF, DMSO, and TEP. Polydye solutions were used to impregnate a number of items including plastics (polyethylene, polycarbonate, polypropylene, poly(vinyl chloride), polystyrene, nylon 6,6, and SAN), cloth (cotton, denim, and 50–50% polyester fabric), paper, films, and coatings.

Simple dye solutions were compared to solutions containing the polydye. After several days to months, the color of the monomeric dye solutions greatly decreased. By comparison, the polydyes retained decent color for a year under fluorescent lighting. Exposure to outdoor light hastened deterioration of the color of both the dye and polydye solutions. Thus incorporation into a polymer appears to lock in the dye structure and gives it some added stability to ordinary indoor light. In the dark, polydye solutions have remained fluorescent and colored now for 25 years.[15]

Studies were undertaken using an Argon Ion laser operated at 514.5 nm (visible green) as the high energy source. Optically transparent films were cast. The presence of polydye in the samples caused significantly shorter (such as almost 10 times shorter) "burn-through" times compared with those containing an equal amount of the dye.[14] In this study, the polydyes acted to concentrate the radiation dramatically decreasing the burn-though times. By comparison, similar samples except exposed to energy from a carbon dioxide laser operating in the infrared region (1.06 microns; 1060 nm).[6] Here burn-through times were significantly greater. Under these experimental conditions,

the polydyes acted as dispersing agents. The films contained from 10 to 100 ppm of the polydye.

In another set of experiments using the carbon dioxide laser, wood was coated with latex paint containing about 200 ppm polydye. The wood was exposed to laser light in the IR region. In comparison to nonimpregnated latex coatings, the polydye-containing samples exhibited equal and greater burn-through times. Similar results were found for plastics doped with polydyes.[6,15]

The behavior was dramatically different, depending on the frequency range of radiation employed. Thus in the IR region the polydyes act as dispersing agents protecting the material that is coated with it or that contains it. In the visible-UV region the polydye acts as a concentrating agent, enhancing the effect of the radiation.

Each tendency offers industrially important opportunities. For instance, chip fabrication might be enhanced through addition of some polydyes that would allow fabrication through use of lasers employing lower energies. The use of lower energies would result in lower temperatures that, in turn, would protect the chip from thermal induced deterioration at the same energy, though-put would be increased. A similar advantage is achieved when cutting or etching occurs. In contrast, greater stability is needed in some applications to resist potentially damaging laser radiation.

In a nonrelated study, some of the polydyes were tested for their ability to inhibit human Balb 3T3 cells. A variety of polydyes were tested. Those from the Group IVB metallocenes showed little or no inhibition at a level of 12.5 μg/mL. However, similar polydye-containing materials derived form diphenyltin showed good activity to 3 μg/mL and below, making them candidates for further testing in the fight against cancer.[25] These results are consistent with the Group IVB metallocene polydyes having a low toxicity.

III. RUTHENIUM-CONTAINING POLYDYES

Ruthenium-containing polydyes is the focus of this section. Another chapter in this series, (in volume 5) details the use of ruthenium-containing coordination polymers in solar energy conversion efforts. These two chapters describe two major aims: first, modification of the accepting and emitting energies of the ruthenium center and, second, to assist in attracting light that can be subsequently harvested by the ruthenium center, thus increasing the converted quantum yield of harvest light. The current effort is aimed at incorporating dyes into the ruthenium-containing polymers.[26–31]

Polymers were synthesized from the reaction of cis-dichloro-bis(2′2-bipyridine)-ruthenium II, $Ru(bipy)_2Cl_2$, with dyes which were suspended in an 80% by volume methanol aqueous solution. This mixture was reflexed on a steam bath for about six hours, after which the methanol allowed to evaporate. The reaction mixture was cooled over night. The solution was washed with benzene to remove unreacted diamine and washed with chloroform to remove unreacted $Ru(bipy)_2Cl_2$. The remaining liquid was removed under vacuum giving the polymer as a solid, generally in good yield.

The polymer, **9**, from $Ru(bipy)_2Cl_2$ and 6-butoxy-2,6-diamino-3,3′-azodipyridine, diazopy is produced in 89% yield. It is soluble in DMSO, methanol, ethanol, and slightly soluble in chloroform. It is insoluble in benzene, carbon tetrachloride, acetone,

and hexane. It has a molecular weight of 1.4×10^5 Daltons which corresponds to a degree of polymerization of about 180.

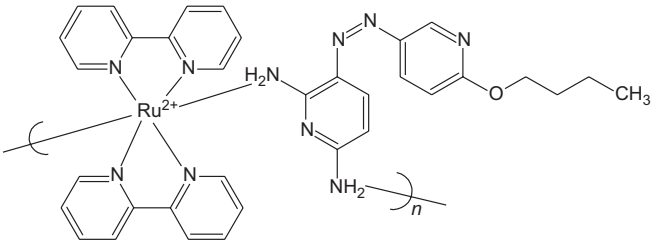

9

The type of bonding between the ruthenium and the amine dye is coordination. The UV–Vis results are an important aspect to light harvesting. Spectra were obtained in DMSO.

The $Ru(bipy)_2Cl_2$ has an octrahedral geometry with absorption bands at 557, 379, and 300 nm with the 300 nm band being the λ_{max} absorption in the middle of the UV region. These bands are associated with a eg to t_2g d-electron transition. Substitution of the chloro ligands by amines should cause a change in the energy for d-electrons to undergo an eg to t_2g transition.

The diazopy dye itself has two bands at 291 nm, and the λ_{max} absorption band is at 454 nm. The polymer product shows a number bands, with the bands appearing at 495, 437, 355, 328, 295, 266, and 252 nm. There is a broad band on the higher side of 500 nm that probably corresponds to the 557 nm band found in $Ru(bipy)_2Cl_2$. The λ_{max} band for the dye that appeared at 454 nm is now at 437 nm, still in the blue region of visible light. The λ_{max} for $Ru(bipy)_2Cl_2$ that appeared at 300 nm is now at 295 nm for the polymer.

The polymer from $Ru(bipy)_2Cl_2$ and diazopy has all the bands from the two reactants essentially the same except for the λ_{max} band for the dye at 454 nm, which is missing. However, the bands are broader for the polymer and the 454 nm band is now probably lost within this broadening caused by the $Ru(bipy)_2$ moiety. The product also contains a large peak at 295 nm. The 295 nm band is the λ_{max} for the product, as is the 300 nm for $Ru(bipy)_2Cl_2$. There are also broad peaks at 355 nm and 495 nm and a less intense peak at 252 nm. It is interesting, that the λ_{max} for the dye itself at 454 nm now corresponds to a much smaller peak at 437 nm.

A similar polydye, **10**, was formed from the reaction of $Ru(bipy)_2Cl_2$ and N,N′-bis(3-aminophenyl)-3,4,9,10-perylenetetracarboxylic diimide. This product was formed in 85% yield and had a DP of 33,000 by light-scattering photometry.

A brief presentation of the UV–Vis spectrum of the monomers and polymer from the diimide product follows. As noted above, $Ru(bipy)_2Cl_2$ has bands at 557, 379, and 300 nm. The diimide shows a band at 529 nm. The Ru-diimide polymer has adsorption bands at 529, 429, 373, and 299 nm. The bands at 373 and 299 nm are derived from the Ru-dibypy moiety, whereas the band at 529 nm is derived from the diimide moiety. The 299 nm band is the λ_{max} absorption band. The band at 429 nm is a new combination band.

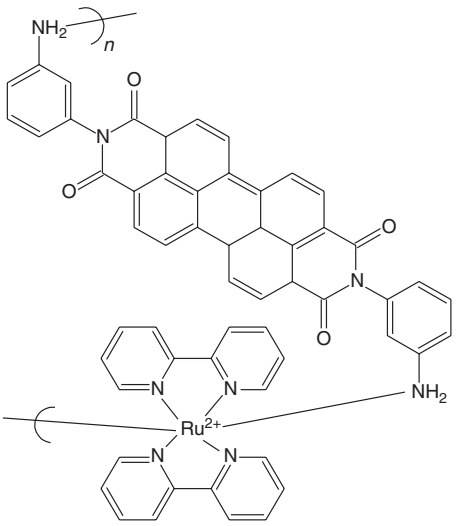

Product of $Ru(bipy)_2Cl_2$ and N, N'-bis(3-aminophenyl)-3,4,9,10-perylenetetracarboxylic diimide

10

The broad spectral bands of the polymer may be viewed as positive with respect to the polymer accepting a wide range of light wavelengths. Emission spectra were not taken of the materials.

Similar products will continue to be studied as the search for using solar energy continues.

IV. HEMATOPORPHYRIN-CONTAINING POLYDYES

While much of our work has focused on the optical properties of polydyes, other properties have also been examined. Here one other area will be noted.

Porpyrins are an essential part of light harvesting by plants. However, there is an increasing interest in understanding and accomplishing selective separations on a molecular level employing constrained chelating sites such as those found in porphyrins. Some of this effort is aimed at looking at natural and natural-like materials such as the porphyrins that selectively uptake metal ions that eventually perform selective functions. It should be possible to synthesize porphyrin-containing assemblies that selectively bind ions that subsequently perform specific functions. These functions include selective catalytic, electrical, binding, and photon activities. It may be possible to construct materials that contain several important sites by combining porphyrins with other moieties that can also exert specific behaviors. Each site can perform a separate or related activity, including light harvesting and catalysis.

Porphyrins are heterocyclic compounds containing pyrrole units. They constitute major components in the human body and within plants and are essential agents for life. For instance, the iron–hematoporphyrin complex is the active component of

hemoglobin and serves as the site for oxygen transfer. Another important porphyrin is the cobalt-porphyrin complex, which is know as vitamin B_{12}. Chlorophyll is a magnesium–porphyrin derivative.

Hematoporphyrin IX (HPIX) was the first porphyrin isolated from natural materials, obtained by the sulfuric acid treatment of blood. HPIX, and some derivatives, are commercially available and have been reported to offer a wide variety of uses. They are used as sensitizes in cancer physiotherapy.[32] These compounds are selectively concentrated by neoplastic tissues, and accordingly the tumors can be distinguished by selective fluorescence under UV light.

HPIX is a macrocyclic "tetrapyrrole" structure with four methyl, two propionic acid, and two ethanolic sidechains. The two propionic acid and two ethanolic chains react with Group IVB metallocene dichlorides, giving crosslinked polymers as **11.**

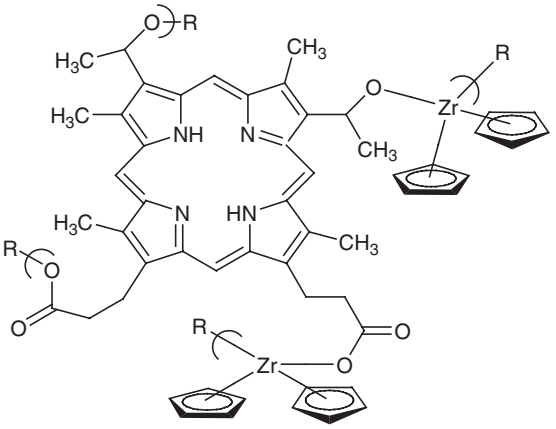

11

HPIX is one of the most unstable of the natural porphyrins commonly employed in the laboratory because of the presence of labile hydroxyethyl sidechains.[33] Thus synthesis of polymers from HPIX must be accomplished rapidly and under mild conditions.

In the present study Ni ion is being absorbed. The adsorbent species (solid phase) are the three Group IVB products obtained from the interfacial polycondensation reaction between HPIX and the Group IVB metallocene dichlorides[34–36] and two commercially available ion exchange resins. Adsorption is the physical or chemical bonding to the surface.

Porphyrin-containing materials are known to retain selected metal ions through chelation and through adsorption involving the pi electron cloud. Porphyrin polymeric materials may offer advantages in comparison to the monomeric porphyrin, because of the added structural features within the polymeric structures. Three major ions known to be retained by porphyrins in general are zinc, copper, and nickel.

Metal ion incorporation into porphyrin molecules is believed to occur through an intermediate, called the sitting-atop-complex, SAT.[37] The metal ion rests on top of the porphyrin before it is completely incorporated. This mechanism has been verified by UV and IR spectroscopy. The active species involved in metal

incorporation are the metal cation and the neutral porphyrin.[38] For chelation to occur, the porphyrin must be in the liquid state. Since the polymers are insoluble, chelation studies were not performed, rather liquid–solid interface metal adsorption studies were carried out.

Adsorption processes depend on the chemical and physical properties of the phases, interfaces, and adsorptives. The solid or bulk phase is critical in controlling the adsorption process. The physical composition of the solid surface also plays a role in adsorption. Spaces available on the surface may be of several kinds. Generally, the edges, corners, and surface defects are more exposed, giving them a higher capability to interact than less exposed portions. Thus surface roughness is important because this roughness allows more exposure of the solid to the metal ion.

Coulombic and polar factors can also influence absorption. For instance, if the surface of the adsorbent molecules are polarizable and the molecules of the adsorptive contain permanent dipoles, then an interaction between the two favor adsorption.

The surface area and specific surface area for the metallo-porphyrin polymers and two commercially available resins was determined. The surface area of the commercially available resins is much greater than the surface areas of the polymers. This is mainly due to a designed high degree of porosity present in these the two resins.

Metal adsorption studies were performed by treating the polymeric materials with solutions of nickel acetate at known concentrations followed by a determination of the concentration of the nickel solution after equilibrium was reached. The exchange capacity of two commercially available resins was also determined. Results appear in Table 1.

Table 1 Adsorption of Nickel Plus Two Ions[36]

	Ni^{+2} Adsorbed		
Material	mmole	mmole/gram of Resin Used	mmole/cm^2 Specific Surface Area
Ti	2.02×10^{-5}	2.02×10^{-4}	306
Zr	0.00	0.00	0.00
Hf	0.00	0.00	0.00
Dowex 50 × 8-200[a]	2.37×10^{-5}	2.37×10^{-4}	1.03×10^{-3}
Amberlite MB1[b]	2.31×10^{-5}	2.31×10^{-4}	1.21×10^{-3}

[a]Initial nickel ion concentration = 2.77×10^{-5} mmole
[b]Initial nickel ion concentration = 2.59×10^{-5} mmole

The results are consistent with the titanocene product having a greater exchange capacity efficiency than either of the two commercial resins. It must be remembered that these studies were performed at low concentrations of the nickel ion, which may correspond to the lower region of equilibrium concentration of an

isotherm. It is possible that if the study was performed at saturated equilibrium concentrations, the exchange capacity for the commercial resins would be higher than the values found for the titanocene product. Even so, under the employed conditions the titanocene product out performed the commercial resins.

V. SUMMARY

The use and diversity of metal-containing polydyes has only been touched, and a large potential exists for medical, electronic, catalytic, photonic, and separations applications. There exists a large number of degrees of freedom with respect to the choice of the metal, metal oxidation number, combination of metals, and dyes and the use of combinations of dyes. This allows those with a good imagination to see a whole host of problems where such metal-containing polydyes might offer a solution.

VI. REFERENCES

1. G. Wilkinson, P. Pauson, J. Birmingham, F. A. Cotton, *J. Am. Chem. Soc*. 75, 1011 (1953).
2. C. Carraher, *Polymer Chemistry*, Dekker, New York, 2003.
3. J. C. Chien, *Homogeneous Polymerization Catalysis*, Prentice-Hall, Englewood Cliffs, NJ, 1993.
4. W. Kaminsky, H. Sinn, *Transition Metals and Organometallics as Catalysts for Olefin Polymerization*, Springer-Verlag, New York, 1988.
5. C. Carraher, R. Linville, T. Manek, H. Blaxall, R. Taylor, L. Torre, in *Conductive Polymers*, R. Seymour, ed., Plenum, New York, 1984.
6. C. Carraher, V. Foster, R. Linville, D. Stevison, R. Venkatachalam, in *Adhesives, Sealants, and Coatings for Space and Harsh Environments*, L-H. Lee, ed., Plenum, New York, 1988.
7. C. Carraher, R. Schwarz, M. Schwarz, J. Schroeder, *Org. Coat. Plast. Chem*., **42**, 23 (1980).
8. C. Carraher, R. Schwarz, M. Schwarz, J. Schroeder, *Org. Coat. Plast. Chem*., **43**, 798 (1981).
9. C. Carraher, J. Kloss, *PMSE*, **64**, 229 (1991).
10. C. Carraher, R. Schwarz, J. Schroeder, M. Schwarz, *J. Macromol. Sci.-Chem*., **A15**(5), 773 (1981).
11. C. Carraher, R. Schwarz, J. Schroeder, M. Schwarz, in *Interfacial Synthesis, Vol. III: Recent Advances*, C. Carraher, J. Preston, eds., Dekker, New York, 1982.
12. C. Carraher, V. Foster, R. Linville, D. Stevison, *PMSE*, **56**, 401 (1987).
13. C. Carraher, A. Li, J. Kloss, A. Lombardo, *PMSE*, **70**, 38 (1993).
14. C. Carraher, J. Kloss, F. Medina, A. Taylor, *PMSE*, **68**, 253 (1993).
15. C. Carraher, unpublished data.
16. P. W. Morgan, *Condensation Polymers by Interfacial and Solution Methods*, Wiley, New York, 1965.
17. C. Carraher, S. T. Bajah, *Polymer*, **15**, 9 (1974).
18. C. Carraher, L. Torre, H. M. Molloy, *J. Makromol. Sci.-Chem*., **A15**, 757 (1981).
19. C. Carraher, S. Jorgensen, *J. Polym. Sci*., **16**, 2965 (1978).
20. C. Carraher, R. Nordine, *Makromol. Chemie*, **164**, 87 (1973).

21. C. Carraher, R. Nordin, *J. Polym. Sci. A-1*, **10**, 521 (1972).
22. C. Carraher, S. T. Bajah, *Br. Polym. J.*, **7**, 155 (1975).
23. C. Carraher, R. Frary, *Makromol. Chemie*, **175**, 2307 (1974).
24. C. Carraher, S. T. Bajah, *Polymer*, **14**, 42 (1973).
25. D. Siegmann-Louda, C. Carraher, J. Lupo, D. Sneeden, J. Ross, *PMSE* (in press).
26. C. Carraher, Q. Zhang, *Metal-Containing Polymeric Materials*, Plenum, New York, 1996, 109.
27. C. Carraher, A. Taylor-Murphy, PMSE, **76**, 409 (1997).
28. C. Carraher, A. Taylor-Murphy, *PMSE*, **86**, 291 (2002).
29. C. Carraher, Q. Zhang, *PMSE*, **73**, 398 (1995).
30. C. Carraher, Q. Zhang, *PMSE*, **71**, 505 (1994).
31. C. Carraher, Q. Zhang, C. Parkanyi, *PMSE*, **71**, 398505 (1994).
32. T. Dougherty, J. Kaufman, A. Goldfarb, K. Weishaupt, D. Boyle, A. Mittleman, *Cancer Res.* **38**, 2628 (1987).
33. K. Saitoh, J. Sugiyama, N. Suzuki, *J. Chromatogr.,* **358**, 307 (1986).
34. C. Carraher, J. Haky, A. Rivalta, D. Sterling, *PMSE*, **70**, 329 (1993).
35. C. Carraher, A. Rivalta, J. Haky, *PMSE*, **74**, 149 (1996).
36. C. Carraher, A. Rivalta, J. Haky, *Functional Condensation Polymers*, Kluwer New York, 2002.
37. E. B. Fleischer, J. H. Wang, *J. Am. Chem. Soc*., **82**, 3498 (1960).
38. D. Dolphin, *The Porphyrins, Vol. V: Physical Chemistry Part C*, Academic Press, New York, 1978.

CHAPTER 4

Metallopolymer Nanocomposite–Macromolecular Metallocomplexes as Precursors for Polymers, Polymer Inorganics, and Bionanocomposites

A. D. Pomogailo

Institute of Problems of Chemical Physics, Russian Academy of Sciences, Chernogolovka, Moscow Region, Russia

CONTENTS

Macromolecules Containing Metal and Metal-Like Elements, Volume 7: Nanoscale Interactions of Metal-Containing Polymers, edited by Alaa S. Abd-El-Aziz, Charles E. Carraher Jr., Charles U. Pittman Jr., and Martel Zeldin.

I. INTRODUCTION

Major discoveries of the 20th century can be mainly related to nuclear power engineering, space exploration, and development of nanomaterials. Even if the former two items seem to be taken for granted, the latter is highly disputable since all fields have made fundamental contributions to the breakthroughs in science. Speaking in support of nanomaterials, the nanoworld is extremely broad. It is practically impossible to find any field in the natural sciences that is not in some way or another connected with nanostructures. Such terms as *nanophase*, *nanohybrid*, *nanocrystalline*, *nanoporous* materials, *nanochemistry*, *nanophysics*, *nanostructures*, *nanocrystals*, *nanophase* geometry, *nanosize* hierarchy and architecture, *nanostructured* organic networks, molecular and *nanolevel* design, and *nanotechnology* are currently most frequently cited in the scientific literature as applied to the scale and dimensional phenomena.

The particles participating in various biological processes—including supramolecular functional systems to which belong enzymes, liposomes, and cells—occupy a peculiar place in nanochemistry. Also included as nanomaterials are fullerenes and nanotubes. These materials are used in a number of new reactions, catalytic and sensor systems, fabrication of new compounds and nanocomposites with previously unknown properties. They are a part of materials for microelectronics, structures with nanogeometry for information-recording systems, and are used to transform various solar radiations. In biology and medicine they are novel medicinal preparations and their carriers to human organs.

Nanos means "dwarf" in Greek. A nanometer (nm) equals 10^{-9} m. Materials whose individual crystallites or phases making up their structural base (small forms of a substance) are below 100 nm in size in at least in one dimension are called nanostructures. This limit is conditional and is accepted for convenience. The portion of the regions bordering on disordered structures becomes perceptible at this size. It correlates with the characteristic size of many phenomenon (see further). Different metals and their oxides differ in their limiting values characteristic for various physical properties. This ensures certain conventionality for use of the 100 nm value. An important place is occupied in nanochemistry by the particles participating in various biological processes, including supramolecular functional systems to which belong enzymes, liposomes, and cells. The relationship between materials science and the science about nature becomes more and more evident.

The assertions that science and engineering of the 21st century will acquire a nano and angstrom character have proved to be a reality. The limits of miniaturization of separate elements (e.g., density of arranging crystals in microelectronics)

have already been attained in many techniques. This challenges us to search for alternative procedures. For example, fabrication of modern chips is based on planar techniques. A combination of nanolithography (formation of surface drawings as lines and dots at a nanolevel) and etching is employed. Recently developed lithographic procedures are used to reduce their size still more. For example, electronic, ion-beam, and x-ray methods and dry etching—including plasma-chemical, reactive, and ion etching—have advanced. These procedures now reach below the 100 nm size for fabricating components in optoelectronic chips.

Nanophase material science differs from traditional areas by the creation of new principle materials and because of the necessity of designing corresponding instruments for manipulating such materials. Among most promising nanotechnologies for metallic materials are micrometallurgy and nanometallurgy, the laser treatment of material surfaces whose thickness is limited to a few hundreds or tens of nanometers and various kinds of nanoceramics.

The development of fundamentally new structural materials requires achieving functional parameters that are conditioned by the properties of microdomains and developing processes at the atomic and molecular level, in monolayers and nanovolumes.

The science of dealing with nanocomposites, which belongs to the class of composite materials characterized by the nanometer sizes of their structural elements (particles of metals, metalloids, their oxides, chalcogenides, etc.), has arisen in recent years on the borders of different areas of knowledge. In the literature, the terms *hybrid nanocomposites*, *nanohybrids*, and *nanostructural composites* are generally used, and the terms *metallomatrix composites*, *monophase hybrids*, etc. are more rarely used when describing materials consisting of an organic phase (polymer) and a nanodispersed mineral phase. If a polymer of biological origin serves as a component or a precursor of these polymer-inorganic materials, the term *nanobiocomposites* is used.

An organic phase can capture metal-containing particles into a trap of a peculiar kind, viz., into an oxopolymeric network or a polymeric unit with appropriate parameters. Silicon, aluminium, titanium, zirconium, vanadium, molybdenum oxides, glasses, clays, layered silicates and zeolites, metal phosphates and chalcogenides, iron oxychloride, and graphite are used as inorganic precursors. Zeolites (molecular sieves) are of particular interest since methods for controlling their pore sizes are well known. Not only carbon-chain but also organoelement (generally, organosilicon), polymers are used as a polymeric component. In the resulting nanocomposite materials, distances between networks and layers formed by polymeric and inorganic ingredients and sizes of particles formed, including metal-containing particles, are nanometric.[1–3]

Generally, hybrid nanocomposites exhibit a synergism of the properties of the initial components. These compounds are characterized by an enhanced mechanical strength and thermal stability and provide optimum heat transfer.[4,5] In metallomatrix composites, the strength and hardness of soft metals, for example, of aluminium, are enhanced. These materials possess good thermochemical, rheological, electrical, and optical properties.[6–8] These compounds are used as chromatographic carriers, membrane materials,[9] optical and magnetic materials, components of polymeric compositions, and carriers and catalysts of various reactions.

Currently, numerous procedures for the preparation of nanocomposite materials are available. Recently, the major synthetic approaches (e.g., evaporation of elemental metal with its deposition on polymeric matrices, plasma-induced polymerisation, vacuum evaporation of metals, thermal decompositions of precursors in the presence of polymers, and reduction of metal ions using different procedures including electrochemical) have been surveyed in books and reviews.[1–3] However, the uniform distribution of ingredients is generally difficult to achieve when hybrid nanocomposites are prepared with the use of the above-mentioned procedures resulting in the nonuniformity of the properties of the material. The following three principal procedures are most commonly employed:

1. The sol-gel method.
2. The intercalation of polymers and nanoparticles into layered structures (including polymerization in situ) using approaches applied in the chemistry of intracrystalline structures ("guest-host" systems).
3. A combination of polymerization and formation of nanosize particles, which provides homogeneous dispersion of an inorganic component (which is often a specific filler) in a polymeric matrix.

In the last decade, these procedures, particularly the first and second methods, have received primary attention. The properties and procedures for the synthesis of metallopolymeric Langmuir-Blodgett (LB) films are being extensively studied. The results of investigations in this field are summarized in a number of monographs and reviews[10–34] as well as in special issues of journals. Note that nanocomposites containing not only synthetic but also natural molecules, including biologically active macromolecules, can be conveniently prepared using the above procedures. These procedures have been used for constructing biosensors, enzyme electrodes and other materials based on enzymes. These materials have already found use in biochemistry, medicine, biotechnology, and the technology of environmental control.

In this chapter, procedures for the preparation of metallopolymer nanocomposites of different types, especially hybrid organic–inorganic ones, are considered from a unified viewpoint and the generality of the processes of their formation in living and nonliving natural objects is demonstrated. This review surveys fresh results and those generally published within the last decade.

II. GENERAL CHARACTERISTICS, CLASSIFICATION OF NANOPARTICLES BY SIZE, STRUCTURAL ORGANIZATION, AND DIMENSIONAL PHENOMENA

Ultradispersed particles can be subdivided by size into three types.[35] (1) nanosize or ultradispersed to about 1–50 nm particles, (2) highly dispersed of 30–500 nm size, and (3) micron size (flocculi) of 100–1000 nm. The micron size

particles consist, as a rule, of individual particles or their agglomerates, representing either monocrystals or polycrystals of the fractal type. The former two types of particles are colloidal and the latter are coarse-dispersed particles.

Aerosol particles of metals of ~50 nm size prepared in normal conditions are spherical or nearly spherical owing to high surface energy of fine particles.[36]

As for the terminology, the most frequently used terms are *ultrasmall particles* and *nanocrystals* to denote nanoparticles of metals whose diameter is within 2–5 to 50 nm, as well as colloidal crystallites and subcolloidal particles. The upper threshold of the size of semiconductin nanocrystals in polymer matrices is the condition that allows for the optical homogeneity of compositions (no scattering by the environment at particle size below a quarter of the light wavelength). The lower boundary is conditioned by the existence of crystalline particles at the interface between the crystalline phase and the quasi-molecular one. Less often the terms *molecular aggregation* and *crystallite clusters* are used.

It is accepted to discern between two types of nanoparticles—namely the particles of an ordered structure commonly possessing 38–40 and sometimes more metallic atoms (e.g., Au_{55}, Pt_{309}, a family of palladium clusters consisting of 500–2000 atoms) called clusters that are about $1 \div 10$ nm in size and nanoparticles proper, which consist of $10^3 - 10^6$ atoms and whose diameter is $10 \div 50$ nm.

Nanoparticles are classified also by the number of atoms N they consist of.[37–41] Clusters, in their turn, are subdivided with a certain share of conditionality into very small, small, and large (in Table 1 diameter 2R for corresponding Na atoms and the relation of N_s to N_v atoms are shown).

As it can be seen, the surface and the bulk appear to be inseparable for very small nanoparticles. For nanoparticles containing 3000 metallic atoms, the relation $N_s/N_v \approx 20\%$ is true, whereas compact metallic particles ($N_s/N_v \ll 1$) are reached only at $N \gg 10^5$. Hence particles by their size can be subdivided into the following four groups (domains):

- Molecular clusters ($N \leq 10$).
- Clusters of a solid body ($N \leq 10^2 \leq 10^3$).
- Microcrystals ($10^3 \leq N \leq 10^4$), and
- Dense substance particles ($N > 10^5$).

Nanoparticles are the objects of supramolecular chemistry, which studies synthesis of molecules and molecular ensembles capable of self-organization owing to their high reactivity and ability to self-assemble. The resultant formations have a loose

Table 1 Classification of Nanoparticles and Clusters by Size

Very Small	Small	Large
$2 < N \leq 20$	$20 < N \leq 500$	$500 < N \leq 10^7$
$2R_{NA} \leq 1.1$ nm	$1.1\text{ nm} \leq 2R_{NA} \leq 3.3$ nm	$3.3\text{ nm} \leq 2R_{NA} \leq 100$ nm
Surface and inner volume are inseparable	$0.9 \geq N_s/N_v \geq 0.5$	$0.5 \geq N_s/N_v$

branching and most often fractal structure. They are called fractal clusters, fractal aggregates, or fractal filaments.[42] These formations are characterized by diminishing mean density of the substance bulk as they grow at preserved self-similarity (scale invariance). These fractal structures are frequently formed in the thin-film metal–polymer nanocomposites. They are also critical objects in representing percolation structures, appearing when isolated clusters join into a large conducting one. The fractal phenomenon is a peculiar criterion for visualizing the level of the system disordering. Like in the living nature, the forces that serve the base for formation of these artificial systems are related to nonvalent interactions.

Ligand-protected particles form, as a rule, solid powders that cannot be used immediately (e.g. in electronics) since common pressing, sintering, or hot pressing are inapplicable due to intensive recrystallization. Their great advantage is that even 30-nm stabilized nanoparticles become soluble in specific solvents, from nonpolar ones (pentane) to water. Nevertheless, organization of such particles is a serious problem and nanoparticles having almost ideal properties can become useless unless the problem is solved. Their structure can be three-dimensional (3D; commonly cross-linked by spatial molecules of various length), two-dimensional (2D; e.g., self-organized ligand-stabilized particles on solution surface, often with participation of linking blocks), or unidimensional (1D; quantum dots, quantum wires, and even quantum cables). 3D, 2D, and 1D materials are in extensive use today (Table 2).

The degree of particle dispersion significantly effects their activity, which varies with particle growth. Properties of nanoparticles as a function of their size is a fundamental problem in chemistry and physics of ultradispersed states. Investigations have proved that nanoparticles exhibit so-called dimensional effects in case their structural parameters are commensurable in at least one direction (or are less) with

Table 2 Typical Nanomaterials

	Size (approximate)	Materials
1D nanocrystals and clusters (quantum dots)	1–10 nm diameter	metals, semiconductors, magnetic materials, LB films
Other nanoparticles	1–100 nm diameter	ceramic oxides
Nanowires	1–100 nm diameter	metals, semiconductors, oxides, sulfides, nitrides
Nanotubes	1–100 nm diameter	carbon, layered metal, chalcogenides
2D arrays (of nanoparticles)	a few nanometers squared to a micron squared	metals, semiconductors, magnetic materials, polymer films
Surfaces and thin films	1–100 nm thick	various materials
3D structures (superlattices)	A few nanometers in all three dimensions	metals, semiconductors, magnetic materials, consolidated material, nanostructured materials
Nanoparticles in polymers	3–100 nm	metal–polymer nanocomposite

the correlative radius of one or another chemical or physical phenomenon (e.g., with the free path length of electrons for electrokinetic properties or phonons, with coherent length in a superconductor, size of a domain for magnetic characteristics, size of Frank-Reed's loop for dislocation sliding, length of mechanical defects of dislocation or disclination type and so on). They are characterized by the quantum-dimension effects (i.e. the classical physical laws are substituted by the rules of quantum mechanics). In other words, when the size of a solid or liquid particle diminishes down to 100 nm and less, quantum-mechanical effects start to be more and more noticeable. The effects are displayed in variation of the quantum-crystalline structure of the particles and their properties.

At least three characteristics are responsible for the effects.[43] First, this is commensurate with size, with one of several fundamental values of the substance or characteristic length of some process in it that evokes various dimensional effects. Second, the expanded specific surface and raised surface energy of nanoparticles at a limited number of atoms and uncompensated electronic links effect their lattice and electronic subsystems. And, third, severe conditions of their formation (high or low temperatures and process rates, exposure to powerful radiation sources, etc.) transform nanoparticles into a nonequilibrium (metastable) state. The mentioned factors ensure the specifics of the atomic structure of just a separate nanoparticle and probably changes in the atomic and crystalline structure of a nanomaterial as a whole. Thus a strictly periodic lattice that is typical of a crystal does not answer the minimum of energy of a nanoparticle, but its stability corresponds to an inhomogeneous strain and, in case of multicomponent materials, to an inhomogeneous distribution of components and phases by the particle radius.

A great variety of imperfections have been detected in the atomic structure of nanoparticles, including variations in the interatomic distance, increasing mean square shifts of atoms, defectiveness, microdistortion, amorphization, inhomogeneous strain; structural, concentration, and phase inhomogeneity of nanoparticles; and stabilization of high-temperature phases. Specific heat, susceptibility, conductivity, and some other critical characteristics of metals change significantly as nanoparticles reach the nanoscale. Besides, their specifics are imposed by a nonmonotonous dependence of the basic characteristics, such as melting point, pressure of recombination of the crystalline structure, ionization potentials, binding energy per metal atom, change in interatomic distances, optical and magnetic parameters, electronic conductance, and electron–phonon interactions, upon cluster size and the number of atoms M.

Formally,[41] nanoparticles of various sizes are treated as a linkage between the classical objects of chemistry and physics of solids (Table 3).

Table 3 Classification of Nanoparticles by the Fields of Investigation

Chemistry		Nanoparticles				Physics of Solids
Atom	$N = 10$	$N = 10^2$	$N = 10^3$	$N = 10^4$	$N = 10^6$	Compact substance
0.1		1 nm	2 nm	5 nm	10 nm	100 nm
			3 nm	7 nm		

Table 4 Different Methods of Synthesis and Investigation of Nanomaterials

Scale (approximate)	Synthetic Methods	Structural Tools	Theory and Simulation
0.1–10 nm	covalent synthesis; reduction procedures; sol-gel synthesis; intercalation methods	transmission infrared spectroscopy (TIRS); UV and visible electronic spectroscopy (UVS–Vis); nuclear magnetic resonance (NMR); electron-spin resonance spectroscopy (ESR); diffraction methods; scanning probe microscopy (SPM)	electronic structure
<1–100 nm	self-assembly techniques; Langmuir-Blodgett (LB) technique; biomineralization	scanning electron microscopy (SEM); transmission electron spectroscopy (TES); atomic force microscopy (AFM); x-ray photoelectron spectroscopy (XPS); extended-ray absorption fine structure (EXAFS)	molecular dynamics and mechanics
100 nm–1 μm	dispersion; microencapsulation; biosorption; processing modification		coarse-grained models, hopping, etc.

Its important that, in contrast to homogeneous materials, nanoparticles have extremely developed interfacial surfaces that show excess energy; thus they are often called energy-saturated systems. Properties peculiar to them serve as the base for relating them to the fifth aggregate state of the substance.[44] These materials are the subject of a new developing scientific branch: physicochemistry of nanoparticles (sometimes called nanochemistry or the physics of clusters). Successes in this field are closely related to the development of synthesis methods (Table 4).

The range of production methods of nanoparticles is extremely broad. They can be grouped into physical (phase transformations of the first order in the absence of chemical reactions) and chemical. Among commonly used physical methods employing aggregations of free molecules and most widely spread clusters of ions are condensation procedures. The condensation procedure includes the assembly of nanoparticles from individual metal atoms and molecular and cluster groups. Upon reaching certain dimensions and a definite physical interface, the atoms associate; and after a transient state, they become nuclei of a new phase. This results in the formation of some equilibrium and stable (like in micelle formation) structure. Modifications of procedure will be analyzed in detail in other chapters, but note that the majority of these modifications are complementing rather than competing methods.

Less frequently dispersion methods are employed that consist of disintegration of the macroscopic phase of the substance (coarse-dispersed particles in colloidal mills, agitators, ultrasonic, high-frequency and electric-arc crushing, etc.). They all belong to forcible methods since a perceptible amount of work is spent on breaking the links, although sometimes a spontaneous dispersion of substances is feasible under specific conditions.

Among chemical methods, the reduction of metal compounds in solutions in the presence of various stabilizers has been in extensive use for more than 100 years. The reducers can be hydrogen and hydrogen-containing compounds (e.g., tetrahydroborates, citrates of alkali metals, hypophosphates, alcohols, metal–organic compounds, and high-energy radiation). The kinetic parameters of the reduction reactions depend on the nature of the agent to be reduced and the conditions thereof. Chemical methods include various modifications of electrochemical synthesis, thermal decomposition of unstable covalent metal-containing compounds (including metal–organic ones) and molecular complexes. Common features for the processes of nanoparticle formation are the high rate of their nucleation and low growth velocity. This aspect is the key to their promising use and the search for the means of exercising various types of synthesis. Their general drawback is the formation of polydispersed colloids within a wide range of particle distribution by size. At the same time, many of the methods aimed at production of nanoparticles furnish a chance for a researcher to choose a synthesis procedure in response to concrete purposes and requirements.

It is worthwhile mentioning a new direction in physicochemistry of nanoparticles: chemistry of gigantic clusters. A number of synthesis methods for compounds with metal–metal links whose nuclearity reaches several hundreds have been elaborated lately. It was noted earlier that severe conditions of synthesis (i.e., the large specific area S_{sp} of nanoparticles, which is also characterized by small-size morphological elements) can induce variations in the nanoparticles physicochemical properties and even the violation of the expected atomic structure.[45] Extremely high (or low) temperatures and velocities of the processes and various outer effects (e.g., fast condensation or quenching) assist in formation of nonequilibrium, so-called frozen states in growing *j*-nuclei particles.

The developed interface, excess energy of the surface atoms (e.g., change in Helmholtz energy ΔF at dispersion of a homogeneous metal of V volume till the particle radius r is ΔF ($r = 3\sigma V/r$), where σ is energy increase of the system at a new interface formation of a unit area) and lowered activation energy of various reactions promote utterly high activity of the particles. This is why energy-saturated nanoparticles obtained in strongly nonequilibrium conditions enter into highly intensive interactions with the components of the medium they are formed in. Even when they are formed in an inert atmosphere, they spontaneously enlarge and result in a powder of an usual dispersivity.

Nevertheless, exclusively high activity of nanoparticles can be sometimes helpful, although there arises a tedious problem of their stabilization for transportation and storage.

However, strong passivation of their activity, especially at catalysis, may actually be undesirable. Therefore, passivation should preserve high chemical activity of

nanoparticles. Note that in the absence of stabilizers, nanoparticles are typical lyophobic colloids having low aggregate stability. In this connection, the choice of the efficient means to control chemical passivation of nanoparticles is considered as one of the most important trends in this field of investigations. Solution of this problem is facilitated by high sorption capacity of such particles toward surfactants and a number of high-molecular compounds. As a result of steric stabilization, the formations transform into a structure with a nucleus encapsulated into a sort of lyophilic steric barrier consisting of a continuous layer of solvate polymer chains. Sometimes only a minimum amount of the polymer stabilizer is used needed just to overcome the coagulation threshold but often, especially when nanocomposites are produced, the share of nanoparticles is low in contrast to the protecting cover. The role of polymers cannot be reduced to only screening of particles as it will be a strongly simplified approach to the problem of stabilization. In reality, its mechanism is extremely intricate and a series of urgent problems touching on interactions of polymers and nanoparticles, though having more than a hundred years' history, remain still unsolved.

In this chapter I present the current state of three aspects in physicochemistry of nanoparticles critical for understanding structure and properties of nanocomposites. This also relates to adsorption and chemisorption of macromolecules on nanoparticle surfaces from solutions; the generation of interfaces; phenomena of surface conductivity; and specific interactions that depend on the chain origin and length, its conformation, the composition of copolymers and so on. In polyelectrolytes similarly charged with nanoparticles, hydrophobic polymers are inclined to associate ionic groups and form domains as microphases of ion regions.

Physicochemical properties of polymer surfactants that present macromolecules with both hydrophobic and hydrophilic fragments are to be considered as stabilizers of ultradispersed state in all the above-cited processes. Along with the topochemistry, interactions which condition the morphology of future nanocomposites must also be considered. The stabilization mechanism is based on structural and mechanical constituents of stability in dispersed systems and spatial networks of the coagulation structure type and formation of adsorption-solvate structured films on nanoparticle surface.

Block copolymers based on polar and nonpolar comonomers are found in some solvents in the form of invert micelles, and their structure is separated at the microphase level. Nanoparticles are formed in the nuclei from a polar monomer like in a micelle (a peculiar nanoreactor—a domain), and they are covered by blocks of a nonpolar monomer (crown) serving as a stabilizer (a hairy ball structure). In this case, we deal with the realization of the ligand-controlled synthesis of nanoparticles. Modern trends in this field are

- Stabilization of concentrated and highly concentrated systems.
- Surface stabilization in LB film dendrimer-template nanocomposites.
- Matrix insulation processes based on the formation of a polymer stabilizer in the presence of dispersed nanoparticles.

The production methods of nanocomposite materials that are, by their essence, a polymer matrix, where nanoparticles and clusters are randomly distributed (a totality

of adjoining discrete particles in the form of aggregates of indefinite shape and size) do not differ formally from the traditional approaches to nanoparticle synthesis without polymers. These procedures are covered at length in this chapter. Nanoparticles in these systems serve as a dispersed phase, whereas the polymer matrix serves as a dispersed medium. In other words, nanoparticles are as if microencapsulated in the polymer shell. On the other hand, 1D, 2D, and 3D nanoparticle composites whose nanoparticles are localized only on the surface of powders, fibers, films, and nanocomposites have become recently widely applicable.

Nanocomposites can be produced by various methods: by generating nanoparticles in a specially prepared polymer matrix, less often by polymerization or polycondensation of corresponding precursors, and very rarely by creation of the materials in a single stage with simultaneous shaping both nanoparticles and the polymer shell. The latter way is complicated by strict requirements correlating velocities of the processes. In fact, these two completely different processes take the same kinetic paths, including nucleation, growth, and breakage of material chains.

In spite of the abundance of such methods and the modifications currently being studied or already elaborated, the number of those carried to completion or potential realization is not numerous. In this connection, a group of methods of metal coating application on polymer surface by evaporation should be mentioned. Nanocomposites with high content of metal particles can be obtained by thermal decomposition of the corresponding metal carbonyls (chiefly in thermoplastics). Still, the broadest sphere of activities in the field lies in chemical reduction of metal compounds in the presence of polymer matrix. This is, however, a complex, multistage process that includes the formation of unstable low-covalent forms of metals undergoing then a spontaneous decay and metal isolation. Along with stabilization of these highly reactive particles in statu nascendi the polymer matrix comparatively often controls the size and sometimes shape of the forming nanoparticles, the rate of their crystallization, the formation of percolation structures, self-organized growth of cluster formations, and so forth. In some circumstances, the macroligand is the factor that helps register the formation and even isolate intermediate particles or clusters of specific sizes.

In fact, all of these methods and their modifications for producing nanocomposites of nonmetallic type also fit the synthesis of multimetallic materials, providing additional difficulties in identification of their structure are excluded. In the course of preparing multimetallic nanocomposites, various complex physicochemical transformations take place that bring about inhomogeneities and various phases at the microlevel. The processes have been comprehensively studied on the example of metal–polymer systems with bimetallic inclusions of Pd-Pt, Pd-Cu, Pd-Au, etc. and triplet ones (i.e., Y-Ba-Cu). Preliminary synthesis of polymers is especially convenient in the synthesis of structurally homogeneous materials. It employs the polymer matrix with metal salts dispersed in it on a molecular level. This procedure is also used to prepare multicomponent steels of M50 type. Yet a number of problems are still waiting their solution concerning matrix structure and composition effect on the physicochemistry of nanoparticle nucleation and growth, and the formation of individual phases of metals and their alloys in multicomponent systems.

The polymer matrix remains, as a rule, indifferent in the reactions of nanocomposite formation. They are frequently accompanied (especially in subsurface layers) by polymer destruction and abrupt reduction of molecular mass, crosslinking, and formation of spatial structures (sometimes by isomerization of polymer units). This results in the loss of matrix solubility and fracture of the polymer crystalline phase followed by its transfer into amorphous state and rupture of separate links (more often halogenide, ether and epoxide ones). Nevertheless, a critical factor that ensures the degree of interactions between the polymer and nanoparticles is the formation of complexes and even chemical metal compounds and salts of arsenic, bis-arsenic and some other π-complexes of metals and chelate cycles of various composition with participation of polymer functional groups. When it has either been proved or presumed that the matrix and nanoparticles interact with each other, the systems are called polymer-immobilized systems. This is especially evident for the examples of polymer-immobilized clusters and polycyclic formations with the identified structure, including the heterometallic types (individual clusters in contrast to set in nanoparticles). They are produced from functionalized in a specific manner (chiefly by phosphorus-, nitrogen- and oxygen-containing groups); polymers made through polymer-analogous transformations leave intact the polymer chain and cluster skeleton. A perspective direction is producing these materials by the polymerization and copolymerization of cluster-containing monomers (by a simultaneous formation of the matrix and nanoparticles similar to nanocomposites).

An original variant of producing nanoparticles stabilized by a polymer matrix presents a combined pyrolysis of polymers and metal-containing precursors. The origin of precursors introduced into the polymer matrix may exert a strong effect on its thermal decomposition. High-temperature thermolysis (depolymerization) results in monomers and some other products, and is accompanied by graphitization of the matrix and nanoparticles. Conditions during pyrolysis (gaseous medium, ligand environment, metal nature, etc.) might influence directions of thermolysis through various means and lead to formation of different nanoparticles, including metal, oxide, carbide, sometimes nitride ones that are encapsulated into either a crosslinked polymer matrix or carbon-containing shell. In addition, nanoparticles of transient metals and their lowest-order oxides with a deficient structure turn out to be most efficient inhibitors of high-temperature thermal and thermooxidative destruction of polymers. Approaches that are based not only on the pyrolysis of polymer-immobilized polynuclear metal complexes but also on the controlled thermolysis of metal-containing monomers with a series of stages seem to be most promising in this respect. These stages also include the formation of metal polymers presenting self-regulating systems in which synthesis of the polymer matrix, nucleation, and growth of nanoparticles are running simultaneously.

For a long time, synthesis of new monomers under optimum kinetic regimes has been the major way of obtaining novel materials. Significant achievements have been attained in this field. Recently, however, much effort has been made searching for ways to modify known materials and procedures. In particular, much effort has been given toward developing hybrid polymer–inorganic nanocomposites. What is common in these materials and the topic of this book is the nanometer parameter

(i.e., distances between networks and layers formed by the polymer and inorganic ingredients) and the nanosize of the forming particles, including metal-containing ones.

One of the most rapidly developing areas of study involves developing sol-gel methods of producing hybrid materials and the intercalation of polymers and nanoparticles into layered systems in terms of chemistry of intracrystalline structures, like guest-host. Of no less importance is the fact that the majority of these procedures employ available substances and reagents that are ecologically safe and convenient for deriving highly dispersed materials. Much of this effort involves the hydrolysis that presupposes condensation of metal and metalloid alcoholates in polymer-forming compounds or, less frequently, in polymer solutions. The major effort is to study and understand the part played by interactions between phases of inorganic and polymer components. Special attention is paid to the network polymer–inorganic composites (their networks can form either sequentially or simultaneously from corresponding precursors) whose components enjoy strong covalent and ionic chemical bonds. Multiple attempts and various modifications of the above-named procedures have been reviewed in scientific literature; but just a few of them seem to be reliable. Furthermore, fewer involve investigations of the kinetic regularities and nucleation mechanisms. At the same time, initiated by practical demands, intensive elaboration of nanosize (soft template systems, etc.) and polymetallic ceramics based on sol-gel synthesis is currently under way.

Special interest is being paid to the study of polymer intercalation into porous and layered nanostructures. Intracrystalline cavities of the host represented by inorganic oxides (silicate layers), metal chalcogenides with a regulated system of nanosize pores and channels are filled with atomic or molecular guest structures, which are clusters, nanoparticles, coordinate structures of CdS type, synthesized in in situ polymer units. The most challenging type of intracrystalline reactions is the inclusion of monomer molecules into the guest pores followed by their postintercalation conversion into the polymer, oligomer, or hybrid sandwich products. This method is currently used to fabricate polyconjugate-conducting nanocomposites based on polyaniline, polypyrrole, and others. Thus induced encirclement of the nascent polymer, including self-assembling polylayered nanocomposites, is characterized by a high degree of ordering and perfected properties.

Clusters and nanoparticles in LB films are promising materials for molecular designs, especially in respect to developing self-organized hybrid nanocomposites. Metal-polymer LB films and their properties are being actively investigated and synthetic approaches to this problem are being developed. One more aspect in understanding nanostructures is the recognition that they are bridges to modeling surfaces and biological processes, as objects of supramolecular chemistry and structural chemistry of intermolecular links.[46] Although only the first steps have been made in this direction, one can perceive the far-reaching vistas in applying the described techniques for the generation of self-organized layers at the molecular level.

Hybrid nanomaterials are widely found in the living nature. Interactions between metal-containing particles, biopolymers (proteins, nucleic acids, polysaccharides) and cells are critical in enzymatic catalysis, geobiotechniques, biohydrometallurgy, and

biomineralization. Perfection of the processes occurring at their formation and principles of self-regulation evoke admiration from those striving to imitate and model such systems in the creation of synthetic analogues approaching living organisms. This is especially true for polynuclear metal enzymes as well as biosorption and biomineralization processes. Thus microbes work hard, like gold diggers extracting nanoparticles from gold until visible gold grains are found. Clusters and nanoparticles serve as models for a series of biological concepts that are objects of biomimetics and bioinorganic chemistry. Practically all approaches to the production of nanocomposites analyzed in this book (polymer-immobilized cluster and nanoparticles, sol-gel syntheses, layered intercalation compounds, LB films, etc.) are intensely used for biopolymers and biocomposites. Good success has been attained (1) in modeling polynuclear nonhemic complexes of iron (methane monooxigenase components), (2) in designing photosystems for oxygen isolation from water in a similar way as enzymatic process, (3) in biochemical nitrogen fixation, (4) in using nanoparticles in the diagnosis of pathogenic and genetic diseases through their aggregation in complementary oligonucleotides, and (5) in creating of metal–enzyme preparations, to name a few.

When the microorganisms are combined with colloidal metals, they concentrate bacteria, which is preceded by their adsorption on the cell surface and is followed by assimilation and precipitation of the metal–bacterial mass. This procedure can become a reliable selective method for removing bacteria (owing to selective affinity to metals) and the collective recrystallization coarsening of metal particles (microbiological geotechnology). The same colloidal and chemical interactions as in the synthetic polymers form the basis of these phenomena. Note that, frequently encountered in nature, biogenous formations can be formed in the course of biomineralization and bioconcentration, providing the matrix (template) exercises a strict control over nucleation and growth of materials with a perfected structure. This leads to the generation of materials with a complex hierarchic structure similar to that present in biological nanocomposites. Although it is extremely difficult to reproduce intricate and accurate bioinorganic reactions under laboratory conditions, a set of complex processes, including microencapsulation of active enzymes into a sol-gel matrix, production of biosensors, enzymatic electrodes, components of optical meters, and some others have already been successfully performed.

The fields where clusters and nanoparticles encapsulated into the polymer matrix can be adopted are, in fact, unbounded. Here, we'll enumerate only the most important already realized processes.

Nanoparticles are commensurable in size with boron's radius of excitons in semiconductors. This governs their optical, luminescence and redox properties. Since the intrinsic size of nanoparticles is commensurable with that of a molecule, this ensures specifics of the kinetics of chemical processes on their surface.[47] Current investigations are concentrated on the study of boundary regions between nanoparticles and the polymer because these interfaces are responsible for the behavior of adsorption and catalysis.

The majority of investigations in nanoparticles has an interdisciplinary character with respect to the methodologies of a number of scientific domains, including physicochemistry, materials science, biotechniques, and nanotechnology, that are

required to gain insight in this area. The science about nanocomposites has sprung in the recent decades[1–3] at the junction of various fields of knowledge and almost at once started to yield practical results. The enrichment with new notions and wide spectrum of knowledge recently presented allows a provisional review of the topic to occur. The present chapter is aimed at generalizing the state of the art in this progressing boundary of science.

III. PROBLEMS OF STABILIZATION OF METAL NANOPARTICLES BY POLYMERS

The high chemical activity of nanoparticles with developed surfaces is the main reason why various, often strongly undesirable, spontaneous processes occur. Nanoparticles are sensible to inclusion of impurities through binding at high solution concentrations during boiling or agitation under the action of radiative energy. These processes are commonly irreversible. One of the most important goals is to raise stability of nanoparticles to allow storage and transportation. With this aim, various stabilizers are used. Previously they were low-molecular organic compounds (carbonic acids, alcohols, amides, and other) and natural polymers (gelatin, gum arabic, agar-agar, starch, cellulose, and so on). At present, synthetic polymers are more frequently employed. Synthetic polymers solve two problems at once—that is, stabilization of nanoparticles and introduction of a polymer ingredient into the nanocomposite.

First attempts to quantitatively estimate stabilizing capabilities of polymers date back to Faraday's time.[48] Steric stabilization becomes probable because spatial dimensions of at least comparatively low-molecular compounds are commensurable with the range of London's forces of attraction or even exceed them. If the diameter of a macromolecule of a linear polymer coincides with the root-mean-square (rms) distance between its ends then the relationship between the mean geometric radius of the particle $\langle r^2 \rangle^{0.5}$ versus polymer molecular mass M can be expressed by the following relationship:[49]

$$\langle r^2 \rangle^{0.5} \approx 0.06 M^{0.5}$$

For a polymer with $M = 10^4$, $\langle r^2 \rangle^{0.5} = 6$ nm and at $M = 10^5$ the value reaches 20 nm. Consequently, macromolecules with $M > 10^4$ are of the sizes needed to stabilize colloidal particles (macromolecules are, of course, to induce repulsion of particles).

It should be emphasized that stabilization of metal nanoparticles by high-molecular compounds presents a major branch of polymer colloidal modern science. Modern polymer colloidal science studies generation regularities of dispersed systems with highly developed interfaces, their kinetic and aggregation stabilities, different surface phenomena arising at the interface, and adsorption of macromolecules from liquids on solid surfaces.[50] The theory of improving stability of colloidal particles by polymers has been treated in detail elsewhere.[51–56] This chapter focuses on basic questions that are connected with nanoparticles and nanocomposites.

Potential energy of attraction U_r between two spheres of the particles of radius r and minimum distance l_o between their surfaces can be given by the following equation

$$U_r \approx Ar/12l_o \text{ at } r \gg l_o,$$

where A is the efficient Hamaker's constant with energy dimensionality.

By its order of magnitude the constant stands close to the kT parameter for latex particles, although in metal dispersions it can be much higher. For example, for PMMC, PS, Ag, and Al_2O_3, constant A equals 6.3×10^{-20}, 6.15×10^{-20}, 40.0×10^{-20}, 15.5×10^{-20} J, respectively.[57] Note for comparison that the energy of attraction of two latex particles 120 nm in size is ~10 kT for each set of particles at a distance of 1 nm and 2 kT at a distance of 5 nm. This is sufficient for coagulation in case the repulsion between particles is absent as far as by its absolute value energy of attraction exceeds the heat energy of the particles equal to ~3/2 kT of three translation degrees of freedom.

To describe the stabilization mechanism of nanoparticles by polymers it is better to apply to the theory of "molecular solder"—so-called strong adhesive interactions between components.[58,59] At the base of the theory lies representations on structural and mechanical factors of stability of dispersed systems and spatial nets of the coagulation structure type. A requisite condition of the stabilizing effect of a high-molecular compound is an adequate activity (diophilic property) of a metal nanoparticle surface in relation to the polymer forming an extremely strengthened adsorption-solvate structurized film on the dispersed phase surface. Protecting polymers generate rather strong structural networks on nanoparticle surfaces within the bulk dispersed phase. The degree of steric stabilization varies in transitions from the formation of structures with adsorption layers through the structurization of the whole volume of the dispersion medium. Specifically stable are adsorption layers arising at considerable concentrations of high-molecular substances. They represent peculiar film gels, so called lyogels, that are highly solvated by the dispersion medium. At specific conditions, a structural network appears in the solution where metal particles are grouped so that they form chains of different shapes and lengths. The lyophobic colloidal particles serve to connect there links of different and similar macromolecules.[49]

Keep in mind that several processes are running simultaneously in the system and that they influence one another. These are processes of enlargement of the particles and macromolecular adsorption on the surface of original and forming particles. For all that, aggregation stability depends on the relationship of the coagulation to adsorption velocity constants. The amount of sole coagulated on a unit area in certain time is calculated[59] by the equation

$$q = (C_0 - C_{eq})V_1S_1/m_2S_2,$$

where C_0 and C_{eq} are the initial and equilibrium mass concentrations of sole and metal, correspondingly; V_1—its volume; m_2—polymer mass; S_1 and S_2 are specific surfaces of metal sole and polymer, respectively.

This is why modeling of adsorption and coagulation processes presents a considerably complex problem. We shall confine the discussion just to the enumeration of the most prominent phenomena.[49–54] In case of added macromolecules, one can observe homosteric and intensified steric stabilizations as well as flocculation (phase separations, substitution coagulation, and crystallizing coagulation) and heterosteric stabilization (selective flocculation, heteroflocculation, phase separation). If free macromolecules are taken, substitution stabilization, flocculation and phase separation occur. The efficiency of sorption processes, to which coagulation of nanoparticles also belongs, is determined by the overall balance of surface forces at interaction of different nature phases.[60]

When two metal nanoparticles covered by a layer of adsorbed soluble polymer chains approach to a distance less the total thickness of adsorption layers, the polymer layers start to interact (Fig. 1). The interaction brings about steric stabilization and leads, in a majority of cases, to repulsion between the colloidal particles. It was repeatedly attempted to clarify its nature and determine its magnitude. Most frequently the problem is studied in terms of changing the Gibbs's energy when two particles are covered by an adsorbed polymer that are approaching one another from infinity.

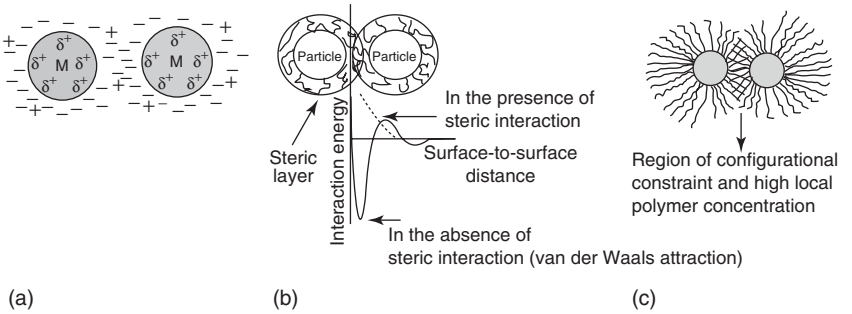

Figure 1 Stabilization of nanoparticles by polymers. (**a**) Electrostatic stabilization. (**b**) Steric stabilization. (**c**) region of high polymer concentration.[51]

The quantitative contribution of the polymer constituent into the interaction energy of particles is a function of both polymer adsorption layer parameters on the surface (share of elementary links of a macromolecule contacting the surface, degree of its covering by the polymer, amount of the polymer in the first (dense) layer, layer thickness, and so on) and those of macromolecules in the solution.

Adsorbed on the surface of dispersed particles, polymer chains lessen the attraction energy by steric reasons (the minimum distance to which particles can approach increases) and because they change the efficient Hamaker's constant value. The attraction energy in expressions for U_r dependence on $\grave{A}$ is the function of not only interaction constants of dispersed phase A_1, dispersion medium A_2 and the phase with the medium A_{12}, but of Gamaker's constant for adsorption layer A_3 too. The effect of polymer adsorption layers on molecular attraction of particles has been described theoretically.[50–53] Below is an expression for U_r, based on the Lifshits macroscopic theory

$$U_r = -\frac{1}{12}\left(A_2^{1/2} - A_1^{1/2}\right)^2 (r/I_0)$$

and an equation to consider unlagging London's forces in microscopic approximation (Fig. 2):

$$U_r = -\frac{1}{12}[(A_2^{1/2} - A_3^{1/2})^2(r + \delta)/(r - 2\delta) + (A_3^{1/2} - A_1^{1/2})^2(r/1_0) + 4(A_2^{1/2} - A_3^{1/2})^2(A_3^{1/2} - A_1^{1/2})^2(r + \delta)/(1_0 - \delta)(2 + \delta/r)]$$

In principle, polymer layers adsorbed on nanoparticles can be considered as an unusual medium—namely, a polymer solution specifying interaction forces between the dispersed phase particles. Evidently, the interaction between particles is negligibly weak when the adsorbed molecules are densely packed on the surface and the macromolecules nearly lie on it. As soon as the particles approach and adsorbed polymer layers superimpose, the loops engage, and there occurs an interaction whose model is shown in Figure 2.

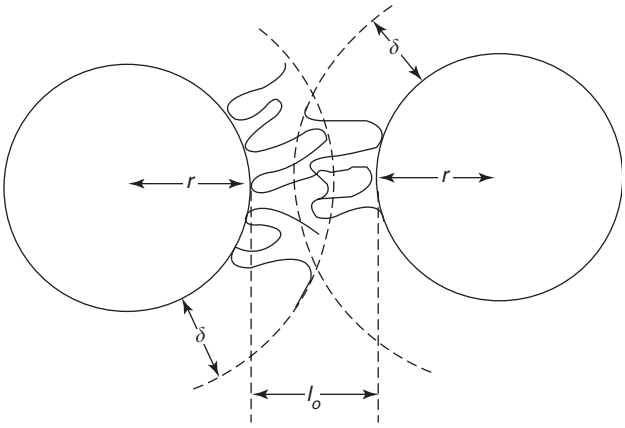

Figure 2 Linkage of the polymer loops on the surface of colloidal particles.[51]

Precisely this superimposing region serves as the medium (polymer solution). Interpenetration of two adsorption layers evokes the appearance of two effects related to a lessened amount of conformations in the macromolecular chain (leading to the loss of configuration entropy and, consequently, to growth of the system free energy) and varied concentration of links in the zone of overlapping. This is accompanied by a variation in the polymer–solvent interaction and generation of the local osmotic pressure. The first of the effects is called entropic and the second is the effect of osmotic pressure.

The total interaction energy of two colloidal particles with adsorbed polymer layers is described by the equation,

$$U = U_1 + U_2 + U_r$$

where U_1 is the effect of osmotic pressure; U_2, entropic effect; U_r, interaction energy of particles.

The interaction energy at mixed polymer blends is given by the expression

$$U_1 = \frac{4}{3}\pi BkTC_a^2(\delta - I_0/2)^2(3r + 2\delta + I_0/2)$$

where π is osmotic pressure; B, the second virial coefficient determining the interaction between the solvent and substance solved; C_a, polymer concentration in the adsorbed layer.

Entropic effect can be calculated using statistical mechanics; however, the equations are complex. Calculation results show that energy of interaction U_2 is on the order of U_1.

U_1, U_2, and U_r dependencies on l_0 are presented in Figure 3. It is clearly seen that at distances twice as big as $\delta(2\delta)$, U_1 and U_2 turn to zero. Energy U_r is conditioned by the long-range London's forces, so the total energy of interaction U reaches its minimum value at a longer distance than 2δ. At a right-hand particle approach the transition through point U_{min} means coagulation of particles. For the process of particles interacting with the adsorption layer one can take that the condition $U_{min} < 5kT$ which corresponds to repulsion and $U_{min} > 5kT$ which corresponds to coagulation. The depth of the potential well U_{min} is determined by a number of factors, including polymer molecular mass, solvent–particle interaction, particle size and so on. With

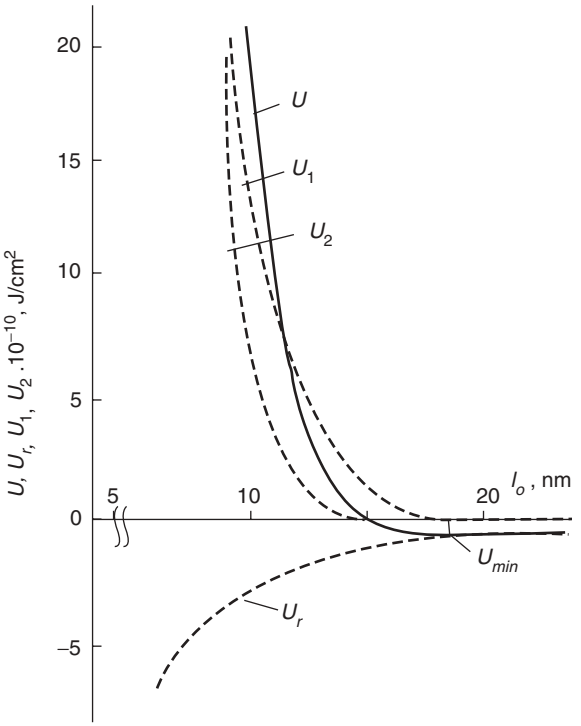

Figure 3 The interaction energy of the particles with their surface-adsorbed polymer layers.[53]

increasing polymer molecular mass, due to the formation of loops, the adsorption layer thickness increments to and curve U_1 (Fig. 3) shifts to the right. As a result of a growing thickness, U_{min} diminishes and the repulsion intensifies. The increasing total amount of the adsorbed polymer elevates C_a making U_1 increase and the value of U_{min} decrease. Once the solvent–particle interaction is intensified, the thickness of the layer of adsorbed loops increments leading to the growth of the second virial coefficient B.

A through examination of two kinds of entropic effects is appropriate. The first one presupposes desorption of polymer chains as a result of a lessened entropy of the system. This augments the interphasal free energy and results in particle repulsion. The second kind of entropic effect is characteristic of nondesorbed polymer chains when a simultaneous breakage of a great amount of polymer links with the surface of colloidal particles occurs. This is in fact improbable. It presumes that the adsorption equilibrium between the polymer and particles remains invariable during particle collisions. So the free energy grows as a result of decreased entropy induced, in turn, by redistribution or compression of adsorbed links in the interaction zone. Two limiting cases are to be mentioned when using a constant adsorption model. They are interpenetration of adsorption layers without constriction of the adsorbed polymer chains (effect of mixing) and compression of the layers without overlapping (effect of bound volume). Both cases are idealized since it is impossible to separate these two phenomena in real systems. Nevertheless, proceeding from general considerations, the effect of bound volume will dominate at high concentrations of polymer units on the surface when polymers with low-molecular mass are adsorbed and the interacting surfaces converge very close to one another. The effect of mixing prevails when the surface is only slightly covered by the polymer, high-molecular compounds are adsorbed, and the distance between particles of the dispersed phase is substantial.

A notion of enthalpic (ΔH), entropic (ΔS) and mixed (enthalpy-entropic) stabilization at interpenetration of polymer chains has been described.[51] The mixing energy is

$$U = \Delta H - T\Delta S$$

The generalized Flory-Huggins' parameter characterizing thermodynamics of polymer–solvent interaction can be presented as a sum of two constituents $\chi = \chi_h + \chi_s$, where χ_h is the parameter of mixing enthalpy and χ_s, an additional entropic parameter specifying both volume effects of mixing and various structural transformations (e.g., rupture and formation of hydrogen bonds, conformation change.).

Evidently, at endless dilution $\Delta H \to (-k)$ and $\Delta S \to (-\psi)$, where $k = \chi_h$ and $\psi = \frac{1}{2} - \chi_s$.

Proceeding from above considerations it's easy to define conditions under which one or another type of steric stabilization dominates (Table 5).

A number of polymers show negative k and ψ values in water solutions. This is connected with the destruction of hydrogen bonds with increasing polymer concentration in the system. In this case, stabilization will be enthalpic. At the same time, the majority of polymer solutions in nonpolar media display positive k and Ψ,

Table 5 Comparison of Types of Steric Stabilization[51]

K	Ψ	ΔH	ΔS	$\Delta H/\Delta S$	U	Stabilization Type
−	−	+	+	>1	+	enthalpic
+	+	−	−	<1	+	entropic
+	−	−	+	$><1$	+	mixed

so far as the entropic stabilization can be expected. Systems with enthalpic type of stabilization show a tendency to lose stability when heated. Entropic systems tend to flocculate when cooled.

It should be noted that adsorption of water-soluble polymers with numerous hydrophilic groups by nanoparticles imparts a considerable water-absorbing capacity to the dispersed phase surface. As a consequence, the role of the solvation factor gains strength for stability. To our regret, the latter phenomenon has been insufficiently studied. Nevertheless, data on hydrophilic properties of stabilizer macromolecules and temperature to stability ratio of polymer-containing dispersions prove that the structural constituent of the wedging pressure plays a critical role in the mechanism of stabilizing colloidal solutions using high-molecular compounds.[61]

As the synthesis of metallopolymer complexes precedes the formation of metallopolymer nanocomposites, let us consider briefly these problems.

IV. BASIC CONSIDERATIONS OF THE COMBINATIONS OF MACROMOLECULES AND METALS

Metal-containing macromolecules or macromolecular metal complexes consist on the combination of

- Organic or inorganic macromolecules.
- With metals in different states such as metals–metal clusters, metal ions, metal complexes–chelates.

These materials are well-known from their active and selective function in biological matter. The increasing knowledge about natural metal-containing macromolecules stimulates chemists to synthesize artificial systems. The newly developed materials can exhibit unusual properties for new applications due to the introduction of metals in polymers. Therefore chemists, physicists, biologists, physicians, and engineers are involved in this interdisciplinaric subject where a macromolecule and a metal atom are combined in one material.

The activities in this field are summarized in some monographs and several reviews.[62–82] We will classify the different combinations of macromolecules and metals. Due to various macromolecules and various metal components such as metal–metal clusters, metal ions, metal complexes rather numerous possible

combinations exist. Therefore, it is essential to introduce a classification for the architecture of these materials.

When considering typical organic polymers, for example, based on polystyrene, polyethyleneimine, polymethacrylic acid, polyvinylpyridines, polyvinylimidazoles, and others, the mainchain of these polymers can be linear or crosslinked. In several cases, a metal is part of the polymer chain leading to new structural units. Inorganic macromolecules like silica, different kinds of sol-gel materials, and molecular sieves can also be included if these macromolecules are modified in such a way to carry as active part one metal component employing different kind of bonds.

The various combinations of macromolecules and metal components will be classified as follows:[81]

Macromolecular complexes (MMCs) that contain at a macromolecule, a metal ion or metal complex interacting ionic by bonds (electrostatically), donor-acceptor bonds (coordinative bonds), or covalent bonds (Fig. 4). In these, the metal MMC is a specific pendant substitute.

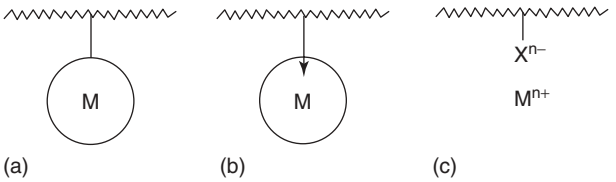

Figure 4 Binding of metal particles to a macromolecule (**a**) covalently, (**b**) coordinatively, and (**c**) electrostatically.[81]

Another type of MMC considers the situation of the ligand and/or metal (metal complex) being part of 1D, 2D or 3D macromolecular structures (Fig. 5).

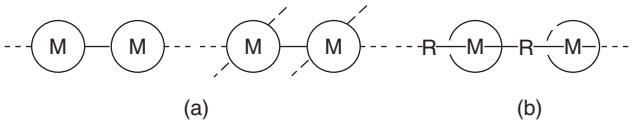

Figure 5 Metal complex part of (**a**) a polymer chain via the ligand and (**b**) a polymer chain via the metal.[64]

Note these macromolecules are completely destroyed after removal of the metal atoms, whereas in the first case, the macromolecular chain remains after the metal atoms are removed.

Finally, there are MMCs with nanosized particles or clusters being incorporated into an organic or inorganic macromolecule where primary bonding does not occur (Fig. 6).

Because, in most cases, no clear IUPAC nomenclature exists for metal-containing macromolecules or macromolecular–metal complexes, it is nearly impossible to obtain detailed information on them using *Chemical Abstract* literature

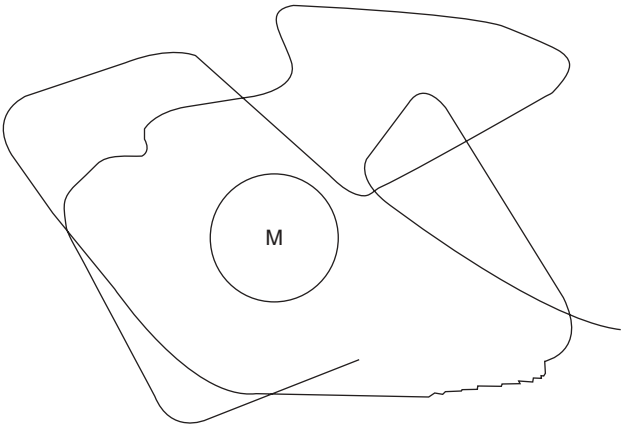

Figure 6 Metal complex or metal cluster/nanoparticles incorporated into macromolecules.[64]

searches. One has to look for each individual metal, metal ion, metal complex, metal chelate, ligand, or polymer to find the appropriate literature citations.[82]

Analogous to low-molecular-weight metal complexes, the kind and strength of the metal to ligand (M–L) bond is determined on one side by the ionization potential and electron affinity of the metal ion and on the other side by the Lewis base or donor properties of the ligand atoms or groups. The metal to ligand bonds can have more covalent or more ionic character, and factors like ion exchange equilibria have to be considered. But in contrast to low-molecular-weight complexes, the situation with high-molecular-weight counterparts is much more complicated.

The presence of low-energy vacant *d*-orbitals in transition metals of IVA-VII or VIII groups of the periodic table of the elements opens the possibility to fill them with electrons donated by various molecules possessing high-energy orbitals with *n*-unshared pairs of electrons of heteroatoms (π-type complexes) such as amines, ethers, and phosphines. The energy levels also can be completed by p-electrons (pi-type complexes), donated by unsaturated or aromatic compounds with relatively low ionization potential. The ligands with vacant π*-antibonding orbitals can be affected as p-acceptor of electrons of the metal. In these cases another type of the interaction is realized—so-called reverse π-binding.

For the polymer ligands, the same considerations can be applied as for low-molecular-weight ligands. The main differences between formed bonds are displayed in long-range actions. Particles (ion–ion, ion–molecule, molecule–molecule) can interact over a long range electrostatically and over the short range approximately as the sum of covalent radii caused by covalent or coordinative bond formation. The total complex binding energy (combination of electrostatic and donor acceptor) increases with increasing particle contact.

As mentioned above, the interactions in the macromolecular ligand (MX_n) systems can be classified as covalent, coordinative, ionic, charge-transfer, and chelate bindings. The macromolecular ligands interact with MX_n either through one bond—the

monodentate binding (when MX_n possesses only one coordination vacancy or group able to be substituted by the polymeric ligand)—or by polydentate binding. The latter can be carried out via both an intramolecular and intermolecular mechanism.

In the case of linear or branched carriers, the macrocomplexes I (scheme 1), as a rule, are soluble in organic solvents and their structure is identified rather easily. As the solubility of the bridged macrocomplexes II decreases, they are more stable and have a less dense structure. The complexes III with the intermolecular bridge bonds are insoluble and they are difficult to define.

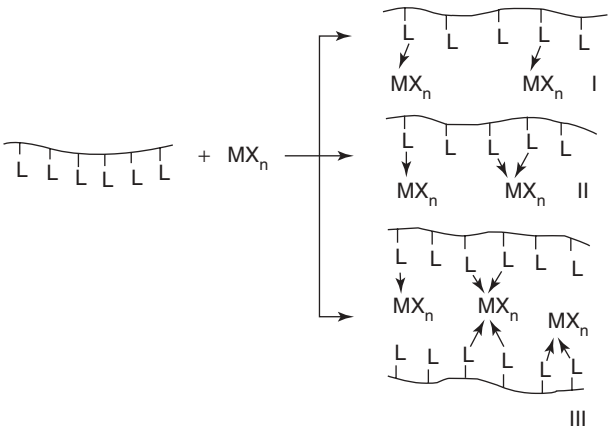

Scheme 1

Progress in many fields of metal complex catalysis is connected with immobilized catalytic systems, which are characterized by physical or chemical bonding of one of the components or a catalytic complex bound to a solid support carrier. However, the relatively low stability of the metal to polymer bond leads, during catalysis, to a weak point in such immobilized metal complex catalysts. The immobilization of metals by chelating polymers, which ensure a stable multicenter bond between the metal, and the polymer support provides the simplest method for overcoming the above disadvantage.

Macromolecular metal chelates (MMChs) are high-molecular-weight compounds that incorporate metal chelate cycles. The problems of the chemistry of MMChs have attracted increased attention by investigators during recent years.[65,76,83–87] It is useful to examine three levels of the spatial organization of the MMCh:

- The local level, which reflects the chemical structure of a single unit in the chain molecule (the nature of the complex forming metal and of the electron donating atoms, the ring size, the steric structure of the ring, etc.).
- The molecular level, which is determined by the chemical structure of the polymer chain (the chain length, the elemental composition of the repeating units, the shape and conformation of the chain, etc.).

- The supermolecular level, which reflects the nature of the intermolecular interaction of the macromolecules and the degree of their mutual order (scheme 1).

Besides C, N, O, S, P, Si, which are well known as chain-forming or participating elements, most other elements of the periodic system are capable (except hydrogen, the noble gases, and the 12 elements of Group 1 A and VII B) to be part of a polymer chain. These elements include many metals or semimetals. In the following text a few characteristic examples are described.[71,81] The most common routes for the preparation are

$$m\text{A}-\text{L}-\text{MX}_{n-\text{a}}-\text{L}-\text{A} \xrightarrow[-2m\ \text{A-B}]{+m\ \text{B-R-B}} \text{---}[-\text{MX}_{n-\text{a}}-\text{L}-\text{R}-\text{L}-]_m\text{---}$$

Scheme 2

- Syntheses of a bifunctional metal complex–chelate → reaction with the same molecule or another bifunctional reagent → purification from starting materials → analytical characterization → investigation of properties (scheme 2).
- Preparation of a bifunctional or higher functional low molecular weight ligand → reaction with a bifunctional or higher functional metal ion → purification → analytical characterization → investigation of properties (scheme 3).
- At first preparation of a high-molecular-weight ligand using different methods → then metallation.

$$m\,\text{L}-\text{R}-\text{L} \xrightarrow[-m\,(\text{aX})]{+m\,\text{MX}_n} \text{---}[-\text{MX}_{n-\text{a}}-\text{L}-\text{R}-\text{L}-]_m\text{---}$$

Scheme 3

Many polymers are less soluble and therefore difficulty to characterize. Especially the results of older reports did not include careful analysis, and the proposed structure should be verified again.

The incorporation of metal ions into a polymer chain—directly or via ligands—offers unique materials with properties that differ significantly from those of conventional organic polymers. The different range of coordination numbers especially of transition metal ions can allow the preparation of polymers with unusual conformational, mechanical, and morphological characteristics. All above considered types of MMCs can be also obtained by polymerization and copolymerization of metal-containing monomers.[88]

V. TYPICAL FORMATION PROCESSES AND THE STRUCTURE OF NANOMETRIC METAL PARTICLES IN POLYMERS

The difficulties of preparing polymer-immobilized nanoparticles are due to a rather poor reproducibility of many synthetic procedures and to rapid oxidation of nonnoble metals particles by potential oxidants at the colloid formation stage. Virtually all of the known methods for producing polymer-immobilized nano particles are at least two-stage processes: They include molecular dispersion (atomisation or reduction) and subsequent condensation of atomic metal into nanoparticles. These stages occur in a rapid succession and virtually form a complex process of nuclei formation and growth of a solid metallic phase. The very notion of a "solid phase nucleus" is somewhat equivocal. A cluster containing 25 Pt atoms has the adsorption properties of a bulk metal.[89] On the other hand, the collected ionic groups in gold chloride reduction start to display properties characteristic of the metal nucleus only after the accumulation of 300 or more Au atoms.[90]

The aggregation of polymer-immobilized nanoparticles on polymeric powders, films, or fibers could be the simplest method for their preparation. Such studies have been carried out mostly on mineral supports, though there are also reports using nonstabilized hydrosols (8–12 nm) and organosols (4–11 nm) of Fe, Zn, and Cu on the surface of Dacron (lavsan) and polycaprolactam (capron) fibers.[91] The formation rate is higher on the lavsan fibers, which is explained by the formation of the surface M–O bonds. The lowest aggregation rate is characteristic of the iron sol. These materials are heterogeneous: The nanoparticles are localized only on the polymer surfaces.

A. Technique of the Atomic Metal Evaporation

Cryochemical depositions (most frequently, vacuum deposition at pressures of 10^{-1}–10^{-4} Pa) of atomic (gaseous) metal on thin (~1000 nm) polymeric supports are attractive technologically. Polymer supports are usually high-molecular-weight paraffins, polyesters, oligo-olefins and polyolefins, polydienes, vinyl-siloxan and phenyl-siloxane polymers. The naked metal atoms are first deposited at temperatures of 77K and above.[91–97] Then small clusters are stabilized at low temperatures. In these systems, both homocluster and heterocluster particles are formed and stabilized at an evaporation rate of 10^{-8} mol min^{-1}. As shown in scheme 1, a single metal atom initially forms bonds with two functional groups (arene rings, or oxygen atoms) (stage I, scheme 4). This is followed by a metal–polymer chain growth stage (II). Finally, stabilization of clusters by ligands takes place (III). The stabilization may also result from the trapping of clusters into a highly viscous metal–polymer network (IV) and the enlargement of these cluster particles (V).

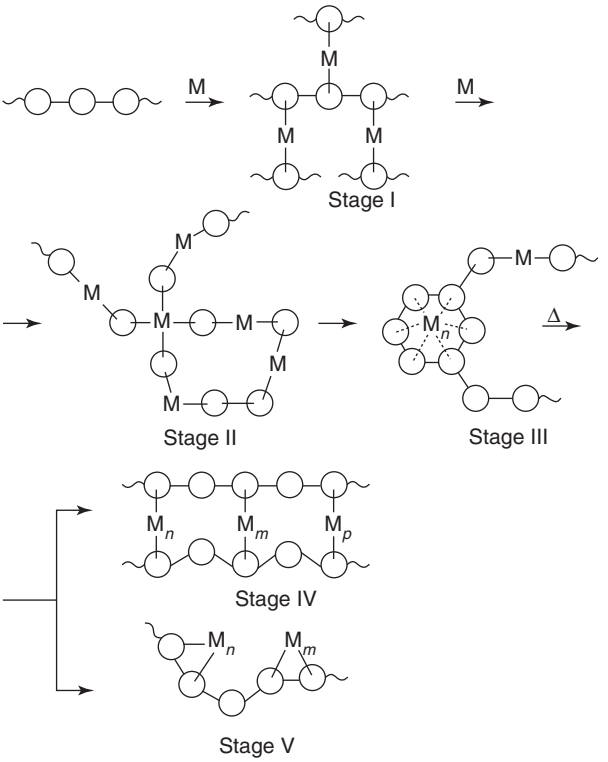

Scheme 4

As a rule, deposition results in the formation of mini-clusters. Their size depends on the process conditions and the nature of the metal. Transition metals are used in most cases. Cr clusters contain 2–3 metal atoms, those of Mo contain 2–5 metal atoms, and clusters of other metals include not more than 10 atoms.*

In principle, the kinetics of metal vapor condensation is analogous to the coagulation kinetics of an ideal suspension. There are unstable states, which can be described by the Smoluchowski equation for fast coagulation.

Spectral techniques have been used for the identification of polymer-immobilized clusters. For example, monomers, dimers, and trimers of molybdenum immobilized on poly(methylphenylsiloxane), absorb at $\lambda_{max} = 318$, 418, and 502 nm, respectively, whereas the tetranuclear and pentanuclear clusters absorb at $\lambda_{max} = 598$ and 640 nm, respectively. This makes it possible to follow the growth of cluster particles. According to scheme 5, this process comprises a number of consecutive irreversible bimolecular reactions:

*These formations are thermally stable only below 290K and disintegrate rapidly under the action of oxygen (even under a pressure of 1 mm Hg). Note for comparison that the energy of Cr–Cr and Mo–Mo bonds are 150 and 400 kJ mol^{-1}, respectively.

$$M + L \xrightarrow{k_1} ML,$$

$$ML + L \xrightarrow{k_2} ML_2,$$

$$ML_2 + M \xrightarrow{k_3} M_2L_2,$$

$$\cdots\cdots\cdots\cdots\cdots\cdots\cdots$$

$$M_{n-1}L_2 + M \xrightarrow{k_n} M_nL_2,$$

Scheme 5

where M is a metal and L is a ligand.

The formation of clusters may be regarded as a continuous deposition of metal atoms on a polymeric film over the time t at the rate W; then the corresponding rate equations are

$$\frac{d[M]}{dt} = W - \sum_{j=0}^{p} k_m[M][M_jL_2]$$

$$\frac{d[M_nL_2]}{dt} = k_m[M]\{[M_{n-1}L_2] - [M_nL_2]\}$$

The concentration of cluster nuclei M_nL_2 of various nuclearities on the polymer may be expressed in general form as

$$\frac{[M_nL_2]}{[ML_2]} = [M_0]^{n-1} = \frac{2^{n-1}}{n[L_0]^{n-1}} = k[M_0]^{n-1}$$

where M_0 is the total mass of metal atoms deposited on the polymeric film over time t.

Generally speaking, the cryochemical condensation of metals on cooled matrices leads to the formation of a variety of cluster series. These are interpreted[98] as a set of clusters with the monotonically increasing nuclearity having the same ligand composition (M_nL_m, where $n = qx$; x is the nuclearity of the simplest member of this series and q is an integer). In these series, the basic structural elements (the simplest building blocks) are individual metal atoms. In contrast the series per se are models of the atom by atom growth of metal particles. One can follow the course of their formation via the addition of individual bricks, which are elements of the nucleus formation.

The cryochemical method allows the preparation of both homometallic and heterometallic polymer-immobilized cluster particles. Thus the consecutive or simultaneous deposition of metal vapors of different elements (e.g., Mo and Ti or Ti and Cr), especially at high concentrations, yields the nonsolvated bimetallic clusters $M^1_xM^2_y$. These clusters are close in size to the colloidal particles (Cr_xTi_y) (scheme 6) or to small clusters. For example, cluster Mo_xTi_y includes 13 atoms.

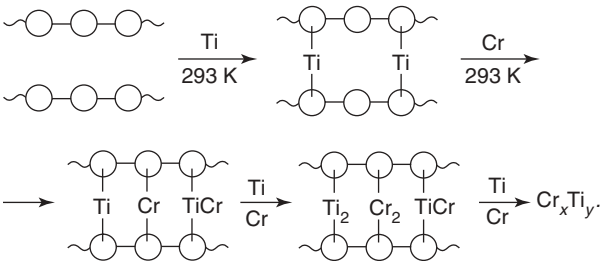

Scheme 6

The particles formed are chemically bound with the polymer and possibly cause crosslinking.

Control of the evaporation conditions also allows the preparation of polymer-immobilized nanoparticles. For example, colloidal silver was obtained with the particle size of 1.0–20 nm (the colloidal Ag particles less than 40 nm in diameter absorb light at ~400 nm).[99] The dispersion of gold nanoparticles (mean particle size ~2 nm) in poly(diphenylbutadiyne) has been obtained by cocondensation of vapor of Au and diacetylene on a support at 77K.[100]

Different versions of cryochemical synthesis have been developed using the protective properties of polymers.[101] For example, an oscillatory contour is applied for the electrical condensational dispersion of metals. In nonpolar media, dispersions of Ag, Al, Bi, Cd, Cu, Co, Mo, Fe, Ni, Zr, Pt, Sn, and W particles (1–10 nm) are stable only in the presence of stabilizers (the synthetic rubbers SKD, SKB-35) that can form 3D structures in solution. In their absence, immediate coagulation takes place.

Evaporating solid polymeric particles (accompanied by considerable pyrolysis) and codepositing the volatile products (mostly radicals) with the metal vapor are used less often. This technique is employed for the formation of 10-nm-diameter copper islets in a polyethylene matrix. The explosive evaporation of a metal wire coated with a polymer and pulsed mechanochemical interactions (of the Bridgeman anvil type),[102] etc. are the modifications of this method. Recently, interest has been shown in the ionic spraying of metals onto polymeric surfaces. Studies of the vacuum deposition of Au and Zn on PE and PTFE should be noted.[103,104]

The low-temperature condensation of Cr vapor with macromolecular matrices containing aromatic rings (oligobenzyl, oligoarylene, benzene -*m*-xylene copolymer) was used for the preparation of macromolecular sandwich-type Cr complexes.[105] The direct reaction of atomic metal with the matrix is prevented by the joint condensation of the metal and solvent (e.g., chromium and diglyme).[106] This makes it possible to replace the direct metal–matrix interaction by exchange of one stabilizing ligand for another high-molecular-weight ligand (this procedure is called resolvation). Nonionogenic surfactants are sometimes used for the replacement of dispersive medium. Thus the silver organosols with 3–12-nm-diameter particles, obtained cryochemically in acetone were subsequently stabilized with 0.2% Triton X-100 solution in water. Then these silver organosols were incorporated into

a crosslinked polyacrylamide gel.[107] The solvent and the polymer used in the cryochemical synthesis both affect the reaction direction and the product stability.

Resolvation may precede the preparation of polymer-immobilized nanoparticles. For example, the cryochemical synthesis of colloidal Ag particles is performed in acetone, which is then replaced by formamide. This dispersion is stable for a few days. The system Ag (2–5 nm) formamide is used as a solvent in the preparation of crosslinked polyacrylamide gel.[108] Three different synthetic resolvation methods are documented.[109] In the first version, a Co-nonadecane system obtained by the cryochemical method was mixed with a solution of a polymer in nonadecane with subsequent sonication. In the second version, the nanoparticles of Co or Ni in toluene were added to a solution of low-pressure polyethylene (LPPE) in toluene at 363K. The third variant employs a toluene polymer solution cooled from 383K to 185K. The resulting gel-like system was mixed with nanoparticles obtained cryochemically and subjected to sonication. These techniques make it possible to virtually preclude the aggregation of particles at all intermediate stages. However, along with the peptization and resolvation, more complex interactions of nanoparticles with the solvent may take place.

The matrix is affected by the metal atoms present during the preparation of polymer-immobilized nanoparticles. A sharp decrease in the molecular weight of polymers (in particular, in the case of oligoarylenes)[106] is observed. The loss of matrix solubility also occurs. In some instances, ester and other bonds are cleaved. Futhermore, the interaction of polymer functional groups with metal atoms yields new products (e.g., terminal chlorine atoms from benzyl cloride in the oligobenzyl matrix in the presence of Cr results in the formation of $CrCl_3$). The interaction of atomic zinc with the polymer surface is accompanied by a profound destruction of the polymeric layers below the surface. Zinc also reacts with the degradation products.[103,104]

B. Preparation of Polymer-Immobilized Nanoparticles by Plasma Polymerization

Plasma polymerization (in a glow discharge) is initiated by ions, excited molecules, and high-energy photons. The monomer vapor pressure during polymerization in plasma is too low (10^{-3}–10 mm Hg) to allow the production of polymers by conventional plasma methods. Polymer formation can occur from relatively simple compounds (CH_4, CF_4, benzene, chlorobenzene, perfluoropropane); less often, by more complex compounds. For example, homogeneous coatings enriched in beryllium are prepared by the thermal evaporation of Be with the concomitant deposition of a plasmopolymer of *trans*-but-2-ene.[110] Mixtures of gaseous monomers with argon are often used. The chain mechanism of the polymer growth does not play a substantial role during the deposition of polymers from the gas phase. Chain propagation in plasma polymerization occurs via a rapid stepwise mechanism with the predominance of polyrecombination reactions between active particles. These products are regarded as polymers, but they have little in common with "normal" polymers because of their structural peculiarities. As a rule, plasma polymers are 3D

highly crosslinked products, especially when produced by extended (5–10 min) plasma treatments. Two competitive processes take place in plasma polymerization: polymer formation by deposition from the gas phase and the etching (destruction) leading to its removal. The relationship between these processes at each specific site is determined by the energy of excited particles, their concentration, and the surface temperature, as well as by the nature of the monomer (e.g., polymerization predominates in the case of C_3F_8).[111]

Plasma polymerizations permit of thin (50–100 nm), virtually defect-free films on most supports. Polymerizations in plasmas are not restricted by the choice of material and the support's shape. Therefore, this technique is well suited for the preparation of microencapsulated nanoparticles (the so-called metal-doped polymeric films).[112]

Thin composite films are formed by simultaneous polymerization of compounds during the vacuum evaporation of metals. Modifications have been reported using different modes of preparation and introducing nanoparticles.* One version includes simultaneous evaporation of a monomer and metal from different sources, while another relies on the combination of plasma polymerization and metal evaporation.[116] Plasma-induced graft polymerization of traditional monomers (e.g., vinylimidazole on a capron film)[117] was carried out during metal evaporation. The plasma polymerization of organometallic compounds is of special interest.[118] For example, plasma-induced polymerization of diethylberyllium is remarkable for the simplicity of the equipment required.[110]

The preparation of polymer-immobilized nanoparticles most often involves combined targets including a metal and a polymer. The target material is sprayed by plasma. The sprayed product is deposited, as a rule, outside the plasma zone. It is convenient to use a Mo, Cu, or Au cathode as the metal source. In trifluoropropanemetal systems obtained by sprayed plasma the metal content in the thin-film product amounts to 18–26 wt%. Metallopolymers with formal compositions of $(C_3F_4O_{0.6}Mo_{0.3})_n$ and $(C_3F_{3.9}O_{0.3}Cu_{0.3})_m$ have been prepared and characterized.[113] An aluminium-containing material with enhanced adhesion properties is produced by the spray plasma polymerization of CH_4 using aluminium as the electrode material. Even at a relatively low frequency (10 kHz), the electrode surface is bombarded so strongly that physical sputtering of Al takes place with its inclusion into the growing macromolecule. The metal atoms are uniformly distributed over the bulk of the deposited material.

The volume fraction (or the filling factor) of the metal embedded into the metallopolymeric material is calculated by equation:[119]

$$r = \frac{S_r - C_f}{S_m - C_f}$$

where S_r is the density of the metal-containing film, C_f and S_m are the densities of the metal-free film and the metal, respectively. The parameter r may vary from 0.1 to 1.0. This parameter reflects the structure of the polymer-immobilized nanoparticles. Thus

*The conditions of low-temperature plasma generation and the technology of plasmochemical processes are describes.[113–115]

at low r values and short plasma treatments, the plasma polymerization of benzene with silver yields quasi-2D particles.[120] The distribution pattern of the silver particles in the polymer depends on the plasma polymerization conditions and the filling factor. For example, the transmission electron microscopy has shown[121] that the composite plasmapolymer-silver films include three different structural regions with different r values: the metallic region composed basically of the metal particles that incorporate polymer inclusions (Fig. 7a,b), the percolational region in which there are no aggregated metal particles and the formation of interacting cluster particles is initiated (Fig. 7c), and the region in which the cluster particles are completely isolated by the polymer, (i.e., microencapsulated polycrystalline silver particles exist) (Fig. 7d–h). This structure is similar to colloidal particles of the Cu, Au, and Ag encapsulated with thin shells. This group also includes the particles of Au;[111,113,122–124] Co, Al, and Mo in fluoropolymers; Cu in polyethylene; Ag in a polymer obtained from chlorobenzene;[116] and benzene.[120] The distribution of gold nanoparticles in a polymer resulting from the plasma treatment of the C_3F_8–Au mixture has been studied in detail.[111,119] The mean size of gold particles is 5.5 nm ($r = 0.15$). The 5–10-nm silver crystallites in thin composite films were formed by polymerization of chlorobenzene and vacuum evaporation of Ag.[116] High Ag levels lead to particle diameters from 100 to 200 nm. Special studies have shown that neither AgCl nor silver carbide are formed.

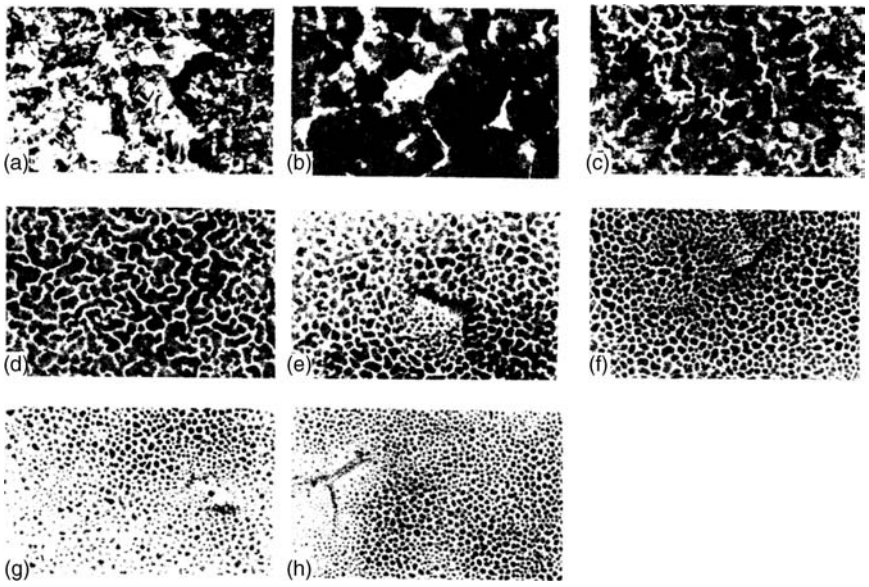

Figure 7 Electron micrographs of composite plasmopolymer–Ag Wlms. The degree of filling decreases on moving from panel **a** to panel **h**.[119]

In summary, the polymerization in a glow discharge makes it possible to produce thin polymeric films of controlled size on the surface of nanoparticles prepared

in situ. The complexity of this technique resides in the fact that it is difficult to control the rate of metal sputtering and metal incorporation into the polymer formed.

C. Preparation of Metal Sols in Polymers by the Thermal Decomposition of Precursor Compounds

Heating volatile metal compounds (such as metal carbonyls, π-allylic complexes, formates, acetates, and other organometallic compounds) in organic media or in the gas phase leads to their degradation. The metals or their oxides are liberated in the form of a dispersed phase. An example is the decomposition of iron pentacarbonyl (scheme 7).

$$Fe(CO)_5 \longrightarrow Fe_2(CO)_9 \longrightarrow Fe_3(CO)_{12} \longrightarrow Fe_n^0$$

Scheme 7

If these reactions are carried out in the presence of polymers, it is the simplest and apparently the most widespread method for the introduction of large (sometimes up to 90 wt%) quantities of colloidal particles of pure metals into polymeric compositions. This method underlies numerous processes intended for the preparation of polymer-immobilized ferromagnetic nanoparticles via the chemisorption of macromolecules on metal particles formed in situ. This is pertinent to the thermolysis of metal carbonyls.

Stable homogeneous polymer-immobilized dispersions of Fe, Co, Cr, Mo, W, Mn, Re, Ni, Pd, Pt, Ru, Rh, Os, and Ir colloidal particles can be produced using two thermal decomposition methods from their precursor compounds.[125,126] The first method employs an active polymer solution (containing amino, amide, imine, nitrile, hydroxyl, or other functional groups) in an inert solvent. The labile metal compound is added to this solution gradually. Favorable conditions are created for the chemisorptive polymer–metal interactions. Then the thermal decomposition is performed (100°–170°C). Sometimes the solution or suspension is subjected to different types of irradiation. The second method relies on the use of a passive polymer that reacts with the metal complex after it loses at least one ligand (for example, a CO). The gradual addition polymers such as polystyrene, polybutadiene, and copolymers of styrene and butadiene to an inert solvent containing the initial complex at the reaction temperature is accompanied by the dissociation of a ligand and the binding of the anionic complex with the passive polymer. Then the thermal degradation is performed.

The particle growth stage of this multistage process has much in common with the transformations taking place during the condensation of metal vapor on polymeric matrices (discussed above). The thermolysis of cobalt carbonyl and iron carbonyl[1] in the presence of polymers is well studied. For instance, the thermolysis (408K) of $Fe(CO)_5$ in a xylene solution of either *cis*-polybutadiene or a block copolymer of styrene and butadiene for 24 h under argon proceed through several consecutive stages, leading to the formation of $[C_8H_{12}Fe(CO)_3]$ units (scheme 8).

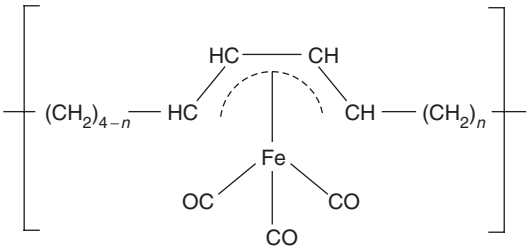

$n = 1, 2, 3.$

Scheme 8

The initial stage involves the formation of a highly reactive anion $Fe(CO)_4^-$, which interacts with isolated double bonds, followed by double bond isomerization and the formation of π-complexes with the iron tricarbonyl residues. The final product is composed of the η^4-(butadienyl)irontricarbonyl units with both *trans-trans-* and *cis-trans*-tetramethylene groups. Since the iron tricarbonyl complexes with two nonconjugated double bonds are unstable, no complexes between two polymer chains are formed. The reaction of iron carbonyls with low-molecular-weight nonconjugated dienes is accompanied by the double bond migration.

Three resonance structures represent the reaction product between an iron carbonyl and vinylallenes (scheme 9):[127]

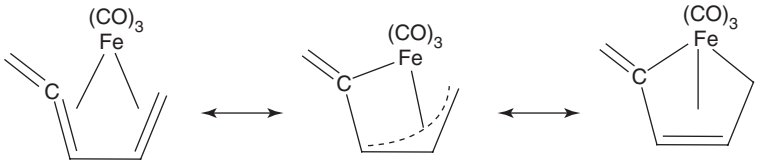

Scheme 9

A characteristic feature is that the same type of carbonyl complexes bound with allyl fragments in the polymer chains were detected on immobilization of $Co_2(CO)_8$ or $Fe_3(CO)_{12}$ within polystyrene-polydiene block-copolymers.[128] The thermal decomposition of these π-allyl complexes results in nanoparticles. The $Cr(CO)_3$ fragments in polystyrene are bound via η^6-complexed benzene rings.[129]

The nanoparticle sizes depend on numerous factors, including are the nature of the polymer disperser. A molecular weight of about 100,000 is optimum. Other factors include the nature of the functional groups (L) and the solvent. The cobalt-containing polystyrene–polybutadiene copolymer forms a nonmagnetic phase of cobalt clusters ~1 nm in diameter when annealed in vacuum at 493K for 2 h. Alternatively, thermolysis at 473–573K leads to the formation of 3–10-nm particles. Increasing the thermolysis temperature to 623K leads to the enlargement of cobalt

nanoparticles to 50 nm and the appearance of the ferromagnetic properties in the materials formed.

The nature of the solvent plays an important role. Metal carbonyls disproportionate in basic solvents (e.g., in DMF) to form ionic complexes in which metal atoms have a 2^+ formal charge (scheme 10). The product compositions of identified by IR spectroscopy varied with the extent of the substitution by carbonyl groups:

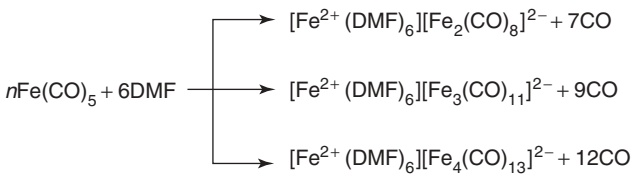

Scheme 10

In the general case (scheme 11):

Scheme 11

where Nu is a nucleophile (Py, *N*-methylpyrrolidone, etc.), $x = 2$–6; $n = 2$, $m = 8$, or $n = 3$, $m = 11$, or $n = 4$, $m = 13$. Under these conditions, dicobalt octacarbonyl is transformed according to the scheme 12:

Scheme 12

Basic solvents and high temperatures favor the binding of metal carbonyls to polymers. Stable colloidal dispersions are formed on the thermolysis of carbonyls in dilute polymeric solutions. For example, iron dispersion containing 5–10-nm particles have been produced.[128] Nanoparticles of this type are very reactive. Particles smaller than 10 nm are superparamagnetic, while the magnetic hysteresis is observed for particle sizes between 10 and 20 nm.

The size of Co particles may be prepared within the range from 2 to 30 nm with a narrow size distribution range by controlling the reaction temperature, the concentration of reagents, and the polymer composition (e.g., terpolymer of methyl methacrylate/ethyl acrylate/vinylpyrrolidone)[102] in a solvent like toluene with a low dielectric constant. It is important that polymers containing large numbers of polar groups can form particles of a smaller size. The same result is achieved by decreasing the metal carbonyl concentration in the polymer.

Nucleophilic fragments of macroligands, (such as those in styrene/*N*-vinylpyrrolidone copolymer catalyze the degradation of metal carbonyls, as shown in scheme 13:[125]

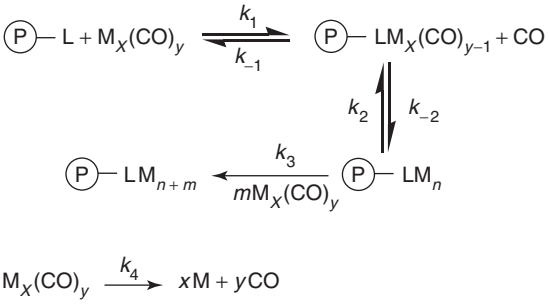

Scheme 13

Ligand functional groups on the polymer first form a soluble macromolecular complex. The loss of CO transforms complexes into polymer-immobilized cluster particles M^0. The subsequent growth of these particles leads to the formation of a nanoparticle. Initiation, growth of particles, and termination by simple disproportionation of metal carbonyl on the particle surface all occur.

The reaction rate on the polymer should be higher than the metal carbonyl decomposition rate in solution. Thus in scheme 13 the following should hold:

$$k_1 + k_2 - k_{-1} - k_{-2} > k_4$$

$$k_3 > k_4$$

Two major pathways in the thermolysis of metal carbonyls in polar media are realized. First, the disproportionation products react with the polymeric chain and initiate the side reactions of crosslinking, destruction, and isomerisation of the chain as well as the immobilization of mononuclear carbonyl complexes. For example, the polybutadiene containing 92% *cis*-1,4-; 4% *trans*-1,4-; and 4% 1,2-units ($M = 246\,000$) undergoes isomerization when reacted with $Fe_3(CO)_{12}$ for 2 h at 350K.[126] This increases the *trans*-1,4 content to 76%. Simultaneously, significant particle enlargement occurs as the hot metal atoms form 1–10-nm nanoparticles (scheme 14).

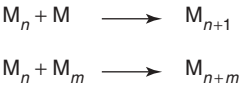

Scheme 14

The binding of small, insufficiently grown particles (M_n) by the polymer (scheme 15) generally

Scheme 15

produces nonmagnetic materials. Introduction of metal particles that are large compared to the interchain distances and the size of crystalline blocks and crosslinks results in the perturbation of the polymer structure and deterioration of its mechanical properties. The competition between both routes determines the ratio of thermolysis and diffusion rates. Both diffusion toward the hot metal centers in the matrix and thermolysis depend on the nature of the reacting particles and the reaction conditions. These processes are considerably influenced by the oxidative or reductive character of the medium.

The thermolysis conditions for metal carbonyls in polymeric matrices and the size of nanoparticles thus formed are given in Table 6.

Rapid unimolecular degradation of solutions of metal compounds in molten polymers, in the natural cavities of polyethylene, polypropylene, polytetrafluoroethylene matrices forms metal-particle-containing polymers; these materials were given the collective name Claspol.[130] In this process, the melt temperature should co siderably exceed the temperature to degradate the carbonyl complexes. Carbonyls are used as dilute solutions under conditions providing for the most rapid and omplete removal of ligand from the reaction system. This technique offers a number of advantages. On the one hand, higher temperatures increase the extent of carbonyl decomposition and reduce the yield of byproducts, on the other hand. In addition, in contrast to solutions, the melts preserve the close order of the initial polymer structure, while the cavities may host the particles formed. The polymer-immobilized particles thus obtained are characterized by a relatively high dispersity and homogeneous distribution over the polymer volume.[130] Macromolecules are irreversibly sorbed on their surface. The metal particles are primarily localized in the amorphous regions of the matrix. Segmental displacement of the amorphous phase is difficult owing to reduced free volume and possible crosslinking. The polymeric materials formed display enhanced thermal resistance. For example, the T_m of atactic polypropylene, modified with metal clusters, is increased by 50–80°C and this material acquires a monolithic pseudocrystalline structure.[130] The recurrent metal clusters spacing is concentration dependent. Iron, for example, forms 9–12-nm particles at high concentration (20–30 wt%) and 20–22-nm particles at low concentration (2–3 wt%) with a narrow particle size distribution (half-width ~1 nm). The presence of the metal phase does not affect either chemical or mechanical properties of such materials since the strong nanoparticle–polymer interactions lead to pseudocrystalline materials. In other words, at definite ratios of ingredients, these products are homogeneous metallopolymers.

Of particular interest is the thermolysis of metal carbonyls in the halogen-containing matrices. PTFE may be modified by Fe^{3+} or Mn^{4+} oxides by the sorption of the corresponding metal carbonyls and their subsequent oxidative decomposition using $KMnO_4$ or H_2O_2.[131] The oxide particles are incorporated into the amorphous regions of PTFE.

Nanoparticles are usually prepared in polar solvents that form intermediate complexes with the carbonyls (schemes 10–13). These complexes then react with the

Table 6 Thermal Decomposition of Metal Carbonyls in Polymeric Matrices[3]

$M_a(CO)_b$	Polymeric Matrix	Thermolysis Conditions	Nanoparticles Content (wt%)	Nanoparticles size (nm)
$Co_2(CO)_8$	without polymer	toluene		>100
	copolymer MMA-vinylpyrrolidone (90:10)	chlorobenzene	75	6–25
	polychloroprene	toluene	93	30–60
	copolymer vinylchloride-vinylacetate—vinyl alcohol (91:6: 3)	chlorobenzene	75	7–47
	PS	toluene	75	10–30
	copolymer styrene-acrylonitrile (88:12)	toluene	75	6–13
	atactic PP	toluene	75	>100
	polyesters	toluene	75	6–20
	polyurethane	toluene	75	5–30
	tercopolymer MMA-ethyl acrylate-vinyl-pyrrolidone (33:66:1)	toluene		20–30
$Fe(CO)_5$	Polystyrene-block-polybutadiene	dichlorobenzene, 145°C		7–8
	polybutadiene	decalin, 140–160°C		5–15
	cis-polybutadiene	xylene, 135°C		
	polybutadiene	decalin, 150°C		~6
	copolymer styrene-butadiene (5.8:1)	decalin, 150°C		~6
	copolymer styrene-4-vinylpyridine (1:0.05) the same	*o*-dichlorobenzene	2	~6
	(1:0.1) polyvinylidene fluoride	*o*-dichlorobenzene DMF, 140°C	1.8	~16 5–15
	cis-polybutadiene natural rubber	1% solution of dioxane-xylene, 135°C	37	
		8% solution of dioxane-xylene, 125°C	17	
$Fe_3(CO)_{12}$	*trans*-polybutadiene	benzene, ethanol, 80°C	23	
	copolymer styrene-butadiene (25:75)	benzene, 80°C	8	
	polybutadiene (81% repeat 1.2-chains)	benzene-dimethoxyethane, 80°C	16	
$Fe(CO)_5$	PE melt	—	1–29	1.5–7
	PP (isotactic, melt)	—	5	
	PP (atactic, melt)]	—	5–30	
$Cr(CO)_6$	PTFE (fluoroplast-40), melt	—	0.5–4	1–5

Table 7 Rate Constants and Activation Energies for the Decomposition of $M_x(CO)_y$-PVF (140°C, DMF).[132]

System	$k \times 10^{-5}/s^{-1}$	E_a/kJ mol^{-1}
PVF-$Fe(CO)_5$	8.41	142.59
PVF-$Fe_3(CO)_{11}^{2-}$	12.2	51.62
PVF-$Co(CO)_4$–	104	45.80

fluorinated polymers.[132] The main factors influencing the selectivity of $Fe(CO)_5$ or $Co_2(CO)_8$ reactions with polyvinylidene fluoride (PVF) during thermolysis have been discussed.[130–132] IR spectroscopy indicates that the adsorption leads to the formation of $[Fe^{2+}(DMF)_6][Fe_3(CO)_{11}]^{2-}$-PVF and $[Co^{2+}(DMF)_6][Co(CO)_4]_2^-$-PVF complexes. Kinetic studies to elucidate the mechanism of their degradation were carried out by IR spectroscopy. The thermolysis of both intermediates was first order; however, the rate constant and the activation energies of these two processes are substantially different (Table 7).

The thermolysis rate constant for polymer-immobilized cobalt carbonyl is one order of magnitude higher than that for iron carbonyl (Table 7). This is consistent with the cobalt carbonyl anion's higher reactivity versus the iron carbonyl anion. A high activation energy for the decomposition of neutral $Fe(CO)_5$ in PVF compared with E_a for the immobilized carbonyl reflects differences in the mechanisms of these reactions. The thermolysis of Fe or Co carbonyls in PVF in situ leads to the formation of metallic domains in the polymeric matrix. When the same carbonyls are bound within the polymer, homogeneously distributed ferromagnetic particles 5–10 nm in diameter are produced. The mean surface area per particle varies from 80 to 700 nm^2. The electron diffraction analysis of these systems has revealed the formation of γ-Fe_2O_3 and FeF_2 particles in the product from $Fe(CO)_5$.[131] Co, Co_2O_3, and CoF_2 were formed from $Co_2(CO)_8$.[131] The appearance of metal fluorides is associated with the cleavage of C–F bonds from the polymer.

Clearly, two parallel processes occur in these systems. The major process leads to the formation of nanoparticles upon thermolysis. In addition, a side process consists of the attack by metal ions upon the polymer chain. This is accompanied by various transformations of the polymer itself (destruction, crosslinking, binding of metal complexes). The formation of ZnF_2 was reported [103,104] via reaction of atomic zinc with the PTFE surface.

The precise nature of the bonding between clusters or nanoparticles to the polymeric matrixis is not fully known. Neither is the topography of these interactions. Nonetheless, it is obvious that the reactivity of the metal centers formed in the course of decomposition is a critical factor controlling the character of interaction between the polymer and the metal particle.

In the thermal degradation (especially, in the oxidative atmosphere), immobilized polynuclear complexes with volatile ligands may form nanoparticles of metals and their oxides. Sometimes admixtures of metal carbides are also present. Thus

heating poly (η^6-phenyl methacrylate)—$Cr(CO)_3$ films at 423K produced a mixture of chromium oxides enclosed in a crosslinked polymer matrix[133] (scheme 16).

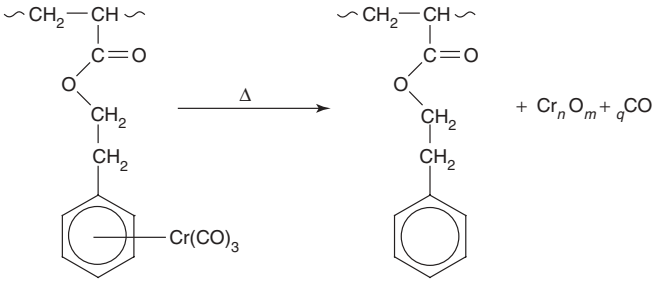

Scheme 16

Thermolysis of the copolymers of acrylonitrile or styrene with (η^4-hexa-2,4-dieneyl acrylate)iron tricarbonyl in air at 473K leads to the formation of Fe_2O_3 nanoparticles.[129] The distinctive feature of nearly all polymers of this type is that they do not melt during or after the decomposition step, apparently because crosslinked structures are formed. Since the metal oxides are the final products of the oxidative decomposition of any metal-containing polymer, the possibility of the replacing toxic $Fe(CO)_5$ by polyvinylferrocene has long been debated.

Less often, metal carbonyls are replaced by other precursor compounds. Examples include metal formates, acetates, and oxalates, and various organometallic compounds. Recently, a metal-polymer composition of the Claspol type was obtained by the thermolysis of a triethylenediamine complex of copper formate $[Cu(En)_3](HCOO)_2$ in PS using dimethylformamide as the common solvent.[134] This complex disintegrates at 170°C to form metallic copper in a highly dispersed state. This temperature is 20°C lower than that of the thermolysis of the initial pure copper formate complex. The polymer has a catalytic effect on the thermal degradation of this complex. The reactive centers of the polymer favor the formation of metal particle nuclei, which are centers of aggregation. This is followed by the thermolysis and redistribution of the copper complex. The maximum quantity of copper that can be incorporated into PS is 10%.

PTFE increases the decomposition temperature of cadmium oxalate trihydrate.[3] Moreover, the products of cadmium complex degradation, in turn, increase the temperature at which an intensive degradation of PTFE begins. The thermal decomposition of the highly dispersed copper formate leads to the formation of a metal–polymer composition (20–34% Cu).[1] The maximum on the nanoparticles granulometric composition curve corresponds to ~4 nm. No chemical interaction between the components was observed. The decomposition of a fine dispersion of palladium hydroxide in polyvinyl chloride (PVC) results in spatial structures with highly dispersed Pd particles ($S_s = 26\ m^2\ g^{-1}$) in the nodes. This process increases in the temperature required for complete dehydrochlorination of PVC. The thermolysis of cobalt acetate in the presence of PS, PAA, and poly(methyl vinyl ketone) proceeds

at a much higher temperature and leads to the formation of metal clusters that catalyse the electroreduction of oxygen.[135]

The preparation of a highly dispersed Cd phase regularly distributed in the PS bulk has been reported.[3] PS was mixed with dibenzylcadmium in THF followed by removal of the solvent and decomposition of the organometallic compound at 130°C. Materials containing 1.4 – 4.3% of Ni or Co were obtained from the bisarene complexes $(C_6H_5CH_3)_2M$, where M = Ni, Co, by their rapid degradation in LPPE at temperatures higher than the decomposition temperature of these complex.[109] Cobalt nanoparticles with a mean particle size of ~1.6 nm and narrow particle distribution were prepared[136] by hydrogenation of the organometallic compounds into the amorphous regions of PS, high-pressure polyethylene (HPPE), PTFE, and polyacrylates. This was followed by their structural modification and formation of clusters as exemplified by $(\eta^5\text{-}C_5H_5)Mn(CO)_3$.[137] To this end, fluids are used in their supercritical state (CO_2 under a pressure of 8–25 MPa at 30–40°C).* According to another protocol,[140] dimethyl(cyclooctadiene)platinum(II) was dissolved in CO_2, and this solution was used to impregnate thin films of poly(4-methylpent-1-ene) or PTFE. The reduction of this system by thermolysis or hydrogenolysis yields polymer-immobilized Pt particle nano-composites with Pt particle sizes of 15–100 nm.

Despite many studies of this sort, no literature discusses thermolysis in polymer-immobilized carbonyl-hydrides, substituted (mixed) carbonyls, or mixed metal carbonyls (such as $Co_2Ir_2(CO)_{12}$, $H_3FeRu_3(CO)_{15}$, $Fe_2Ru(CO)_{12}$, or $MM'(CO)_n$, where M = Mn, Re; M′ = Cr, Mo, W). Data on the thermolysis of metal carbonyls in thermosetting plastics are also meager. The only thing known is that heating degradable metal carbonyls that are introduced into an epoxy resin leads to the deposition of nano-particles on the surface of the polymer formed. The highly reactive metal particles may initiate the opening of the epoxy ring with the formation of 3D polymer structures.

D. Synthesis of Polymer-Immobilized Nanoparticles by Reductive Methods

Reduction is the most common technique to prepare polymer-immobilized nanoparticles. Two different types of reduction can be considered. The first type, or the impregnation method, consists of the chemical reduction of metals from solutions or suspensions of their salts. Ammoniacal solutions of Cu, Cr, and Ag hydroxides are often used. Electrochemical or radiation-induced reduction in the presence of macroligands have also been employed. The reduction of mononuclear metal complexes chemically bound with polymers represent the second type. The impregnation method is more widely applied because it better meets the needs of catalysis. In particular, metal blacks, ultradispersed powders, etc. are prepared. For example, Raney nickel is stabilized by incorporating it into the silicone rubber[141] followed by vulcanization at room temperature.

*The interest in the processes occurring in supercritical Xuids has sharply increased over the recent years,[138,139] especially in the reactions in supercritical CO_2.

Au, Fe, and Cr sols were prepared by the reduction of their hydroxides by hydrazine hydrate in a matrix of water-soluble polymers, and dispersions of particles of Pd (1–2 nm) and Au (1–13 nm) were obtained in synthetic rubber films.[142] Polymeric films prepared from aqueous solutions of PVAl and $AgNO_3$ were treated with photographic reducing agents (hydroquinone, *p*-phenylenediamine, pyrogallol, etc.) to produce the corresponding metallocomposite materials.[143] Monodispersed hyperfine powders of gold [143] and platinum[144–147] were prepared by the reduction of their salts in the presence of protective colloids.

Natural polymers (gelatin, gum arabic, agar, proteins and products of their hydrolysis, sodium protalbuminate, starch, cellulose and its derivatives) and polymeric compounds soluble in organic media (synthetic rubbers, naphthenic acids) are often used as protective high-molecular-weight compounds in the production of sols of silver, mercury, bismuth, copper, and platinum group metals by the reduction of corresponding ions. (β-Cyclodextrin may also be employed as a stabilizing agent for colloidal particles of Rh, Pt, and Pd (1–100 nm).[148] Ultrafine particles of Ni (5–20 nm) were prepared from $Ni(NO_3)_2$ by reduction with hydrogen following the particle diffusion into gel membranes of cellulose acetate.[149] The adsorption of ions by protective polymers (discussed earlier) creates favorable conditions for the concomitant appearance of a large number of colloidal metal nuclei. The metal that was reduced was mostly consumed to form these nuclei, while only a small quantity remained for their growth. As a result, only small nanoparticles were formed. The high aggregative resistance of the sols also favored small nanoparticles.

The radiation-chemical and photo-induced reduction is preferred to the reduction by hydrogen when it is necessary to prepare small particles with a narrow size distribution.[150] A characteristic example is the preparation of blue silver in the process of γ-irradiation of slightly alkaline aqueous solutions of $AgClO_4$ containing 2-propanol and PAA.[151,152] The blue silver is a linear Ag cluster stabilized on a polymer molecule. In the course of radiation-chemical reduction, the Ag clusters are transformed through a number of successive stages into a polymer-immobilized colloidal silver.

Treatment of colloidal Pd, obtained by the radiation-chemical reduction of Pd^{2+} in an aqueous solution of PAA, with H_2 does not increase the particle size. Ohly hydrogen sorption on the nanoparticle surface occurs.[152]

The impregnation method does not rule out the chemical interaction between the compound to be reduced and the polymeric matrix. The absence of chemical interaction between the metal and the polymer is an exception rather than the rule. For example, in the systems based on polymers devoid of functional groups (polyacetylene and MX_n) the macromolecule plays the role of a specific ligand. This hampers the multicenter association of metal complexes and prevents their enlargement. Condensation of a metal in a liquid phase occurs at the moment its ion undergoes reduction. The formation of a supersaturated solution of metal atoms is not necessary. Nanoparticle nuclei formation occurs spontaneously, at the sites of largest metal ions concentration. Particle growth results from the reduction of ions adsorbed on the surface. Apparently, this process has much in common with the growth of particles in the course of cryochemical synthesis.

The mechanism underlying the reduction of metal ions chemically bound with polymers is rather complex. It has been elucidated in detail using the formation of

clusters of zero-valent Pd, Ru, Rh, Ag, Os, Ir, Pt, Au, and Ni as the examples.[153–155] When solutions of these metal salts in proton-donating solvents are boiled in the presence of polymers several chemical transformations take place. An example is a solution of $RhCl_3$ in aqueous methanol in the presence of poly(vinyl alcohol) (scheme 17).

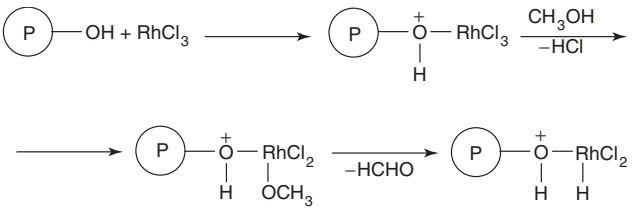

Scheme 17

At the start of this complex process, $RhCl_3$ coordinates with PVA. An oxonium product is formed, which is further transformed via an alkoxide intermediate into a polymer-bound hydride complex. Finally a colloid forms, resulting from the disproportionation of these rhodium hydrides and subsequent growth of particles (scheme 18).

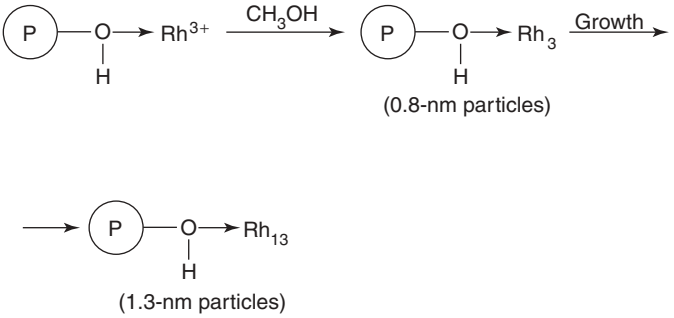

Scheme 18

The Rh_{13} nuclear clusters have the structure of a face-centered cubic lattice structure with a rhodium atom coordination number equal to 12. These clusters are 4 nm in diameter. They interact with the protective polymer owing to electrostatic attraction or to physical adsorption. The formation of coordination bonds is also possible.

Changing the nature of the medium, (ethanol, butanol, toluene-butanol), introducing additional ligands (e.g., PPh_3), or using various polymers (e.g., PVPr, copolymer of MMA with *N*-vinyl-2-pyrrolidone or polyacrylamide gel), permits the preparation of metallopolymers with cluster particles of different sizes (0.9–4 nm for Rh^0 and 1.8 nm for Pd^0). These particles are stable in the protective colloid. They have a narrow size distribution and high stability. They remain in the gel over a pH range from 2 to 12. Thus the water-soluble polymers act as protective colloids, while alcohols serve as reducing agents.

The reduction of $NiCl_2$ by $NaBH_4$ in ethanol in the presence of PVPr generates a nickel boride sol.[3] This method is suitable for the preparation of organosols of noble

metals. It proved to be useful in the synthesis of colloidal dispersions of polymer-protected bimetallic Pd–Pt or Pd–Au clusters.[155–157] They were produced by the joint reduction of $PdCl_2$ and H_2PtCl_6 or $HAuCl_4$ in the presence of PVPr (by boiling in methanol or enlightenment with visible light). The products remained stable for a few months at room temperature. The size of Pd–Pt and Pd–Au clusters was ~1.5 and 3.4 nm, respectively. This method was also used to prepare polymer-protected bimetallic Pt-Co colloids with Pt:Co ratios of 3:1 and 1:1.[158]

The diffusion of ions to be reduced into the polymeric matrix is an obstacle to the synthesis of metal colloids. For example, reduction of Ni^{2+} with $NaBH_4$ in aqueous methanolic solution within porous isotropic isotactic polypropylene (PP) has been carried out using the method of countercurrent diffusion.[159] The following consecutive stages are involved: (1) penetration of metal ions and the reducing agent into the polymeric matrix, (2) in-depth diffusion of reagents, and (3) the reduction itself. The size of the nanoparticles formed depends on the reaction conditions and the parameters of the porous polymeric structure. This technique allows the microencapsulation of metal crystallites (3–10 nm in diameter) assembled in polycrystalline aggregates. Nickel particles prepared by the reduction in the polymeric matrix resisted oxidation in water for over 2 weeks. Dry particles remained unoxidised for 6 months.[160] In contrast, the nickel obtained in the absence of polymers rapidly oxidised in water and air. Apparently, polymer shielding prevents further growth of particles and also provides their high resistance to oxidation. The macromolecules trap and stabilize the metal nuclei by cooperative interactions of chain segments during matrix recognition by the growing chain during polymerization.

Immobilized complexes (including mononuclear ones) undergo different transformations leading to the increased nuclearity during reduction. For example, Rh, Ru, and Pt compounds fixed by ion exchange on the completely fluorinated resin Nafion (Fig. 8), undergo reduction in a flow of H_2 at 473K. Metallic clusters are formed with sizes of 2.8, 3.3, and 3.4 nm, respectively.[161] Cations of Ag, Cu, Rh, Ru, Pt, and Ir bound to perfluoroethylenesulfonic acid or to a partially sulfated PS oxidise CO, NO,

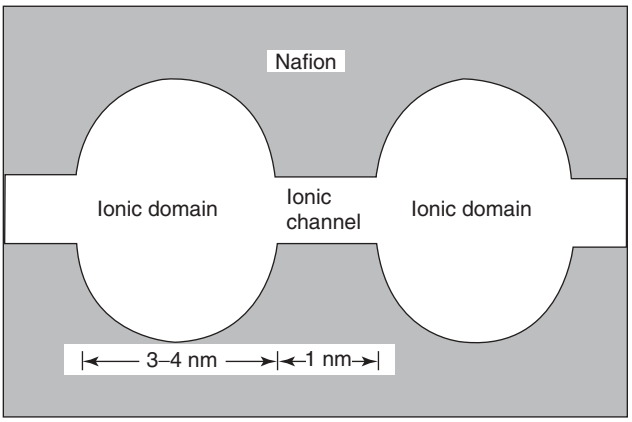

Figure 8 Ionic Domains in the Nafion Ion-Exchange Resin.[161]

NH_3, N_2H_4, and C_2H_2 at 373–473 K. This gives metal particles 2.5–4.0 nm in diameter.[162]

The formation of polymer-immobilized metalloclusters during catalytic reactions is a rather common, especially for complex organometallic catalysts deposited on polymers.[73,79] This may cause both activation (e.g., in hydrogenation reactions) and deactivation (in particular, in reactions of ionic-coordination polymerization). Transformations of immobilized Ni^{2+} during ethylene dimerisations were studied by magnetic susceptibility measurements in strong magnetic fields (up to 70 kOe at 4.2K. Under these conditions, the susceptibility of different spin states depends nonlinearly on the magnetic field strength (described by the Brillouin's function), which made it possible to establish the distribution of nickel states over the magnetic moment values. Evidence exists for the formation of 1-nm microparticles containing 10–30 Ni atoms that display no ferromagnetic (supermagnetic) properties. Polymer-immobilized cobalt catalysts are used for butadiene polymerization. A considerable proportion of Co^{2+} ions in these catalysts are reduced to the metallic state in the absence of polymerized monomer.[3] About 90% of total ferromagnetic cobalt is localized in the relatively large particles 10 nm in diameter.

E. Electrochemical Methods for Preparing Polymer-Immobilized Nanoparticles

The electrochemical and electroflotation methods are widely used to prepare of chemisorbed macromolecules bound to colloidal metal particles generated in situ. Electrochemical polymerization reactions are heterogeneous: They are initiated on the electrode surface, while other stages (chain growth or termination) occur, as a rule, in the liquid phase. The yield of a polymer depends on the chemical and physical nature of the electrodes and their surface, electrode overvoltage, potential under which the reaction occurs, and electrical current density. The nature of the electrode material (metals or alloys, thin metallic coats, etc.) determines the characteristics of electron-transfer initiation and polymerization. Direct electron transfer between the electrode and monomer, cathodic deposition, and anodic solubilization of metals are optimum for electrochemical polymerization. Metal salts are the precursors of nanoparticles, which may act as specific electrochemical activators. Nanoparticles can influence activations through direct chemical binding to the monomer and by virtue of transfer, decomposition, or catalytic effects. Nonetheless, electrochemical polymerization has found only limited use in the preparation of polymer-immobilized nanoparticles.

The preparation of metal organosols by electrolysis in a two-layer bath proved to be more suitable than electrochemical polymerization.[163] The upper organic layer of the electrolytic bath is a dilute solution of a polymer in an organic solvent, sometimes, supplemented with a small amounts of surfactant. The polymer interacts with the nascent colloidal metal particles near the interface between layers.

Less often, nanoparticles are formed on polymers by means of electrophoretic and electrochemical deposition of metals onto an added polymeric suspension. The metallopolymer formation results from the polarizational of polymer and metal particles during deposition on the electrode followed by chemisorption of macromolecules at the metal surface at the moment of its reduction. This process includes

several stages, such as discharge of M^{n+} ions, crystallization of deposited metal, a number of parallel electrochemical reactions, etc. The contributions from different stages depend on the concentration of the dispersed phase and electrolyte, and the particle charge. The ratio of these contributions determines the transition from polymer-immobilized nanoparticles to high metal content electrochemical plating.

Polymeric particles shield and block, the surface of the electrode and metal particles. Therefore, electrophoretic polarization appears, which has an appreciable effect on the process of metal electrocrystallization. The polymer is often deposited as a separate phase (liquid or solid) on the electrode surface. The polymer may cause significant kinetic restrictions to the transfer of ions, electrons, or neutral particles through this new layer.[163] The extent of those restrictions depends on the permeability of polymeric coating. Coating the anode with an insulating polymer layer reduces the electrode activity and the current amplitude.[164] This inconvenience can be partly eliminated by the use of liquid electrodes, such as the dropping mercury electrode.

In one example, colloidal Pd particles are obtained by the electrolysis of aqueous solutions of palladium chloride at pH 1 in a two-layer bath in the presence of a hydrocarbon solvent and epoxy dianic resin or PVA.[3] Electrolysis results in the formation of colloidal palladium organosols stabilized by the chemisorption of the polymer. Metallopolymers containing up to 90–95% of Pd remain after the removal of solvent and residual electrolyte. They are formed under high cathode polarization where concomitant elimination of hydrogen adsorbed on the nanoparticles (5.5–7.8 nm in diameter) occurs.

The combined Ni nanoparticles deposition and PTFE suspension from the sulfamic-acid electrolyte during nickel-coating at room temperature leads to polymer inclusion into the Ni deposit.[164] The polymer may contribute up to 20 wt%. The process is controlled by varying the cathode current density and the concentration of the suspension introduced. The relationship between the homocoagulation and heterocoagulation interactions of metal particles and polymer is determined by the rates of electrochemical deposition and the trapping of Ni in the PTFE systems. [165]

The electrode material may become the precursor of noble metals nanoparticles. Polypyrrole films containing functional groups, such as 4,4′-dipyridyl, alkylammonium, may serve as protectors in this case. [166–169] Bimetallic Pd-Pt or Pd-Rh nanoparticles incorporated into such films are also used for the electrocatalytic hydrogenation.[170] Fine dispersions of iron powders (~200 nm) formed electrochemically may be used as modifying coatings of various materials.[171] How polymeric dispersions effect the reduction of metal ions depends on the concentration and composition of both electrolyte and dispersed phase, the charge and size of polymeric particles, and the mode of electrodeposition.

The thermal techniques have substantial advantages over the electrochemical ones because the latter occur with considerable degradation of the dispersive medium, noticeable oxidation of the colloidal particles formed, etc.

F. Preparation of Polymer-Immobilized Nanoparticles During Polymerization (Polycondensation) Stage

Methods for the simultaneous formation of the matrix and nanoparticles are of special interest. A large number of techniques is reported mostly in the patent literature.

The early studies demonstrated the possibility of initiating polymerization by intensive mechanical dispersion of certain inorganic substances, including metals (Fe, Al, Mg, Cr, W) in vinylic monomers. The degree of polymerization of styrene, vinyl acetate, acrylonitrile, or MMA depended on the dispersion intensity. The fresh metal surfaces play the role of catalyst and initiator. These surfaces are the sites of electron transfer from the surfaces metal atoms to the monomers to form ion-radical initiating particles. Colloidal particles of Au, Tl, and Pt were found to influence substantially the bulk and solution polymerization of styrene.[1,3]

Sometimes, organometallic compounds are used instead of bulk metals for the preparation of polymer-immobilized nanoparticles. Adding of relatively small quantities of organo-cadmium compounds has virtually no effect on the initial rate of radical polymerization of MMA.[172] Cadmium nanoparticles may be obtained by two routes: (1) from organometallic compounds, such as bis(triethylgermyl)cadmium, which decompose at a temperature close to that of polymerization, or (2) by heating the composition formed, which includes a cadmium component whose decomposition temperature is higher than that of MMA polymerization. Alkyl derivatives of cadmium serve this purpose. Organocadmium compounds of this type lower the molecular weight (M_n) of the PMMA formed. For example, PMMA's M_n decreases from 800 to 60 kDa in the presence of 2.5 wt% of these compounds.[172] Chain transfer at the organometallic compound is the probable cause. The formation of nanoparticles in the monomer–polymer mixture is represented in scheme 19.

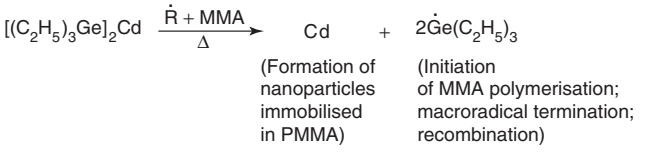

Scheme 19

The size of Cd nanoparticles formed at the polymerization stage increases from 6.3 nm to 300 nm as the content of the initial cadmium compound in the monomeric mixture increases from 8 to 40 wt%, respectively. Compositions formed on heating contain larger nanoparticles that have the regular hexagonal structure characteristic of Cd crystals.

The critical process parameters are the ratio of the rates of decomposition of the organometallic component and the polymerization of the corresponding monomer, and the sedimentational resistance of metal dispersions formed in the monomer. Apparently, this also holds true for solidifying systems. For example, colloidal Pb is incorporated into thermally generated epoxy-thiocol resin at the moment of its formation by thermolysis. In this case, internal stresses existing in solidified systems should be considered.[173]

Highly stabile nanoparticles result by combining in situ photopolymerization (acrylamide and *N*, *N*′-methylene-bis-acrylamide, nonfiltered light from a DRSh-250 mercury lamp) and photoreduction of highly stable Ag^+ ions.[107] The

nascent specimens remain stable in air for a few weeks, and films remain unaltered for a few months. The ≤20 nm Ag particles are comparable with nanoparticles prepared by low-temperature condensation of vaporized metals. A modification of this method was reported recently[174] where metal vapors and monomers capable of low-temperature polymerization were simultaneously condensed on a support at liquid nitrogen temperature. The metal used were Ag, Pb, Cd, or Mg and *n*-xylylene was the monomer. *n*-Xylylene yields poly-*n*-xylylene films with regularly distributed nanoparticles more or less homogeneous in size in this process. The formation of these films was induced by UV irradiation at 80K or heating to 130–160K.

Other modifications of this method for the preparation of nanoparticles in polymers have been reported. In one modification, catalysts containing highly dispersed transition metals particles immobilized in films were obtained by the electrolytic oxidative polymerization. A monomer derived from mercaptohydroquinone was electropolymerized in the presence of platinum group metals. These metals were incorporated by electrochemical deposition.[175]

Not all of the approaches discussed in this section are equally developed. The priority is given to the reduction techniques. The role of the dispersive phase is mostly played by carbon-chain polymers and less often, by condensation-type polymers. The immobilization of nanoparticles is nearly always accompanied by chemical interactions of the particles formed with the matrix, in contrast to mechanical mixtures of metals with polymers. Further developments in the preparation of polymer-immobilized nanoparticles[176–190] have been documented.

VI. PREPARATION OF HYBRID NANOCOMPOSITES BY THE SOL-GEL METHOD

Optimum procedures for the preparation of composite materials should not produce effluents of environmental consequence. This is a characteristic of the sol-gel method (sol-gel or spin-on-glass process). The latter method allows one to exclude numerous washing stages because the reagents do not contaminate the final product. The sol-gel method is convenient procedure for preparing dispersed materials (ceramers). Sol-gel polymerization of inorganic compounds forms metallooxo polymers in solution. This involves the following stages: (1) preparation of a solution, (2) formation of a gel, (3) drying, and (4) thermal treatment. Metal alkoxides $M(OR)_n$ (M = Si, Ti, Zr, VO, Zn, Al, Sn, Ce, Mo, W, lanthanides, etc.; R = Alk or Ar), are used, which hydrolyze upon addition of water, as the starting compounds. The reactions are carried out in organic solvents. Subsequent polymerization (condensation) affords a gel, for example, when $n = 4$ (scheme 20).

$$M(OR)_4 + 4H_2O \longrightarrow M(OH)_4 + 4ROH,$$

$$mM(OH)_4 \longrightarrow (MO_2)_m + 2mH_2O.$$

Scheme 20

In this method, hydrolysis and condensation are catalyzed by the same compound (by acid, base or, sometimes, by a nucleophilic catalyst, such as NaF).[14,191] These reactions with $Si(OR)_4$ have long been known. Apparently, the preparation of monodisperse TiO_2 particles by hydrolysis of alkoxides was described first by Barringer and Bowen.[192,193]

The real process is much more complicated and occurs by multiple-route mechanism. Generally, metal oxoalkoxides $MO_n(OR)_m$, including polynuclear compounds, are formed as intermediates. Thus hydrolysis of $Ti(OR)_4$ proceeds in two stages.[27,194] Nucleophilic replacement of the alkoxy group by the hydroxy group is followed by condensation where oxo and hydroxo bridges are formed. The rates of these reactions are comparable.[195] $Ti_xO_y(OR)_{4x-2y}$ compounds were isolated and characterized.[196] In general, the controlled synthesis of hybrid nanocomposites from zirconium alkoxysilanes and alkoxides proceeds according to scheme 21.[195]

1. Formation of complex 1:

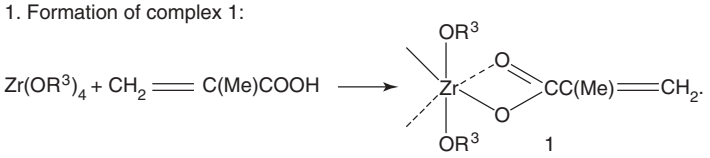

2. Hydrolysis:

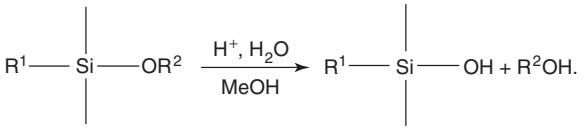

3. Condesation to form latent water:

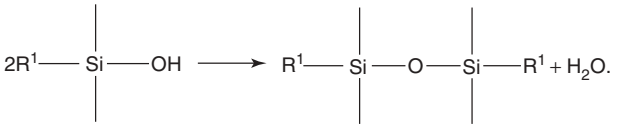

4. Addition of complex 1 and removal of free and latent water by condesation:

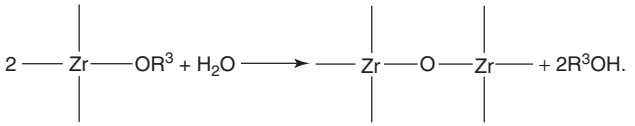

4. Addition of a photoinitiator:

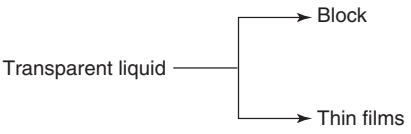

Scheme 21

The following variables are of great importancein these types of reactions: (1) the use of catalysts, including polymeric catalysts such as polystyrenesulfonic acid;[197] (2) the nature of the alkoxy group and of the metal (for example, $Ti(OBu)_4$ is hydrolyzed almost 150 times more slowly than $Ti(OEt)_4$);[198] (3) the use of mixed alkoxides, particularly chelating ligands such as β-diketonate, α- or β-hydroxy acids, and polyols; (4) the degree of alkoxide association of (e.g., in the case of $[Ti(OEt)_4]_m$ $m = 2$ or 3); and (5) the formation of oxo or alkoxo cluster structures during hydrolysis (e.g., $Ti_{18}O_{22}(OBu)_{26}(acac)_2$). The reactivity of $M^{IV}(OR)_4$ alkoxides increases in the series $Si \ll Sn$ and $Ti < Zr < Ce$.[199] The ionic radius of the M atom (0.04 and 0.06 nm; and 0.064, 0.087, and 0.102 nm, respectively), its coordination number (4 and 6; and 6, 7, and 8, respectively), and its degree of unsaturation (the coordination number minus the valence; 0 and 2; and 2, 3, and 4, respectively) all increase in the same order.[200] The H_2O:$M(OR)_4$ ratio (γ) is of prime importance. For example, sol-gel hydrolysis of $VO(OPr^n)_3$ generates a homogeneous transparent gel with an alkoxide polymer network in *n*-propanol if $\gamma = 3$. However, when $\gamma > 100$, the resulting gel acquires a quite different structure, which prevents the formation of an inclusion compound. Gel formation is also affected by the nature of the medium, the initial alkoxide concentration, the presence of a stabilizer and the reaction temperature.[201–203] The thermal effects on $Ti(OR)_4$ hydrolysis in ROH increases when $\gamma = 0.2-1$, and then remain virtually unchanged. This corresponds to the replacement of one alkoxy group by the hydroxy group.[204] $TiO_x(OBu)_{4-2x} \cdot \gamma BuOH$ was obtained upon hydrolysis of $Ti(OBu)_4$ in butyl alcohol via intermediate $TiO(OBu)_2$.[198,204] The *x* and *y* values increased as the solution concentration of titanium alkoxide increased. Unfortunately, the effect of solvent (generally, alcohols) on these processes has received little attention in experimental studies. It is known that hydroxy-containing compounds (for example, AlkOH, HOH or R_3SiOH) play an active role in transesterification (scheme 22).

$$M(OR^1)_4 + nHOR^2 \longrightarrow M(OR^1)_{4-n}(OR^2)_n + nHOR^1.$$

Scheme 22

The metal alkoxides affect substantially these reactions.[205–207] Thus $Ti(OPr^i)_4$ and $OV(OPr^i)_3$, cocondensates act as catalysts in transesterification of tetramethoxy- and tetraethoxysilanes (TMOS and TEOS, respectively) during sol-gel nanocomposite preparation.[208]

The sol-gel process involves hydrolysis, polymerization (chemically controlled condensation) of a gel precursor, nucleation and growth of particles followed by their agglomeration.[209,210] TMOS and TEOS are most often used as precursors. They form silica gel structures that serve to host a dopant (guest), within specific cage. Nucleation proceeds through formation of polynuclear complexes. Their concentrations increase slightly above supersaturation. From this time on, new nuclei do not form. Only the available nuclei grow, similar to the analogous formation of nanosized particles in polymers.[3] A gel can be impregnated with ions of different metals during the gelation stage.

The resulting oxopolymers exhibit ultrathin porous networks with pore sizes of 1–10 nm similar to the structures of zeolites. Their specific surface area (S_{spec}) varies in the range of 130–1260 $m^2\ g^{-1}$, depending on the conditions. Their bulk densities are 0.05–0.10 g cm^{-3}. Thus molecular sieves based on silicon oxides were prepared by the sol-gel method in the presence of surfactants.[211,212] They were characterized by different mesopore structures and S_{spec} of ~1000 $m^2\ g^{-1}$. Hydrolysis of $Ti(OEt)_4$ produced a powder with a surface area of 200–300 $m^2\ g^{-1}$. Futhermore, the S_{spec} of $Ti(OBu)_4$ hydrolysis products strongly depends on the concentration of the initial alkoxide solution and attains 490 $m^2\ g^{-1}$ at the concentration of 1.0 mol L^{-1}. Concentrated aggregatively stable hydrosols (up to 40 wt% of TiO_2) were prepared[213] by secondary dispersions of dried xerogels of the sol (the TiO_2 content is ~85 wt%) at 100°C for 2 h. This sol contains crystalline ~3 nm TiO_2 particles, which are a mixture of rutile and anatase polymorphs, with the latter slightly predominating. Brookite is rarely formed. Single crystals of the anatase phase are often metastable in these systems. Compounds containing labile vinyl, methacrylate, epoxy, and other functional groups can act as crosslinking agents (scheme 21). Conditions for removal of volatile components determine the product texture. Prolonged air drying generates coarse-dispersion xerogels due to coalescence of gel particles. Highly dispersed aerogels are formed when conditions preclude capillary forces from acting. Thermal treatment completes the formation of the structure and texture of the product.[10,214–218]

The sol-gel polycondensation of highly dispersed silica gel in a polar solvent is applied for the microencapsulation of photochromic fluorescent compounds,[219] scintillators,[17] and porphyrins. A sol-gel matrix for encapsulation is prepared by simultaneous hydrolysis of $Si(OEt)_4$-$Zr(OBu)_4$ and other alkoxides.[220–222] Thermally stable materials for use in nonlinear optics can be prepared by introducing azo dyes into TMOS by the sol-gel method.[223] Although these systems are not considered in this review (except for biologically active systems; see below), they are structurally similar to nanocomposites and are prepared by analogous procedures. Thus introducing of a solution of perylene in methyl methacrylate (MMA) into a xerogel followed by thermal or UV polymerization, afforded a coimpregnated SiO_2-polymethyl methacrylate-dye system.[224,225] A sublimation/dehydration method was developed for impregnated gels,[226] which prevents redistribution of labile components in the matrix during drying.

Sol-gel materials are classified by their mode of formation and types of bonds between organic, organometallic, and inorganic components.[17] Organic groups introduced into $R^1_nSi(OR^2)_{4-n}$ serve two functions:[227,228] modify a network (ORMOSIL, organically modified silicates) and form a network (ORMOCER, organically modified ceramics). However, this classification has not yet received ample recognition. Low- and high-percentage composites contain 2–30 vol% and 45–75 vol% of ceramic content, respectively. A material under the name *rubber ormosil* (based on TEOS and polydimethylsiloxane with $M_w = 1700$) contains more than 70 vol% of an inorganic component.[229,230]

Hybrid nanocomposites may be classified by the type of interphase interactions between components. For example, nanocomposites whose macrostructures are determined by the presence of van der Waals, hydrogen or hydrophilic–hydrophobic

interactions are known. Amorphous inorganic nanocomposites prepared from silicon-, titanium-, aluminium-, or zirconium-containing oxopolymers formed in situ in a medium of a soluble organic polymer belong to this group. This process involves the homogeneous formation of a nanosized filler in a medium of a polymer composites with poly(*n*-butyl acrylate), polyphosphazene, polyvinylpyrrolidone (PVPr), and poly(*N,N*-dimethylacrylamide) matrices were prepared according to this procedure.[231–235] An alternative procedure involves the insertion of a polymer (or its precursor) into an oxogel, formed by mixing of metal alkoxide.[233] The polymer may also be impregnated into pores of an oxide xerogel network. Organic molecules or polymers may also be inserted as guests into nanocomposites of other types.

The single-stage formation of oxogels and polymers is exemplified by sol-gel polymerization of the silanised monomers such as *N*-[3-(trimethoxysilyl)propyl]-pyrrole,[236,237] 2,5-bis(trimethoxy-silyl)thiophene,[238] and trimethoxysilylferrocene derivatives.[239]

Hybrid network composites where organic and inorganic components are linked through strong covalent or ionic bonds have been prepared according to two procedures: (1) the formation of secondary networks within primary networks, which are functionalised as required; and (2) the simultaneously formation of two different networks (including interpenetrating networks) from molecular precursors of a different nature that undergo different reactions (polyaddition, polycondensation, metathesis polymerization, hydrolysis-condensation, etc.). This simultaneous network formation is in a early state of development. Reliable examples realized by this approach are few in number.[240–242] Initially, attempt were made to use solutions of polymers. However, gel formation a was accompanied by uncontrolled phase separation to yield a heterogeneous materials. More homogeneous sol-gel materials were prepared[243] by simultaneous acid-catalysed hydrolysis and condensation of HO-(polyethersulfone)-OH (PES) and TEOS or TMOS in DMF (scheme 23).

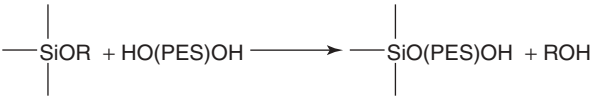

Scheme 23

Inorganic and polymeric components are linked by chemical bonds. Thus poly(ethersulfone) chains are linked through —SiO_2— units. Their condensation affords nanoparticles (Fig. 9).[244]

Bonding of TEOS, diethoxydimethylsilane or their mixture with sulfonate groups of perfluoroalkylsulfonate ionomers (Nafion) in which SO_3H^+ groups form 3–5-nm clusters affords a hybrid heterogeneous material Nafion/SiO_2 (Nafion/ORMOSIL[245–249]). Differential scanning calorimetry demonstrated a shift of the broad endothermic peak of Nafion H^+ at 215°C to a lower temperature as the ratio of the components of the reaction mixture was changed. This endotherm is associated with

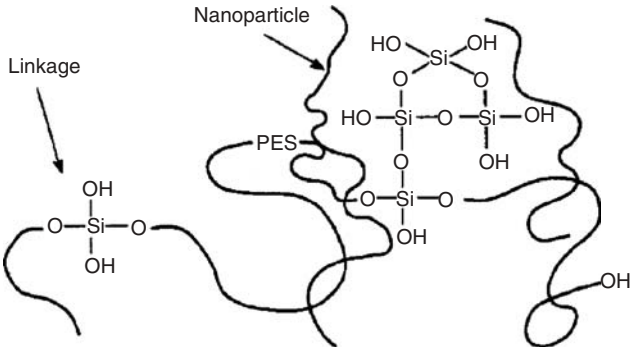

Figure 9 Formation of a hybrid nanocomposite in the reaction of HO-(polyethersulfone)-OH with bridging—SiO_2—groups.

condensation between the Nafion's sulfonate functions and the silanol groups. Sol-gel condensation of TEOS and styrene-maleic anhydride copolymer in the presence of a binding agent—(3-aminopropyl)triethoxylsilane—generated a covalent bond between polymeric and inorganic components.[250] In this case, particles with sizes <20 nm were formed (scheme 24).

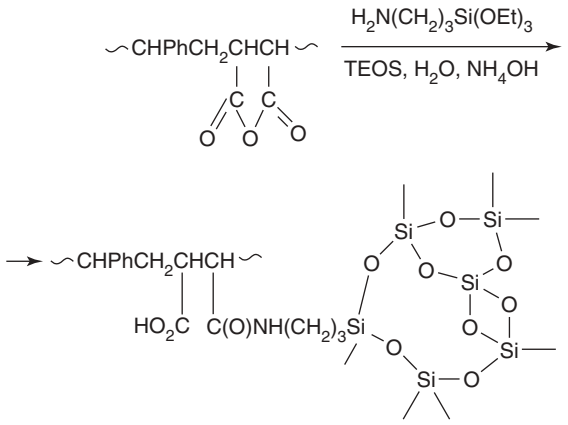

Scheme 24

A series of monolithic hybrid materials containing 23–100 vol% of an inorganic component were prepared by the sol-gel method starting from SiO_2 and the copolymer of methyl methacrylate with 3-(trimethoxysilyl)propyl methacrylate.[251,252]

Polyimide composite materials containing nanosized SiO_2 or TiO_2 particles possess the high mechanical strength due to their ability to form 3D inorganic

networks.[253,254] Polyimide-polysilsesquioxane* composites were prepared simultaneously condensing and imidizing, 1,1-bis(4-aminophenyl)-2,2,2-tri-fluoro-1-phenylethane with a derivative of pyromellitic anhydride and aminophenyl-trimethoxysilane at 250–350°C.[255–260] This gave hybrid nanocomposite films containing 32–70% of homogeneously dispersed SiO_2 particles with sizes of 0.5–7 nm (scheme 25). Polyamide-SiO_2 compositions were prepared in situ by suspending aminobutyric acid–modified SiO_2 nanoparticles in polymerized ε-caproamide at high temperature.[261,262] This approach provides homogeneous distribution of SiO_2, which improves the mechanical properties of nanocomposites. For example, the glass-transition temperature rises and the rate of crystallization increases.

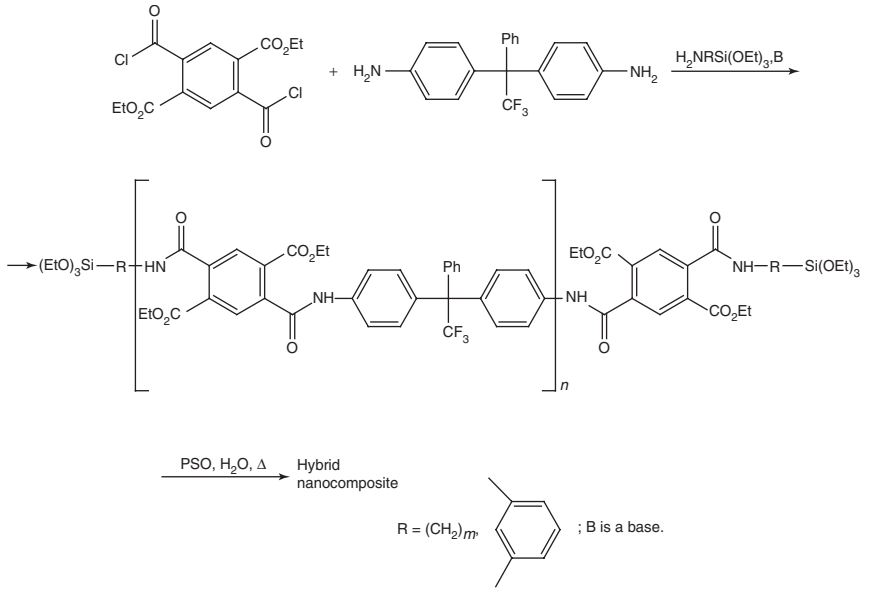

Scheme 25

Analogous nanocomposites were also prepared[17] based on polyimide analogs, such as polyoxazolines, containing triethoxysilane groups.[263–265]

Ring-opening metathesis polymerization accompanied by free-radical addition of cyclic alcohols appears to be the optimum procedure for the synthesis of hybrid SiO_2-polymer nanocomposites exhibiting minimum shrinkage.[31,265–268] The synchronous

*Polysilsesquioxanes (PSO) belong to a class of 3D organosilicon oligomers of the general formula $(RsiO_{1.5})_n$ containing the inorganic cubic Si_8O_{12} nucleus. These compounds have polyhedral structures with different symmetries and are key intermediates in the formation of various nanocomposites.[255] Thus the synthesis and properties of hyperelastic materials, which have been prepared by copolymerization of 4-methylstyrene and oligomeric silsesquioxane macromers, have been reported recently.[256]

formation of interpenetrating networks occurs as a result of competitive polymerization and hydrolysis of silicon alcoxide catalyzed by NaF and followed by condensation (scheme 26).

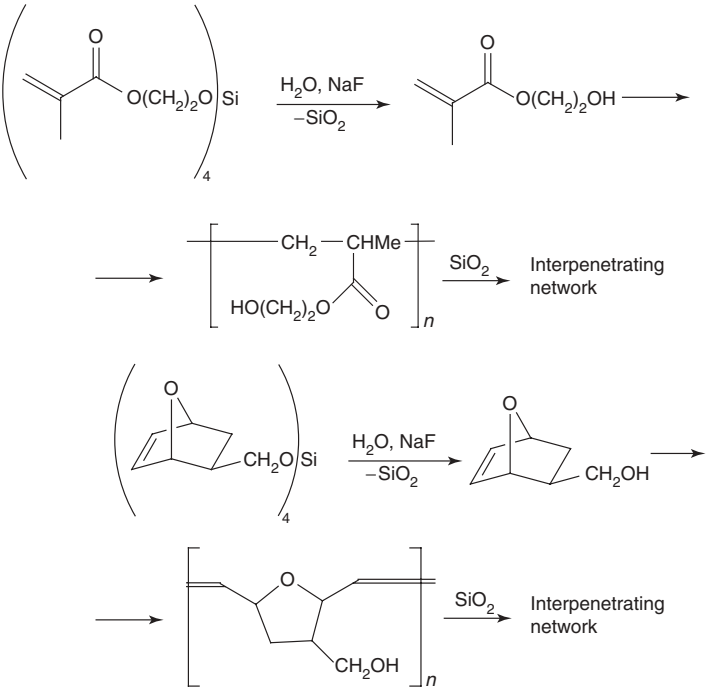

Scheme 26

Sols are thermodynamically unstable systems with high surface free energies. They should be stabilized by controlling pH of the system. Nanosized particles or their precursors are stabilized during sol-gel reactions, by adsorption of special monomeric molecules on the sol surface.[269–272] For example, carboxylic acids and polymeric acids[259,273] are strongly bound to the surface of SiO_2, ZrO_2, TiO_2 or Al_2O_3 particles. Amines adsorb specifically on metallic Pd or Au particles. Thiols are even more specific reagents for Au. Controlled hydrolysis of bifunctional molecules containing a double bond along with hydrolyzed silane or ZrOR groups affords precursors (scheme 21) which convert into ~2-nm ZrO_2 particles. The double bonds in these systems can undergo copolymerization with methacrylic acid (MAA). The latter also acts as a surface modifier.

$Zr(OR)_4$ is readily hydrolyzed. Direct hydrolysis produces a $ZrO_2 \cdot nH_2O$ precipitate, which is unsuitable for the preparation of a homogeneous composite. In strongly acidic media, a flocculent hydrated gel layer is present on the surface of these particles. This layer helps prevent aggregation.[274] It is believed[275] that this layer makes it possible to perform repeated peptisation of ZrO_2 from a xerogel. When

bound to MAA, $Zr(OR)_4$ is hydrolyzed more slowly. Therefore well-dispersed nanosized ZrO_2 particles are formed in the presence of latent water. Silanes modified with MAA undergo copolymerization. The resulting silicon-containing polymer is then used as a matrix material for nanosized zirconium particles (Fig. 10).[229] Another convenient procedure for nanocomposite synthesis involves dispersion copolymerization of monomers containing trialkoxysilyl groups.[276–280]

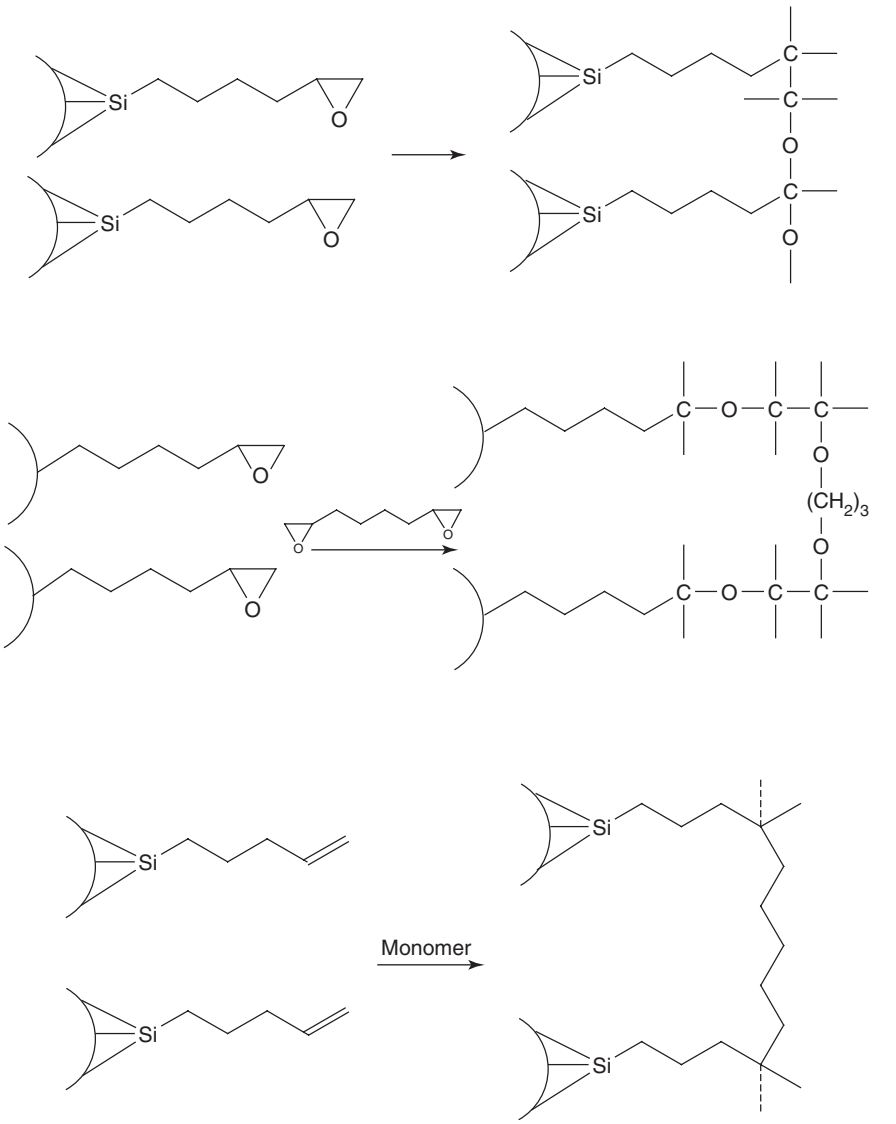

Figure 10 Use of functionalized silanes for crosslinking the organic and inorganic components of the system.

Thus statistical copolymerization of silicon-magnesium monomers affords beads of 100–500 nm from which organic compounds are removed on heating to 1000°C in the presence of wet air (scheme 27). The final particles sizes are ~100 nm.[281]

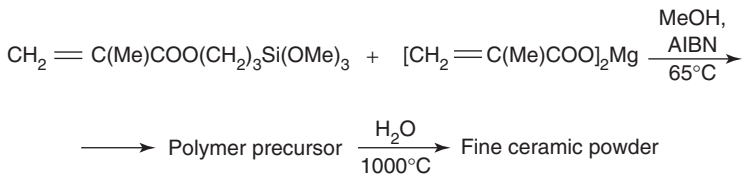

Scheme 27 AIBN is an initiator [2, 2′-azobis(isobutyronitrile)].

A nanocomposite material was prepared by mixing methacryloxypropyltrimethoxysilane[229] with equimolar amounts of $Zr(OR)_4$ and MAA. The trimethoxysilane function was hydrolyzed and condensed in the presence of 0.5 M HCl, and then H_2O was added. A photoinitiator and alcohol were introduced into the resulting mixture. The alcohol is used to control the viscosity. When a support was submerged in the mixture, a thin film of a photosensitive material deposites.

Hybrid nanocomposite materials have been prepared from alkoxy derivatives of Ti and V of the general formula $Ti(OR^1)_3(OR^2)$[282] or $OV(OR^1)_{3-n}(OR^2)_n$,[283] respectively. In these monomeric units R^2OH can be ethylene glycol monomethacrylate, 2-hydroxyethyl methacrylate, furfuryl alcohol, 1,1-dimethylpent-4-en-2-yn-l-ol, propargyl alcohol, or other unsaturated alcohols, that are able to undergo polymerization. Radical polymerization of these metal-containing monomers affords polymers with sidechains containing alkoxy groups of titanium[284] or vanadium.[285] Methacrylic acid reacts with alkoxy derivatives of titanium yield metal-containing monomers $CH_2{=}C(Me)COOTi(OR)_3$ (R = Et, CH_2Bu^t or Bu^t).[286] Nontoxic, self-polished and anticontamination coatings were prepared from these monomers by free-radical copolymerization with methacrylic acid or by etherification of the resulting polymer and titanium tetraalkoxide.

Polytitanosiloxanes were prepared in one stage by simultaneous controlled cocondensation of $Si(OEt)_4$ and $Ti(OPr^i)_2(acac)_2$.[287] A ladder polymer containing Si-O-Si and Si-O-Ti units is formed. Their ratio depends on the conditions. This ratio determines the time to gel formation and if fiber ceramics can form upon annealing of the material (500–900°C).[288] The structures, growth mechanism and the properties of siloxane composites containing the silicon, titanium and mixed titanium-silicon phases have been thoroughly reviewed.[289]

The sol-gel synthesis[290] of titanium-silicon nanocomposites based on perfluorosulfonate ionomers was reported. Also the preparation of nanosized particles (10–50 nm) derived from $Ti(OR)_4$ and $Zr(OR)_4$ within matrices of styrene/4-vinylphenol copolymer was performed via the sol-gel method.[291] These approaches can also be used for the surface activation of polymers. For example, hydrofobic perfluorinated polymers such as polytetrafluoroethylene (PTFE) or copolymers of

tetrafluoroethylene with hexafluoropropylene were treated with $SiCl_4$ followed by controlled hydrolysis to produce a hydrofilic surface.[292,293]

Titanium and silicon alkoxides have been used as crosslinking reagents for polysaccharides, cellulose derivatives, vegetable oils, etc.[294,295] These polymers contain highly active hydroxy groups that form oxopolymers in situ. Organic networks are also formed in similar reactions of low-molecular-weight compounds containing several hydroxy groups. For example, anthracenobisresorcinol and its derivatives polymerize with $(Pr^iO)_2TiCl_2$.[296]

Cocondensation of macromers containing trialkoxysilyl groups with modified polystyrene (PS), polyoxazoline, polyimide, polyethylene glycol (PEG), polyetherketones, polymethyl methacrylate, and derivatives of polytetramethylene oxide was established as convenient procedure for the preparation of telechelic polymer networks.[259,297–303]

The insertion of highly dispersed SiO_2 particles into a polymerized system is also widely used for the preparation of nanocomposite materials. Although a survey of this area is beyond the scope of the present review, several prominent examples are worth noting. Spherical SiO_2 particles possessing a high specific surface act as peculiar dispersing agents in aqueous media. Raspberry-shaped composite particles (100–300 nm) were formed in both polyaniline-SiO_2 and polypyrrole-SiO_2 systems.[304–309] During redox polymerization of pyrrole initiated by $FeCl_3 \cdot 6H_2O$-$(NH_4)_2S_2O_8$ spherical and fiber-shaped SiO_2 particles were introduced.[310] The particle sizes varied from 80 to 200 nm as the SiO_2: polypyrrole ratio changed.

Lithographic composites based on SnO_2, have been prepared by oxidation and cross–linking in films.[311,312] Tin-containing polymers (e.g., poly(4-[(trimethylstannyl)-methyl] styrene was synthesized[313–315] and used as a precursor of SnO_2). Photoirradiation of this polymer followed by pyrolysis in air gave simultaneous formation of SnO_2 particles and a polymer network. Pyrolysis cleaved the C-Sn bonds to benzyl and trimethylstannyl radicals. The former react with atmospheric oxygen on film surfaces. The Me_3Si radicals undergo recombination to form networks.

Hybrid nanocomposites containing nanosized Au[316] and TiO_2 particles[317] were prepared using reverse micelles. Addition of didodecyldimethylammonium bromide to toluene formed reverse micelles into which $AuC1_3$ and a gel precursor (TEOS) were introduced. The $AuC1_3$ was reduced by $LiBH_4$-THF. Subsequent hydrolysis and condensation gave wet gels impregnated with Au particles. The gold particle sizes depended on the H_2O: Si ratio and the concentration of the surfactant. Colloidal gold particles were stabilized with dodecanethiol[318] after immobilization on the surface of highly dispersed SiO_2 with the bifunctional aminosilane $(MeO)_3Si(CH_2)_3$-$NH(CH_2)_2NH_2$.[17] Subsequent treatment of these particles with thiol resulted in the cleavage of the bonds to SiO_2 and the particles became labile. Repeated immobilization–stabilization events led to the growth of 2D highly ordered ~10-nm-thick layers of linked particles (Fig. 11).

Reverse micelles were prepared using sodium bis(2-ethylhexyl)sulfosuccinate (SBES).[319] For example, $Ti(OPr^i)_4$ was dissolved in reverse micelles formed from isooctane, SBES, and calculated amount of water. Slow diffusion of the alkoxide into micelles was followed by hydrolysis and condensation. These micelles serve as

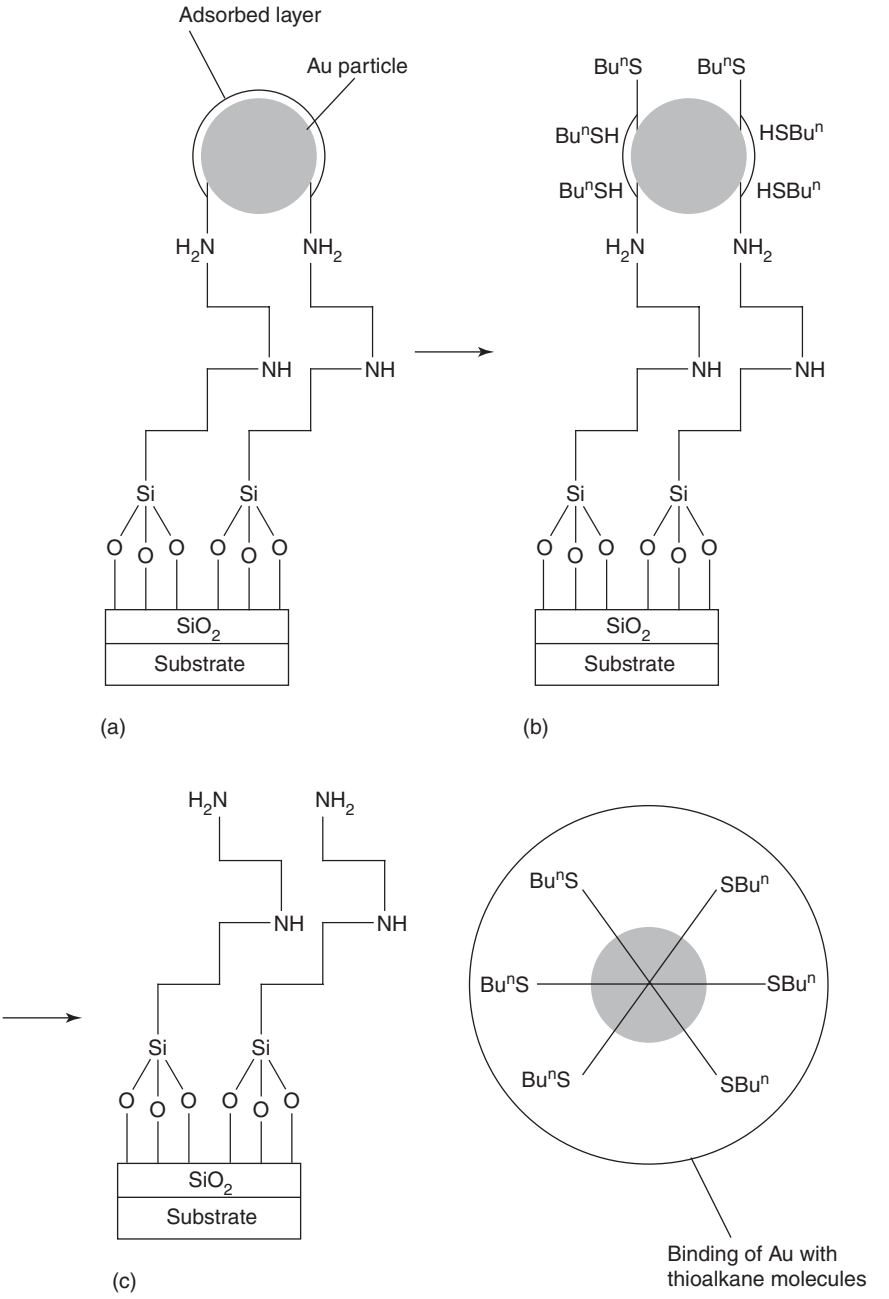

Figure 11 Preparation of hybrid materials through the use of reverse micelles. **A** immobilization of colloidal Au particles. **B** exchange of alkanethiol molecules and cleavage of the Au–NH_2 bonds. **C** The complete binding of Au particles with thioalkane molecules.[318]

microreactors. This procedure was used for the preparation of TiO_2 nanoparticles, which were extracted and dispersed in a solution of fluorinated polyimide. When this polymer–TiO_2 composite was deposited on a glass plate followed by thermal treatment at 300°C under N_2 for 30 min an optical film wave guide was formed. Therefore, one advantage of the solution preparation of these nanocomposites is the ability to form transparent films (yellow titanium complexes are not formed). The thermal stability of these materials (4% of TiO_2) is almost identical to that of the initial polymer. This indicates that the thermal characteristics of the host polymer remain virtually unchanged upon impregnation of TiO_2. Simple mixing of a polyimide solution and a sol-gel precursor, which leads to phase separation, is sufficient to form a polymer–inorganic nanocomposite in some cases.

Epoxysilane groups can also form networks.[320–323] Thus alkoxysilane (**2**) is a binder providing the compatibility of TEOS with polyacids.

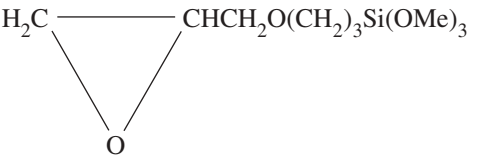

The SiO_2/ethylene oxide-epichlorohydrin copolymer compositions were 71:29–29:71 in gel-sol hybrid nanocomposites. Acid condensation of TEOS in THF afforded an inorganic network.[324,325] These networks have also been prepared from alkoxy derivatives of aluminium.

The morphology and fractal structures of these materials were studied. The structures of these aggregates are characterized by the fractal dimension D ($1 \leq D \leq 3$).[326] This D is the exponent relating the weight of the M particles to their characteristic size R in the equation

$$M \approx \mathrm{R}^D$$

For surface fractals with uniform density, $D = 3$. The self-similarity or scale invariance of the fractal aggregate implies that the structure of the aggregate, on the average, remains unchanged over any extended interval and any its portion is similar to the aggregate as a whole. When refering to a surface, the $D = 2$ corresponds to a smooth surface, and $D = 3$ corresponds to the maximum roughness.

The fractal dimensions of polymeric and colloidal samples of the TiO_2 aerogel with high values of S_{spec} were compared. These samples were prepared by the sol-gel method and dried with CO_2 in the supercritical state. These values are virtually identical (2.6–2.8). The fractal surfaces of colloidal particles are only slightly less regular than those of polymeric aerogels.[327] This indicates that the nanolevel morphology is determined in the early stages of there formation and depends only slightly on the conditions of the synthesis. However on the mesolevel, the synthesis conditions determine morphology.

Studies of TEOS condensation in a polysiloxane network demonstrated[14,289] that fractal models typical of solutions were not observed on matrix polymerization. The entropy of the mixture decreases due to the high matrix polymer molecular weights resulting in phase separation. Particular conditions are required to prevent phase separation. However, phase separation always occurs when the concentration of SiO_2 is >5%, which enhances the mechanical strength of composites. When TiO_2 nanoparticles were precipitated in situ, the maximum bulk domains (up to 5%) were formed. These nanocomposites rank below systems with SiO_2 in strengths.[328]

The sol-gel method is especially useful for performing template syntheses, where nanocomposites are assembled from components under conditions where a strictly defined stereochemical orientation of the reagents exists. These conditions and the tiny micelle sized reaction volumes promote the mild template synthesis where assembly occurs under normal conditions. This procedure was used[329] for the preparation of tubular semiconducting nanostructures of TiO_2 derived from $Ti(OPr^i)_4$, commercial Al_2O_3 template membranes with the pore diameters of 22 and 200 nm,[330] fibrous ZnO structures generated from zinc acetate,[331] and fibers from WO_3.[332,333] These materials are excellent photocatalysts. Template synthesis is described in more detail in Section VIII. Sol-gel template syntheses in fibers, nanotubes, or microporous and nanoporous membranes have been described in detail in several reviews (Section XI). Template procedure were used for the preparation of fibrous electrode materials based on V_2O_5[334] and semiconducting oxide materials, including MnO_2,[335] Co_3O_4,[336] ZnO, and WO_3. The template synthesis of nanotubes or nanowires of semiconductor-conductor materials was performed[330] from TiO_2 within Al_2O_3 pores followed by polymerization of monomers.[337,338] These methods have been highly developed in the last few years.[339–355]

VII. SOL-GEL PREPARATION OF NANOHYBRID MULTIMETALLIC MATERIALS

Heterometallic ceramic nanocomposites, such as perovskites with the ABO_3 structure, can be synthesised through sol-gel routes. Film and epitaxially oriented materials possess specific ferroelectric, piezoelectric, and pyroelectric properties and are widely used in electronics and optoelectronics.[356] The naturally occurring mineral perovskite, $CaTiO_3$, has the pseudocubic crystal lattice. The classical perovskite synthesis is illustrated by considering $PbTiO_3$. $PbTiO_3$, is generally prepared by calcination of a mixture of PbO and TiO_2. These solids are ground using a vibrational mill at temperatures higher than 600°C. However, PbO is toxic, and its presence in the final product is undesirable. The sol-gel preparation of $PbTiO_3$ is free from these drawbacks.[357] A mixture of $Ti(OPr^i)_4$, $Pb(AcO)_2 \cdot 3H_20$, ethylene glycol and citric acid in a ratio of 1:1:40:10, respectively, was stirred at 50°C. Then the resulting citrate metal complexes were subjected to polymerization at 130°C and then pyrolysis at 300°C. The resulting powdered precursor was calcined in air at 400–600°C for 2 h to obtain thin $PbTiO_3$ films, which retained the properties of a bulk material. Different versions of the solgel syntheses of $PbTiO_3$ were described in the literature in detail. Thus polymeric

films, which were prepared by mixing $BaTiO_3$ with solutions or melts of polymers, were studied.[358,359] However, in this case particles were nonhomogeneously distributed and their agglomeration occurred. An alternative hydrothermal procedure for the synthesis of these nanocomposites was proposed.[360] $BaTiO_3$ particles were prepared from $Ba(OH)_2$ and titanium diisopropoxide bis(ethylacetoacetate) at temperatures higher than 100°C in a polybutadiene-polystyrene block copolymer matrix, etc.[361] These materials might serve as components of conducting compositions.[362] Structurally homogeneous $BaTiO_3$ nanocomposites can be prepared only by using the sol-gel method (scheme 28).[363] One version of this procedure involves solid-phase polymerization of organometallic precursors followed by pyrolysis.[364]

$$Ba + Ti(OPr^i)_4 + CH_2{=}C(Me)COOH \longrightarrow$$

$$\longrightarrow BaTi[OOCC(Me){=}CH_2]_6 \xrightarrow{200^\circ C} \{BaTi[OOCC(Me)CH_2]_6\}_n \longrightarrow$$

$$\longrightarrow BaCO_3 + TiO_2 \xrightarrow{600^\circ C} BaTiO_3$$

Scheme 28

Polymerization of $BaCO_3$, $SnCl_2 \cdot 4.5H_2O$, ethylene glycol and citric acid (1:1:40:10) were also used to prepare[365] $BaSnO_3$ with the perovskite structure. The synthesis was analogous to that of $PbTiO_3$ (see above) but at a different temperature. Other multicomponent perovskite ceramics such as $SrTiO_3$, $NdAlO_3$, $SrBi_2Ta_2O_9$, and superconducting ceramics $YBa_2Cu_3O_{7-\delta}$, were also prepared by the sol-gel method (see below). The use of metallochelates and decomposition of organometallic precursors to these sol-gel syntheses has been described in more detail.[366] Single-phase thin $KTiOPO_4$ films, which exhibit remarkable optical properties and high thermal stability, can be prepared from $Ti(OEt)_4$, KOEt and different sources of phosphorus ($(EtO)_2P(O)(OH)$, $(EtO)P(O)(OH)_2$, $P(OH)_2Me$, $P(OMe)_3$, etc.).[367] $(Bu^nO)_2P(O)(OH)$ is the optimum phosphorus source.

Heteropolymetallates, such as Keggin's acids $H_3PW_{12}O_{40}$ and $H_4SiW_{12}O_{40}$, may be incorporated into organic–inorganic polymetallic nanocomposites.[17,270] These materials possess good electrochemical properties and can be potentially used in holography. Nanocomposites based on these materials can be prepared by mixing polymetallates (spheres of diameter ~1 nm) with TEOS and tetraethylene glycol or by introducing polymetallates into organosilanes.

Specific oxometallates containing W-O-Si units were synthesised by the reactions of substituted trichlorosilanes $RSiCl_3$ ($R{=}CH_2{=}CH$, $CH_2{=}CHCH_2$, $CH_2{=}C(Me)CH_2$ or $CH{=}CHPh$) with the polyanion $K_4SiW_{11}O_{39}$. Cluster-containing monomers with the composition $(SiW_{11}O_{40}(SiR_2)_2)^{4-}$ were formed.[17] Polymerization was carried out under the action of radical initiators to form polymers with heteropolyoxymetallate sidechains. These products were characterized by ^{13}C and ^{29}Si NMR spectroscopy. The polymer yield and chain length depend on the

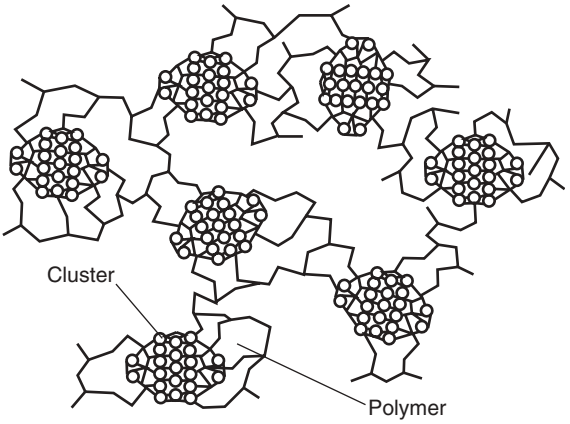

Figure 12 Structure of the hybrid polymer–inorganic material based on the $(SiW_{11}O_{40}[Si(CHPh\text{-}CH)_2])^{4-}$ polyanion.[17]

reactivities of the unsaturated R groups and increase in the series $CH_2CH \ll CH_2{=}CHCH_2 < CH_2{=}C(Me)CH_2 \ll CH{=}CHPh$. The polymer structure is shown in Figure 12. The syntheses of the transition-metal oxoclusters $Nb_4(\mu_2\text{-}OMc)_4(\mu_{12}\text{-}O)_4(OPr^i)_8$, $Ti_6O_4(OEt)_8(OMc)_8$ (OMc is methacrylate), and $Zr_{10}(\mu_4\text{-}O)_2(\mu_3\text{-}O)_4(\mu_3\text{-}OH)_4(\mu_2\text{-}Opr^n)_8 \cdot (Opr^n)_{10}(AllylAc)_6$ (AllylAc is allyl acetoacetate) has been accomplished[368] by controlled hydrolysis of metal alkoxides in the presence of complex-forming agents (OMc or AllylAc). These compounds consist of the metal oxide nucleus surrounded by peripheral ligands, which can undergo polymerization. The latter are responsible for the formation of a cluster network. The construction of stable nanoblocks ensembles requires that clusters possess high lability and reactivity. For example, the thermodynamical stability and resistance to hydrolysis of titanium oxo clusters depend both on size and the oxo(alkoxo) group: titanium ratio. Polymerization should be performed in anhydrous organic solvents.[369]

Three-dimensional oxovanadium borophosphates with open frameworks[370–372] and polyboroazinylamines have been synthesized. Polyboroazinylamines are precursors metal-containing matrix composites containing metal borides and nitrides.[373]

Modification of materials prepared by the sol-gel method with different transition metals are being extensively studied.[374,375] For example, mesoporous M41S was prepared from molecular sieves NCM-41 or MCM-48, modified with solutions of NH_4VO_3 or $ZrOCl_2$ in a mixture with polyoxoethylene stearate. NH_4VO_3 or $ZrOCl_2$ solutions acted as precursors of transition metal ions.[376] Nanoparticles (50–60 nm) of cobalt carbide immobilized within a silica matrix were obtained (scheme 29).[377]

Mesopores in the MCM-41 matrix were modified[378] with the *trans*-$[Co(en)_2Cl_2]^+$ or $[Co(en)_3]^{3+}$ complexes (en is ethylene-diamine) stabilized by ammonium salts. Hydrolytic condensation of cyclopentadienyltitanium trichloride with silsesquioxane (the product of incomplete condensation of cyclopentyltrichlorosilane) was followed by calcination of titanium-containing oligosilsesquioxane. This afforded microporous titaniumsilicon oxides with S_{spec} of up to 780 $m^2\ g^{-1}$.[379]

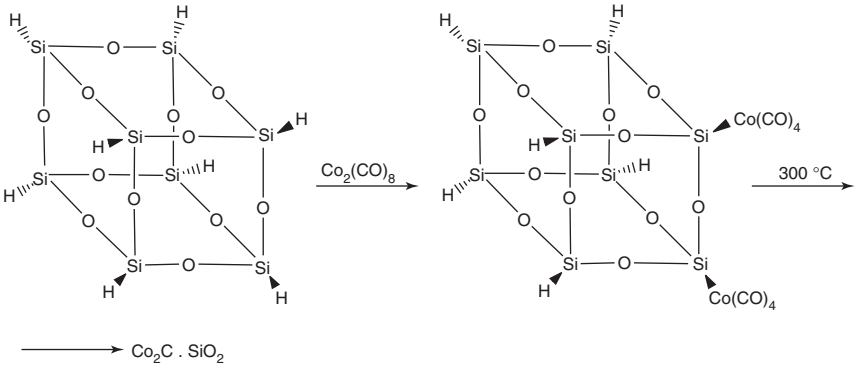

Scheme 29

During sol-gel polymerization, metal clusters can be introduced. Thus the trihydrosilyl group was inserted into known cluster, $(\mu_3\text{-HC})Co_3(CO)_9$. It was then subjected to heterocondensation (scheme 30).[380]

A unimodal distribution of the particles was observed in the resulting xerogel. The particles ranged from 10 to 46 nm (with an average diameter of 25 nm). The Os_3, PtSn, Fe_2P, Co_2P, and Ni_2P nanoclusters can be introduced into composites analogously. Complexes with a bifunctional ligand containing the reactive alkoxy- or hydroxysilyl group were incorporated.[381] The insertion of Pd^{2+}[382] and Cu^{2+} ions into poly(ethyltrimethylsilane) formed was described.[383] The structure of the organometallic–inorganic diblock copolymer poly(ferrocenyldimethylsilane-dimethylsiloxane) was studied.[384] In hexane, this copolymer exists as long rod-shaped cylindrical micelles in

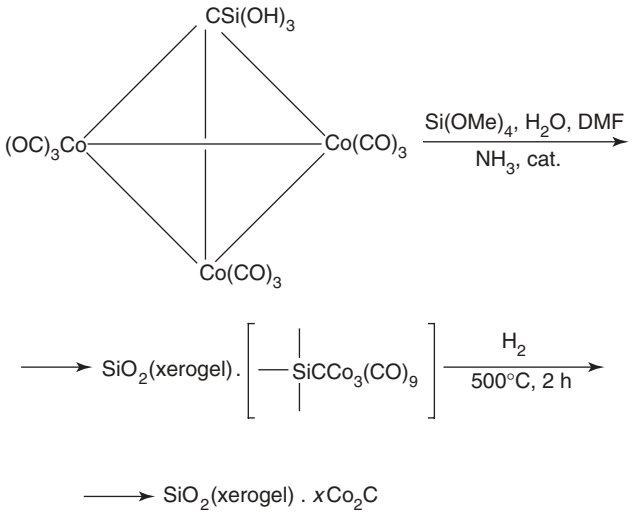

Scheme 30

which the iron-containing nucleus is located in a case formed from polydimethylsiloxane blocks. These micelles comprise up to 2000 polymeric molecules and decompose to form short cylinders containing ~700 molecules when sonicated.

Metal complex catalysts (Section XII) are bound to an inorganic matrix through bidentate phosphorus–containing ligands $[Ph_2P(CH_2)_2CO_2]EO_x(OR)_{3-2x}$ type (E = Ti or Zr; R = Alk).[385] The reactions of these ligands with tungsten carbonyl afforded $W(CO)_5[Ph_2PXEO_x(OR)_{3-2x}]$. These are potential precursors for sol-gel synthesis. Cocondensation of these precursors gave xerogel nanocomposites composed of a SiO_2 (xerogel)$\cdot x M_yP_z$[386–388] (M = Ru, Ga or In, y = z = 1; M = Pt, y = 1, z = 2; M = Fe, Co, Ni or Rh, $y = 2$, z = 1; M = Cd, y = 3, z = 1; M = Pd, $y = 5$, $z = 2$), and even bimetallic SiO_2 xerogel/Zn(Cd)GeP_2 composites.[387] The $[\eta^6\text{-PhSi(OMe)}_3]\cdot Cr(CO)_3$ complex was immobilized in a highly dispersed amorphous xerogel ($S_{spec} = 500–1800\ m^2\ g^{-1}$) during fluoride catalyzed sol-gel polymerization.[389] This allowed the preparation of a single-phase inorganic oxide/organic network polymer hybrid containing (1,4-phenylene)siloxane nucleus-shell bridges.[389] Vacuum thermolysis (393K, 24 h, < 1 Torr) of this composite eliminated of carbon monoxide to form zero-valent 1.0–10.0 nm chromium nanoparticles in pores of the xerogel (Fig. 13). At 1 atm pressure, thermal elimination of CO proceeded only at 400°C, forming low-oxidation-state chromium.[390]

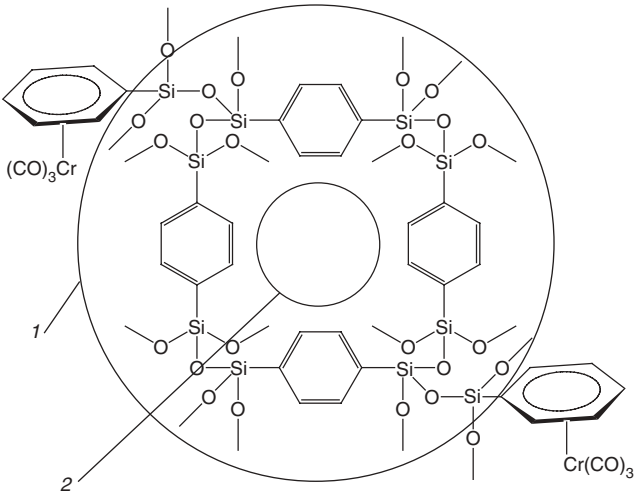

Figure 13 Structure of a single-phase hybrid of the nucleus—shell type. *1*, a shell; *2*, a nanoparticle of zero-valent chromium.[390]

Polysilanes have also been complexed with metal carbonyls. Tricarbonylmolybdenum groups were introduced into poly(methylphenylsilane) upon treatment with $Mo(CO)_3Py_3$.[391]

Nanolayer silanization TiO_2, $A1_2O_3$ or Fe_2O_3 surfaces and the introduction of Fe_2O_3 into silicate, $CaCO_3$, and $BaSO_4$ mesopores is widely practiced.[392]

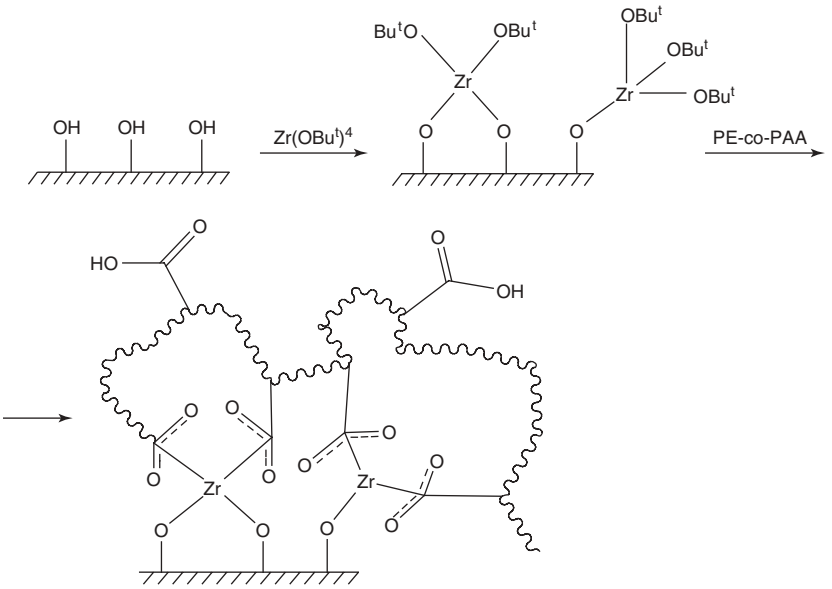

Scheme 31

Generally,[393–396] a thin layer of silanol derivatives and a dimethylsiloxane oil are deposited on inorganic surfaces, which is followed by heating to 250°–280°C. Siloxane bonds are cleaved, and the terminal groups of the polymer chains react with hydroxy groups of inorganic surfaces. Futhermore the polymer chains are crosslinked through methylene and siloxane bridges or oligomers. This forms particles that are stable to hydrolysis and extraction. In a related process, $Zr(OBu^t)_4$ modified the aluminium surfaces.[397] Zirconium groups are linked when treated with poly(ethylene-acrylic acid) copolymer (PE-co-PAA) containing 5 wt% acrylic acid (scheme 31).[398]

The adsorption properties of these materials are changed by the formation of a hydrophobic layer, and the material becomes moisture stable. When Ti and Au layers 5 and 50 nm thick, respectively, were deposted on an activated polydimethylsiloxane surface, ordered structures were formed.[399,400]

The surfaces of metals or metaloxides are often coated in powder technology particles to form structures of the core-shell type. Such particles exhibit additional useful properties. Thus SnO_2 or In_2O_3 particles have been coated with chelating polymers swelled in water. For example, polymers containing In^{3+}-SiO_2 or In^{3+}-Sn^{2+}-SiO_2 as well as Ag^+ have been used in such coating processes. These particles exhibited the surface conductivity and were used to prepare thermally stable conducting films possessing antistatic properties.[401–403]

Several procedures for including a polymer into the structure of an inorganic material by the sol-gel method are available. Thus siloxanes containing two different functional groups can be used. One of these groups reacts with a reacting function

on the macromolecule and the second group reacts with the sol-gel precursor. This bonds polymer to the sol-gel network. Sometimes special binding or surface coupling agents are added. For example, the surface of highly dispersed SiO_2 was modified with aminobutyric acid. The resulting product was dried, dispersed in ε-caproamide and subjected to initiated polymerization at 90°C.[404] When the concentration of SiO_2 particles was ≤5 wt% (the distance between the particles was 50–110 nm), they were homogeneously distributed in the composite. At concentrations of >10 wt%, aggregation of particles starts.

Layered nanohybrid materials (Section VIII) were prepared[405] by the reactions of $Zn(OH)_2$, ZnO, or a Zn/Al alloy with carboxylic acids or their oxychlorides. The guest to host ratio in these composites varies from 0.75:0.25 to 0.9:0.1. The particle morphologies changes from fibrous to platelet, depending on the nature of the reacting components. The interlayer distance increased in the range of 1.61–2.01 nm.

Recently, the sol-gel procedures for preparing alumoxane ceramics from carboxylates of the general formula $[Al(O)_x(OH)_y(OOCR)_z]_n$, were analyzed.[406] $M(acac)_n$ complexes ($M = Ca^{2+}$, Mn^{2+}, Y^{3+}, etc.) can be incorporated into ceramics during the reaction.[407,408] Metallic Co and Fe and their alloys, formed by hydrogen reduction of the corresponding nitrates, were dispersed in an aluminosilicate matrix. The matrix was synthesized from $(BuO)_2A1OSi(OEt)_3$ by sol-gel reaction. This product possesses dielectric properties. Nanocomposites were formed that contain ~20 nm particles and possess magnetic properties (Fig. 14).[409]

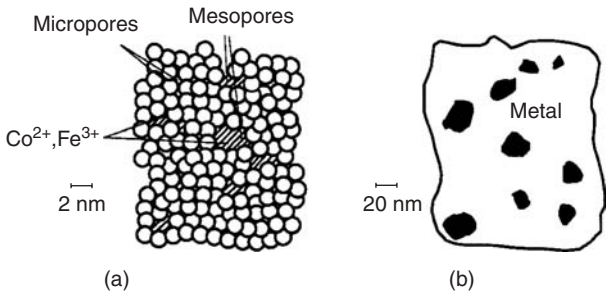

Figure 14 Diffusion and adsorption of metal ions in pores of the host and the structure of the composite (**a**) before and (**b**) after thermal treatment.

One of new trends today in sol-gel chemistry is the use of supercritical carbon dioxide as a solvent during sol-gel polymerization or for extraction of the resulting product.[410] The initial alkoxysilane is mixed with anhydrous 99% HCO_2H and sol-gel polymerization of the mixture is then carried out in supercritical CO_2 in an autoclave (40°C, 41.4–55.2 MPa). Gel formation proceeds over 12 h and then CO_2 is slowly removed (8 h). This procedure favors for the formation of highly porous monolithic composites with the mesopore and macropore architectures.[410] Components that sharply enhance the ability of SiO_2 to adsorb water may also be introduced at the stage of formation. For example, selective water adsorbents, such as $CaCl_2$ and LiBr, bind up to 53 wt% of H_2O.[411,412]

Colloidal dispersions of 33-nm-diameter trimetallic Au–Pb–Cd particles, containing gold core surrounded with a 18-nm-thick lead shell are formed by γ-irradiation of corresponding metals salts.[413] Nanocomposites with three or more different metals are multimetallic nanohybrids. Studies of their structures is a challenging task. Nevertheless, these materials have already been used as precursors in the production of superconducting ceramics, special multicomponent steels, etc. Traditionally, polymer is formed in a previously prepared inorganic matrix or the polymer is inserted into the latter. Multimetallic nanocomposites are prepared in situ within a polymeric matrix or simultaneously with polymer matrix formation.

Standard methods for the preparation of blends in the production of high-T_c superconducting ceramics (direct mixing of oxides, carbonates, oxalates, nitrates, and other metal salts) give rather poorly reproducibility.[414] This is due to the heterogeneity inherent in grinding and mixing of the solids and to complex physicochemical and mechanochemical conversions that occur in the course of sample preparation. As a result, microheterogeneities appear and both conducting and nonconducting phases are formed. This results in low-quality high-T_c superconducting ceramics with a blurred superconducting transition (Meissner effect). A structurally homogeneous $YBa_3Cu_4O_8$ superconducting ceramic was formed when the initial $Y(NO_3)_3 \cdot 6H_2O$, $Ba(NO_3)_2$ and $Cu(NO_3)_2 \cdot 2H_2O$ reagents were mixed on the molecular level by dissolution. After evaporation of the solvent, a homogeneous dispersion was obtained that was a precursor for a high-T_c superconducting ceramic. Composite materials may be made by introducing the high-T_c superconducting ceramic into a polymeric matrix. Alternatively, this ceramic can be prepared in the presence of a polymeric matrix. An example of the first case is the introduction of a dispersed high-T_c superconducting phase (such as $YBa_2Cu_3O_{7-\delta}$, $(Pb_xBi_{1-x})_2Ca_2 \cdot Sr_2Cu_3O_y$[414] or $T1_2Ba_2Ca_2Cu_3O_y$[415] with $T_c \sim 90$K, 110K, and 125K, respectively) into a polychlorotrifluoroethylene, polyvinylchloride, or rubber matrix. Ceramic contents of 50–75% were made.[414,415] The optimum compositions combine the high T_c, good magnetic properties, and magnetic levitation of a high-T_c superconductor with the mechanical strength, flexibility, processing simplicity, and resistance to media effects of a polymer. In addition, the preparation of composites allows the elimination of such drawbacks as the high porosity, friability, and susceptibility to degradation exhibited by the high-T_c ceramics. However, rather large (micrometer) ceramic particles are inserted into a polymer according to this procedure.[415]

The ceramic may be prepared in the presence of the polymer matrix (second method referred to above). Matrices containing metal ions dispersed on the molecular level can be used. Nanosized particles formed in the course of polymerization or polycondensation are also considered members of this class. Metal ion citrate chelates can be dissolved in aqueous solutions of acrylamide. The acrylamide is polymerized in the presence of radical initiators and chain carriers (*N,N,N′,N′-tetraethylene*-diamine) to form a gelatinous phase.[416] This traps the metal cations into a polyacrylamide gel much as occurs in the sol-gel synthesis. After calcination, ultrathin multicomponent oxide powders, such as $YBa_2Cu_3O_{7-x}$ or $LaAlO_3$, were obtained.[416] $YBa_2Cu_3O_{7-x}$ ceramics were made using acrylic or methacrylic acid as the metal ion chelating ligands.[417] Polymer-salt solutions of polymeric alcohols or

acids, PEG or PVPr have been used.[418–420] The sizes of all salt crystals formed in the presence of a polymer are substantially smaller than those obtained upon crystallization from pure salt solutions. This is associated with complex formation in solutions as well as with adsorption of macromolecules on the crystallization nuclei. Recrystallization may occur simultaneously due to the presence of concentration gradients of the components within the thickness of the surface layers. Homogeneous films are most often formed because they form both on the surface and also in the solution volume. It is essential that the final ceramic crystallites sizes in the powders, resulting when the polymer is destroyed during calcining, should be approximately equal to their sizes in films.

Such polymer conversion methods were used to prepare Y^{3+}, Ba^{2+}, and Cu^{2+} complexes with poly(methacrylic acid)[421,422] and YBC chelates with polyamides.[423,424] Gel formation with poly(vinyl alcohol) (PVA) can also be used.[425] The superconducting ceramics based on these metallopolymers have T_c values = 80–92K, and critical current densities (J_c) of 150–160 A cm^{-2}. Films and fibers in addition to powders, can be prepared from these ceramics. YBC-epoxy composites are also suitable for this purpose.[426]

Moreover, long(>200 cm) fibers 1 mm in diameter were formed from thermoplastic gels of Y-123 ceramics and PVA.[427] Calcined fibers exhibited values of T_c = 92–94K. These fibers form materials characterized by different J_c values, depending on the degree of saponification (DS) and the Y-123 ceramic content of these materials.[428–430] The minimum critical current density occures when DS = 67 mol%, and the maximum value ($J_c = 3.5 \times 10^4$ A cm^{-2}, 77K) when DS = 81 mol%. The critical current density is also affected by the conditions of treatment (calcination and pyrolysis), which is associated with the peculiarities of the distribution of the ceramics over the fibers. High-T_c superconductor nanocomposites have also been prepared by polymerization of acrylic acid in an aqueous solution of Y^{3+} nitrate and Ba^{2+} and Cu^{2+} acetates.[417]

One of the most promising approaches to the polymer synthesis of high-T_c superconductors involves copolymerization of metal-containing monomers.[431] If metal ions are bound to the monomer before copolymerization, these ions are distributed in the polymer more uniformly. Acrylate or acrylamide complexes of Y^{3+}, Ba^{2+}, or Cu^{2+} were dissolved in a minimum amount of methanol mixed in a molar ratio of 1:2:3, dried and subjected to solid-phase copolymerization.[432] Acrylamide complexes of Bi^{3+}, Pb^{2+}, Sr^{2+}, Ca^{2+}, and Cu^{2+}, in a molar ratio of 2:0.3:2:2:3, were made by the same procedure; but copolymerization was then carried out in concentrated aqueous solutions.[433] The organic phase was destroyed by calcination from the resulting metal-containing copolymers. The properties of these high-T_c superconducting ceramics are shown in Figure 15. Analysis of the temperature dependence of the electrical resistance (R) demonstrated that these ceramics behave as metals[433] at $T < T_c$. The T_c values of these ceramics are not as high as those of single crystals.

The properties of polycrystalline samples depend to a greater extent on the quality of intergrain contacts than on the structure of grains as such. The widths of superconducting transitions in the range of 0.1–0.9 of the value corresponding to complete resistance drop is no more than 2–3 K. This is close to the characteristics

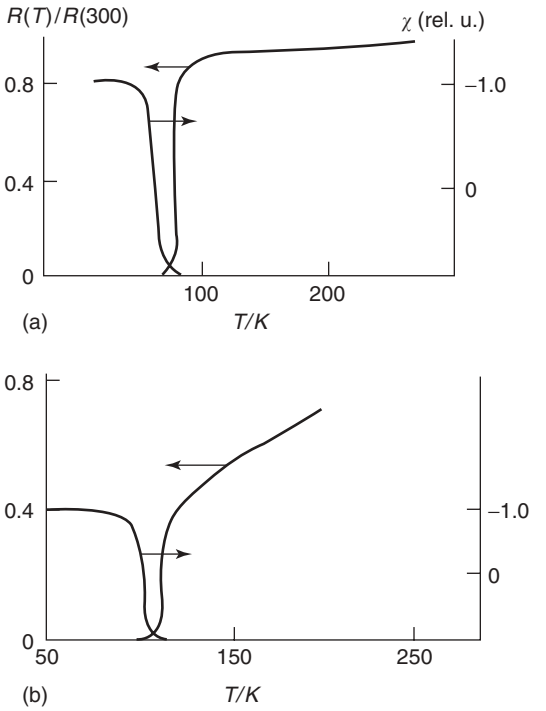

Figure 15 Temperature dependence of the electrical resistance and the magnetic susceptibility of high-T_c superconducting ceramics. (**a**) Ceramics from a copolymer of Y, Ba, and Cu acrylates. (**b**) Ceramics prepared by spontaneous copolymerization of acrylamide complexes of Bi, Ca, Sr, Pb, and Cu.

of the best samples of high-T_c superconducting ceramics. The temperature dependence of the magnetic susceptibility (χ) also indicates a sharp transition and the presence of only the superconducting phase. In this case, the diamagnetic shielding volume of the phase, estimated from a lead reference compound, reaches 100%.[431] Superconducting bismuth cuprates are of particular importance. Developing a reproducible synthesis of these cuprates is a challenging task. Generally, these ceramics contain admixtures of a phase with $T_c = 85$K due to the microheterogeneity and the successive phase transitions[414] 2201 $\rightarrow$ 2212 $\rightarrow$ 2223. Products prepared by spontaneous copolymerization are reproducible single-phase samples with $T_c = 110$K and a critical current density of up to 240 A cm^{-2}. Apparently, this approach can also be used for the preparation of other single-phase nanocrystalline materials.

The preparation of multicomponent M50 steels (alloys of Fe, containing 4.0 wt% Cr, 4.5 wt% Mo, 1.0 wt% V, and 0.8 wt% C) may become an important application for nanostructured polymetallic materials. These steels are primarily used in aircraft construction for the preparation of support bearings, gas turbine engines, etc.[434,435] Generally, M50 steels contain substantial amounts of micron-size carbon particles. These particles initiate the formation of fatigue cracks in bearings.

Mechanical properties of these materials would be improved as grain sizes deposited on the defects decrease (healing of microcracks). The grain sizes can be reduced by employing a process in which organometallic compounds are converted to colloidal particles using the polymeric surfactant PVPr.[434] The surfactant and precursors are subjected to ultrasonic irradiation (sonochemical synthesis) in dry decalin. After removal of the solvent and the gaseous phase, colloidal particles are obtained with average diameter of 7 nm. These particles exist as a homogeneous alloy. Another procedure[435] involves the chemical reduction of metal chloride precursors of M50 steel ($FeCl_3$, $MoCl_3$, $CrCl_3$, or VCl_3) with lithium triethylborohydride in THF. This is followed by removal of solid LiCl by sublimation in vacuo at high temperature. These approaches will also be useful in the design of magnetic materials, such as polymetallic nanosized particles of the $LaSrCr_xNi_{1-x}O_{4+\delta}$ type. Thus a procedure for the preparation of the $La_{1-x}Sr_xMnO_3$ ceramics ($x = 0$, 0.2, 0.4, or 0.6) has been recently proposed.[436] This procedure involves preliminary polymer binding of certain metal nitrate ratios with a gel precursor from PEG ($M_w = 20{,}000$). Autoignition of the polymer occurred at 300°C, with the nitrate ions serving as an oxidizing agent. Subsequent thermal treatment of the combustion product afforded a homogeneous perovskite phase (see above). Its morphology and S_{spec} (1–7 $m^2\,g^{-1}$; the sizes of crystallites were 24 – 150 nm) depended on the ratio of reagents and reaction conditions employed. A ceramic with cadmium and lanthanum additives, having an overall composition $Pb_{0.85}Cd_{0.05}La_{0.10}Ti_{0.975}O_3$, was prepared by the sol-gel method from metal acetates and $Ti(OBu)_4$.[437] Thin silicon films were coated with this material by concentration of the solution (before drying). Subsequent thermolysis was carried out according to a standard procedure.

VIII. INTERCALATION OF POLYMERS INTO POROUS AND LAYERED NANOSTRUCTURES

Sometimes products prepared by sol-gel reactions or by intercalation can be distinguished only by their past history. No less than 5000 studies dealing with the problems of intercalating of organic, organometallic, and inorganic compounds as well as with the properties of the resulting products had been published up to 1994.[438] However, the major body of information has been obtained since then.

Natural layered silicates, (the smectite clays) are most often used for the preparation of nanocomposites under consideration. Their structures, selected physicochemical properties, and the nature of their active surfaces have been considered in a review [439] and in monographs.[20,440] Clays are widespread minerals. Hectorite and montmorillonite $[AlMg(OH)_2(O)_4]^{5-}[Si_2O_3]^{4+}[Na,nH_2O]^+$ (MMN) are typical clays, with structures of the type to which mica belongs. Crystals of MMN consist of alternating tetrahedral silicate layers of cations condensed with negatively charged octahedral layers of metal oxides. However, unlike mica, these minerals undergo ready cation exchange, including transition metal ions exchange. Exchange occurs predominantly in layers containing solvated sodium cations. Intracrystal cavities can swell when they are

filled with organic solvents. The degree of swelling depends on the nature of the cations within the layers and on the negative charge density on the silicate layers. Aluminosilicates and magnesosilicates belong to clays whose nature is determined by the type of the octahedral metal. Mg^{2+} and Al^{3+} can isomorphically replace Al^{3+} and Si^{4+}, respectively, within the lattice. The cations are hydrated and the clay layers readily swell to accommodate large cations or substantial amounts of water. In addition, most of inorganic oxides contain surface hydroxy groups, which actively bind metal ions. Crystalline rigid host matrices with a regular system of nanometer-size pores are well studied.[20,441–444] These pores can be occupied by atomic or molecular guest structures such as clusters, nanosize particles, inorganic coordination polymers of the CdS type, large C_{60} fullerene type molecules, and polymer units synthesized in situ.[20,441–444] Thus intercalation of buckminster fullerene functionalized with ethylenediamine into a mica-like silicate of the fluorohectorite type has been described.[441] Many procedures for the introduction of polymers into host matrices are available. When polymers penetrate between the individual clay layers, the process is called intercalation; it increases the interlayer spacing. When clay layers are completely separated and their individual sheats are surrounded by matrix, the clay is said to be exfoliated. These hybrid nanocomposites are of technological interest because their properties are substantially improved compared to those of materials filled according to a standard procedure.[445–447] For example, these materials prepared by thermal synthesis are generally metastable (in particular, due to flaking of the polymer from the inorganic component).

The properties of intercalated hybrid nanocomposites are determined by a number of characteristics, particularly, by the sizes of their inner open-pore systems. These properties were considered in many reviews.[20,448–452] Intercalating systems are divided into two types according to their architecture and properties.[450] The first type are characterized by the presence of rigid pores with a constant volume, the parallel isolation of lattice channels and the interrelation between the channels of the network. The location, the concentration and the spatial distribution of guests are governed by the topology, the chemical nature and the reactivity of the inner surface of the host. The lattice solid can be additionally dispersed and functionalized or long-chain surfactants can be intercalated into the solid. In addition, the choice of guests is limited by the minimum size of crosslinked channels, which leads to selective intercalation into induced spatial matrices (of the types of molecular sieves or membrane films). The second type of system of hosts are characterized by a low dimensionality of the lattice (i.e., by the structures of the layers or chains). This results in flexible pores. Their sizes can be adapted to the size of the guest. In layered systems, the basal (intralayer) space is often ~ 5 nm. The layer thickness in perovskite varies from 0.5 to 2.2 nm. The matrix lattice that holds the guest may have no effect on the intercalation–deintercalation process. This is true for dielectric lattices of zeolites, layered aluminosilicates, metallophosphates, etc., where the intercalation behavior is determined primarily by the acid–base and exchange properties. Lattices possessing the electronic conductivity (semiconductors and metals) are a special case. Upon intercalation, redox reactions with electron (ion) transfer occur in these materials, resulting in a substantial change in the physical properties of the host matrix.

The inclusion of monomer molecules into pores of a host that is followed by their controlled conversions into polymeric, oligomeric, or hybrid-sandwich products (postintercalation conversions in situ) belong to the most interesting group of intracrystalline chemical reactions. This field has been rather well studied.[453–455] Intercalation of the appropriate monomer causes delamination and dispersion of host layers. This can be accompanied by polymerization to form a linear or crosslinked polymeric matrix. This procedure was used to the insert polyesters,[456] PVPr,[457–459] and poly(ethylene oxide) (PEO)[460] into silicates and to insert PVPr,[461] polyimide,[462,463] and poly(ε-caprolactam)[446,447] into kaolin. When polymerization was performed within kaolin, the resulting composites were nondelaminated products. The most interesting hybrid nanocomposites were prepared from conducting polymers such as polyaniline,[464,465] poly(2-ethylaniline), poly(*p*-phenylene), polythiophene, polypyrrole,[466,467] or pyrolyzed polyacrylonitrile[468] in different matrices.[469–471] A diversity of procedures can be used for two purposes: the enclosure of a polymer into a gel and the use of salt solutions of the corresponding polymers. Polyaniline hydrochloride in an acid–methanolic solution or a sulfonium salt of poly(p-phenylene) in many solvents are examples. Early studies have been reviewed.[438] Thus oxidative polymerizations of pyrrole, dithiophene,[472,473] tetrahydrofuran,[474] or aniline[475] in an FeOCl lattice have been described. Intercalated aniline forms hydrogen bonds with chlorine atoms of the FeOCl lattice, and polymerization occurs along the lattice diagonal.[101] However, the conductivity of the resulting polymer is somewhat decreased. This lattice appeared to be suitable for oxidative polymerization of aniline introduced from an aprotic solvent.[472,476,477] The molecular formula of the resulting product was $(C_6H_5NH_2)_{0.28}FeOCl$.* Zigzag polymer chains, $M_w = 6100$, are comparable with the FeOCl lattice. The chains are extended along the direction of the host crystal and along the hydrogen bonds between the NH groups and the chlorine atoms of the lattice layers. The Fe^{2+}: Fe^{3+} ratio is ~1 : 9. The polymeric intercalate behaves as a *p-type* semiconductor (the conductivity of a single crystal is 1.5×10^{-2} S cm^{-1}). Its prolonged oxidation in air afforded a mixture of polyaniline and β-FeOOH. The use of the α-$RuCl_3$ matrix, which is structurally similar to $FeCl_3$, was proposed[481] for the preparation of lamellar nanocomposites. The oxidative polymerization product of aniline in this matrix has the composition $(C_6H_5NH_2)_xRuCl_3$ $(0.5 < x < 0.6)$. Its conductivity at room temperature is ~2 S cm^{-1}, which is more than three orders of magnitude higher than that of the initial α-$RuCl_3$.

Postintercalation polymerization of aniline was carried out in air at 130°C within phosphate layers of α-$Zr(HPO_4)_2 \cdot (H_2O$,[482,483] $VOPO_4$, [484] $HUO_2PO_4 \cdot 4H_2O$,[483–486] layered acidic zirconium-copper phosphates,[19] and layered double hydroxides;[487] in layers of $HM^1M^2O_6 \cdot H_2O$ (M^1 = Nb or Ta; M^2 = Mo or W),[488–490] molybdenum

*The method consist of quantitative removal of a polymer from an inorganic host, by repeated dissolution. Such investigations could be important for the analysis of polymers in these hybrid materials. Although studies on the extraction of polymers from layered nanocomposites have been reported,[6,477–479] this field is poorly understood. Recently, rapid and quantitative extraction of PEO from the $K_x(C_2H_4O)_4$-$M_{1-x/2}PS2$ composite (M = Mn or Cd) with an aqueous tetraethylammonium salt under normal conditions has been carried out.[480] This process was analyzed in detail and the kinetic regularities were revealed.

sulfide,[491] porous zeolites of the mordenite type,[492,493] and MCM-41;[492] and in layers of perovskite,[494] mica-like silicates,[495] etc.[496] The resulting products are generally dielectrics. Polyoxometallates as host matrices can serve as ideal models of molecular batteries because they contain a small number (generally 6–8) of W or Mo atoms linked through oxygen bridges. Their spatial and electronic structures were adequately characterized.[497] Electrochemical polymerization of pyrrole in Keggin's structures $H_3PM_{12}O_{40}$ (M = W or Mo) was described.[498,499] Sometimes additional chemical reactions are carried out with the aim of converting these products into nanocomposites. For example, $(Bu_4N)_5Na_3[(l,5\text{-COD})M \cdot P_2W_{15}Nb_3O_{62}]$ (M = Ir or Rh; 1,5-COD is 1,5-cyclooctadiene) was reduced with hydrogen in acetone.[500,501] These hybrid nanocomposites can be completed with phosphomolybdate anions (scheme 32). The product compositions exhibit the formula $C_6H_5N \cdot (PMo_{12}O_{40})_{0.116}$. Photochemical polymerizations of the diacetylene 3,5-octadiyne in layers of Mg, Mn, or Zn phosphates were also reported.[452]

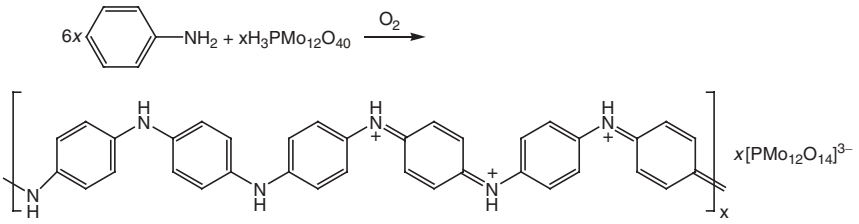

Scheme 32

Under the appropriate conditions, monomers occupy virtually the entire space of pores or the whole interlayer space. Subsequent oxidative polymerization[492] was carried out in the presence of molecular oxygen (as an electron acceptor) and a redox-active host that catalyzes electron transfer. Layered silicates containing metal ions are of particular interest because they initiate polymerization of an intercalated monomer. Thus when Na^+ ions in hectorite are replaced by Cu^{2+} or Fe^{3+}, styrene can be polymerized[316] both in the pores and on the surface. The polymer has a brush-like structure, which indicates that the inorganic surface possesses an orienting effect. This effect decreases as the chain grows away from the surface.

N-Vinylcarbazole is polymerized in MMN at 64°C or in benzene at 50°C due to the presence of cations in the MMN.[502] The thickness of the intercalated layer of guest–host particles in this nanocomposite is 33 ± 10 nm, and the conductivity (10^{-6} S cm^{-1}) is 10 orders of magnitude higher than that of polyvinylcarbazole.

Polystyrene exists in two forms[328] when intercalated into MMN. One form possesses enhanced rigidity due apparently to a higher degree of ordering. The improvement in physicochemical properties of intercalated polystyrene was observed also in a model PS-MMN system.[503]

Redox intercalation polymerization of aniline, pyrrole, and dithiophene using a V_2O_5 xerogel affords polyconjugated anisotropic polymers.[504–506] Intercalation is

accompanied by polymerization. The chain growth initially occurs within the xerogel and is associated with transport of molecular oxygen. The V_2O_5 xerogel acts as a catalyst. A conducting polymer with different polyaniline:V_2O_5 ratios is formed by interaction with the mixed-valence (V^{4+}/V^{5+}) host lamellae, which are ordered along one direction. The material consists of alternating layers of vanadium oxide and the polymer. Physicochemical studies demonstrated that polyaniline was formed as a salt. Aging of the material in air facilitates both partial oxidation of the inorganic framework and oxidative binding of polyaniline in the intralamellar space. The resulting polymer is frozen in place due to the formation of NH···OV hydrogen bonds. A detailed analysis[501,507] of the insertion of aniline, its competitive polymerization into MoO_3, and the formation of the nanocomposite $(C_6H_5NH_2)_{0.24} \cdot MoO_3$ structures was carried out. Low-temperature intercalation procedures were also examined. Polyaniline chains expanded the inorganic layers and changed the potential surface, thus decreasing the polarizability of the lattice.* The polyaniline chains intercalated within MoO_3 oxidize $(NH_4)_2S_2O_8$.[507] Oxidative polymerization of aniline, pyrrole, or thiophene monomers intercalated in layered aluminosilicates affords highly oriented host–guest layers. Radiation polymerization of acylonitrile and acrylic acid in MMN inclusion compounds afforded stereoregular (most likely syndiotactic) polymers.[32]

Many interesting procedures exist for the synthesis of 1D nanocomposites based on matrix intercalation. An aqueous Au colloid particles (12 nm) stabilized with citric acid were introduced into pores of a Al_2O_3 filtration membrane with an average pore diameter of 20 nm. Then oxidative polymerization of pyrrole was performed in situ inside these pores by adding an aqueous $Fe(C1O_4)_3$ solution.[509,510] After dissolution of the membrane in 0.5 M KOH, a suspension of 1D colloid-polypyrrole nanostructures was obtained (Fig. 16).

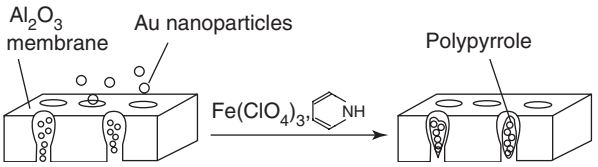

Figure 16 Template synthesis of 1D Au–polypyrrole nanostructures in an Al_2O_3 membrane.

TiO_2 particles (~ 20 nm diameter prepared from $TiCl_3$, pH 2.5) can be obtained at the surface of a photochemical electrode to construct solid light-sensitive solar cells.[511,512] Simultaneously, polypyrrole, which is formed on electrochemical polymerization of pyrrole adsorbed in the electrode's pores, precipitates on these particles.[511,512] These structurally controlled templates are analogues of self-assembling supramolecular ensembles. The procedure for the preparation of supramolecular systems for

*The geometric structures and vibrational properties of complexes of polyenes with aluminium atoms as a constituent were studied by the ab initio quantum-chemical method in the Hartree- Fock approximation.[508]

molecular recognition is analogous to the above-considered preparation of nanobiocomposites.[511,513,514]

One-dimensional parallel polyaniline chains can be prepared in situ, while encapsulated into structures with wide pores and large (the diameter is ~3 nm) channels. These chains are fiber-like and exhibit microwave conductivity.[492,515,516]

An alternative to in situ polymerization involves direct intercalation of macromolecules into layered structures. Silicates are most often used. The insertion of polymer molecules into layered host lattices is of interest from different points of view. First, this insertion process leads to the construction of organic–inorganic polylayered composites. Second, the intercalation physical chemistry by itself and the role intercalation plays in the gain of electronic conductivity are of interest. This becomes important in the construction of reversible electrodes[449] or when improving the physicomechanical properties of nylon-layered silicate nanocomposites,[517,518] hybrid epoxide clay composites,[463] and nanomaterials based on hectorite and polyaniline, polythiophene or polypyrrole.[519]

The insertion of PEO into mica-like sheet silicates in the reactions of a melt of the polymer with the host Na^+- or NH_4^+-exchanged lattice is one of the few examples of direct polymer intercalation.[520] Poly(ethylene oxide) is also inserted into the lamellar networks of $V_2O_5 \cdot nH_2O$, MoO_3,[478,479,521–523] $MnPS_3$, $CdPS_3$,[521,524] etc. Thus an aqueous solution of PEO ($M_w = 10^5$) reacts with an aqueous gel of $V_2O_5 \cdot nH_2O$ to form a composite after removal of water. In this case, the interlayer distance increases from 1.155 to 1.32 nm. Alkali metal ions react with PEO to form inclusion compounds. These can also be inserted into layers of ionic silicates, for example, into MMN. The distance between the layers of the PEO–Li^+ salt complexes intercalated into MMN is 0.8 nm, the PEO chain adopts a slightly strained helicoid conformation in these locations.

Poly(ethylene oxide)-LiX systems find wide application as polymeric electrodes and solid electrolytes. This topic has been discussed in detail in several monographs.[525–527] These systems are often used in combination with ceramic fillers such as $LiA1O_2$, Al_2O_3, and TiO_2. One example will be discussed.[528] Nanosized TiO_2 (13 nm) or Al_2O_3 (5.8 nm) particles (10 wt%) were dispersed in acetonitrile with $LiC1O_4$. Then PEO was added ($LiC1O_4$:PEO molar ratio was 1:8). The conductivity of the resulting polymer–inorganic nanocomposite is 10^{-4} and 10^{-5} S cm^{-1} at 50° and 30°C, respectively. A new series of hybrid polymer–inorganic electrolytes was prepared by cocondensation of $LiAl(OR)_2H_2$ with organosilicon precursors.[529] This series contains aluminium in the main chain and Li^+ ions.

The intercalation of polymers[530] (PS,[531] PEO,[520] polypropylene,[532–534] etc.) from their melts into a silicate lattice is also a promising procedure. Molecular dynamics calculations and the kinetics of formation of these intercalates were considered in this study.[530] A new line of investigation involves direct hydrothermal crystallization of silicate layers from a polymer gel.[535,536] This approach extends the range of intercalated polymers because it allows one to use compounds that do not contain functional groups.

Activation of surfaces, layers and host pores by ultrasonics, is of importance in a process in which Ni particles (10–40 nm) were deposited on submicrospherical

silica gel.[537] When a solution of $Ni(CO)_4$ in decalin was sonicated, the Ni–C bonds were cleaved simultaneously with activation of the SiO_2 surface. Adsorbed water was removed from SiO_2, Si–O–Si bond cleavage occurred, and free Si–O bonds were formed. An alternative procedure involves the reaction of metallic nickel with activated surface silanol groups to form Si–O–Ni bonds. These centers serve as nuclei for further growth of Ni particles. Amorphous superparamagnetic Ni clusters were converted into a crystalline ferromagnetic material at 400°C. This mechanism is realized to some extent for other dehydrated surfaces as well. For example, Al_2O_3 and metal carbonyls $M(CO)_n$ form Al–O–M structures.[538] Gold nanosize particles were stabilized in a silica gel monolith.[539] Thermolysis of rhodium carbonyl on the Al_2O_3 surface afforded small Rh clusters.[540]

Nanocomposites can be self-assembled as $(M/P)_n$ multilayers, where M and P are nanosize oppositely charged layers of an inorganic component and a polymer, respectively. These composites are worthy of special notice bacause they possess a variety of valuable properties. They may be used in optical engineering for the production of displays.[541–547] A great variety of procedures for the layer-by-layer assembly of polyelectrolytes and clays,[548–553] lamellar zirconium phosphates,[554] and colloidal metal particles[555,556] were proposed. Anionic MMN and positively charged poly(diallylmethylammonium chloride) (PDAMAC) is an example of a system that can assemble layer by layer. The mechanism by which these materials form on the surface of nanoplates from glass, quartz, silver, gold, and even Teflon was considered in detail and the defect formation processes were studied.[557] Successive submersion of plates into a solution of the P component or in a suspension of M leads to an increase in the number of layers (n). Each layer that formed is accompanied by an increase in the thickness of the P and M layers by 1.6 and 2.5 nm, respectively. The formation of multilayers involves several stages. First, adsorption on the substrate surface occurs. This event is determined by electrostatic and van der Walls interactions. The structural hierarchy of the M layers provides limitless possibilities for their application as templates for the insertion a great variety of molecules and clusters,[24,558–562] between swollen layers or inside the M plates while being located on the surface. Second, the M component is strongly and irreversibly adsorbed on the oppositely charged polymeric electrolyte to form a closely packed plane-oriented layer. Irregular M layers cannot provide complete coating of intercalated layers due to new stacks are overlapped. Interphase irregularities, which are independent of the nature of the substrate, exceed the thickness of the M/P layer. The control over the process can be performed by applying an external stress to the system during self-assembly. In practice, a wide variety of these procedures were realized. For example, the PDAMAC polyelectrolyte and SiO_2 nanoparticles (25 nm diameter) were successively deposited on the surface of a polystyrene latex. A three-component polylayered material is formed by adsorption (Fig. 17) in which the thickness of one, two, and four SiO_2- polymer layers are 60, 120, and 240 nm, respectively. Multilayer self-assembly was also used to prepare nickel phthalocyaninetetrasulfonate–PDAMAC nanocomposites with an average M/P layer thickness of 1.05 nm.[563]

Layered nanostructures were prepared[564] using liquid-crystalline polymers containing ionic groups; MMN or hydrotalcite $[AlMg_2(OH)_2(OH)_4]^+[0.5\ CO_3, OH,$

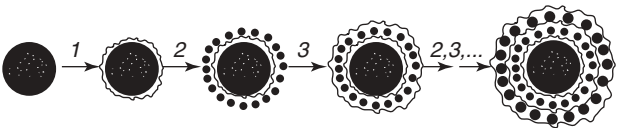

Figure 17 Self-assembly of a polylayer composite based on PS latex, SiO_2, and poly(diallylmethylammonium chloride: *1*, adsorption of polyelectrolyte; *2*, adsorption of SiO_3; *3*, adsorption of a polycation.

C1]$^-$ was the inorganic component. The average thickness of the M/P layer pair was estimated at 4.93 nm. Electrostatic self-assembly promotes tight contacts between the components, and the establishment of this molecular organization allows one to prepare new types of liquid-crystalline structures with unusual properties. Layer-by-layer assembly of aluminosilicate-polyelectrolyte nanocomposites appears to be a promising procedure for the design of new membrane materials.[565] This review will not consider hybrid nanocomposites that were prepared by emulsion or gas-phase polymerization of traditional monomers, such as styrene, MMA, aniline, ethylene, or propylene, in the presence of different organophilic minerals. However, these approaches are undoubtedly of interest by themselves.[566] Thus emulsion polymerization of a bisphenol A/epichlorohydrin epoxy prepolymer in the presence of Na^+ $^-$MMN was accompanied by the insertion of the polymer into the basal space of this smectite clay. The layer spacing expanded from 0.96 to 1.64 nm.[567] A monomer micelle rather than the monomer itself was inserted into the body of the swollen host in aqueous media. The resulting composite exhibits a higher thermal stability than that of the corresponding homopolymer. A hydrogel containing 3.5 wt% of MMN[568] was prepared via copolymerization of *N*-isopropylacrylamide and *N*,*N*′-methylenebisacrylamide in aqueous suspensions of MMN.[569] This hydrogel possesses the lower critical solution temperature (~32°C) than that of the nonmodified product.

Layered graphite inclusion compounds have been studied in detail. Graphite can be considered as an aromatic macromolecule. The number of aromatic rings in this molecule is ~1000 and the distance between the parallel planes is 0.335 nm. Since bonding between the parallel carbon layers in graphite is weak (the energy of the interlayer interaction is only 16.8 J mol^{-1}), monomolecular layers of different compounds, including metal ions, can be inserted into graphite to form layered (laminated) compounds.[570] Graphite-inclusion compounds are generally prepared by the reactions of graphite with vapors or solutions of metals in strongly ionizing solvents, with low-boiling chlorides or with cationic metal complexes. These compounds are divided into products of the first, second, and subsequent stages of insertion, depending on the number of carbon layers separating two adjacent layers of the metal inserted. The nature of bonds in these layered systems depends on the nature of the metal. For example, in the cases of Fe, Co, Ni, Mn, and Cu, van der Waals interactions exist. Sometimes when the π-electron density of graphite is transferred to the inserted metal layer, the carbon network of graphite serves as polymeric ligand. In the case of alkali metals, this bond is formed as a result of electron transfer from the metal atoms to the conduction band of the adjacent graphite layer. Electrostatic

interactions occur between the positively charged metal ions and free electrons of the conduction band of graphite.[571]

Upon reduction, the inserted metal ions, may partially leave layered stacks and reduction may occur on the outer surface of graphite. Nanosize particles of titanium are inserted into the imperfect lattice of graphite in this manner.[572] Many metals are inserted into graphite under high pressure in combination with shear deformation.[573] Nanosize cobalt particles inserted into the graphite lattice in this way exhibit unusual magnetic and thermal properties.[574]

Clearly, intercalation chemistry provides virtually limitless possibilities for hybrid nanocomposites construction. Presently, the major effects attendant on the processes of formation of these materials are revealed. The structural organization and properties of these materials have been studied. The number of studies in this field is gradually increasing, and this allows one to predict the design of new types materials. For example, the synthesis of hybrid nanocomposite materials on the base of gallium phosphates containing azamacrocycles, etc. has been reported recently.[575] Studies of ion exchange intercalation of nitrate groups, nucleosidemono-phosphates, and DNA into layered double hydroxides of the $Mg_2Al(NO_3)_2 \cdot H_2O$ type (anionic clays) has began.[576] Nanocomposites containing metal chalcogenide host structural elements are of special interest.[577–584]

IX. METAL CHALCOGENIDE-POLYMER INCLUSION NANOCOMPOSITES

Metal chalcogenide–polymer inclusion nanocomposites are rather well studied. The results of these studies were reviewed.[585,586]

Intercalation into the CdS structure has received much attention.[587] Composite films are generally prepared from a solution of the corresponding precursor followed by in situ synthesis.[588] For example, $Zr(OPr)_4$ in propanol was hydrolyzed with an aqueous solution of acetic acid, and solutions of cadmium acetate and ammonium thiocyanate were added.[589] The composition was coated onto a glass support and treated as in the sol-gel method (Section VI). The cryochemical treatment of gels impregnated with Cd^{2+}, Pb^{2+}, or Zn^{2+} salts, followed by sulfiding with hydrogen sulfide in the gaseous phase, afforded nanosize sulfide particles with sizes ranging from 3–7 to 30–100 nm within a SiO_2 matrix.[226] The formation of the dispersed CuS phase in a polyacrylic acid-poly(vinyl alcohol) matrix proceeds through several stages. These include formation of sulfur-containing copper complexes, the association of these complexes, the formation of amorphous clusters and, finally, development of crystalline CuS nanoparticles.[590] The specific structure of the interfacial layer and limitations imposed by diffusion in the swollen polymeric matrix are responsible for the formation of small (~4 nm) particles, the particle distribution in the matrix and the aggregative stability.

If the anion in MX_2 systems is readily polarized and the cation possesses strong polarizing properties, layered structures develop. The distinguishing feature

Table 8 Properties of Intercalated Polymer–$NbSe_2$ Nanocomposites

Composite	d/nm	Thermal Stability in N_2/°C	Conductivity/S cm^{-1}	T_c(K)
$(PVPr)_{0.14}NbS_2$	2.40	310	140	7.1
$(PEO)_{0.94}NbS_2$	1.96	224	250	6.5
$(PEG)_{0.80}NbS_2$	1.88	233	240	7.0

of MoS_2 or TaS_2 layered materials with low charge density in their layers is their ability to decompose into nanosize building blocks and to form colloidal solutions. A layer of molybdenum atoms is located between layers of chalcogen atoms in molybdenum dichalcogenides. Packs are formed from these triple layers. Bonds within the packs are substantially stronger than those between two different packs linked only through van der Waals forces.[591] The exfoliation procedure has been developed in sufficient detail.[592,593] Plastic superconducting electromagnetic materials have been prepared based on nanocomposites.[594] Intercalation of PVPr, PEO, and PEG from aqueous solutions into monolayers of suspended $NbSe_2$ was reported.[595] The PEG/$NbSe_2$ is of one the best superconductors among layered dichalcogenides ($T_c = 7.2$K).[595] The compositions and the selected properties of these nanocomposites are given in Table 8. A polymer is inserted into the WS_2 phase according to the same mechanism.[596]

$$NbSe_2 + xLiBH_4 \xrightarrow[-0.5xH_2]{-xBH_3,} Li_xNbSe_2 \xrightarrow[-0.5xH_2]{xH_2O,\ -xLiOH,} NbSe_2\ (\text{monolayer}) \xrightarrow{\text{polymer}} \text{polymer} - NbSe_2$$

Delamination occurs by the insertion of a polymer can according to the host–guest mechanism. Then intercalated systems are deposited by removing the solvent or by increasing the concentration of the electrolyte. Direct intercalation of polyalanine into the interlayer space of MoS_2 ($d = 1.037$ nm) through formation of colloidal suspensions has been described.[492]

The polypyrrole–MoS_2 nanocomposite, produced by of oxidative polymerization in situ under kinetically restricted conditions, is a *p-type* conductor. Its electronic conductivity is three orders of magnitude higher than that of the initial MoS_2.[597] Intercalation of PEO into a delaminated suspension of TiS_2 or MoS_2 has been carried out.[598] Nanocomposites of linear polyethyleneimine inside layers of MoS_2, $MoSe_2$, TiS_2, or MPS_3 (M = Mn or Cd)[599] have been made in aqueous solutions. Composites of polyethyleneimine or poly(styrene 4-sulfonate) within $TiO_2 \cdot PbS$ layers possessing semiconducting properties were also made.[600]

Nanocrystals of metal chalcogenide semiconductors immobilized into polymeric matrices exhibit luminescent properties. This is illustrated by nanocrystals of CdSe,[601,602] CdS-Ag,[603] ZnS, and ZnS-CuS.[604,605] Composites based on ZnS-CuS,

contain ~2 nm crystals in a polymeric matrix. They have been prepared by copolymerization of corresponding metal acrylates with styrene, followed by treating of the copolymer solution with hydrogen sulfide in chloroform.[606] These composites possess good photoluminescent and electroluminescent properties. They are also stable. A precipitate did not form even after 1 year from the almost colorless organosol.

Metal chalcogenides with more complex layered structures can also be decomposed and subjected to intercalation.[607] Examples include $PbNb_2S_5$ and $SmNb_2S_4$. In polar solvents, 1D host phases form colloidal systems with MMo_3Se_3 (M = Li, Na or In). These contain monodisperse, negatively charged condensed cluster chains $(Mo_3Se_3^-)_n$. The structures of these systems, called pseudo-1D metals, have been described in detail.[608] They are of interest in the design of materials with a nanowire (or molecular-wire) morphology. Block radical polymerization of dilute ($l0^{-3}$–$l0^{-4}$ mol L^{-1}) solutions of these rigid rods in a solvating monomer (vinylene carbonate) is performed in the presence of a crosslinking agent.[609,610] After rapid solidification, the polymeric matrix provides capture, association, and isolation of the inorganic phase. The nancomposite contains individual isotropic nanowires 0.6–2 nm in diameter and 5–10 nm in length. Polymerization of more concentrated solutions (10^{-2} mol L^{-1}) affords nanocomposites as oriented multiwires (nanocables) 2–4 nm in diameter and ~500–1500 nm in length. Each nanocable contains 5–20 nanowires (Fig. 18). The molecular weight of the inorganic chain is estimated at ~10^5. The conductivity is 10^2–10^3 S cm^{-1}, which is approximately equal to the conductivity of the $(LiMo_3Se_3)_n$ film.

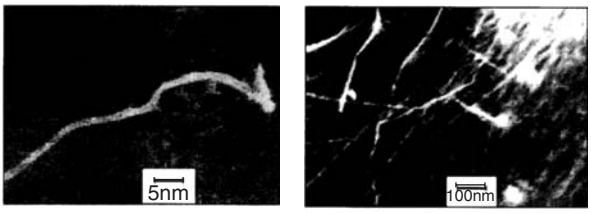

Figure 18 Electron micrograph of a (**a**) nanowire and (**b**) nanocable.[610]

The intercalation of polymers into the interlayer space of chalcogenides is an extensively and fruitfully developing field of the technology for the preparation of nanocomposites. However, many problems are still not completely understood, particularly those associated with the mechanism of insertion and guest–host interactions. Several more examples of these nanocomposites will be noted. Polymeric films containing nanosize particles (10–16 nm) of the chalcogenides ZnS,[611] and Cu_2S-CdS-ZnS with different polymers, CdS,[612] and β-cyclodextrin were described. The inner diameter of the β-cyclodextrin cavity is 1.53 nm.[613] This is substantially smaller than the nanosize particles. Nevertheless, monodisperse complex structures with the participation of β-cyclodextrin are formed. It was suggested[612] that these structures result from the binding of monodisperse complexes with excess sulfide anions and cadmium cations to form CdS-P-cyclodextrin-S^{2-} aggregates.

X. METALLOPOLYMERIC LANGMUIR-BIODGETT FILMS—SELF-ORGANIZED HYBRID NANOCOMPOSITES

Metal-containing nanoparticles inserted into LB films (LBFs) belong to yet another promising class of precursors for the preparation of nanocomposites. Procedures to synthesize of self-organized inorganic surfactant composites have recently been developed. This has made possible the preparation of new 2D composite materials.[211,614,615] Generally, the phase sizes within these materials are no more than 2–10 nm.

Polymolecular LBFs are used to prepare highly oriented ultrathin films possessing special properties, determined by their supramolecular structures. Sensor groups or their precursors possessing nonlinear optical properties can be inserted into these self-organized layers. In some cases, metal complexes, clusters, or nanosize particles are inserted. Finally, LBFs are used as a model for surface and biological processes.[616] Supramolecular ensembles with a periodicity that is intermediate between atomic and macroscopic sizes are the subjects of supramolecular chemistry.

Supramolecular chemistry routes to nanocomposites are still in a primitive state of progress. However, some methodology has already been developed. The preparation of LBFs is modified when they are applied in this methodology.[615] Heterogeneous polar nanolayers are prepared on the surface of a subphase such as deionized water. A constant surface pressure, π, is used, which has the dimensionality mN m^{-1}. This pressure has been measured using a Wilhelmy balance in a specially designed apparatus with two-section baths controlled by microprocessors.[617] Successive LB vertical lifts or Langmuir-Scheffer horizontal lifts in the liquid-crystalline state are used to transfer these layers to a solid support. This allows one to design complex molecular planar structures possessing different properties. Metal particles in LBFs can exist as 2D gases when their surface concentration is small and they do not interact with each other. Three-dimensional states such as gaseous (the distance between the molecules is substantially larger than their sizes), liquid (the distance between the molecules is comparable with their sizes), liquid-crystalline (the lability of the molecule in the plane of the monolayer is retained), and solid states are formed as the 2D gas is compressed.[614]

Two procedures for the formation of nanosized particles within these films are employed. The first procedure combines the principles of colloid chemistry, self-organization and the growth of monolayers.[618–620] The formation of nanosize particles is performed in the presence of stabilization agents and components forming LBFs. Chemical and photochemical reduction of metal salts in aqueous solutions can cause particle formation. The resulting layers act as specific templates.[620–622] This approach is also of interest in studies of biomineralization, including studies using the sol-gel method.

The second procedure consists of LBF deposition on the surface of stabilized nanosize particles followed by insertion of these particles into polylayers. Functional groups participate, including groups on inorganic layers. For example, a LBF based on amphiphilic Ru^{2+} complexes was immobilized on a monolayer of hectorite.[623] Lamellar films and polylayers were formed. LBFs with a specified organization were formed either directly on the surface of colloidal particles or on the water surface. Then

these films were transferred to a support composed of nanosize particles using LB techniques.[624–628] Thus a gold hydrosol stabilized with 4-carboxythiophene was immobilized on a monolayer of octadecylamine.[629] The charge on the film was controlled by changing pH. Multilayer films with different densities of 10 ± 3 nm Au–octadecylamine clusters were prepared according to this procedure.[629] These films contain from 2 to 20 monolayers, where the surface pressure in the monolayer is 25 mN m^{-1} and the film area (A) is 0.37 nm^2 $molecule^{-1}$. The immobilization of nanosize particles on a LBF has a number of advantages over the chemical insertion of metal ions into a LBF followed by the assembly of clusters. The deformation of films is prevented. The ordering in the lamellar phase is not disrupted, and various nanosize bimetallic and polymetallic particles can be used by choosing appropriate hydrosol mixtures. When particles are immobilized on an LBF, adsorption or chemical interactions occur. Furthermore, a higher recognition level is achieved. Examples are provided by self-organization of monolayers composed of alkylsiloxanes, fatty acids, dialkyl sulfides, or thiols on surfaces of Al, Au, SiO_2, etc.[630,631] Thus two processes occur on the mosaic Au-Al_2O_3 surface. First, recognition of the like support (selective adsorption) takes place. Second, self-organization of diphilic thiols on Au regions and acid on Al_2O_3 regions occurs.

The majority of studies were devoted to (1) self-organized hybrid nanocomposites made from mononuclear complexes (in particular, on CdS), (2) procedures for the assembly of nanosize particles from these complexes, (3) investigations of the quantum-dimensional effects typical of semiconducting nanoparticles, (4) and practical applications of these nanocomposites.[632,633] Dispersions of CdS particles (2.65–3.4 nm) stabilized with dodecylbenzenesulfonic acid in $CHC1_3$ spreads over a water surface to form stable monolayers of nanosize particles.[634,635] According to the π-A compression isotherms, an increase in the π value leads to the transition from the gaseous state to a close-packed monolayer of particles. Finally, a polylayer is formed. The resulting LBFs are characterized by $A = 0.65$–1.1 nm^2 $particle^{-1}$, which is close to the corresponding values for the hexagonally packed rigid spheres (0.608–0.887 nm^2 $particle^{-1}$). The transfer of these monolayers to a solid support by the LB method produces polylayers of dimensionally quantized CdS clusters. Their optical density increases linearly as the number of monolayers transferred increases.

The in situ formation of nanosize semiconducting particles in LBFs by reacting metal ions with H_2S or Na_2S has been described.[636–638] For example, sulfiding layers of cadmium, zinc, or lead behenates $(C_{21}H_{43}COO)_2M$ afforded 100-nm-thick films (34 layers) containing sulfides of these metals.[639,640] The films are anisotropic. The resulting nonspherical nanosize (5–10 nm) particles form the cluster layers possessing pores. CdSe nanoparticles form on treatment of films of cadmium arachidate $(C_{19}H_{31}COO)_2Cd$ with a H_2Se vapor. This occurs in the interlamellar space of films in the solid phase and is accompanied by substantial deformation and even by disruption of the lamellar structure.[641]

Multilayer LBFs are often prepared from cadmium stearate,[642] magnesium stearate,[643] and α-Fe_2O_3.[644] Self-organized films of silver stearate (8–14 layers) were formed in hydrophobic layers of stearic acid. The film was transferred to electrodes ($\pi = 25$ mN m^{-1}) and then electrochemically reduced in a neutral or acidic solution to form 2D Ag clusters (20–30 nm).[645] These films also contained Ag clusters of the sandwich type. Self-organized metal-containing LBF ensembles are often used for

the modification of the electrochemical properties of electrode surfaces on the molecular level.[646–647] These ensembles are exemplified by self-assembling LBFs of $C_8H_{17}C_6H_4N{=}NC_6H_4O$ -$(CH_2)_3COOH$ and $X(CH_2)_2SH$ (X = OH, COOH), which are linked though a hydrogen bond and deposited on Au. These systems are electrochemically stable and their behavior is predictable and reproducible.

One promising electrochemical synthetic approach involves the formation of 2D (Langmuir) nanosize particle monolayers under a monolayer surfactant matrix. These surfactants are present on the surface of an electrolytic solution during kinetically controlled electroreduction in an electrochemical circulating cell.[648,649] Two-dimensional aggregates of silver particles are formed only when a monolayer of a surfactant carries a negative charge. The LBF technique can be used in conjunction whith controlled precipitation and hydrolysis of iron salts within surfactant layers[650] for preparing new nanomaterials. The layer thickness is determined by the concentrations of Fe^{2+} and Fe^{+3} salts as well as of their oxides in aqueous solutions and also by the redox $Fe^{2+} \Leftrightarrow Fe^{3+}$ equilibrium (oxidation by H_2O_2). The properties of self-assembling iron–surfactant nanocomposites containing 1, 2, 3, or 6 layers of iron oxide depend on their sizes. These composites exhibit superferromagnetism and occupy the first step in the hierarchy of nanocomposite magnetic materials (scheme 33).

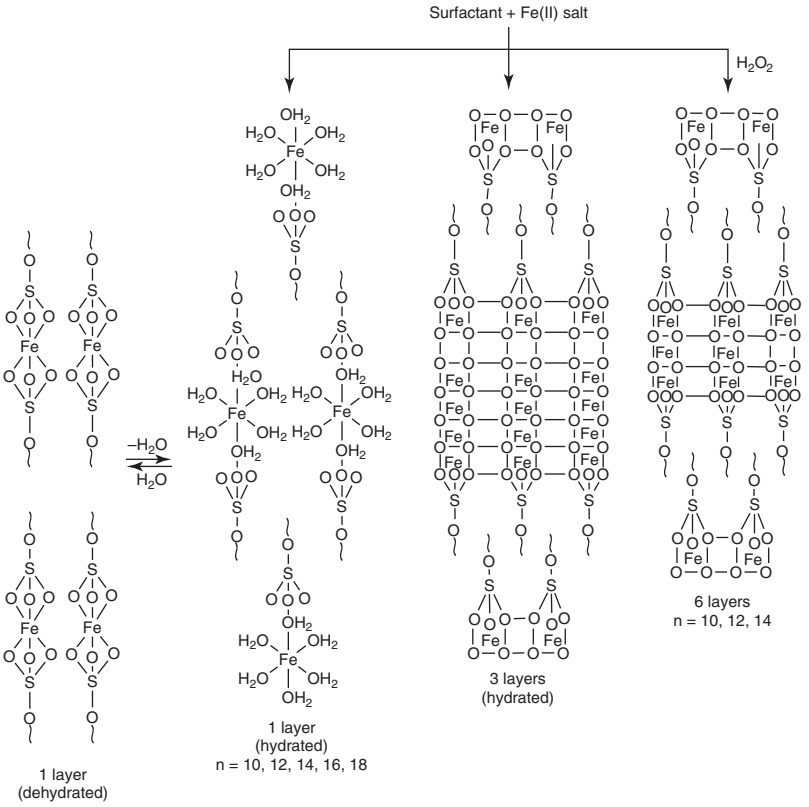

Scheme 33 *n* is the number of carbon atoms in a surfactant.

Magnetic LBFs can be prepared based on heterobimetallic oxo complexes such as Cr^{3+}–Fe^{2+}–Cr^{3+},[651] or by sulfiding bimetallic Pb-Cd or Zn-Cd stearates.[652] Classical LBFs can be prepared from either low-molecular-weight compounds or polymeric systems. High degree of hydrophobicity can be imparted during the formation of monolayers, if the chain is functionalized by polymer-analogous reactions or by grafting sidechains, which can respond to the external factors. The polymerization of functional monomers and their copolymerization with monomers serving as spacer units have been used. In principle, diphilic LBFs have higher stability than polymolecular films of low-molecular-weight compounds. These materials support the required monolayer density upon formation of a film (an equilibrium pressure of spreading of monolayers is a more rigorous criterion for their thermodynamic stability). It is necessary to introduce functional groups of different types into LBF monolayers to solve some problems. For example, a redox pair can serve as functional groups. However, serious limitations emerge when employing low-molecular-weight reagents because diphilic compounds are not mixed at the molecular level and phase separation occurs. The use of polymers allows one to solve this problem. The effect of the composition, the structure of polymers and copolymers, and the external conditions on the formation and properties of organized polymeric monolayers and LBF on surfaces were analyzed in a detailed review.[652] LBFs were formed the using polymeric metal complexes based on porphyrins and phthalocyanines.[653,654] For example, polymers with diphilic properties can be obtained by copolymerization of long-chain α-alkenes with maleic acid, maleic anhydride, and other compounds.[655] In these polymers the carboxyl group is a convenient site for binding a metal complex. The use of 4-aminomethylpyridine to open anhydride rings generates groups capable of bonding metals possessing coordination vacancies in the polymer. This procedure was used for binding tris(phenanthrolino)iron(II) sulfate or bis(salicylidenoaminopropyl)aminocobalt(II) to diphilic copolymers, including those of maleic acid–pyridinemonoamide with octadecene or maleic acid–picolinemonoamide with *N,N*-diocta-decylacrylamide.[656] The dependence of surface tension π on the area of the monolayer per molecule (A) at the air–water interface is shown in Figure 19. The type of isotherm for the film formation is determined by the concentration of a metal complex. Its dimensions are substantially larger then the area of monomeric units (it is assumed that a cubic complex molecule is located nearly parallel to the water surface). At complex concentrations higher than 10^{-7} mol L^{-1}, this fact is of considerable importance in the organization of a monolayer. After compression ($\pi = 25$ mN m^{-1}), a stable homogeneous monolayer is formed. However, this stability is lost at concentrations of ~10^{-4} mol L^{-1}.

One monolayer of a multilayer system can contain metal complexes of two different types. Metal bonding by two functional groups possessing opposite properties prevents phase separation.

Recently, the preparation of monolayer and polylayer LBFs from a carbazole containing copolyimide and copper phthalocyanine has been reported.[657] The stacked molecular organization of the layers and small intermolecular distances in these LBFs ensure the high mobility of the charge and impart the good photoconducting properties.[658]

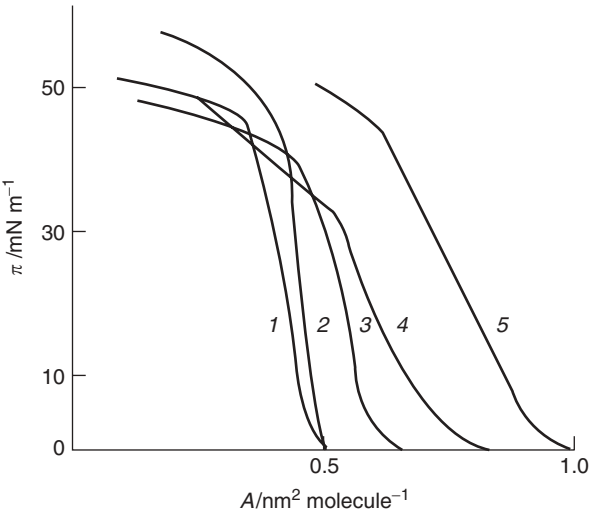

Figure 19 Film formation isotherm for maleic acid—pyridinemonoamide—octadecene copolymers on different subphases. *1*, An aqueous solution of an alkali with pH 10; *2–5,* solutions of [bis(salicylideneaminopropyl)amine]cobalt[659] (II). The concentrations (mol L^{-1}) are *2*, 10^{-7}; *3*, 10^{-6}; *4*, 10^{-5}; and *5*, 10^{-4}.

Regular nanocomposite ensembles organized in LBF miltilayers are also constructed through electrostatic interactions between charged sol nanoparticles dispersed in a subphase and charged monolayers of the surface. This can occur between anionic nanoparticles and a cationic polyelectrolyte.[548] This procedure was used for the synthesis of regular nanowire Tl_2O_3-PVC–arachidic acid composites (PVC–polyvinylcarbazole) made from crosslinked polycationic PVC. This PVC was prepared by electrochemical polymerization of *N*-vinylcarbazole in the presence of $NaC1O_4$, and a thallium oxide sol (*n*-type semiconductor).[659] The resulting polymeric layer (2.7 nm) serves as a template coated with regularly organized Tl_2O_3 particles (3.2 nm). The resulting 5.5 -nm-thick monolayers can be transferred layer by layer to the hydrophobic surface ($\pi = 25$ mN m^{-1}). This method could gain wide acceptance because electrochemical polymerization allows one to produce many positively charged conducting polymers, including polyaniline, polypyrrole, and polythiophene.[660]

This mechanism also occurs during the formation of self-organized TiO_2 layers on SO_2-functionalized polymer surfaces[661] as well as in the preparation of ordered TiO_2 layers on poly(sodium 4-styrenesulfonate) (PSS). TiO_2 particles (~3 nm) were prepared by acid hydrolysis of $TiCl_4$. They formed organized layered structures on surfaces of cationic polymers like superthin (~1 nm) PSS or PDA-MAC.[662] Optically transparent LBFs organized on the molecular level and containing up to 120 layers (60 bilayers) were formed on surfaces of such substrates as metal, silicon, or a polymer cleaned with a 5% *N*-2-(2-aminoethyl)-3-aminopropyltrimethoxysilane solution. The thickness of these bilayers was estimated at 3.6 nm. It is expected that this procedure will allow one to realize semiconducting metal–dielectric structures containing

nanosize *p-n-, p-n-p-, n-p-n-,* etc. units. Polylayer (2–12 layers) films of hybrid nanocomposites with N → Cd coordination bonds have been prepared by the reaction of poly(4-vinylpyridine) (P4VP) with nanosize particles of cadmium sulfide.[663]

LB monolayers containing tris(2′2-bipyridine)ruthenium(II) have received much attention for use in sensors.[664–667]

Nanocomposites made of clusters in a Langmuir monolayer are of interest for the design of metal-film materials used in the electronics and for modeling the structures of fixed catalysts. For example, $Os_3(CO)_{11}(NCCH_3)$ reacts with self-organized layers of (3-mercaptopropyl)trimethoxysilane on a gold surface. This results in the disruption of the well-organized thiol surface to form (1.0–2.2 nm) cluster aggregates.[668] Layer-by-layer adsorption of 1D and 2D $[Cd_4L_4]^{8+}$ octahedral complexes on monomolecular poly(ethyleneimine hydrochloride) and polystyrenesulfonate films on silicon is an efficient method for preparing new metal-containing supramolecular thin films.[669]

Metal clusters in LBF deposited on the surface of highly oriented pyrolytic graphite (HOPG) have been applied to solve many catalytic problems and to prepare stable reproducible tunnel nanostructures. $Rh_4(CO)_{12}$ and $(NEt_4)_2[Pt_{12}(CO)_{24}]^{2+}$ clusters sorbed onto HOPG from organic solvents were studied by scanning tunnel microscopy.[670] Under laser irradiation, these clusters underwent decarbonylation and transformation to highly dispersed Pt 1.8×0.5 nm crystallites bound to the graphite surfaces.[671] Procedures were developed for the deposition of isolated naked silver clusters on the HOPG surface with a topography characterized by planar dimensions of 3–5 nm and a height of 2–3 nm. Futhermore, a technique for the assembly of their ligand shells from PPh_3 was developed.[672] The voltammetric characteristics were measured of individual clusters on freshly cleaved HOPG. These clusters were inserted into monolayers of stearic acid, and their transfer to the HOPG surface also afforded cluster-containing LBFs.[673] In the resulting monolayer, cluster molecules form an ordered 2D lattice. The problem of fixing of clusters on the surface was solved in this way and reproducible one-electron tunneling was realized at room temperature. The regular insertion of clusters (Pd_3, Pt_5, and Pd_{10}) into LBFs and their voltammetric characteristics have been analyzed.[674] A multilayer LBF was transferred from a monolayer of stearic acid at the surface of $MgCl_2$ aqueous solutions to the HOPG surface in the disrupted state; the surface per molecule is 0.15 nm^2, $\pi = 36$ mN m^{-1}.[494]

The examples above demonstrate that metal-containing LBFs, including those based on nanosize particles and clusters, are of considerable interest for the preparation of organized hybrid nanocomposites.

XI. NANOMETER-SIZE PARTICLES, CLUSTERS, AND POLYNUCLEAR STRUCTURES IMMOBILIZED IN BIOPOLYMERS AND THEIR ANALOGS

The interaction of metal ions and nanoparticles with biopolymers and cells plays a highly significant role in the enzymatic catalysis, geobiotechnology, and

biohydrometallurgy. Natural and genetically engineered microorganisms are of practical interest for the geomicrobiological transformation of heavy metals. Their vital activity occurs under extreme conditions (high temperature and pressure, highly acidic or basic media, strong salinity, the presence of metals at levels toxic for common microorganisms). This group of microorganisms is named metallophiles in analogy with thermophiles, halophiles, acidophiles, etc.

The extent of selective metallophilicity of microorganisms is believed to be determined by a number of factors, including (1) the selective direction of motion of the colloidal particles relative to microorganisms, and (2) the nature and strength of the chemical bonding of particles on the surface. Covalent bonds to the surface are predominate.

The genetically predetermined specialization of microorganisms for the interaction with definite metals is a consequence of selective metallophilicity. A rigorously determined system of cells from definite species and a metal (or a group of related metals appear under natural conditions. Flocculation of cells by colloidal metal particles leads to the formation of rather large (up to 50–60 nm) bioskeletal aggregates undergoing sedimentation in aqueous media.[675]

The binding of metals is effected by bacteria, yeasts, fungi, numerous algae, and some protozoa. This extends the potential for biochemical transformation and transfer of metals under natural conditions.

The coagulation of metal sols is one manifestation of the colloidal–chemical binding. The best studied is the easily prepared and stable gold sol. The heterocoagulation of these sols produces biopolymer-immobilized nanoparticles. These particles are mixed aggregates of living microorganisms and nanoparticles. Many of them possess specific properties determined by the processes occurring in the diffusion layers of cells. Many properties are associated with the electrical heterogeneity of their surface.[676] These processes induce sol particles to bind and simultaneously decrease their coagulation threshold due to the increased counterion concentrations. These highly dispersed biogenic aggregates are widely distributed in nature as economically important metal ores, etc. In fact, the very idea of immobilization of metallocomplexes on polymers originated with natural systems.

A. The Formation of Metallobiopolymeric Systems

The peculiarities of the interaction of microorganisms with metal sols largely depend on the nature of the metal. The best studied are the colloids of gold.[675] Colloids of other noble metals, as well as those of iron, copper, and manganese have been investigated to a lesser extent. Biosorption is the novel approach to the metal recovery from the dilute solutions. Biosorption is often caused by polysaccharides. Microorganisms and algae allow the extraction of up to 100% of lead, mercury, zinc, nickel, cobalt, manganese, chromium, uranium, and some other elements from dilute aqueous solutions.[676] Up to 96–98% of gold and silver, up to 84% of platinum, and 93% of selenium can also be removed from dilute solutions.[677] Bacterial polysaccharides are also effective in the recovery of radioactive elements, copper, and cadmium from solution (Table 9).

Table 9 Sorption of Metals by Microorganisms[677]

Metal Sorbed	Microorganisms	Metal Content (mg per 1 g dry cells mass)
U, Th	denitrifying bacteria	140
	Rhizopus arrhizus	180
U	*Pseudomonas aeruginosa*	≤ 560
	Saccharomyces cerevisiae, Pseudomonas aeruginosa	100–150
	Biosorbent M *(Penicillum chrysogenum)*	80–120 (purification of waters containing <0.05 mg L^{-1} of elements)
Ag	Bacterial community of *Ps. maltophila, Staphylococcus aureus* and unidentified forms	≤300

The bacterial concentration of metals is preceded by their adsorption on the cell surface with subsequent assimilation. This can be accompanied by enlargement of sol particles (flocculation) and the adsorption and deposition of a coarse metal–bacterial mass (heterocoagulation). As with systems based on synthetic polymers, the sol with particle size of ~10 nm proves to be the most stable.

An distinctive feature of colloid–bacterial interactions is the diversity of forces including mechanisms of electrostatic, molecular, and chemical origin. One example are the coccal bacteria *M. luteus* (with the mean size of 2000 nm) isolated from an auriferous placer. They form packages of 4–8 cells that effectively sorb gold particles (up to 10 mg of Au per 1 g wet biomass). However, they do not induce heterocoagulation. Instead, one cell binds, on the average, 10^4 colloidal gold particles.

The attachment of colloidal particles of metals and their compounds to the cell surface occurs mainly through metabolic products with such functional groups as -S-, $-COO^-$, $PO(OH)O^-$, $-NH_3^+$. In contrast to positively charged proteins (trypsin, papain, lysozyme, RNAse),[678] the negatively charged proteins (human serum albumin, soybean trypsin inhibitor) do not cause flocculation of gold particles. The flocculation of sol on lysozyme it occurs only in a narrow range of enzyme concentrations ($1–10\,\mu g\,mL^{-1}$), while higher concentrations stabilize the sol and enhance the aggregational stability of the system.[678] Consecutive stages of metal colloid flocculation and stabilization occur with the increasing concentration of certain synthetic polymers, such as polyethyleneimine and nonionogenic polyethyleneoxide.

Some differences should be noted in the behavior of proteins and synthetic polymers. First, proteins differ in their selectivity toward different dispersed phases during flocculation. This selectivity is determined by electrostatic factors and by specific binding by sulfhydryl and amino groups of amino acid residues.[679] Second, the biopolymer's native structure is of prime importance for promoting sorption. For

example, partial destruction of the polysaccharide skeleton of bacterial cell walls by lysozyme reduces considerably their ability to induce sorption.

The cells of monoculture tissues (*Pseudomonas* sp., *Bacillus cereus, Bacillus* sp., *Bacillus subtilis*) grown under similar conditions differ significantly in their ability to accumulate metal particles on their surface. This accumulative ability was observed to correlate with the flocculating capacity of preparations isolated from the cells (Fig. 20).[678]

Figure 20 The cell of associative tissue culture in the presence of colloidal gold particles ($\times$ 35,000).[678]

There is experimental evidence for the binding of metal particles on the surface of cells by their carbohydrate or glycoprotein structures. A ~50 kDa glycoprotein that binds colloidal gold was isolated from different cells (including *B. subtilis*) by butanol extraction. The specificity of binding of different compounds by this protein decreases in the series[679] Au $>$ Pt $>$ MnO_2 $>$ Al_2O_3. Liposomes are the closest models of biomembranes, having no effect on the aggregative stability of gold. However, liposomes modified by this glycoportein actively sorb particles of metals. Apparently, the glycoprotein is bound with lipids in the bacterial cell wall. In fact, it is the increased level of glycophospholipids and the extended branching of fatty acid residues that determine the ability of *M. luteus* cells to survive under extreme conditions of high Au concentrations.[679]

The recrystallization and enlargement of dispersed metal particles occurs on the surface of living cells after adsorption and heterocoagulation. Thus biopolymer–colloidal gold particles must redissolved to eventually form larger particles by recrystallization.

The surface of bacteria may contain several independent metal-binding sites (M). This process is described by the equilibrium

$$M + L \rightleftharpoons ML$$

The symbol L designates the binding site on the bacterial surface, while ML stands for the bacterium–sol particle complex. The total number of binding sites (n), the quantity of bound metal particles (v), and the association constant $K = [ML]/[M][L]$ may be calculated by the Scatchard equation:[680]

$$\frac{v}{[L]} = nK - vk$$

For example, the *M. luteus* cells have two types of independent gold-binding sites.[675] One of these sites is hydrophilic, and binding results from electrostatic interactions ($K_1 = 3.85 \times 10^9$ L mol^{-1}, $\nu_1 = 4.7 \times 10^3$). The second type of binding site functions via an oxidative process of gold complex formation ($K_2 = 4.6 \times 10^8$ L mol^{-1}, $\nu_2 = 4.3 \times 10^3$).

The processes of accumulating heavy metals by cells occupy a special place. The most important cell components for this process are the low-molecular-weight (5–10 kDa) metal-binding thioneins proteins. These proteins are rich in SH groups, which accumulate both the metals essential for the cell (Cu, Mn, Fe, Co, Cr, Mo) and unessential ones. These proteins consist of two separate subunits. Each subunit binds metal ions into a polynuclear metal–thiol cluster surrounded by cysteine residues. For example, Cd- and Zn-thioneins contain 7 metal atoms each, of which 4 are bound with 11 cysteine residues (M_4Cys_{11}) in a C-terminal A-cluster, while 3 metal atoms are bound with 9 cysteine residues (M_3CyS_9) in the N-terminal B-cluster.[680] At the same time, Ag and Cu form M_{12} metallothioneins containing 6 metal atoms in each domain.

The biological function of thioneins is, most likely, the storage and detoxification of heavy metals. Apparently, the accumulation of metals is associated with intense reduction, localization, and adhesion on the outer membrane of metal particles formed. During the adaptation period, the cells can acquire a plasmid imparting resistance to the metal. This ability is realized through the increased rate of metal ions reduction. Thus natural selection may result in the formation of metal-tolerant microbial strains.[681]

Two aspects of nanoparticles immobilization on biopolymers should be mentioned.[682] First, most of the heavy metals bind simultaneously to several protein macroligands with a specific spatial environment and conformation. Triple complexes may also form composed of protein/metal/nucleic acid (metal = Au, Pt, Pd). Perhaps the presence of these structures provides the anticarcinogenic effect achieved on introduction of these metals into organisms. Second, heavy metals, such as Au(I), react with native Zn-, Cd-, and Co-thioneins by replacing selectively Zn and even Cd when added in excess. This process is characterized by only minimal changes in the protein conformation.

Metalloclusters play an important role in bacterial mineralization,[683–686] and their investigation is the subject of a new branch of science called bioinorganic solid-state chemistry. This field studies the formation and structure of nanoscale materials in biological environments. A characteristic example is the formation of nanoparticles on the base of ferritin (Fig. 21).[686] A nanoparticle of Fe_3S_4 is deposited in the inner part of the protein shell through chemical transformations under mild conditions. The process is simplified when a metal-free apoferritin is used for this purpose. For

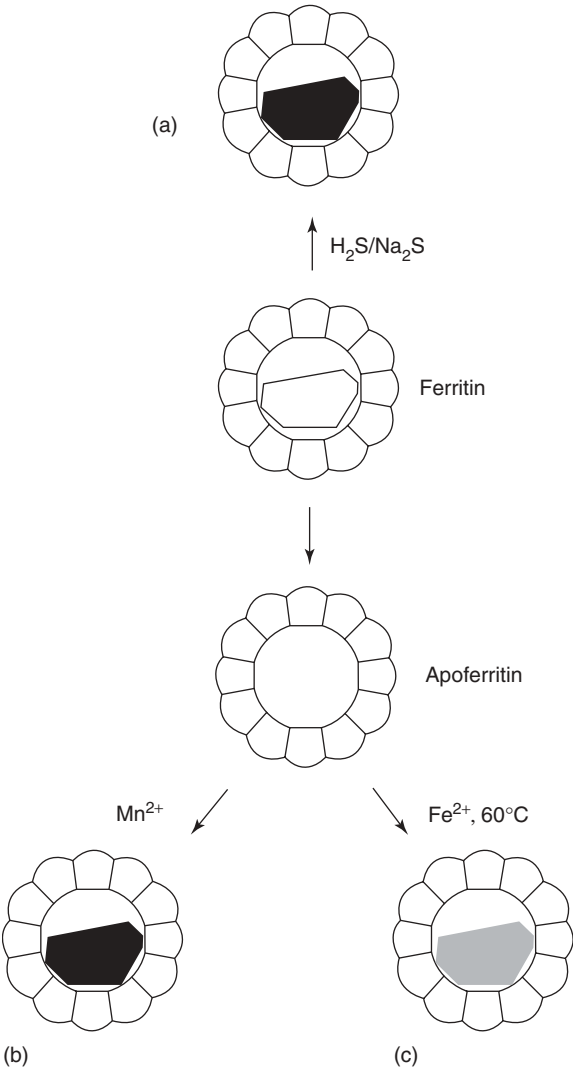

Figure 21 Synthesis of nanophase materials based on ferritin:[686] (**a**) Fe_3S_4; (**b**) Mn_2O_3; (**c**) Fe_3O_4.

example, the biopolymer-immobilized Mn^{3+} oxides particles (8 nm) are obtained upon oxidation Mn^{2+} to Mn^{3+}. This route is also effective for preparing nanoscale biomaterials based on Ag_2O and especially calcium phosphates structures ($Ca_{10}(PO_4)_6(OH)_2$, $Ca_8H_2(PO_4)_6$, etc.) which are important components of osseous tissues.

Special attention should be given to the intraferritin generation of in situ Fe_3O_4 deposits with definite crystallochemical characteristics.[687] This leads to the formation of ferromagnetic proteins, which are used to prepare magnetic images for

clinical purposes. This is clearly seen in electron micrographs of bacterial magnetite.[688] This intracellular product is composed of Fe_3O_4 crystals arranged in a chain parallel to the longitudinal axis of *Coccus* and *Spirillum* bacteria (Fig. 22). These magnetically ordered (magneto-tactical) bacteria orient themselves (move) even in weak (0.25–0.5 G) magnetic terrestrial fields by performing navigational functions within the living organisms.

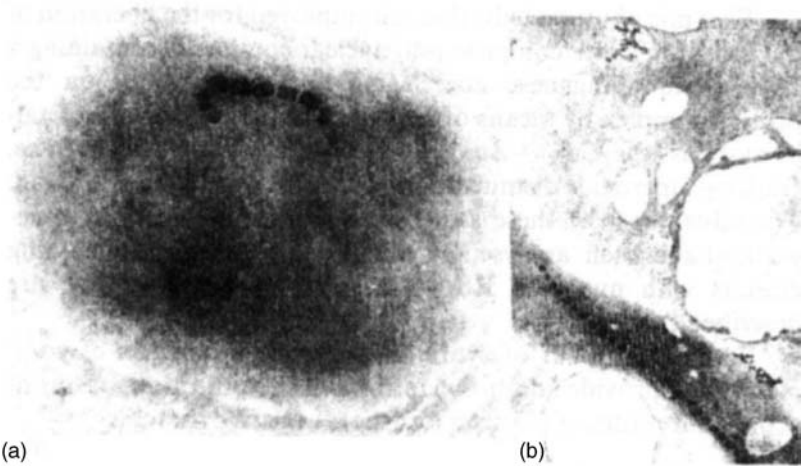

Figure 22 Electron micrographs of (**a**) *Coccus* bacteria with a chain of nine intracellular crystals and (**b**) Spirillum cells with a chain of cubic octaedral crystals. The cell length is 3 μm, the size of each crystal is ~50 × 50 nm.[686]

The complexity and precision of such bioinorganic reactions require the strict ordering and control of particle size and morphology, tasks that are difficult to achieve under laboratory conditions.

Heterometallic clusters of ferredoxin with the composition $[MFe_3S_4]$, where M = Zn, Co, Mn, are known.[683] They are present, in particular, in the *Pyrococcus furiosus* cells.[684] Bacterial methods may be effective in the preparation of finely dispersed precursors of superconducting high-temperature ceramics and other materials.[683,684]

Metalloprotein preparations are often used in medicine to regulate enzyme activity and to devise new drugs with narrow targeted action. Colloidal compounds of calcium and magnesium with plant proteins are employed for the regulation of gastric juice acidity.[689–697] A finely dispersed Fe_3O_4 complex with serum albumin is administered intravenously as an x-ray contrast agent. Colloidal gold and its biopreparations have been used since ancient times as medicines and many of them are known to be effective antiarthritis drugs. Colloidal gold is widely used in immunochemical studies as an electron-dense cytochemical marker in electron microscopy. The hydrophobic character of metal particles and the existence of electrostatic

charge on their surface have allowed the development of specific markers with numerous macromolecules. These include antibodies, lectins, enzymes, proteins, glycoproteins, and polysaccharides.

Special attention should be given to the microbial geotechnology (i.e., to the extraction of metals from their ores, concentrates, embedding rocks, and solutions by means of microorganisms and their metabolites).[677] The bacterial leaching of copper and uranium has long been used on the industrial scale.[677,678] This process includes fragmentation of ores and preparation of pulp, bacterial leaching of the target metal, filtration, neutralization of solid residues, and cyanation.

B. Polynuclear Metalloenzymes as Components of Nanobiocomposites

Metal-containing protein systems important for biocatalysis and metabolism may be divided into four main groups:[698] enzymes (containing Mn, Fe, Co, Cu, Mo), redox proteins, transport proteins, and storage proteins. The last two groups regulate the concentration of metal(s) at specific sites in the organisms. Kidney proteins, which bind and withdraw heavy metals from living organisms, are also sometimes classified in these groups. The biological functions of these proteins and the types of interactions within them have been reviewed.

A typical representative storage protein is ferritin. This iron-storing protein contains 24 identical subunits with an inorganic core composed of 4500 iron atoms in the form of a basic hydrophosphate $(FeOOH)_8(FeO—OPO_3H_2)$. This core has a diameter of 7.3 nm, and its structure is similar to that of synthetic polymers considered above.[699]

The distinctive feature of this large group of redox biocatalysts is the presence of several interacting transition metal atoms in one protein molecule. Today, over 100 enzymes are known that include several atoms of iron, copper, molybdenum, or manganese. In many of proteins the arrangement of atoms into polynuclear ensembles has been established. Such ensembles are especially common in metalloproteins containing non-hem iron complexes linked by oxy-, hydroxy-, and alkoxy-bridges. Binuclear iron complexes (with the $Fe_2O(OCOR)_2$ core) were found in hemerythrin, ribonucleotide reductase, and acid phosphatase.[700] Polynuclear $Fe^{2+}Fe^{3+}$ complexes are thought or known to exist in numerous enzymes. Examples include the Fe_2S_2 groups in ferredoxin and the high-nuclearity oxocenters of iron in the metal structures within such iron-storage proteins as ferritin and hemosiderin, and in the structures of magnetotactic microorganisms mentioned above.

During biological nitrogen fixation, the active enzyme form is produced by the action of both iron- and iron-molybdenum-containing proteins (including 32–34 Fe and 2 Mo atoms), with natural electron donors (ferredoxins, flavodoxins) in the presence of ATP. The molybdenum nitrogenase cofactor may have the structure $MoFe_6(SR)_6L_3$; the MoFe- and VFe-proteins (nitrogenases) were isolated from *Azotobacter vinelandii* and *A. Chroococcum*.[701]

Enzymic photosystems that are employed for the liberation of oxygen from water contain polynuclear complexes with a cubane-like manganese core Mn_4O_2,[702] which is immobilized on the protein complex by carboxyl groups. The bimetallic

Cu^{2+} -Zn^{2+}-containing superoxide dismutases, Cu_2Co_2-superoxide dismutases, and some others deserve mention. The advantages of these structures with shared nuclear frameworks have been analyzed in detail.[701] Biopolymers, which include Rh_6,[703] Ru_3,[704] and Fe_4[705] clusters, have been described.

Many studies of synthetic oligopeptide models of such metal complexes may provide additional information on the mechanisms of action and routes of electron transport in native proteins.

C. Preparation of Template Synthetic Nanobiocomposites by the Sol-Gel Method

The sol-gel method provides considerable possibilities for the preparation of a series of nanohybrid materials in which biologically active macromolecules can be encapsulated at the stage where ceramic, glass and other inorganic composite formation occur.[706,707] The biological components can be enzymes; catalytic antibodies; noncatalytic proteins; polynucleic acids; and microbial, plant, and animal cells.[708–711] These can be used in biocatalysis, for immunodiagnostics, as biooptical agents, various adsorbents, etc.[706,712–718]

Active enzymes were encapsulated into a sol-gel matrix for the first time in 1990.[719] About 60 different types of hybrid bioceramic materials with inorganic matrices made from silicon, titanium, and zirconium oxides; TiO_2-cellulose composites; etc. were described.[720] Recently, bioceramic sensors, solid electrolytes, electrochemical biosensors, etc. have been surveyed in a review.[721] The moderate temperatures and mild hydrolytic and polymerization conditions in sol-gel reactions of alkoxides make it possible to trap proteins during matrix formation. This prevent proteins denaturation. The high stability of the trapped biomolecules, the inertness, the large specific surface, the porosity, and the optical transparency of the matrix facilitate use of sol-gel immobilization. The principal approaches are considered below.

Proteins, such as copper-zinc superoxide dismutase, cytochrome, myoglobin, hemoglobin, and bacteriorhodopsin, were encapsulated into porous silica gel matrices prepared by the sol-gel method. The matrix effectively retains these biomolecules without loss in their enzymatic activity, and it changes their spectral properties.[722] The matrix does not preclude the approach of small molecules to the reaction center and does not hinder transport of the reaction products. Heterogenizing glucose oxidase and peroxidase, for use in solid-phase glucososensors, was carried out using the same sol-gel procedure. The spectral characteristics of a gel containing oxalate oxidase and peroxidase changed upon storage in aqueous solutions of oxalic acid.

Antibodies bound by sol-gel encapsulation are used in medicine, immunochromatography, immunosensors, etc. Immunoglobulins that are trapped retain their ability to bind external antigens from solutions.[723] Antibodie 14D9 catalyze hydrolysis of cyclic acetals, ketals, epoxides, etc. when incorporated in sol-gel matrices.[724] The ability of a sol-gel matrix containing 10% PEG and antiatrazine antibodies to bind atrazine was studied.[725] This matrix recognizes and binds atrazine and widely distributed herbicides. In this case, neither leaching of antibodies nor nonspecific physical sorption of atrazine on the ceramic matrix occurs. The activity did not decrease

for at least 2 months. In contrast, the activity in solutions decreased by 40% in this period. In addition, the use of the sol-gel method excludes the need to purify immunoglobulin. It should be emphasized that these materials have other advantages, such as the enhanced thermal and pH stability, ease of monitoring enzymatic reactions both in pores and in the body of the matrix by spectral methods, the convenience of storage, the ability for reuse, etc.[723]

Enzymes, which act as bioreactors, were immobilized according to such sol-gel procedures (Sections VI and VII). Certain chemically active terminal groups of enzymes and ceramic dopants such as Sn-Cl, were used (scheme 34).[726]

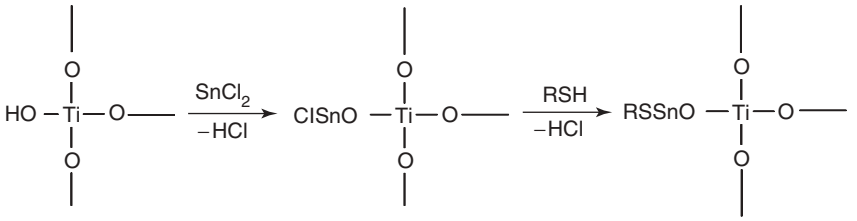

Scheme 34 R is an enzyme.

For example, alcohol dehydrogenase has been immobilized into nanotubes of TiO_2, which were prepared by sol-gel template synthesis. This enzyme retained its ability to oxidize ethanol for more than 4 days (NAD^+ cofactor, phosphate buffer, pH 8).[727] Since these TiO_2 nanotubes were open at both ends, this configuration allowed their use as a flow reactor. Examples of bound enzymes acting as bioreactor are large in number. They also involve covalent binding of antibodies to functionalize sol-gel films.[723]

Procedures for modifying the surfaces of metal oxides,[728,729] silicates, siloxanes, and hybrid sol-gel polymers with polyols such as glycerol and their ethers are of considerable interest. Polyol modification is followed by binding trypsin, cytochrome c, superoxide dismutase, glucose oxidase, phospholipase D, etc. Bioencapsulants exhibit activities that are almost identical to that of nonimmobilized enzymes. In addition, the former possess the high stability and exhibit the substantially better properties than materials prepared by the standard sol-gel method. Vinyl groups are grafted to the surface of SiO_2 particles by treating aminosilica gel with acryloyl chloride. The copolymerization of the surface-treated silica with acrylamide and acrylic acid or *N*,*N*-dimethylaminopropylacrylamide and a crosslinking agent has been carried out in the presence of glucose oxidase.[730] After removal of the glucose oxidase protein from these nanocomposites, a molecular imprint (template) remains. This template recognizes glucose oxidases in protein mixtures.[731] This molecular imprinting (template) approach is based on the formation of porous silicate films about a specific reagent using sol-gel polymerization. The reagent is then removed. Template films thus prepared have a higher affinity for 3-hydroxytyramine than for structurally related molecules, including serotonin, dihydroxynaphthalene, etc. These films do

not possess an affinity for negatively charged or large molecules, including the Tyr-Gly-Gly peptide. Apparently, the film porosity well as steric, hydrophobic and electrostatic interactions play an important role in controlled penetration of different molecules through this film.

The formation of an organized material by the sol-gel method can be performed by three procedures.[732,733] The first is formation of self-assembling organic templates (transcription syntheses). The second is cooperative assembly of ensembles from the template molecule and sol-gel building blocks (synergistic syntheses). The third procedure is morphosynthesis in which organized nonlinear chemical environments (reaction fields) are used for the construction of models.[734] A combination of these methods (integrated synthesis) is also possible. This strategy (reaction ensemble → replication → metamorphism) resembles the general scheme of mineralization. The template-directed syntheses of ordered mesoforms, organoclays, and microframework structures, including those using bacterial templates, exemplify this strategy. In particular, the coat of the one-celled algae *Emiliania huxleyi* consists of radially arranged hammer-shaped single crystals of calcite, which are crystallographically oriented and have a specific species form. The crystallographic orientation is retained in fossil casts, which indicates the control over nucleation on the molecular level (Fig. 23).[735]

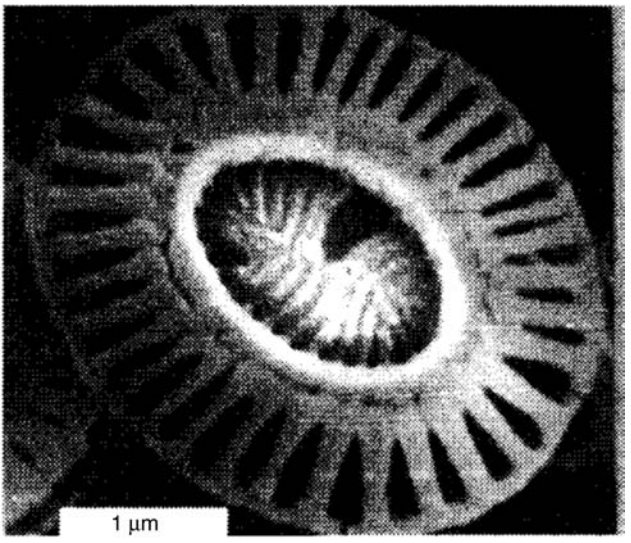

Figure 23 Electron micrograph of a *Coccus*-like coat on the one-celled algae *Emiliania huxleyi.*[735]

This fact is most pronounced in the reproduction of hierarchic macrostructured organized silica gels. Multicellular fibers from *Bacillus subtilis* (Fig. 24) can serve as an example of scaled organic 3D templates. Nanosize magnetic (Fe_3O_4), semiconducting (CdS) or TiO_2 particles were prepared first and then incorporated into

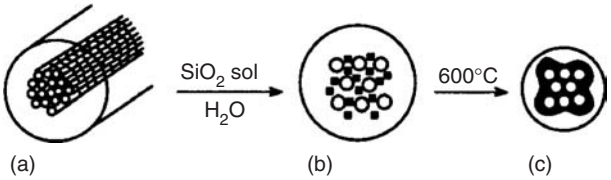

Figure 24 (**a**) Formation of an organized macroporous SiO_2 structure aided by the use of bacterial templates, (bacterial filaments) with the structure of multicellular fibers. (**b**) Mineralization of interfibre spaces of filaments. (**c**) Formation of a macroporous replica upon drying.[736]

macroscopic filaments upon swelling in colloids.[736] Dried fibers (500 nm diameter) were coated with a thin (30–70 nm) layer of aggregated colloidal particles. Negatively charged magnetic colloids exhibit the good permeability and reproduce the bacterial superstructure. Neutral CdS particles partially penetrate into the filament, but their major portion remains on the surface of the filament. Positively charged TiO_2 sols form only a surface coating. Removal of a bacteria from a magnetic composite upon heating led to structural collapse.

In summary, nanohybrid materials are widespread in nature and are of considerable importance both in nonliving and in living systems.[706,712] Binding and decomposition of different organic compounds lead to nanocomposites. Nature's cycling of compounds and energy and the formation of many useful minerals occur with the participation of nanohybrid materials. The design of molecularly organized self-assembled systems, including nanobiomaterials, offer outstanding possibilities. The protein environment is favorable to the preparation of complicated but organized products. For example, perovskites ($BaTiO_3$, $SrTiO_3$ or $NaNbO_3$) whose synthetic analogs were considered in Section VII can be involved in processes of bioaggregation.[737] It is believed[738,739] that finely monodispersed precursors of high-T_c superconducting ceramics could be formed based on bacterial objects.

XII. APPLICATION OF POLYMER-IMMOBILIZED METAL NANOPARTICLE AND METAL CLUSTER NANOCOMPOSITES

As noted above, metallopolymer nanocomposites have found diverse and sometimes unexpected applications in the fields of chemistry, physics, and biology. This largely stimulated further studies of their structure, function, and formation.

Attention was focused on the properties and practical application of nanocomposites when considering synthetic problems. Undoubtedly, these synthetic problems merit detailed consideration. In this review, only the major problems are briefly analyzed.

The interaction of nanoparticles or clusters with traditional polymers improves the physicomechanical properties and performance of composites. Properties improve because particles form ionic and coordination crosslinks, restricting the mobility of polymer chains or their segments. Other cohesional and adhesional interactions also further restrict mobility.

The incorporation of metal nanoparticles into a polymer (polymeric shell) may lead to changes in the properties of the polymer matrix itself. The properties of the immobilized nanoparticles or clusters also may be modified, in particular, by their passivation. An in-depth analysis of these changes goes beyond the scope of this review. Therefore, we shall dwell here only on the most essential properties.

Hybrid nanocomposites are primarily used for the preparation of plastic materials possessing semiconducting and superconducting properties. This includes nanowires on polymeric matrices, films with special properties, and special-purpose ceramics, including membranes, luminophors, antireflection and reflecting coatings on optical units, carriers and catalysts, reinforcing agents for plastics and rubbers, binders, and adsorbents for pharmaceutical and cosmetic industries.

A. Modification of Polymer Matrices by Nanoparticles

Virtually all of the methods used to prepare polymer-immobilized metal nanoparticles are associated with the metal–matrix interactions, especially at the interface. The incorporation of species as small as nanoparticle substantially perturbs the polymer structure.[740] The extent of these structural changes depends on the concentration of nanoparticles, which serve as knots of the emerging structural network. An Fe + FeO mixture is formed from the decomposition of iron oxalate in HPPE. The presence of as little as 1% of this highly dispersed mixture alters the sizes of polymer lamella and spherulite, increases the molecular anchoring density in the fluctuational network, and increases the proportion of oriented polymeric chains.[3] This results in a considerable increase in the impact elasticity of the material, its tensile strength, and its resistance to cracking. The overall structuring processes in the polymer phase occur in different ways in the presence of nanoparticles. The interaction of nanoparticles with each other (especially at high concentrations) leads to the formation of coagulated structures. At low nanoparticle levels, the formation of coagulational structures is impossible. The polymer matrix itself undergoes structural changes. These processes are accompanied by changes in the temperatures of vitrification, fluidity, thermal destruction, and in the thermomechanical parameters (as a rule, they increase). This is caused, as noted above, by the restricted mobility of macromolecules due to their interaction with the nanoparticle surfaces and also with the formation of secondary structures.

The Claspols (Section V.3) are obtained by the thermal decomposition of metal salts and carbonyls in polymers melts (PE, PTFE, etc.). Particles appear in Claspols that reduce the mobility of molecular chains, thereby increasing the thermal resistance of polymeric compositions.[130] As noted above, the decomposition of a fine palladium hydroxide dispersion in PVC leads to the formation of network structures. These networks contain the highly dispersed metal in their PVC encapsulated knots,

thereby raising the temperature required for complete dehydrochlorination of the polymer. Nanoparticles produced by the thermal degradation of copper oxalate[134] increase the size of the polyamide crystallites, the interaction energy between the structural elements, and the strength; but they reduce the overall degree of the polymer crystallinity. The water of crystallization released during the decomposition of cadmium oxalate trihydrate[1] accelerates the crystallization of structural elements, decreases the cohesion energy, and leads to a looser polymer matrix. The π-complexes of iron tricarbonyl within polystyrene-butadiene block copolymers influence the segmental mobility of the polybutadiene microphase in the softening temperature range.[128] Even when present at levels below 2 wt% Fe, these tricarbonyl iron groups manifest an ordering effect, which increases the macromolecule rigidity. At higher metal concentrations, this effect is enhanced owing to the development of a physical network. The dispersed metals/metal oxides formed in situ appear to be promising modifiers of the polymer fluidity. Of special interest is the method by which nanoparticles can inhibit the thermo-oxidative destruction of temperature-resistant polymers.[3] This inhibition takes place due to the binding of oxygen by highly effective metal nanoparticle oxygen acceptors, which are formed directly in the polymer matrix.

There are numerous examples where the adhesive properties have been improved in polymer-nanoparticle systems. Tribological coatings (of Ni-PTFE type) are characterized by the homocoagulational interaction between the polymer and nanoparticles that occurs at the moment of their isolation on the electrode.[165]

SiO_2, TiO_2, CdS, $CaCO_3$, and $BaSO_4$ nanoparticles, including those formed by the sol-gel method, are used as specific fillers because they improve material properties at a substantially lower concentration in a matrix than those prepared with the use of standard fillers. Thus when fillers are mechanically dispersed into composites using mixing equipment (the size particles is ~1 μm or larger) it is necessary that up to 40–50 wt% of the filler should be used in polyisopropylene to attain the required reinforcing effect. In sharp contrast, the same effect is achieved by dispersing only 0.6 to −0.8 wt% of a filler in situ.[741] Highly filled (up to 75 wt%) composite materials made from nanosize particles of the high-T_c superconductor $Tl_2Ba_2Ca_2Cu_3O_y$-($T_c = 125$K) in polychlorotrifluoroethylene possess improved physical, mechanical, and thermal properties and stability to atmospheric moisture.[743] These materials can be used for the design of cryoelectronic instruments, levitation equipment, and magnetic screens.

Recently, attempts to describe the viscoelastic properties of a composite have been made which account for the specific interactions between segments of the macromolecules and the active centers of the nanoparticles.[742] The Kerner equation relates the elastic modulus of a composite upon simple extension to the portion φ of the inorganic phase present. This treatment was modified when applied to systems with strong nanoparticles–polymer interactions. The equilibrium mechanical properties of a complex of colloidal particles and macromolecules were described based on scaling theory.[742] Some segments of the polymer chain are adsorbed at active centers on the particle surfaces. These constitute polynodes of the nanocomposite network.[742] Under deformation and temperature changes, some segments leave the

surface and the fragment of the macromolecular chainlinking the surfaces of two particles is increased by the same number of the segments. Two nontrivial conclusions can then be made: (1) The elastic properties of the composite are not only determined by the filled volume fraction but are also inversely proportional to the linear size of the particles; (2) the shift modulus of the nanocomposite, unlike the shift modulus of nonfilled polymeric networks, does not approach zero as the temperature is extrapolated to zero. These conclusions agree well with the relaxation mechanical properties of the composite as well as with the dependence of its viscosity on the molecular and structural parameters. These parameters include the energy of interaction between the macromolecular segments and the active centers on the nanoparticle, the number of macromolecular segments, their size, the φ value, the particle size (the diameter is $\leq$30 nm), and the temperature.

B. Electrical and Magnetic Properties

Atomic and electronic processes that occur at the polymer–nanoparticle interface largely determine the unique properties of nanocomposite. These materials become electrical conductors only at definite component ratios when conducting chain-type coagulated structures are formed instead of matrix systems. In other words, the fractal clusters formed upon cohesion of nanoparticles serve as current-conducting channels. The highest conductivity is attained when the metallopolymeric material is permeated by interconnected chains of conducting particles that are in contact. This forms an electrical percolation network that exceeds the percolation threshold. As a rule, this is achieved at a nanoparticles content of ~50 vol%.

These materials find extensive uses in microelectronics for the production of circuit boards, flexible cables, in the production of highly dispersed conducting coatings, and in both film and membrane technology.[423] They are also applied as precursors in the preparation of superconducting ceramics.[743] Materials with a superconductivity transition temperature of 90K were obtained on the from polycondensed Y-, Ba-, and Cu-based chelates.[741] This transition temperature is still higher (110K) in the polymeric composites containing bismuth ceramics.[743] Nearly all of the methods described in Section V are used to prepare ultradispersed metal polymers in polymeric matrices, including the vacuum metallization of polymers. The magnetization curve, magnetic permeability, coercive force, magnetic hysteresis loop, and magnetostriction of these magnetic materials, ferroplastics, or ferroelastics depend on their prehistory, the nature of the polymer and the nanoparticles, and the concentration and structural state of particles. Their properties can vary over wide ranges. For instance, the magnetic behavior of the Ni-HPPE and Co–HPPE systems depends on the cryosynthesis conditions.[109] The irreversible interaction of Ni clusters with the matrix takes place in the Ni–HPPE system above 370K. In the Co–HPPE system, the form of the thermomagnetic curve is completely changed at 470K due to the enlargement of Co particles.

The peculiarities of the magnetic behavior have been studied for systems obtained by the reduction of metal salts in the medium of a swollen polyacrylic acid interpolymeric complex with an urea-formaldehyde oligomer.[160] Similar studies have

been made on materials formed by the thermolysis of iron arenecyclopentadienyl cationic complexes and arylenecarborane oligomers.[102] Similar studies were carried out on composites obtained by the thermal and oxidative decomposition of Co and Fe carbonyls in PVF matrices and on those prepared by the hydrogen reduction of organocobalt percursors and Ni carbonyl in epoxy resin films using different solidification conditions.[744] The conductivity and the percolation parameters of the latter system depend on the internal stresses arising during solidification. Magnetic particles are often introduced in such gels as silicone,[745] polyacrylamide,[746] latex spheres,[747] and others. Conducting Ag-containing films are produced by the reduction of $AgNO_3$ in PVAl.[143] Ferroplastics, which are sometimes formed in magnetic fields (for example, neodymium ferrites, in 3–30-G fields), have been subjected to mechanical (pressing, processing on Bridgeman anvils), thermal,[748,749] and other impacts. In recent years, these studies have been developed extensively.[750–754]

Of interest is the preparation of thin (3–7 nm) magnetic coatings, obtained by electrochemical deposition, on the surface of self-assembling thin films of the LB type. Such coatings as α-Fe, magnetite Fe_3O_4, and admixtures of Fe_2O_3, may be formed on organosilanes.[755] Polymer-immobilized particles are formed in statu nascendi in magnetic fields. These materials seem to be rather promising as drug carriers, for magnetic recording of information, for magnetic separation, as materials possessing the magnetic-optical properties, and as magnetic fluids.[756] The magnetic fluids are colloidal solutions with strong magnetic properties. Polymers such as oligoorganosiloxanes serve as carriers operating under extreme conditions (wide temperature range, vacuum, aggressive and biologically active media).

Let us briefly consider the conducting properties of hybrid nanocomposites. Conducting properties are manifested only with particular inorganic component to polymer ratios in which current-conducting channels of fractal metal-containing clusters are formed in a polymeric matrix for one reason or other. The highest conductivity is achieved when the composite is converted into a network of interrelated current-conducting chains. This is where a percolation structure is achieved.[757] To put it differently, critical concentrations of the filler φ_{cr} (the percolation threshold) exist above which ($\varphi > \varphi_{cr}$) the conductivity sharply increases.

With a knowledge of the percolation threshold, the minimum necessary filling to give conducting composites can be predicted. For example, φ_{cr} for epoxysilicon resin filled with spherical particles of dispersed nickel is 0.25, and the critical parameter (X_{cr}), determined by the number of bonds at conducting nodes in the lattice of the solid, is 0.30.[758]

The conductivity of metallopolymeric nanocomposites is substantially affected by the dispersity of an inorganic component. Different nanocomposites are characterized by different relationships between the conductivity and the metal content. The percolation threshold of composites containing layered polypyromellitimide films filled by inserted silver particles is attained at a filler content >9 wt%. When nanosize silver particles (10–15 nm), were prepared by thermolysis of a solution of silver acetate in poly(pyromellitamide acid), they became uniformly distributed over a film. This composite does not exibit conducting properties at the same filler content. The dielectric characteristics of films ($\sigma = 10^{-15} - 10^{-12}\,S\,m^{-1}$) are retained at a high

filler level, which is associated with the presence of a substantial fraction of dielectric polymeric interlayers between conducting filler particles.

It is possible to enhance the conductivity of polymeric composites by the formation of a core-shell fillers, where the core could be either conductor or dielectric and the shell is a conductor. This is of practical interest in the technology of the production of glues and varnishes. For example, the conductivity of dielectric SnO_2 particles coated with a silver layer (8 vol%) is substantially increased to $\sigma = 1 \times 10^{-3}$ S m^{-1}), versus only $\sigma = 2 \times 10^{-7}$ S m^{-1} for a mechanical mixture of SnO_2 and 16 vol% of Ag powders.[759] The silver layer was prepared by thermally treating an Ag(I)-containing polymer.

Multicomponent metal-containing hybrid nanocomposites find use in the production of electrode materials for galvanic cells.[760] High-T_c superconducting ceramics, for example, have attracted attention. Materials prepared by the sol-gel method are used as piezoelectric ceramic fillers in acoustic converters as well as in the medical diagnostics. Thus coatings with dense homogeneous microstructures, possessing the enhanced mechanical strength and improved piezoelectric characteristics, were formed by sheet rolling (413K, 20–30 MPa) polymer–ceramic mixtures of polyvinylidene fluoride with up to 65 vol% $PbTiO_3$.[761]

The electrochemical preparation of thin (3–7 nm) magnetic coatings has considerable promise. In particular, organosilanes are coated with a film containing α-Fe (70 at% of Fe), magnetite Fe_3O_4 and an admixture of Fe_2O_3. Sometimes magnetically active particles are introduced into gels, such as silicon,[762] polyacrylamide,[763] and poly(ethylene oxide) gels.[764–765]

Ferroplastics are often formed in magnetic fields to improve the electrophysical and magnetic characteristics of nanocomposites. In this case, magnetic orientation occurs. Thus, neodymium ferrite is prepared in of 3×10^{-4}–3×10^{-3} T intensity magnetic fields, and then it is subjected to the pressing,[763] treatment between Bridgman's anvils[765] or a combination of these procedures.[766] Magnetically filled matrices are produced with oriented chain structures, which are used for the production of varnishes and films and are of considerable interest in data-recording systems. The formation of coatings under hardening conditions in a variable magnetic field prevents precipitation of nanoparticles. Instead, nanoparticles are either concentrated closer to the film surface or uniformly distributed throughout the body of the film. Organometallic ferromagnetics based on polymetalloorganosiloxanes possess peculiar magnetic properties.[766,767]

C. Polymer-Immobilized Nanoparticles as Optical Materials and Semiconductors

The composite materials in polymeric optical media and nanoparticles possess a unique set of the optical (visible light range) and semiconductor properties. The ease of mechanical processing and the film-forming properties of these materials permit their use for the preparation of dispersive optical elements, band light filters, etc. To this end, the condensation products of Au with a large excess of a diphenylbutadiyne, or its polymer, are most often used.[100] The metallopolymers produced

contain 7–16% of metal with a mean particle size of ~2 nm. The composite material is characterized by a 200-fold increase its third-order optical coefficient. Thin films of Au- and Ag-fluorocarbon plasma polymer possess good optical properties.[116,119]

Homogeneous composite materials with high absorption and refraction indices suitable for the production of optical elements have been prepared: polymeric glasses made from transition metal sulfoselenides, Ag and Cu halide photochromic glasses, and holographic emulsions of Ag halide nanoparticles in gelatin. As a rule, the semiconductor components concentration in a polymeric binder (4-VPy, PVA1, *etc.*) does not exceed 0.1%.

The methods of the assembly of semiconductor components directly within polymeric matrices have found extensive applications. For example, nanocrystals of CdS and ZnS are obtained by reacting their salts and H_2S in polymeric solutions. The cadmium sulfide (~50 nm particles) content in these materials may be as high as 50%.[768] The optical characteristics of gelatin films depend on the $PbCrO_4$ particle size.[769] Effective control of the $PbCrO_4$ particle size may be realize by varying the copolymer composition and thereby the size of ionomer domains (Fig. 8).[770,771] Thus the mean size of CdS particles in toluene solutions of the block copolymer of styrene with acrylic acid increases from 1.8–2.3 nm to 3–5 nm as the number of acrylic units in the ionic block increases from 4 to 32. Materials of this type have promise in the systems for solar-energy accumulation and transformation.[772,773]

Hybrid polymer–inorganic nanocomposites can exhibit a unique combination of the optical and semiconducting properties associated with the sensitivity of plasmon vibrations (the frequency, the intensity, the shape, and the width of the band) to the nature of the matrix to the morphology of the nanocomposite and also to the particle size. The interactions between the electronic and atomic subsystems changes substantially as the linear sizes of semiconductor particles decrease to values comparable with the electron wavelengths. This is manifested in the quantum dimensional effects. These effects include nonlinear optical effects, doubling of the frequency of the incident radiation (generation of the second harmonic) and the blue shift of the exciton absorption band. The ability of these nanocomposites to form films and the ease of their treatment make it possible to use them for the preparation of dispersing optical elements, band-pass light filters and other high-quality thin-film coatings (only ~5–20 nm thick). These thin-films are used in optoelectronics. Integrated circuits are produced using planar technology, which combines nanolithography and the etching. New techniques are aimed at decreasing the features sizes of optoelectronic integrated circuits to <100 nm. These techniques include electron-ray, ion-beam, and x-ray lithography as well as new procedures for dry etching (plasma-chemical, reactive ionic, etc.).

Almost all materials of this kind are characterized by nonlinear optical properties manifested in a substantial strengthening of the lightwave's local field. The latter is characterized quantitatively by its third-order susceptibility, the nonlinear refractive indices, and the nonlinear absorption coefficient. These effects are widely used in spectroscopic practice (local nonperturbing diagnostics methods, electron-optical image converters, etc.). This is particularly true of sol-gel glasses based on CdS and nanohybrid composites based on polymers and SiO_2 (or V_2O_5), LBFs,

etc.[774] When the sizes of semiconducting nanosize particles are much smaller than the wavelength of the exciting field ($\ll \lambda/20$), the nonlinear optical properties manifest themselves. Thus quantum points appear in nanocomposites (quantum-point polymers).[775–777] A definite relationship exists between the wavelength of the exciting radiation and the sizes of nanoparticles. Nanocomposites of this type can be used as the active layers of light-emitting diodes.[778,779]

Procedures to insert of transition metal ions into polymers in the stage of the sol-gel synthesis or intercalation have been mentioned in previous sections. These materials find use in the preparation of colored light guides, displaying a broad spectrum of applications, from storage elements to highly sensitive detectors.

D. Catalysis Using Polymer-Immobilized Nanoparticles and Clusters

The Group VIII metal colloids were among the first known hydrogenation catalysts for organic compounds. In the 1940s, PVAl, PVA, and PMMA were used to protect these colloids.[780,781] Later, silk fibroin, nylon, PETF, etc. were used to this end.

Catalysts of this type are of prime theoretical interest since they allow modeling of the size effects on the catalytic activity. They may be used to exemplify basic theories of the catalysis: multiple theory, theory of active ensembles, and theory of skeletal catalysis. Many attempts were made to assess the influence of catalyst particle size on activity. For example, the size of nickel particles was varied from that of an individual atom to that of the bulk metal.[782] Quantitative estimates were made of the effect of the Ni_n/SiO_2 and Ni_nCu_m/SiO_2 particle size on the course of hydrogenation.[783] Similar studies were performed of the behavior of deposited polynuclear complexes in the hydrogenation and isomerization of alkenes.[784,785]

The application of polymer-immobilized cluster and nanoscale particles provides a chance to understand the relationship between homogeneous, heterogeneous, and enzymic catalysis.[786] Some features of these particles resemble homogenous catalysts: They are obtained from ordinary, soluble metal compounds by an increase in nuclearity; the polymer often functions as a macroligand influencing the stereochemical environment; and they can function under temperatures below 100°C. At the same time, major properties of heterogeneous systems also are present: reactions occur at the interface, the activation of the substrate results from adsorption on the surface, and the catalyst is easily separated from the reaction products and may be regenerated. The peculiarities of enzymic catalysis, such as substrate enrichment, structural correspondence, favorable orientation of reacting molecules, and additional activation of the substrate by the multicenter catalytic system are also easily simulated using polymer-immobilized clusters and nanoparticles. For example, introduction of neodymium ions into ultradispersed Pd particles, immobilized in water-soluble polymers, exerts a promoting effect in acrylic acid hydrogenation.[787,788] This effect results from an increase in substrate concentration due to additional coordination interactions with neodymium ions.

Cryochemical combination of Ag, Pd, or Pt with liquid oligoesters, polyesters, and polydienes allows the of polymer to be reached. This critical loading is reached

when the concentrations of metals exceed the coordination possibilities of polymers. Subsequent deposition of such polymer-immobilized nanoparticles on carbon powder may lead to the formation of Ag_n^0/C, Pd_n^0/C, and Pt_n^0/C systems. These are traditional catalysts for numerous processes. Nanoparticles of Pt incorporated in glass–carbon matrices belong to this type of catalyst.

Polymer-immobilized nanoparticles can manifest high activity and selectivity as exemplified by ionic-coordination polymerization, hydrogenation, and oxidative transformations.[786] The catalytic activity depends on the nature of the polymer and the size of nanoparticles. After the removal of heavy Pt particles by centrifugation (20,000 rpm), the transparent supernatant containing about 20% of the initial Pt in a finely dispersed form manifests much higher activity during catalytic liberation of hydrogen from water.[37] The size of the remaining Pt particles is critical for their catalytic activity to be manifested irrespective of the nature of the protecting colloid.

The regioselectivity observed in the hydrogenation of undecenoic and oleic acids on clusters stabilized by surfactants or polymers is of special interest.[146] The surfactant micelles surrounding a cluster stabilize it and also orient the unsaturated fatty acids appropriately (Fig. 25).

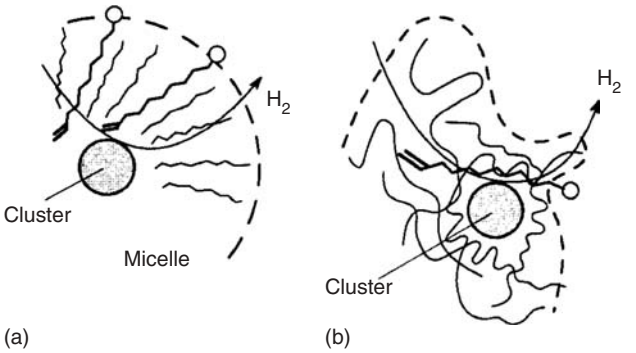

Figure 25 A proposed mechanism of the hydrogenation of unsaturated fatty acids in (*a*) micellar and (*b*) polymeric systems.[146]

The double bond in a linear polymer is more accessible to nanoparticles since such macromolecules are in a chaotic molecular motion.

Polymer-immobilized bimetallic Pt-Co colloids exhibit high selectivity (up to 99.8%) in the reaction of hydrogenation of cinnamaldehyde to the corresponding alcohol.[789] The application of polymer-protected nanoparticles is expected to lead to the discovery of new specific effects in catalysis. The cluster $[Pt_{15}(CO)_{30}]^{2-}$ fixed on Sephadex is used to catalyze of the hydrogenation of selective redox-active cofactors.[790]

Let us consider the use of hybrid nanocomposites in catalytic hydrogenation. During catalysts formation and hydrogen adsorption, dislocations are fixed at

interblock boundaries of polymer-stabilized nanoparticles. These particles have highly active surfaces and developed internal structures. A polymeric matrix hinders the smoothing of numerous defects during catalyst aging. A knowledge of the surface composition and S_{spec} and the possibility to control these parameters are of prime importance in the catalysis. The inherent size of nanosize particles is comparable with the molecular sizes of the compound subjected to catalytic conversion. This fact is responsible for the characteristic kinetics and mechanism of the reactions occuring at nanosize particles. In particular, the high efficiency of colloidal metall catalysts in multiple-electron processes results from the fact that these catalysts are reservoirs, that can readily incorporate electrons.

Polymer-stabilized metal nanoparticles are excellent models for studying the influence of the dimensional effects on the catalytic activity. Composites based on nanosize particles of platinum and other metals that are incorporated into glassy carbon matrices can be assigned to the same type of catalysts.[791] Of particular interest are catalysts based on organic–inorganic hybrid materials in which catalytically active metals incorporated into an oxide network are dispersed. For example, highly dispersed heterogeneous catalysts in a SiO_2 network prepared from substituted alkoxysilanes are known (scheme 35).[792]

$$MY_n + nAXSi(OR)_3 + xSi(OR)_4 \xrightarrow[-ROH]{NH_3,\ H_2O}$$

$$\longrightarrow Y_m(AXSi_{3/2})_n \cdot xSiO_2 \xrightarrow{O_2,\ \Delta} MO_y \cdot (x+n)SiO_2 \xrightarrow{H_2,\ \Delta}$$

$$\longrightarrow M \cdot (x+n)xSiO_2$$

Scheme 35

A protective polymeric coating prevents poisoning of a metallopolymeric catalyst by potential catalytic poisons of the dibenzothiophene type.

Nanocomposites exhibit the high catalytic activity for hydrogen elimination under visible light[793] [(e.g., the ethylenediaminetetraacetate (electron donor)-$Ru^{2+}(bipy)_3$ (photocatalyst)-methyl viologen (electron acceptor) system). Substantial success has been achieved in charge separation as well as in the design of efficient photocatalysts from semiconducting nanomaterials prepared by the sol-gel method.[794,795] The additional introduction of transition metal ions like copper[796,797] during formation of these materials substantially enhances photocatalytic reaction efficiency. These catalysts also exhibit high activity in the low-temperature oxidation of CO.[798,799]

The use of polymer-protected nanoparticles can contribute new features to catalysis. A platinum sol as well as Pt on Al_2O_3 are well-known enantioselective hydrogenation catalysts.[800] The possible uses of hybrid nanocomposites in catalysis are far from all realized.[801]

XIII. CONCLUSION

The most topical theoretical problems for the formation of clusters and nanoparticles in polymeric matrices involve questions about structural-morphological and spatial organization at the local, molecular, and supramolecular levels. Among such problems are the thermodynamic peculiarities of cluster and nanoparticle formation. An analysis has recently been performed using macrochelates.[802] The most important problem seems to be the nanoparticle stabilization by polymer monolayers and LBFs. A insufficient number of studies have been carried out on this topic. Thus the nature of the adhesion at the interfaces formed still remains obscure.

Nanoparticle passivation should be accomplished to allow time for the preservation of their energy-rich state. A highly significant theoretical and practical problem is to control the surface processes or processes in thin subsuperficial layers of polymer granules, films, or fibers. The preparation of self-assembling colloidal layers of Au, Ag, and Ag-Au on the surface of plasma-purified PTFE is of interest. The PTFE surface and those of other polymers had been premodified by hydrolyzed alkoxysilanes containing functional groups.[803] When such surfaces are contacted with dilute solutions of monodisperse colloids, the assembly of nanoparticles takes place. They form as a monomolecular layer, which is 5–70 nm thick in the case of Ag and 5–20 nm thick in the case of Au and Au-Ag.

Further progress is expected in the development of novel methods for the preparation of polymer-immobilized clusters and nanoparticles. A promising direct synthesis of these products is the dissolution of zero-valent metals into polymer solutions that function as macroligands. Subsequent recrystallization of particles then occurs, much like what occurs in biological systems (Section XI). Stabilization of nanoparticles and clusters during polymerization of micelle-forming monomers could become a significant practical method.

Research into such small particles requires further development and the application of modern physical-chemical methods. Visualization of the surface structure at the atomic level needs further study by means of scanning tunnel microscopy, transmission electron microscopy, ferromagnetic resonance, small-angle x-ray scattering, x-ray photoelectron spectroscopy, etc.

The polymer-immobilized nanoparticles are already used for many tasks associated with the surface modification, such as metallization, imparting of antistatic and magnetic properties, design of new materials for photography and cinematography, and design of efficient fibrous filter materials, permitting the isolation and concentration of precious metals. Specifically, surface metallization is required to decorate plastics, to modify polymeric films, to make tribological coatings, and for other purposes. The coatings made of polymer-immobilized nanoparticles derived from Be and plasmopolymers have found unexpected applications in thermonuclear synthetic reactions.[110]

It should be noted that metal clusters can also be formed in fullerenes or nanotubes. Endohedral complexes $M_n@C_{60}$, in which metal clusters are localized in the inner cavities of the spheroidal molecule C_{60}, and organometallic polymers of the type $C_{60}Pd_n$ are known.[804] Nanocomposite materials are also formed upon evaporation of

metals in presence of carbon nanotubes. The clusters of metals (Cr, Ni, etc.) are localized both inside these tubes and on their ends and surfaces (Fig. 26).[805,806] Evaporation of metals in the presence of oxidized nanotubes leads solely to the decoration of nanotube surface with nanoparticles. An analogous pattern is also obtained[807] when lipid structures undergo electrochemical polymerization, followed by metallization. This results in metal-coated polymers having hollow cylindrical shapes several tens of microns long, ~0.5 nm in inner diameters and ~50-nm-thick walls. The similarity of such metal structures with metallophilic microorganisms is a point of interest.

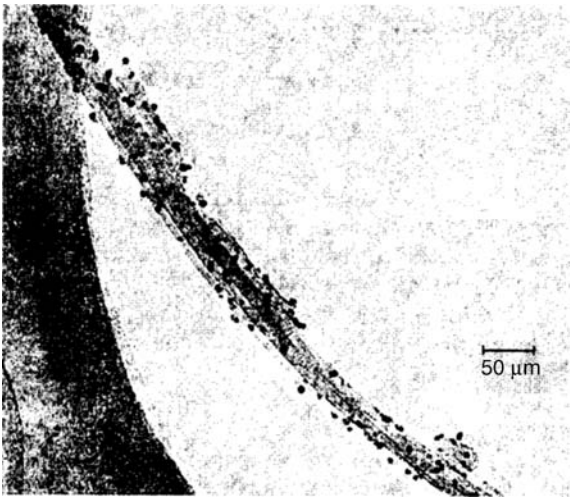

Figure 26 Electron micrograph of oxidized nanotubes decorated with silver.[806]

Biological systems bring about a controllable growth of iron oxide crystals (including magnetite) of a definite size and morphology and with strictly defined crystallochemical characteristics. These structures have, so far, been difficult to achieve under laboratory conditions. Extensive studies of these processes (bioinorganic solid-phase chemistry) will allow one to establish the basic principles of synthetic crystal engineered. The discovery of the selective aggregation of microorganisms with dispersed metals and metal compounds has already laid the foundation for biotechnological enrichment used in metallurgy and for environmental protection. Many of these principles are employed in nanotechnology and are likely to form the basis of the chemistry of highly organized compounds, a new branch of science, including supramolecular chemistry and chemistry of hypermolecular compounds.

To summarize, the chemistry of nanocomposites is progressing rapidly. In the coming years, synthetoc procedures will be developed for making multicomponent materials by ecologically pure solid-state reactions. Procedures for the preparation

of hybrid interpenetrating network materials will be studied in more detail. The mechanism of their phase separation and the structures of the resulting nanocomposites will be elucidated. These materials will be formed from monomers, which are traditionally used for the preparation of network polymers. A search for the optimum modes of new types of lattice formation (host and guest components in intercalated nanocomposites) is still in progress. Studies of intracrystalline host–guest interactions and their effect on the electronic properties of complex systems are being continued. Therefore, it is necessary to reveal the principal mechanisms of pore orientation, crystallization in interlayer formations, and the stereoregularity of the polymer formed. The approaches to prepare organic–inorganic nanocomposites surveyed in this review may be useful in the synthesis of single-phase crystalline nanometal–ceramic products with complex compositions. The use of LBFs, which incorporate isolated cluster molecules or nanosize particles, in molecular electronics may have considerable promise. Finally, nanophase materials technology requires the appropriate scientific support, (e.g., the construction of new instruments and the development of techniques for working with nanosized materials).

Dendrimers, a new class of regular polymers characterized by a tree-type structure, eminating from one center, are attracting great interest.[808] Sometimes they are called cascade polymers or polymers with controlled molecular architecture.[809] Poly(amidoamine) or poly(propyleneamine) with a diaminobutane nucleus are common examples. The terminal fragments, increase exponentially with the number of generations. Organometallic dendrimeric derivatives are also known,[810] as are numerous dendritic macromolecular metal complexes (e.g., ruthenium, palladium, platinum).[811] There are rather large spaces in the interiors of some dendrimers. This makes it possible to use them as molecular containers. Thus they have served in the construction of dendrimer-template nanocomposites.[812,813]

Many processes occur both in living and nonliving systems that provide an impetus to study nanobiocomposites. In this review, a fair, though incomplete, picture is given of nanobiocomposite applications to studies of organized matter and to the preparation of hybrid bioceramic nanomaterials.

The view that the science and engineering will be developed on the nanosize level in the 21st century seems to be realistic because nanometer sizes of individual elements are attained in many traditional technologies.

The structure–property relationships within hybrid nanocomposites are a fundamental problem in modern chemistry and physics. A great deal needs to be done before this problem is solved.

XIV. ACKNOWLEDGMENTS

The author gratefully acknowledges Professors C. Crraher, C. Pittman, and M. Zeldin for the great assistance on the editing the manuscript. The author is also grateful to Mr. A. M. Bochkin and Dr. G. I. Dzhardimalieva for the help in the preparation of the manuscript.

XV. REFERENCES

1. A. D. Pomogailo, A. S. Rozenberg, I. E. Uflyand, *Nanoparticles of Metals in Polymers*, Khimiya, Moscow, 2000.
2. M. Khler, *Nanotechnologie*, Wiley-VCH, Weinheim, New York, 2001.
3. A. D. Pomogailo, *Russ. Chem. Rev.*, **66**, 679 (1997); **69**, 53 (2000).
4. N. J. Di. Nardo, *Nanoscale Characterisation of Surfaces and Interfaces*, VCH, Weinheim, 1994.
5. M. Ruhre, A. G. Evans, M. F. Ashby, J. P. Hizth, eds., *Metal-Ceramic Interfaces*, Pergamon Press, Oxford, UK, 1990.
6. J. P. Lemmon, M. M. Lerner, *Chem. Mater.* **6**, 207 (1994).
7. G. Kickelbick, U. Schubert, *Monats. Chem.*, **132**, 13 (2001).
8. J-F. Nicoud, *Science*, **263**, 636 (1994).
9. C. Guisaro, P. Lacan, *New J. Chem*., **18**, 1097 (1994).
10. C. J. Brinker, G. W. Scherer, *Sol-Gel Science. The Physics and Chemistry of Sol-Gel Processing*, Academic Press, New York, 1990.
11. E.J.A. Pope, S. Sakka, L. Klein, eds., *Sol-Gel Science and Technology*, American Ceramic Society, Westerville, OH, 1995.
12. C. J. Brinker, D. E. Dark, D. R. Ulrich, eds., *Better Ceramics through Chemistry*, Materials Research Society, Pittsburgh, PA, 1986.
13. M. C. Roco, R. S. Williams, P. Alivisatos, eds., *Nanotechnology Research Directions: IWGN Workshop Report. Vision for Nanotechnology R&D in the Next Decade*, Kluwer Academic Publishers, Dordrecht, 2000.
14. M. C. Roco, *J. Nanoparticle Research*, **3**, 5 (2001).
15. H. Schmidt, *Chemistry, Spectroscopy and Applications of Sol-Gel Glasses*, Springer, Berlin, 1992.
16. C. Sanchez, F. Ribot, eds., *Proceedings of the First European Workshop on Hybrid Organic-Inorganic Materials*, Paris, 1993.
17. C. Sanchez, F. Ribot, *New J. Chem*., **18**, 1007 (1994).
18. P. W. Neilson, H. A. Allcock, K. J. Wynne, eds., *Inorganic and Organometallic Polymers* (ACS Symp. Ser., **572**), American Chemical Society, Washington, DC, 1994.
19. T. Bein, ed., *Supramolecular Architecture* (ACS Symp. Ser. **499**) American Chemical Society, Washington, DC, 1992.
20. A. J. Jacobson, M. S. Whittingham, *Intercalation Chemistry*, Academic Press, New York, 1982.
21. E. M. Natanson, Z. R. Ul'berg, *Colloid Metals and Metallopolymers*, Naukova Dumka, Kiev, 1971.
22. R. M. Laine, ed., *Inorganic and Organometallic Polymers with Special Properties* (NATO ASI Ser., **206**), Kluwer Academic, New York, 1992.
23. G. C. Hadjipanayis, G. A. Prinz, eds., *Science and Technology of Nanostructured Magnetic Materials*, Plenum Press, New York, 1991.
24. E. Pelizetti, ed., *Fine Particles Science and Technology from Micro to Nanoparticles*, Kluwer Academic, Dodrecht, The Netherlands, 1996.
25. J-P. Sauvage, ed., *Comprehensive Supramolecular Chemistry*, vol. 9, Elsevier, New York, 1996.
26. G. W. Brindley, G. Brown, eds., *Crystal Structures of Clay Minerals and Their X-ray Diffraction*, vol. 5. Mineral Society, London, 1980.
27. J. Livage, M. Henry, C. Sanchez, *Progr. Solid State Chem*., **18**, 259 (1988).
28. E. Ruiz-Hitzky, *Adv. Mater.,* **5**, 334 (1993).
29. J. M. Ziegler, F. G. Feazon, eds., *Silicon Based Polymer Science. A Comprehensive Resource* (Adv. Chem. **224**), American Chemical Society, Washington, D.C., 1990.

30. J. E. Mark, A.B.R. Mayer, *Eur. Polym. J*., **34,** 103 (1998).
31. M. W. Ellsworth, B. M. Novak, *J. Am. Chem. Soc*., **113**, 2756 (1991).
32. O. L. Glavati, L. S. Polak, V. V. Shchekin, *Neftekhimiya*, **3**, 905 (1963).
33. G. Kiss, *Polym. Eng. Sci*., **27**, 410 (1987).
34. H. Ishida, ed., *Interfaces in Polymer, Ceramic and Metal Matrix Composites*, Elsevier, New York, 1988.
35. Y. I. Krasnokutsky, B. G. Vereschak, *Production of Refractory Compounds in Plasma*, Vyscha Shkola, Kiev, 1987.
36. Yu. I. Petrov, *Clusters and Small Particles*, Nauka, Moscow, 1986.
37. D. Braga, F. Grepioni, *Acc. Chem. Res*., **27**, 51(1994).
38. Y. Kawazoe, T. Kondow, K. Ohno, eds., *Cluster and Nanomaterials. Theory and Experiments*, Springer, Berlin, Heidenberg, 2001.
39. U. Kreibig, M. Volmer, *Optical Properties of Metal Clusters*, Springer, Berlin, 1995.
40. N. Takeo, *Disperse Systems*, Wiley-VCH, 1999.
41. K. J. Klabunde, *Free Atoms, Clusters and Nanoscale Particles*, Academic Press, San Diego, 1994.
42. M. Folner, *The Kinetics of New Phase Formation*, Mir, Moscow, 1986.
43. V. F. Petrunin, *Nanostruct. Mat*., **12**, 1153 (1992).
44. H. Muler, C. Opitz, L. Skala. *J. Mol. Catal*., **54**, 389 (1989).
45. A. P. Alivistatos, *Endeavour*, **21**, 56 (1997).
46. M. N. Vargaftik, I. I. Moiseev, D. I. Kochubey, K. I. Zamaraev, *Faraday Dissc*., **92**, 13 (1991).
47. J.-M. Lehn., *Angew. Chem., Int. Ed. Engl*., **27**, 89 (1988); **29**, 1304 (1990), *Macromol. Chem*., *Macromol. Symp*., **69**, 1 (1993).
48. M. Faraday. Philos, *Trans. R. Soc*., London, **147**, 145 (1857).
49. D. Cabane, R. Duplessix, *J. Physique*, **48**, 651 (1987).
50. B. V. Deryagin, *The Theory of Stability of Colloids and Thin Films. Surface Forces*, Nauka, Moscow, 1986.
51. D. H. Napper, *Polymeric Stabilization of Colloidal Disptrsions*, Academic Press, London, 1983.
52. K.E.J. Barrett, *Dispersion Polymerization in Organic Media*, Willey, London, 1975.
53. G. D. Parfitt, C. H. Rochester, eds., *Adsorption from Solution at the Solid/Liquid Interface*, Academic Press, London, 1983.
54. F. Baran, *Polymer-Containing Dispersed Systems*, Navukova Dumka, Kiev, 1986.
55. N. B. Uryev, *Highly Concentrated Dispersed Systems*, Khimiya, Moscow, 1980.
56. J. W. Goodwin, R. Buscall, eds., *Polymer Colloids*, Academic Press, New York, 1995.
57. J. Visser, *Adv. Colloid. Interface Sci*., **3**, 331 (1972).
58. P. A. Rebinder, in *Selected Works. Surface Phenomena in Dispersed Systems*, G. I. Fux, ed., Nauka, Moscow, 1978.
59. E. D. Schukin, *Colloid. J*., **59**, 270 (1997).
60. M. A. Lunina, M. G. Ivanova, A. A. Khachaturyan, *Colloid. J*., **57**, 825 (1995).
61. G. Parphite, K. Rochester, eds., *Adsorption from Solutions of Solid Surfaces*, Mir, Moscow, 1986.
62. F. Ciardelli, E. Tsuchida, D. Wohrle, eds., *Macromolecule Metal Complexes*, Springer, Heidelberg, 1996.
63. A. D. Pomogailo, V. S. Savosfyanov, *Synthesis and Polymerization of Metal-Containing Monomers*, CRC Press, Boca Raton, FL, 1994.
64. E. Tsuchida, ed., *Macromolecular Complexes, Dynamic Interactions and Electronic Processes*, VCH, New York, 1991.

65. A. D. Pomogailo, I. E. Uflyand, *Macromolecular Metal Chelates*, Nauka, Moscow, 1991.
66. N. H. Ray, *Inorganic Polymers*, Academic Press, New York, 1978.
67. F.G.A. Stone, W.A.G. Graham, eds., *Inorganic Polymers*, Academic Press, New York, 1962**.**
68. C. E. Carraher, J. E. Sheats, C. U. Pittmann, eds., *Organometallic Polymers*, Academic Press, New York, 1978.
69. C. E. Carraher, J. E. Sheats, C. U. Pittmann, eds., *Advances in Organometallic and Inorganic Polymer Science*, Marcel Dekker, New York, 1982.
70. J. E. Sheats, C. E. Carraher, C. U. Pittmann, eds., *Metal-Containing Polymeric Systems*, Plenum Press, New York, 1985.
71. C. U. Pittmann Jr., C. E. Carraher, M. Zeldin, B. M. Culbertson, J. E. Sheats, eds., *Metal-Containing Polymeric Materials*, Plenum Press, New York, 1996.
72. B. K. Kepler, *Metal Complexes in Cancer Chemotherapy*, VCH, New York, 1993.
73. A. D. Pomogailo, *Polymeric Immobilized Metallocomplex Catalysts*, Nauka, Moscow, 1988.
74. F. R. Hartley, *Supported Metal Complexes, A New Generation of Catalysts*, Reidel, Dordrecht, 1985.
75. Y. I. Yermakov, B. N. Kuznetsov, V. A. Zakharov, *Catalysis by Supported Complexes*, Elsevier, Amsterdam, 1981.
76. D. Wohrle, *Adv. Polym. Sci*., **50**, 45 (1983); *Porphyrins Phthalocyanines*, **4**, 418 (2000).
77. D. Wohrle, in *Phthalocyanines, Properties and Applications*, vol. 1, C. C. Leznoff, A.B.P. Lever, eds., VCH, New York, 1989.
78. D. Wohrle, R. Benters, O. Suvorova, G. Schnurpfeil, N. Trombach, T. Bogdahn-Rai, *J. Porphyrins Phthalocyanines*, **4**, 491 (2000).
79. A. D. Pomogailo, *Russ. Chem. Rev*., **61**, 133 (1992).
80. A. D. Pomogailo, I. E. Uflyand, *Adv. Polym. Sci*., **97**, 61. (1990).
81. D. Wohrle, A. Pomogailo, in *Advanced Functional Molecules and Polymers*, vol. 1, H. S. Nalwa, ed., OPA (Overseas Publishers Association), N.V., 2001.
82. *Pure Appl. Chem*., **57**, 151 (1985).
83. A. D. Pomogailo, I. E. Uflyand, *Macromolecular Metal Chelates*, Khimiya, Moscow, 1991.
84. A. D. Pomogailo, I. E. Uflyand, *Plat. Met. Rev*., **34**, 185 (1990).
85. A. D. Pomogailo, I. E. Uflyand, E. F. Vainstein, *Russ. Chem. Rev*., **64**, 857 (1995).
86. M. Kaneko, E. Tsuchida, *J. Polym. Sci., Macromol. Rev*., **16**, 397 (1981).
87. S. K. Sahni, Reedijk, *J. Coord. Chem. Rev*., **59**, 1 (1984).
88. A. D. Pomogailo, *Russ. Chem. Rev*., **72** (2003).
89. M. Moscovits, G. A. Ozin, *Cryochemistry*, Wiley-Interscience, New York, 1979.
90. R. Zigmondy, *Z. Anorg. Chem*., **99**, 105 (1917).
91. G. A. Ozin, M. P. Andrews, in *Metal Clusters in Catalysis*, B. C. Gates, L. Guczi, H. Knosinger, eds., Elsevier, Amsterdam, 265, 1986.
92. K.V.P. Shafi, A. Ulman, X. Yan, N.-L. Yang, C. Estournes, H. White, M. Rafailovich, *Lengmuir*, **17**, 5093 (2001).
93. C. G. Francis, H. Hubert, G. A. Ozin, *Inorg. Chem*., **19**, 219 (1980).
94. G. A. Ozin, *J. Macromol. Sci. A, Chem*., **16**, 167 (1981).
95. M. P. Andrews, G. A. Ozin, *Chem. Mater*., **1**, 174 (1989).
96. G. A. Ozin, M. P. Andrews, C. G. Francis, H. X. Hubert, K. Molnar, *Inorg. Chem*., **29**, 1068 (1990).
97. K. W. Devenish, T. Goulding, B. T. Heaton, R.Whyman, *J. Chem. Soc., Dalton Trans*., 673 (1996).
98. S. P. Gubin, N. K. Eremenko, *Zh. Vses. Khim. O-va im. D. I. Mendeleeva*, **36**, 718 (1991).
99. M. Kerker, *J. Colloid Interface Sci*., **105**, 297 (1985).

100. A. W. Olsen, Z. H. Kafafi, *J. Am. Chem. Soc*., **113**, 7758 (1991).
101. S. P. Solodovnikov, A. Y. Vasilkov, A. Y. Olenin, V. A. Sergeev, *J. Magn. Mater*., **129**, 317 (1994).
102. A. I. Aleksandrov, A. I. Prokofev, V. N. Lebedev, E. V. Balagurov, N. N. Bubnov, I. Yu. Metlenkova, S. P. Solodovnikov, A. N. Ozerin, *Russ. Chem. Bull., (Engl. Trans.)*, **10**, 2355 (1995).
103. A. I. Pertsin, Yu. M. Poshutin, *Polym. Sci., (Engl. Transl.) Ser. B* **38**, 919 (1996).
104. A. I. Pertsin, I. O. Volkov, *Vysokomol. Soedin*., *Ser. B* **38**, 1249 (1996).
105. V. A. Sergeev, L. I. Vdovina, Yu.V. Smetannikov, A.Yu. Vasil'kov, V. A. Tsyryapkin, S. O. Pupynina, *Polym. Sci., (Engl. Transl.)*, *Ser. B* **29**, 431 (1987).
106. V. A. Sergeev, L. I. Vdovina, Yu.V. Smetannikov, E. M. Belavtseva, A.Yu. Vasil'kov, *Zh. Vses. Khim. O-va im. D I Mendeleeva*, **34**, 427 (1989); **36**, 255 (1991).
107. B. M. Sergeev, I. A. Gromchenko, A. N. Prusov, G. B. Sergeev, *Mosc. Univ. Bull., (Engl. Transl.), Ser. 2, Khim.* **36**, 365 (1995).
108. B. M. Sergeev, I. A. Gromchenko, G. B. Sergeev, *Mosc. Univ. Bull., (Engl. Transl.), Ser. 2, Khim.* **35,** 331 (1994).
109. A. Yu. Vasil'kov, P. V. Pribytko, E. A. Fedorovskaya, A. A. Slinkin, A. S. Kogan, V. A. Sergeev, *Dokl. Chem., (Engl. Transl.)*, **331**, 179 (1993).
110. N. C. Morosoff, N. E. Barr, W. J. James, R. B. Stephens, in *The 12th International Symposium on Plasma Chemistry*, J. V. Hebberlleing, D. W. Ernie, J. T. Roberts, eds., University of Minnesota, 1995.
111. E. Kay, M. Hecq, *J. Appl. Phys*., **55**, 370 (1984).
112. L. Martinu, H. Biederman, J. Zemek, *Vacuum*, **35**, 171 (1985).
113. H. Yasuda, *Plasma Polymerisation*, Academic Press, Orlando, FL, 1985.
114. S. A. Krapivina, *Plasmochemical Technological Processes*, Khimiya, Leningrad, 1981.
115. M. Shen, A. T. Bell, eds., *Plasma Polymerisation* (ACS Symp. Ser., **108**), American Chemical Society, Washington, D.C., 1979.
116. G. Kampfrath, A. Heilmann, C. Hamann, *Vacuum*, **38**, 1 (1988).
117. N. Inagaki, S. Tasuka, M. Masumoto, *Macromolecules*, **29**, 1642 (1996).
118. R. K. Sadir, H. E. Saunders, *J. Vac. Sci. Technol*., A **3**, 2093 (1985).
119. J. Perrin, B. Despax, E. Key, *Phys. Rev. B, Condens. Matter*, **32**, 719 (1985).
120. A. Heilmann, G. Kampfrath, V. Hopfe, *J. Phys. D, Appl. Phys.,* **21**, 986 (1988).
121. B. Abeles, P. Sheng, M. D. Coutts, Y. Arie, *Adv. Phys.,* **24**, 407 (1975).
122. J. Perrin, B. Despax, V. Hanchett, E. Kay, *J. Vac. Sci. Technol. A, Vac. Surf. Films*., **4**, 46 (1986).
123. H. Biederman, *Vacuum*, **34**, 405 (1984).
124. L. Martinu, H. Biederman, *J. Vac. Sci. Technol., A, Vac. Surf. Films.* **3**, 2639 (1985).
125. U. S. Pat. 4 **252**, 671 (1981); U. S. Pat. 4 **252**, 672 (1981); U. S. Pat. 4 **252**, 673 (1981); U. S. Pat. 4 **252**, 674 (1981); U. S. Pat. 4 **252**, 675 (1981); U. S. Pat. 4 **252**, 676 (1981); U. S. Pat. 4 **252**, 677 (1981); U. S. Pat. 4 **252**, 678 (1981).
126. M. Berger, T. A. Manuel, *J. Polym. Sci., Polym. Chem. Ed.,* **4**, 1509 (1966).
127. C. E. Kerr, B. E. Eaton, J. A. Kadue, *Organometallics*, **14**, 269 (1995).
128. L. M. Bronstein, S. P. Solodovnikov, E. S. Mirzoeva, E. Yu. Baukova, P. M. Valetsky, *Proc. Am. Chem. Soc. Div. Polym. Mater. Sci. Engin*., **71**, 397 (1994).
129. C. U. Pittman Jr, P. L. Grube, O. E. Ayers, S. P. McManus, M. D. Rausch, G. A. Moser, *J. Polym. Sci., Polym. Chem. Ed. W* 379 (1972).
130. S. P. Gubin, I. D. Kosobudskii, *Russ. Chem. Rev*., **52**, 766 (1983).
131. F. Galembeck, *J. Polym. Sci., Polym. Lett. Ed*., **15**, 107 (1977); *J. Polym. Sci., Polym. Chem. Ed*., 1**6**, 3015 (1978).
132. R. Tannenbaum, C. L. Flenniken, E. P. Goldberg, *J. Polym. Sci., Part B Polym. Phys.* **28**, 2421 (1990).

133. C. U. Pittman Jr, O. E. Ayers, S. P. McManus, *J. Macromol. Sci. A, Chem.* **7**, 737; 1563 (1974).
134. T. Yu. Ryabova, A. S. Chirkov, L. S. Radkevich, N. V. Evtushok, *Ukr. Khim. Zh*., **59**, 1329 (1993).
135. M. C. Alves, O. Tourillon, *J. Phys. Chem*., **100**, 7566 (1996).
136. E. E. Said-Galiev, L. N. Nikitin, Yu. P. Kudryavtsev, A. L. Rusanov, O. L. Lependina, V. K. Popov, M. P. Polyakov, S. M. Khoudl, *Russ. J. Chem. Phys., (Engl. Trans.)*, **14**, 190 (1995).
137. M. Poliakoff, S. Howdle, *Chem. Br*., 118 (1995).
138. S. P. Gubin, *Dokl. Chem. (Engl. Trans.)*, **345**, 490 (1995).
139. P. G. Jessop, Yi. Nsiao, T. Ikariya, R. Noyori, *J. Am. Chem. Soc*., **116**, 8851 (1994).
140. J. J. Watkins, T. J. McCarthy, *Chem. Mater*., **7**, 1991 (1995).
141. A. Tai, Y. Imachi, T. Harada, Y. Izumi, *Chem. Lett*., 1651 (1981).
142. R. Payne, G. Fritz, H. Narmann, *Angew. Makromol. Chem*., **144**, 51 (1986).
143. C.-C. Yen, *J. Appl. Polym. Sci*., **60**, 605 (1996).
144. K. Torigoe, K. Eaumi, *Langmuir*, **8**, 59 (1992).
145. M. Boutanner, J. Kizling, P. Stenius, G. Marie, *J. Appl. Catal*., **20**, 163 (1986).
146. N. Toshima, T. Takashi, *Bull. Chem. Soc. Jpn*., **65**, 400 (1992).
147. J. H. Clint, I. R. Collins, J. A. Williams, *Faraday Discuss. R. Soc. Chem*., **95**, 219 (1993).
148. N. Thoshima, Shokubai, **27**, 488 (1985); *Kobunshi*, **36**, 670 (1987); *Chem. Let*., 1769 (1989).
149. J. Ishiyama, T. Shirakawa, Y. Kurokawa, S. Imaizumi, *Angew. Macromol. Chem*., **156**, 179 (1988).
150. K. Meguro, T. Adachi, R. Fukunishi, K. Esumi, *Langmuir*, **4**, 1160 (1988).
151. A. D. Pomogailo, *Zh. Russ. Khim. O-va im. D. I. Mendeleeva*, **46**(5), 64 (2002).
152. B. G. Ershov, D. A. Troitskii, *Russ. J. Phys. Chem., (Engl. Trans.)*, **69**, 2179 (1995).
153. H. Hirai, H. Chawanya, N. Toshima, *J. Chem. Soc. Jpn. Chem. Ind Chem*., 1027 (1984); *Kobunshu Ronbunshu*., **43**, 161 (1986).
154. H. Hirai, M. Ohtaki, M. Komiyama, *Chem Lett*., 127 (1987).
155. H. Hirai, N. Toshima, in *Tailored Metal Catalysts*, Y Iwasawa, ed., Reidel, Dordrecht, 1986.
156. N. Toshima, H. Liu, *Chem. Lett*., 1925 (1992).
157. N. Toshima, *J. Macromol. Sci. A. Chem*., **27**, 1125 (1990).
158. W. Yu, Y. Wang, H. Liu, W. Zheng, *J. Catal*., A, **112**, 105 (1996).
159. S. V. Stakhanova, N. I. Nikonorova, V. D. Zanegin, G. M. Lukovkin, A. L. Volynskii, N. F. Bakheev, *Polym. Sci., (Engl. Trans.), Ser. A* **34**, 133 (1992).
160. I. M. Papisov, Yu. S. Yablokov, A. I. Prokofev, A. A. Litmanovich, *Polym. Sci., (Engl. Trans.), Ser. A* **35**, 515 (1993); **36** A, 352 (1994).
161. G. D. Chryssicos, V. D. Mattera Jr, A. T. Tsatsas, W. M. Risen Jr, *J. Catal*., **93**, 430 (1985).
162. W. M. Risen, in *Proceedings NATO Advances Research Workshop Structure and Properties of Ionomers*, Villard, Dordrecht, 1987.
163. Yu. F. Deinega, Z. R. Ul'berg, *Electrophoretic Composite Coatings*, Khimiya, Moscow, 1989.
164. E. V. Kuznetsova, *Russ. J. Appl. Chem., (Engl. Trans.)*, **66**, 1155 (1993).
165. N. M. Teterina, G. V. Khaldeev, *Russ. J. Appl. Chem., (Engl. Trans.)*, **67**, 1528 (1994).
166. L. Coche, J.-M. Moutet, *J. Am. Chem. Soc*., **109**, 6887 (1987).
167. I.M.F. Oliveira, J.-M. Moutet, S. Hamar-Thibault, *J. Mater. Chem*., 2, 167 (1992).
168. L. Coche, B. Ehui, D. Liimosin, J.-M. Moutet, *J. Org. Chem*., **2**, 55, 5905 (1990).
169. J-M. Moutet, A. Ourari, A. Zouaoui, *Electrochim. Acta*, **37**, 1261 (1992).
170. J-C. Moutet, Y. Ouennoughi, A. Ourari, S. Hamar-Thibault, *Electrochim Acta*, **40**, 1827 (1995).
171. O. M. Mikhailik, V. I. Povstugar, S. S. Mikhailova, A. M. Lyakhovich, O. M. Tedorenko, G. T. Kurbatova, N. I. Shklouskoya, A. A. Chuiko, *Colloids Surf*., **52**, 315; 325; 331 (1981).

172. Yu. D. Semchikov, N. L. Khvatova, V. G. El'son, R. F. Galliulina, *Polym. Sci., (Engl. Trans.)*, *Ser. A* **29**, 503 (1987).
173. V. V. Vysotskii, V. I. Roldugin, *Colloid J., (Engl. Trans.)*, **58**, 312 (1996).
174. V. V. Zagorskii, A. E. Nasonova, M. A. Petrukhina, G. B. Sergeev, *Mosc. Univ. Bull., (Engl. Trans.), Ser. 2, Khim*. **36**, 159 (1995).
175. T. Arai, I. Yasumoto, *Hyomen*, **29**, 955 (1991).
176. C. V. Stakhanova, N. I. Nikonorova, A. L. Volynskii, N. F. Bakeev, *Vysokomol. Soedin. Ser. A* **39**, 312; 318 (1997).
177. R. Saito, S-I. Okamura, K. Ishizu, *Polymer*, **37**, 5255 (1996).
178. H. S. Zhou, T. Wada, H. Sasabe, H. Komiyama, *Synth. Met*., **81**, 129 (1996).
179. T. S. Ahmadi, Z. L. Wang, T. C. Green, A. Henglein, M. A. El. Sayed, *Science*, **272**, 1924 (1996).
180. W-Y. Yu, H-F. Liu, Q. Tao, *J. Chem. Soc., Chem. Commun*., 1773 (1996).
181. C. B. Murray, C. R. Kagan, M. G. Bawendi, *Annu. Rev. Mater. Sci*., **30**, 545 (2000).
182. R. I. Rudyi, N. V. Cherkashina, L. K. Shubochkin, M. N. Vargaftik, B. N. Novgorodov, D. I. Kochubei, V. N. Kolomiichuk, I. I. Moiseev, *Dokl. Chem., (Engl. Trans.)*, **349**, 490 (1996).
183. S. O'Brien, L. Brus, C. B. Murray, *J. Am. Chem. Soc*., **123**, 12085 (2001).
184. K. Kuraoka, Y. Chujo, T. Yazawa, *Chem. Commun*., 2477 (2000).
185. J. A. Becker, R. Schafer, R. Festag, W. Ruland, J. H. Wendorf, *J. Chem. Phys*., **103**, 2520 (1995).
186. N. Nakashima, Y. Miyata, M. Tominaga, *Chem. Lett*., 731 (1996).
187. F. Remacle, R. D. Levine, *Chem. Phys. Chem*., **2**, 21 (2001).
188. T. G. Shutova, G. V. Butovskaya, V. E. Agabekov, *Russ. J. Phys. Chem., (Engl. Trans.)*, **70**, 2123 (1996).
380. P. Mercandelli, A. Sironi, *J. Am. Chem. Soc*., **118**, 548 (1996).
189. M. Marakami, K. Itami, Y. Ito, *J. Am. Chem. Soc*., **118**, 672 (1996).
190. T. Cunji, I. Sopyan,Y. Abe, *J. Polym. Sci., Part A, Polym. Chem*., **32**, 3133 (1994).
191. D. W. McCarthy, J. E. Mark, S. J. Clarson, D. W. Schaefer, *J. Polym. Sci., Part B Polym. Phys*., **36**, 1191 (1998).
192. E. A. Barringer, H. K. Bowen, *J. Am. Ceram. Soc*., C, **65**, 199 (1982).
193. E. A. Barringer, H. K. Bowen, *Langmuir*, **1**, 414 (1985).
194. G. T. Petrovskii, V. S. Shashkin, A. K. Yakhkind, *Phys. Chem. Glass*, **23**(1), 43 (1997).
195. J. Blanchard, S. Barboux-Doeuff, J. Maquet, C. Sanchez, *New J. Chem*., **19**, 929 (1995).
196. V. B. Aleskovskii, *The Chemistry of Supermolecular Compounds*, St. Petersburg University, St. Petersburg, 1996.
197. A. B. Brennan, H. H. Wang, G. L. Wieres, *Polym. Prepr*., **30**, 105 (1989).
198. N. V. Golubko, M. I. Yanovskaya, S. G. Prutchenko, E. S. Obolonkova, *Inorg. Mater., (Engl. Trans.)*, **34**, 1115 (1998).
199. F. Ribot, P. Toledano, C. Sanchez, *Chem. Mater*., **3**, 759 (1991).
200. R. C. Mehrotra, D. P. Gaur, D. C. Bradley, *Metal Alkoxides*, Academic Press, London, 1978.
201. U. Schubert, F. Schwertfeger, C. Girsmann, in *Nanotechnology. Molecular Designed Materials* (ACS Symp. Ser. **622**), G-M Chow, K. E. Gonsalves, eds., American Chemical Society, Washington, D.C., 1996.
202. B. E. Yoldas, *J. Non-Cryst. Solids*., **82**, 11 (1986).
203. Q. Xu, M. A. Anderson, *Mater. Res. Soc. Symp. Proc*., **132**, 41 (1988).
204. N. V. Golubko, M. I. Yanovskaya, I. P. Romm, *Russ. J. Phys. Chem., (Engl. Trans.)*, **71**, 1747 (1997); **72**, 1023 (1998).
205. K. L. Walther, A. Wokaun, B. E. Handy, A. Baiker, *J. Non-Cryst. Solids*, **134**, 47 (1991).

206. D.C.M. Dutoit, M. Schneider, A. Baiker, *J. Catal*., **153**, 167 (1995).
207. D.C.M. Dutoit, M. Schneider, P. Fabrigioli, A. Baiker, *Chem. Mater*., **8**, 734 (1996).
208. M. D. Curran, T. E. Gedris, A. E. Stiegman, *Chem. Mater*., **10**, 1604 (1998).
209. A. C. Pierre, *Am. Ceram. Soc. Bull*., **70**, 1281 (1991).
210. G. W. Scherer, *J. Non-Cryst. Solids*, **87**, 199 (1986).
211. C. T. Kresge, M. E. Leonowicz, W. J. Roth, J. C. Vartuli, J. S. Beck, *Nature*, **359**, 710 (1992).
212. P. T. Tanev, T. J. Pinnavaia, *Science*, **267**, 865 (1995).
213. L. I. Grishchenko, N. G. Medvedkova, V. V. Nazarov, Yu. G. Frolov, *Colloid J. (Engl. Trans.)*, **55**, 35 (1993).
214. L. L. Hench, J. K. West, *Chem. Rev*., **90**, 33 (1990).
215. H. D. Gesser, P. C. Goswami, *Chem. Rev*., **89**, 765 (1989).
216. G. M. Pajonk, *Appl. Catal*., **72**, 217 (1991).
217. B. O'Regan, J. Moser, M. Anderson, M. Gritzel, *J. Phys. Chem*., **94**, 8720 (1990).
218. R. Kasemann, H. Schmidt, *New J. Chem*., **18**, 1117 (1994).
219. Y. Haruvy, S. E. Webber, *Chem. Mater*., **3**, 501 (1991); **4**, 89 (1992).
220. R. Zusman, C. Rottman, M. Ottolenghi, D. Avnir, *J. Non-Cryst. Solids*, **122**, 107 (1990).
221. B. Dunn, J. I. Zink, *J. Mater. Chem*., **1**, 903 (1991).
222. L. M. Ellerby, C. R. Nishida, F. Nishida, S. A. Yamanaka, B. Dunn, V. J. Selverstone, J. I. Zink, *Science*, **255**, 1113 (1992).
223. P.-H. Sung, T.-F. Hsu, Y.-H. Ding, A. Y. Wu, *Chem. Mater*., **10**, 1642 (1998).
224. R. Reisfeld, D. Brusilovsky, M. Eyal, E. Miron, Z. Burstein, J. Ivri, *Chem. Phys. Lett*., **160**, 43 (1989).
225. E.J.A. Pope, M. Asami, J. D. Mackenzie, *J. Mater. Res*., **4**, 1018 (1989).
226. S. V. Kalinin, A. V. Lukashin, K. V. Tomashevich, A. V. Knot'ko, M. P. Nikiforov, S. Y. Stefanovich, A. A. Vertegel, Yu. D. Tret'yakov, *Dokl. Chem. Technol., Dokl. Chem., (Engl. Trans.)*, **364**, 207 (1999).
227. H. Schmidt, B. Seiferling, *Mater. Res. Soc. Symp. Proc*., **73**, 739 (1986).
228. M. Zeldin, K. J. Wynne, H. R. Allcock, eds., *Inorganic and Organo-Metallic Polymers* (ACS Symp. Ser. **360)** American Chemical Society, New York, 1988.
229. Y. Hu, J. D. Mackenzie, *Mater. Res. Soc. Symp. Proc*., **271**, 681 (1992).
230. J. D. Mackenzie, Y. J. Chung, Y. Hu, *J. Non-Cryst. Solids*, **147/148**, 271 (1992).
231. M. Brust, D. Bethell, C. J. Kiely, D. J. Schiffrin, *Langmuir*, **14**, 5425 (1998).
232. T. Saegusa, Y. Chujo, *Polym. Prepr*., **1**, 39 (1989).
233. C.J.T. Landry, B. K. Coltrain, J. A. Wesson, N. Zumbulyadis, J. L. Lippert, *Polymer*, **33**, 1486; 1496 (1992).
234. K. A. Mauritz, C. K. Jones, *J. Appl. Polym. Sci*., **40**, 1401 (1990).
235. M. Tiki, T. Y. Chow, T. Ohnaka, H. Samura, T. Saegusa, *Polym. Bull*., **29**, 653 (1992).
236. C. Sanchez, B. Alonso, F. Chapusot, F. Ribot, P. Audebert, *J. Sol-Gel Sci. Technol*., **2**, 161 (1994).
237. H. Krug, H. Schmidt, *New J. Chem*., **18**, 1125 (1994).
238. R.J.P. Corriu, J.J.E. Moreau, P. Thepot, M. W. Chi Man, C. Chorro, J.-P. Lere-Porte, J.-L. Sauvajol, *Chem. Mater*., **6**, 640 (1994).
239. P. Audebert, P. Calas, G. Cerveau, R.J.P. Corriu, N. Costa, *J. Electroanal. Chem*., **372**, 275 (1994); **413**, 89 (1996).
240. L. C. Klein, ed., *Sol-Gel Technology*, Noyes, Park Ridge, NY, 1988.
241. P. Calvert, *Nature*, **353**, 501 (1991).
242. Y. Wei, R. Bakthavatchalam, C. K. Whitecar, *Chem. Mater*., **2**, 337 (1990).
243. K. A. Mauritz, R. Ju, *Chem. Mater*., **6**, 2269 (1994).

244. N. Juangvanich, K. A. Mauritz, *J. Appl. Polym. Sci*., **67**, 1799 (1998).
245. Q. Deng, Y. Hu, R.B. Moore, C. L. McCormick, K. A. Mauritz, *Chem. Mater*., **9**, 36 (1997).
246. Q. Deng, R. B. Moore, K. A. Mauritz, *Chem. Mater*., **1**, 2259 (1995).
247. Q. Deng, R. B. Moore, K. A. Mauritz, *J. Appl. Polym. Sci*., **68**, 747 (1998).
248. Q. Deng, C. A. Wilkie, R. B. Moore, K. A. Mauritz, *Polymer*, **39**, 5961 (1998).
249. L. A. Utracki, R. A. Weiss, eds., *Blends, lonomers and Interpenetrating Networks* (ACS Symp. Ser. **395**) American Chemical Society, Washington, D.C., 1989.
250. Z. D. Zhao, Y. C. Ou, Z. M. Gao, Z. N. Qi, F. S. Wang, *Acta Polym. Sin*., 228 (1996).
251. W. Zhou, J. H. Dong, K. Y. Qiu, Y. Wei, *J. Polym. Sci. Part A Polym. Chem*., **36**, 1607 (1998).
252. Y. Wei, D. Jin, D. J. Brennan, D. N. Rivera, Q. Zhuang, N. J. Di Nardo, K. Qiu, *Chem. Mater*., **10**, 769 (1998).
253. Y. Imai, *J. Macromol. Sci*., A **28**, 1115 (1991).
254. A. Morikawa, Y. lyoku, M. Kakimoto, Y. Imai, *Polym. J*., **24**, 107 (1992).
255. A. Provatas, M. Luft, J. C. Mu, A. H. White, J. G. Matisons, B. W. Skelton, *J. Organomet. Chem*., **565**, 159 (1998).
256. A. Romo-Uribe, P. T. Mather, T. S. Haddad, J. D. Lichtenhan, *J. Polym. Sci. Part B, Polym. Phys*., **36**, 1857 (1998).
257. G. V. Kostrelev, M. Yu. Mitrofanov, E. A. Gruzinova, V. S. Svistunov, A. I. Zakharov, N. V. Abysheva, *Russ. J. Appl. Chem., (Engl. Trans.)*, **72**, 488 (1999).
258. J. L. Hedrick, H.-J. Cha, R. D. Miller, D. Y. Yoon, H. R. Brown, S. Srinivasan, R. Di Pietro, R. F. Cook, J. P. Hummel, D. P. Klaus, E. G. Liniger, E. E. Simonyi, *Macromolecules*, **30**, 8512 (1997).
259. M. Nandi, J. A. Conklin, L. Salvati Jr, A. Sen, *Chem. Mater*., **3**, 201 (1991).
260. A. Morikawa, Y. lyoku, M. Kakimoto, Y. Imai, *J. Mater. Chem*., **2**, 679 (1992).
261. Y. Ou, F. Yang, J. Chen, *J. Appl. Polym. Sci*., **64**, 2317 (1997).
262. F. Yang, Y. Ou, Z. Yu, *J. Appl. Polym. Sci*., **69**, 355 (1998).
263. Y. Chujo, E. lhara, H. lhara, T. Saegusa, *Polym. Bull*., **19**, 435 (1988).
264. T. Saegusa, Y. Chujo, *Macromol. Chem. Symp*., **33**, 31 (1990).
265. Y. Chujo, T. Saegusa, *Adv. Polym. Sci*., **100**, 11 (1992).
266. B. M. Novak, C. Davies, *Macromolecules*, **24**, 5481 (1991).
267. M. W. Ellsworth, B. M. Novak, *Chem. Mater*., **5**, 839 (1993).
268. B. M. Novak, *Adv. Mater*., **5**, 422 (1993).
269. P. Judeinstein, *Chem. Mater*., **4**, 4 (1992).
270. P. Judeinstein, P. W. Oliveira, H. Krug, H. Schmidt, *Chem. Phys. Lett*., **220**, 35 (1994).
271. H. Schmidt, *Makromol. Symp*., **101**, 333 (1996).
272. N. N. Khimich, B. I. Venzel', I. A. Drozdova, L. Ya. Suslova, *Dokl. Chem. Technol., Dokl. Chem. (Engl. Trans.)*, **366**, 361 (1999).
273. M. Nandi, J. A. Conklin, L. Salvati Jr, A. Sen, *Chem. Mater*., **2**, 772 (1990).
274. Sh. Yu. Dou, V. V. Nazarov, Yu. G. Frolov, *Colloid J. (Engl. Trans.)*, **53**, 464 (1991); **54**, 119 (1992).
275. E. V. Gorokhova, V. V. Nazarov, N. G. Medvedkova, G. G. Kagramanov, Yu. G. Frolov, *Colloid J. (Engl. Trans.)*, **55**, 30 (1993).
276. M. Kakihana, M. Yoshimura, *Bull. Chem. Soc. Jpn*., **72**, 1427 (1999).
277. Y. Wei, D. C. Yang, L. C. Tang, M. K. Hutchins, *Makromol. Chem. Rapid Commun*., **14**, 273 (1993).
278. Z. H. Huang, K.Y. Qiu, *Polym. Bull*., **35**, 607 (1995).

279. Z. H. Huang, K. Y. Qiu, *Acta Polym. Sin*., 434 (1997).
280. Z. H. Huang, K. Y. Qiu, *Polymer*, **38**, 521 (1997).
281. L. L. Beecroft, C. K. Ober, *Adv. Mater*., **7**, 1009 (1995).
282. G. I. Dzhardimalieva, A. D. Pomogailo, A. N. Shchupik, *Russ. Chem. Bull. (Engl. Trans.)*, 451 (1985).
283. A. D. Pomogailo, N. D. Golubeva, A. N. Kitaigorodskii, *Russ. Chem. Bull., (Engl. Trans.)*, 482 (1991).
284. G. I. Dzhardimalieva, A. O. Tonoyan, A. D. Pomogailo, S.P. Davtyan, *Russ. Chem. Bull. (Engl. Trans.)*, 1744 (1987).
285. A. D. Pomogailo, N. D. Golubeva, *Russ. Chem. Bull. (Engl. Trans.)*, 2139 (1994).
286. M. Camail, M. Humbert, A. Margaillan, A. Riondel, J. L. Veraet, *Polymer*, **39**, 6525 (1998).
287. M. Camail, M. Humbert, A. Margaillan, J. L. Vernet, *Polymer*, **39**, 6533 (1998).
288. T. Gunji, I. Sopyan, Y. Abe, *J. Polym. Sci. Part A, Polym. Chem*., **32**, 3133 (1994).
289. J. M. Breiner, J. E. Mark, *Polymer*, **39**, 5483 (1998).
290. P. L. Shao, K. A. Mauritz, R. B. Moore, *J. Polym. Sci. Part B Polym. Phys*., **34**, 873 (1996).
291. C.J.T. Landry, B. K. Coltrain, D. M. Teegarden, T. E. Long, V. K. Long, *Macromolecules*, **29**, 4712 (1996).
292. M. A. Mohammed, V. Rossbach, *J. Appl. Polym. Sci*., **50**, 929 (1993).
293. C. Rehwinkel, V. Rossbach, P. Fischer, J. Loos, *Polymer*, **39**, 4449 (1998).
294. J. Kramer, R. K. Prud'homme, P. Wiltzius, *J. Colloid Interface Sci*., **118**, 294 (1987).
295. J. Kramer, R. K. Prud'homme, P. Wiltzius, P. Mirau, S. Knoll, *Colloid Polym. Sci*., **266**, 145 (1988).
296. T. Sawaki, T. Dewa, Y. Aoyama, *J. Am. Chem. Soc*., **120**, 8539 (1998).
297. T. H. Mourey, S. M. Miller, J. A. Wesson, T. E. Long, L.W. Kelts, *Macromolecules*, **25**, 45 (1992).
298. Y. Chujo, E. lhara, S. Kure, K. Suzuki, T. Saegusa, *Makromol. Chem. Makromol. Symp*., **42/43**, 303 (1991).
299. G. Broze, R. Jerome, P. Tyssie, C. Marko, *Macromolecules*, **18**, 1376 (1985).
300. J. L. W. Noell, G. L. Wilkes, D. K. Mohanty, J. E. McGrath, *J. Appl. Potym. Sci*., **40**, 1177 (1990).
301. R. H. Glaser, G. L. Wilkes, *Polym. Bull*., **19**, 51 (1988); **22**, 527 (1989).
302. B. K. Coltrain, C.J.T. Landry, J. M. O'Reilly, A. M. Chamberlain, G. A. Rakes, J. S. Sedita, L. W. Kelts, M. R. Landry, V. K. Long, *Chem. Mater*., **5**, 1445 (1993).
303. H. H. Huang, G. L. Wilkes, J. G. Carlson, *Polymer*, **30**, 2001 (1989).
304. M. Gill, J. Mykytiuk, S. P. Armes, J. L. Edwards, T. Yeates, P. J. Moreland, C. Mollett, *J. Chem. Soc., Chem. Commun*., 108, (1992).
305. M. Gill, S. P. Armes, D. Fairhurst, S. N. Emmett, G. Idzorek, T. Pigott, *Langmuir*, **82**, 178 (1992).
306. S. Maeda, S. P. Armes, *J. Colloid Interface Sci*., **159**, 257 (1993).
307. S. Maeda, S. P. Armes, *J. Mater. Chem*., **4**, 935 (1994).
308. S. Maeda, S. P. Armes, *Chem. Mater*., **7**, 171 (1995).
309. N. J. Terrill, T. Crowley, M. Gill, S. P. Armes, *Langmuir*, **9**, 2093 (1993).
310. R. Flitton, J. Johal, S. Maeda, S. P. Armes, *Colloid Interface Sci*., **173**, 135 (1995).
311. T. Tamai, I. Hashida, N. Ichinose, S. Kawanishi, H. Inoue, K. Mizuno, *Polymer*, **37**, 5525 (1996).
312. N. Ichinose, T. Tamai, S. Kawanishi, I. Hashida, K. Mizuno, *Langmuir*, **13**, 2603 (1997).
313. T. Tamai, N. Ichinose, S. Kawanishi, M. Nishii, T. Sasuga, I. Hashida, K. Mizuno, *Chem. Mater*., **9**, 2674 (1997).

314. Y. Kawakami, H. Hisada, Y. Yamashita, *J. Polym. Sci. Part A Polym. Chem*., **26**, 1307 (1988).
315. N. Kato, N. Yamazaki, Y. Nagasaki, M. Kato, *Polym. Bull*., **32**, 55 (1994).
316. A. Martino, S. A. Yamanaka, J. S. Kawola, D. A. Loy, *Chem. Mater*., **9**, 423 (1997).
317. M. Yoshida, M. Lal, N. D. Kumar, P. N. Prasad, *J. Mater. Sci*., **32**, 4047 (1997).
318. T. Sato, D. Brown, B.F.G. Johnson, *Chem. Commun*., 1007 (1997).
319. C. Petit, P. Lixon, M. P. Pileni, *J. Phys. Chem*., **94**, 1598 (1990).
320. L. Mascia, A. Kioul, *J. Mater. Sci*. **13**, 641 (1994).
321. L. Mascia, A. Kioul, *J. Non-Cryst. Solids*, **175**, 169 (1994).
322. L. Mascia, *Trends Polym. Sci*., **3**, 61 (1995).
323. M. Popall, H. Durand, *Electrochim. Ada*, **37**, 1593 (1992).
324. R. A. Zoppi, C.M.N.P. Fonseca, M. A. De Paoli, S. P. Nunes, *Acta Polym*., **48**, 193 (1997).
325. R. A. Zoppi, S. P. Nunes, *Polymer*, **39**, 6195 (1998).
326. B. B. Vandelbrott, *Fractal Geometry of Nature*, Freeman, San Francisco, 1982.
327. F. Meng, J. R. Schiup, L. T. Fan, *Chem. Mater*., **9**, 2459 (1997).
328. T. L. Porter, M. E. Hagerman, B. P. Reynolds, M. P. Eastman, R. A. Parnell, *J. Polym. Sci. Part B Polym. Phys*., **36**, 673 (1998).
329. B. B. Lakshmi, P. K. Dorhout, C. R. Martin, *Chem. Mater*., **9**, 857 (1997).
330. Y. Hamasaki, S. Ohkubo, K. Murakami, H. Sei, G. Nogami, *J. Electrochem. Soc*., **141**, 660 (1994).
331. S. Sakohara, L. D. Tickanen, M. A. Anderson, *J. Phys. Chem*., **96**, 11087 (1992).
332. T. Nishide, H. Yamaguchi, F. Mizukami, *J. Mater. Sci*., **30**, 4946 (1995).
333. J. H. Kim, B. R. Min, C. K. Kim, J. Won, Y. S. Kang, *Macromolecules*, **34**, 6052 (2001).
334. J. B. Bates, G. R. Gruzalski, N. J. Dudney, C. F. Luck, X. Yu, *Solid Slate Ion*., **70/71**, 619 (1994).
335. S. Bach, M. Henry, N. Baffler, J. Livage, *J. Solid Stale Chem*., **88**, 325 (1990).
336. E. Zhecheva, R. Stoyanova, M. Gorova, R. Alcantara, J. Morales, J. L. Tirado, *Chem. Mater*., **8**, 1429 (1996).
337. R. V. Parthasarathy, C. R. Martin, *Nature*, **369**, 298 (1994).
338. V. M. Cepak, J. C. Hulteen, G. Che, K. B. Jirage, B. B. Lakshmi, E. R. Fisher, C. R. Martin, H. Yoneyama, *Chem. Mater*., **9**, 1065 (1997).
339. A. N. Ozerin, E. Yu. Sharipov, L. A. Ozerina, N. V. Golubko, M. I. Yanovskaya, *Russ. J. Phys. Chem. (Engl. Trans.)*, **73**, 277 (1999).
340. M.Z.-C. Hu, J. T. Zielke, C. H. Byers, J. S. Lin, M. T. Harris, *J. Mater. Sci*., **35**, 1957 (2000).
341. T. Werne, T. E. Patten, *J. Am. Chem. Soc*., **123**, 7497 (2001).
342. K. Dahmouche, L. D. Carlos, C. V. Santilli, V. Z. Bermudes, A. F. Craievich, *J. Phys. Chem. B*, **106**, 4377 (2002).
342. G.-H. Hsiue, R.-H. Lee, R.-J. Jeng, *Polymer*, **40**, 6417 (1999).
344. M. Sykora, K. A. Maxwell, T. J. Meyer, *Inorg. Chem*., **38**, 3596 (1999).
345. S. M. De Paul, J. W. Zwanziger, R. Ulrich, U. Wiesner, H. W. Spiess, *J. Am. Chem. Soc*., **121**, 5727 (1999).
346. H. Shiho, N. Kawahashi, *Colloid Polymer Sci*., **278**, 270 (2000).
347. C. Rottman, G. Grader, D. Avnir, *Chem. Mater*., **13**, 3631 (2001).
348. K. Wada, K. Yamada, T. Kondo, T. Mitsudo, *Chem. Lett.*, 12 (2001).
349. R. Hernandez, A.-C. Franville, P. Minoofar, B. Dunn, J. I. Zink, *J. Am. Chem. Soc*., **123**, 1248 (2001).
350. K. Nakane, J. Ohashi, F. Suzuki, *J. Appl. Polym. Sci*., **71**, 185 (1999).
351. A. S. Kovalenko, V. G. Ilin, A. P. Filippov, *Theor. Experiment. Chem*., **36**, 135 (2000).

352. M.-P. Zheng, Y.-P. Jin, G.-L. Jin, M.-Y. Gu, *J. Mater. Sci. Lett*., **19**, 433 (2000).
353. D. Tian, S. Blacher, R. Jerome, *Polymer*, **40**, 951 (1999).
354. T. Ogoshi, H. Itoh, K.-M. Kim, Y. Chujo, *Macromol*., **35**, 334 (2002).
355. S. Kobayashi, K. Hanabusa, M. Suzuki, M. Kimura, H. Shirai, *Bull. Chem. Soc. Jpn*., **73**, 1913 (2000).
356. C. D. Chandler, M.J. Hampden-Smith, *Chem. Mater.*, **4**, 1137 (1992).
357. M. Kakihana, T. Okubo, M. Arima, O. Uchiyama, M. Yashima, M. Yoshimura, Y. Nakamura, *Chem. Mater*., **9**, 451 (1997).
358. D. Geschke, N. Leister, M. Steffen, H.-J. Glisel, E. Hartmann, *J. Mater. Sci. Lett*., **16**, 1943 (1997).
359. K. Nagata, S. Kodama, H. Kawasaki, S. Deki, M. Mizuhata, *J. Appl. Polym. Sci*., **56**, 1313 (1995).
360. D. E. Collins, E. B. Slamovich, *Mater. Res. Symp. Proc*., **255**, 375 (1992); **457**, 445 (1997).
361. H. Kumazawa, T. Kagimoto, A. Kawabata, *J. Mater. Sci.,* **31**, 2599 (1996).
362. I. A. Tchmutin, A. T. Ponomarenko, V. G. Shevchenko, N. G. Ryvkina, C. Klason, D. H. McQueen, *J. Polym. Sci. Part B Polym. Phys*., **36**, 1847 (1998).
363. R. N. Viswanath, S. Ramasamy, *Nanostruct. Mater*., **8**, 155 (1997).
364. H.-J. Glisel, E. Hartmann, D. Hirsh, R. Bittcher, C. Klimm, D. Michel, H.-C. Semmelhack, J. Homes, H. Rumpf, *J. Mater. Sci*., **34**, 2319 (1999).
365. C. P. Udawatte, M. Kakihana, M. Yoshimura, *Solid State Ion*., **108**, 23 (1998).
366. R. W. Schwartz, *Chem. Mater*., **9**, 2325 (1997).
367. K.-I. Noda, W. Sakamoto, K.-I. Kikuta, T. Yogo, S.-I. Hirano, *Chem. Mater*., **9**, 2174 (1997).
368. C. Sanchez, M. In, P. Toledano, P. Criesmar, *Mater. Res. Soc. Symp. Proc*., **271**, 669 (1992).
369. P. J. Pagan, J. C. Calabrese, B. Malone, *J. Am. Chem. Soc*., **113**, 9408 (1991).
370. M. I. Khan, L. M. Meyer, R. C. Haushalter, A. L. Schweitzer, J. Zubieta, J. L. Dye, *Chem. Mater*., **8**, 43 (1996).
371. D. Hagrman, C. Zubieta, D. J. Rose, J. Zubieta, R. C. Haushalter, *Angew. Chem., Int. Ed. Engl*., **36**, 873 (1997).
372. C. J. Warren, R. C. Haushalter, D. J. Rose, J. Zubieta, *Chem. Mater*., **9**, 2694 (1997).
373. C. K. Narula, P. Czubarow, D. Seyferth, *J. Mater. Sci*., **33**, 1389 (1998).
374. C. Y. Chen, H. X. Li, M. E. Davis, *Microporous Mater*., **2**, 17 (1993).
375. A. Corma, *Chem. Rev*., **97**, 2373 (1997).
376. X. Zhang, Z. Zhang, J. Suo, S. Li, *Chem. Lett*., 755 (1998).
377. P. G. Harrison, R. Kannengiesser, *Chem. Commun*., 2065 (1995).
378. A.-R. Badiei, L. Bonneviot, *Inorg. Chem*., **37**, 4142 (1998).
379. K. Wada, M. Nakashita, M. Bundo, K. Ito, T. Kondo, T. Mitsudo, *Chem. Lett*., 659 (1998).
380. J. P. Carpenter, C. M. Lukehart, S. R. Stock, J. E. Witting, *Chem. Mater*., **7**, 2011 (1995).
381. J. P. Carpenter, C. M. Lukehart, S. B. Milne, S. R. Strock, J. E. Witting, B. D. Jones, R. Glosser, J. G. Zhu, *J. Organomet. Chem*., **557**, 121 (1998).
382. M. V. Russo, A. Furlani, M. Cuccu, G. Polzonetti, *Polymer*, **37**, 1715 (1996).
383. S. Bandyopadhyay, S. Roy, D. Chakravorty, *Solis State Commun*., **99**, 835 (1996).
384. J. Massey, K. N. Power, I. Manners, M. A. Winnik, *J. Am. Chem. Soc*., **120**, 9533 (1998).
385. A. Lorenz, G. Kickelbick, U. Schubert, *Chem. Mater*., **9**, 2551 (1997).
386. C. M. Lukehart, S. B. Milne, S. R. Stock, *Chem. Mater*., **10**, 903 (1998).
387. S. C. Goel, M. Y. Chiang, W. E. Buhro, *J. Am. Chem. Soc*., **112**, 5636 (1990).
388. L. I. Halanoui, S. S. Kher, M. S. Lube, S. R. Aubuchon, C.R.S. Hagan, R. L. Wells, L. A. Coury *Jr*, *ACS Symp. Ser*., **622**, 178 (1996).

389. K. M. Choi, K. J. Shea, *J. Am. Chem. Soc*., **116**, 9052 (1994).
390. G. Cerveau, R.J.P. Corriu, C. Lepeytre, *Chem. Mater*., **9**, 2561 (1997).
391. A. J. Wiseman, R. G. Jones, A. C. Swain, M. J. Went, *Polymer*, **37**, 5727 (1996).
392. T. Abe, Y. Tachibana, T. Uematsu, M. Iwamoto, *Chem. Commun*., 1617 (1995).
393. R. F. Soares, CAP Leite, W. Bottler Jr, F. Galembeck, *J. Appl. Polym. Sci*., **60**, 2001 (1996).
394. K. W. Alien, *J. Adhes. Sci. Technol*., **6**, 23 (1992).
395. F. D. Osterholtz, E. R. Pohl, *J. Adhes. Sci. Technol*., **6**, 127 (1992).
396. W. Bottler Jr, R. F. Soares, F. Galembeck, *J. Adhes. Sci. Technol*., **6**, 781 (1992).
397. Y. C. Aronoff, B. Chen, G. Lu, C. Seto, J. Schwartz, S. L. Bernasek, *J. Am. Chem. Soc*., **119**, 259 (1997).
398. S. K. Vander Kam, A. B. Bocarsly, J. Schwartz, *Chem. Mater*., **10**, 685 (1998).
399. P. Bodo, J.-E. Sundgren, *Thin Solid Films*, **136**, 147 (1986).
400. N. Bowden, S. Brittain, A. G. Evans, J. W. Hutchinson, G. M. Whitesides, *Nature (London)*, **393**, 146 (1998).
401. E. Ruckenstein, L. Hong, *J. Appl. Polym. Sci*., **55**, 1081 (1995).
402. E. Ruckenstein, L. Hong, *Chem. Mater*., **8**, 546 (1996).
403. L. Hong, E. Ruckenstein, *J. Appl. Polym. Sci*., **67**, 1891 (1998).
404. Y. Ou, F. Yang, Z.-Z. Yu, *J. Polym. Sci. Part B Polym. Phys*., **36**, 789 (1998).
405. S. Ogata, Y. Tasaka, H. Tagaya, J. Kadokawa, K. Chiba, *Chem. Lett*., 237 (1998).
406. R. L. Callender, J. Harian, N. M. Shapiro, C. D. Jones, D. L. Callahan, M. R. Wiesner, D. B. MacQueen, R. L. Cook, A. R. Banon, *Chem. Mater*., **9**, 2418 (1991).
407. A. Kareiva, C. J. Harlan, D. B. MacQueen, R. L. Cook, A. R. Barron, *Chem. Mater*., **8**, 2331 (1996).
408. C. J. Harian, A. Kareiva, D. B. MacQueen, R. L. Cook, A. R. Barren, *Adv. Mater*., **9**, 68 (1997).
409. E. Mouchon, P. Colomban, *J. Mater. Sci*., **31**, 323 (1996).
410. D. A. Loy, E. M. Russick, S. A. Yamanaka, B. M. Baugher, K. J. Shea, *Chem. Mater*., **9**, 2264 (1997).
411. J. Mrowiec-Bialon, A. B. Jarzebski, A. I. Lachowski, J. J. Malinowski, Yu. I. Aristov, *Chem. Mater*., **9**, 2486 (1997).
412. Yu. I. Aristov, M. M. Tokarev, G. Cacciola, G. Restuccia, G. Di Marco, V. N. Parmon, *Mater. Res. Soc. Symp. Proc*., **457**, 463 (1997).
413. P. Mulvaney, M. Giersig, A. Henglein, *J. Phys. Chem*., **96**, 10419 (1992).
414. P. A. Voznyi, L. V. Galushko, P. P. Gorbik, V. V. Dyakin, A. A. Levchenko, V. V. Levandovskii, V. N. Lysenko, V. M. Ogenko, L. K. Yanchevskii, *Superconductivity. Phys. Chem. Eng.,* **5**, 1478 (1992).
415. L. K. Yanchevskii, V. V. Levandovskii, N. V. Abramov, P. P. Gorbik, P. A. Voznyi, I. V. Dubrovin, M. V. Bakuntseva, *Plast. Massy*, (9),18 (1997).
416. A. Douy, P. Odier, *Mater. Res. Bull*., **24**, 1119 (1989).
417. I. Valente, C. Sanchez, M. Henry, J. Livage, *Ind. Ceram*. **836**, 193 (1989).
418. A. A. Ostroushko, L. I. Zhuravlev, S. M. Portnova, Yu. I. Krasilov, *Russ. J. Inorg. Chem. (Engl. Trans.)*, **36**, 1099 (1991).
419. A. A. Ostroushko, S. M. Portnova, Yu. I. Krasilov, I. P. Ostroushko, *Russ. J. Inorg. Chem. (Engl. Trans.)*, **36**, 823 (1991).
420. A. A. Ostroushko, N. V. Mironova, I. P. Ostroushko, A. N. Petrov, *Russ. J. Inorg. Chem. (Engl. Trans.)*, **37**, 2627 (1992).
421. J.C.W. Chien, B. M. Gong, J. M. Madsen, R. B. Hallock, *Phys. Rev. B Solid State, Ser. B,* **38**, 11853 (1988).
422. J.C.W. Chien, B. M. Gong, X. Mu, Y. Yang, *J. Polym. Sci. Polym. Chem. Ed*., **28**, 1999 (1990).

423. S. Maeda, Y. Tsurusaki, Y. Tachiyama, K. Naka, A. Ohki, T. Ohgushi, T. Takeshita, *J. Polym. Sci. Part A Polym. Chem*., **32**, 1729 (1994).
424. K. Naka, Y. Tachiyama, A. Ohki, S. Maeda, *J. Polym. Sci. Part A Polym. Chem*., **34**, 1003 (1996).
425. H. Tamura, H. Hineta, M. Tatsumi, J. Tanishita, S. Yamamoto, *Chem. Lett*., 1147 (1994).
426. G. Mohazzab, I. M. Low, *J. Appl. Polym. Sci*., **56**, 1679 (1995).
427. P. Catania, W. Hovnanian, L. Cot, *Mater. Res. Bull*., **25**, 1477 (1990).
428. T. Goto, K. Takahashi, *J. Mater. Res*., **9**, 852 (1994).
429. H. Tomita, T. Goto, K. Takahashi, *Supercond. Sci. Technol*., **9**, 363, 1099 (1996).
430. H. Tomita, T. Omori, T. Goto, K. Takahashi, *J. Mater. Sci*., **33**, 247 (1998).
431. A. D. Pomogailo, V. S. Savost'yanov, G. I. Dzhardimalieva, A. V. Dubovitskii, A. N. Ponomarev, *Russ. Chem. Bull. (Engl. Trans.)*, 1096 (1995).
432. V. S. Savost'yanov, V. A. Zhorin, G. I. Dzhardimalieva, A. D. Pomogailo, A. V. Dubovitskii, V. N. Topnikov, M. K. Makova, A. N. Ponomarev, *Dokl. Chem. Technol., Dokl. Chem., (Engl. Trans.)*, **318**, 378 (1991).
433. V. S. Savost'yanov, V. N. Vasilets, O. V. Ermakov, E. A. Sokolov, A. D. Pomogailo, D. A. Kritskaya, A. N. Ponomarev, *Russ. Chem. Bull., (Engl. Trans.)*, **41**, 2073 (1992).
434. K. E. Gonsalves, S. P. Rangarajan, C. C. Law, C. R. Feng, G.-M. Chow, A. Garcia-Ruiz, *ACS Symp. Ser*., **622**, 220 (1996).
435. K. E. Gonsalves, S. P. Rangarajan, *J. Appl. Polym. Sci*., **64**, 2667 (1997).
436. H.-B. Park, H.-J. Kweon, Y.-S. Hong, S.-J. Kirn, K. Kirn, *J. Mater. Sci*., **32**, 57 (1997).
437. X.-G. Tang, H.-K. Guo, Q.-F. Zhou, J.-X. Zhang, *J. Mater. Sci. Lett*., **17**, 1277 (1998).
438. D. O'Hare, *New J. Chem*., **18**, 989 (1994).
439. M. I. Rozengart, G. M. V'yunova, G. V. Isagulyants, *Russ. Chem. Rev*., **57**, 115 (1988).
440. M. L. Occelli, H. Kessler, eds., *Synthesis of Porous Materials, Zeolites. Clays and Nanostructures*, Marcel Dekker, New York, 1997.
441. V. Mehrotra, E. P. Giannelis, R. F. Ziolo, P. Rogalskyj, *Chem. Mater*., **4**, 20 (1992).
442. M. W. Anderson, J. Shi, D. A. Leigh, A. E. Moody, F. A. Wade, B. Hamilton, S. W. Carr. *Chem. Commun*., 533 (1993).
443. A. Gmgel, K. Mmllen, H. Reichert, W. Schmidt, G. Schin, F. Schmth, J. Spickermann, J. Titman, K. Unger, *Angew. Chem*., **105**, 618 (1993).
444. A. Gmgel, A. Kraus, J. Spickermann, P. Belik, K. Muller, *Angew. Chem. Int. Ed. Engl*., **33**, 559 (1994).
445. E. P. Giannelis, *Adv. Mater*., **8**, 229 (1996).
446. P. B. Messersmith, E. P. Giannelis, *Chem. Mater*., **5**, 1064 (1993); **6**, 1719 (1994).
447. P. B. Messersmith, E. P. Giannelis, *J. Polym. Sci., Part A, Polym. Chem*., **33**, 1047 (1995).
448. T. Lan, T. J. Pinnavaia, *Chem. Mater*., **6**, 2216 (1994).
449. W. Muller-Warmuth, R. Schollhorn, eds., *Progress in Intercalation Research*, Kluwer Academic, Dodrecht, 1994.
450. R. Schollhorn, *Chem. Mater*., **8**, 1747 (1996).
451. M. Ogawa, K. Kuroda, *Chem. Rev*., **95**, 399 (1995).
452. G. A. Ozin, *Adv. Mater.* **4**, 612 (1992).
453. A. Blumstein, *J. Polym. Sci. Part A* **3**, 2653 (1965).
454. A. Blumstein, S. L. Malhotra, A. C. Watterson, *J Polym. Sci. Part A-2*, **8**, 1599 (1970).
455. Y. Kojima, A. Usuki, M. Kawasumi, A. Okada, T. Kurauchi, O. Kamigaito, *J. Polym. Sci. Part A Polym. Chem*., **31**, 983 (1993).
456. J. Wu, M. M. Lerner, *Chem. Mater*, **5**, 835 (1993).
457. H. Miyata, Y. Sugahara, K. Kuroda, C. Kato, *J. Chem. Soc. Faraday Trans*., **83**, 1851 (1987).

458. M. Ogata, M. Inagaki, N. Kodama, K. Kuroda, C. Kato *J. Phys. Chem.* **97**, 3819 (1993).
459. A. Hild, J.-M. Sequaris, H.-D. Narres, M. Schwuger, *Colloid. Surf. A* **123/124**, 515 (1997).
460. P. Arada, E. Ruiz-Hitzky, *Chem. Mater*., **4**, 1395 (1992).
461. Y. Sugahara, T. Sugiyama, T. Nagayama, K. Kuroda, C. Kato, *J. Ceram. Soc. Jpn*., **100**, 413 (1992).
462. T. J. Pinnavaia, T. Lan, P. D. Kaviratna, M. S. Wang, *Mater. Res. Symp. Proc*., **346**, 81 (1994).
463. T. Lan, P. D. Kaviratna, T. J. Pinnavaia, *Chem. Mater*., **6**, 573 (1994).
464. S. P. Amies, S. Gottesfeld, J. G. Beery, F. Garson, S. F. Agnew, *Polymer*, **32**, 2325 (1991).
465. S. Maeda, S. P. Amies, *Synth. Met*., **73**, 151 (1995).
466. A. Akelah, N. Salahuddin, A. Hiltner, E. Baer, A. Moet, *Nanostruct. Mater*., **4**, 965 (1994).
467. A. Akelah, A. Moet, *J. Appl. Polym. Sci*., **55**, 153 (1994).
468. G. A. Ozin, A. Kupermann, A. Stein, *Angew. Chem*., **101**, 373 (1989).
469. G. A. Ozin, A. Kupermann, A. Stein, *Angew. Chem., Int., Ed. Engl*., **28**, 359 (1989).
470. T. Bein, *Chem. Mater*., **4**, 819 (1992).
471. B. R. Mattes, E. T. Knobbe, P. D. Fuqua, F. Nishida, E. W. Chang, B. M. Pierce, B. Dunn, R. B. Kaner, *Synth. Met*., **41**, 3183 (1991).
472. M. G. Kanatzidis, L. M. Tonge, T. J. Marks, H. O. Marey, C. R. Kannewurf, *J. Am. Chem. Soc*., **109**, 3797 (1987).
473. M. G. Kanatzidis, H. O. Marey, W. J. McCarthy, C. R. Kannewurf, T. J. Marks, *Solid State Ion*., **32–33**, 594 (1989).
474. C. G. Wu, H. O. Marey, D. C. DeGroot, J. L. Schindler, C. R. Kannewurf, W. Y. Leung, M. Benz, E. Le Goff, M. G. Kanatzidis, *Synth. Met*., **41**, 797 (1991).
475. M. G. Kanatzidis, C. G. Wu, H. O. Marcy, D. C. DeGroot, C. R. Kannewurf, A. Kostikas, V. Papaefthymiou, *Adv. Mater*., **2**, 364 (1990).
476. C.-G. Wu, D. C. DeGroot, H. O. Marcy, J. L. Schindler, C. R. Kannewurf, T. Bacas, V. Papaefthymiou, W. Hirpo, J. P. Yesniowski, Y-J. Liu, M. G. Kanatzidis, *J. Am. Chem. Soc*., **117**, 9229 (1995).
477. R. Bissessur, D. C. DeGroot, J. L. Schindler, C. R. Kannewurf, M. G. Kanatzidis, *Chem. Commun*., 687 (1993).
478. Y. Liu, D. DeGroot, J. Schindler, C. Kannewurf, M. Kanatzidis, *Chem. Mater*., **3**, 992 (1991).
479. Y. Liu, D. DeGroot, J. Schindler, C. Kannewurf, M. Kanatzidis, *Adv. Mater*., **5**, 369 (1993).
480. C. O. Oriakhi, M. M. Lerner, *Chem. Mater*., **8**, 2016 (1996).
481. L. Wang, P. Brazis, M. Rocci, C.R. Kannewurf, M. G. Kanatzidis, *Chem. Mater*., **10**, 3298 (1998).
482. K. J. Chao, T. C. Chang, S. Y. Ho, *J. Mater. Chem*., **3**, 427 (1993).
483. Y. J. Liu, M. G. Kanatzidis, *Chem. Mater*., **7**, 1525 (1995).
484. T. Bein, ed., *Supramolecular Architecture, Synthetic Control in Thin Films and Solids* (*ACS Symp. Ser.*) American Chemical Society, Washington, D.C., 1992.
485. H. Nakajima, G. Matsubayashi, *Chem. Lett*., 423 (1993).
486. Y.-J. Liu, M. G. Kanatzidis, *Inorg. Chem*., **32**, 2989 (1993).
487. T. Challier, C. T. Slade, *J. Mater. Chem*., **4**, 367 (1994).
488. B. E. Koene, L. F. Nazar, *Solid State Ion*., **89**, 147 (1996).
489. N.S.P. Bhuvanesh, J. Gppalakrishnan, *Inorg. Chem*., **34**, 3760 (1995).
490. N.S.P. Bhuvanesh, J. Gopalakrishnan, *Mater. Sci. Eng. B*, **53**, 267 (1998).
491. M. G. Kanatzidis, R. Bissessur, D. C. DeGroot, J. L. Schindler, C. R. Kannewurf, *Chem. Mater*., **5**, 595 (1993).
492. C-G. Wu, T. Bein, *Science*, **264**, 1757 (1993).
493. P. Enzel, T. Bein, *J. Phys. Chem.*, **93**, 6270 (1989).

494. S. Uma, J. Gopalakrishnan, *Mater. Sci. Eng. B*, **34**, 175 (1995).
495. V. Mehrotra, E. P. Giannelis, *Solid State Ion.,* **51**, 115 (1992).
496. I. P. Suzdalev, *Vestn. RFFI*, **1**, 1 (1999).
497. M. T. Pope, A. Miiller, eds., *Polyoxometallates. From Platonic Solids to Antiretroviral Activity*, Kluwer Academic, Dordrecht, 1994.
498. P. Gomez-Romero, M. Lira-Cantu, *Adv. Mater*., **9**, 144 (1997).
499. M. Lira-Cantu, P. Gomez-Romero, *Chem. Mater*., **10**, 698 (1998).
500. J. D. Aiken III, Y. Lin, R. G. Finke, *J. Mol. Catal*., **114**, 29 (1996).
501. J. D. Aiken III, R. G. Finke, *J. Am. Chem. Soc*., **120**, 9545 (1998).
502. M. Biswas, S. S. Ray, *Polymer*, **39**, 6423 (1998).
503. E. Manias, W. J. Han, K. D. Jandt, E. J. Kramer, E. P. Giannelis, *Mater. Res. Soc. Symp. Proc*., **457**, 495 (1997).
504. M. G. Kanatzidis, C-G. Wu, H. O. Marcy, C. R. Kannewurf, *J. Am. Chem. Soc*., **111**, 4139 (1989).
505. M. G. Kanatzidis, C.-G. Wu, H. O. Marcy, C. R. Kannewurf, *Chem. Mater*., **2**, 221 (1990).
506. C.-G. Wu, D. C. DeGroot, H. O. Marcy, J. L. Schindler, C. R. Kannewurf, Y.-J. Liu, W. Hirpo, M. G. Kanatzidis, *Chem. Mater*., **8**, 1992 (1996).
507. T. A. Kerr, H. Wu, L. F. Nazar, *Chem. Mater*., **8**, 2005 (1996).
508. V. Parente, C. Fredriksson, A. Selmani, R. Lazzaroni, J. L. Bredas, *J. Phys. Chem., B*, **101**, 4193 (1997).
509. C. J. Brumlik, V. P. Menon, C. R. Martin, *J. Mater. Res*., **9**, 1174 (1994).
510. S. M. Marinakos, L. C. Brousseau III, A. Jones, D. L. Feldheim, *Chem. Mater*., **10**, 1214 (1998).
511. K. Murakoshi, G. Kano, Y. Wada, S. Yanagida, H. Miyazaki, M. Matsumoto, S. Murasawa, *Electroanal. Chem*., **396**, 27 (1995).
512. K. Murakoshi, R. Kogure, Y. Wada, S. Yanagida, *Chem. Lett*., 471, (1997).
513. G. D. Stucky, in *Progress in Inorganic Chemistry*, vol. 40, J. Lippard, ed., Wiley, New York, 1992.
514. V. Ramamurthy, *J. Am. Chem. Soc*., **116**, 1345 (1994).
515. C.-G. Wu, T. Bein, *Chem. Mater*., **6**, 1109 (1994).
516. R. F. Khairutdinov, *Russ. Chem. Rev*., **67**, 109 (1998).
517. A. Usuki, M. Kawasumi, Y. Kojima, A. Okada, T. Kurauchi, O. Kamigato, *J. Polym. Sci. Part A Polym. Chem*., **31**, 983 (1993).
518. A. Usuki, M. Kawasumi, Y. Kojima, A. Okada, T. Kurauchi, O. Kamigato, *J. Mater. Res*., **8**, 1174 (1993).
519. M. P. Eastman, J. A. Attuso, T. L. Porter, *Clays Clay Miner*., **44**, 769 (1996).
520. R. A. Vaia, S. Vasudevan, W. Krawiec, L. G. Scanlon, E. P. Giannelis, *Adv. Mater*., **7**, 154 (1995).
521. I. Lagadic, A. Lgaustic, R. Cigment, *Chem. Commun*., 1396 (1992).
522. Y.-J. Liu, J. L. Schindler, D. C. DeGroot, C. R. Kannewurf, W. Hiro, M. G. Kanatzidis, *Chem. Mater*., **8**, 525 (1996).
523. L. F. Nazar, H. Wu, W. P. Power, *J. Mater. Chem.,* **5**, 198 (1995).
524. P. Jeevanandam, S. Vasudevan, *Chem. Mater*., **10**, 1276 (1998).
525. N. Furukawa, K. Nishio, eds., *Lithium Batteries with Polymer Electrodes*, Chapman & Hall, London, 1993.
526. M. Annand, J. Y. Sanchez, M. Gauthier, Y. Choquette, eds., *Electrochemistry of Novel Materials. Frontiers of Electrochemistry*, VCH, Weinheim, 1994.
527. F. M. Gray, *Solid Polymer Electrolytes-Fundamentals and Technical Applications*, VCH, Wenheim, 1991.

528. F. Croce, G. B. Appetecchi, L. Persi, B. Scrosati, *Nature*, **394**, 456 (1998).
529. T. Fujinami, K. Sugie, K. Mori, M. A. Mehta, *Chem. Lett*., 619, (1998).
530. J. Y. Lee, A. R. C. Baljon, R. F. Loring, A. Z. Panagiotopoulos, *J. Chem. Phys*., **109**, 10321 (1998).
531. R. A. Vaia, H. Ishii, E. P. Giannelis, *Chem. Mater*., **5**, 1694 (1993).
532. A. Usuki, M. Kato, A. Okada, T. Kurauchi, *J. Appl. Polym. Sci*., **63**, 137 (1997).
533. M. Kato, A. Usuki, A. Okada, *J. Appl. Polym. Sci*., **66**, 1781 (1997).
534. M. Kawasumi, N. Hasegawa, M. Kato, A. Usuki, A. Okada, *Macromolecules*, **30**, 6333 (1997).
535. K. A. Carrado, P. Thiyagarajan, D. L. Elder, *Clays Clay Miner*., **44**, 506 (1996).
536. K. A. Carrado, L. Xu, *Chem. Mater*., **10**, 1440 (1998).
537. S. Ramesh, Y. U. Koltypin, R. Prozorov, A. Gedanken, *Chem. Mater*., **9**, 546 (1997).
538. D. A. Hucul, A. Brenner, *J. Phys. Chem*., **85**, 496 (1981).
539. L. M. Liz-Marzan, M. Giersig, P. Mulvaney, *Langmuir*, **12**, 4329 (1996).
540. P. Basu, D. Panayotov, J. T. Yates Jr, *J. Am. Chem. Soc*., **110**, 2074 (1988).
541. W. Knoll, *Pure Appl. Chem*., **67**, 87 (1995).
542. G. Decher, *Science*, **277**, 1232 (1997).
543. S. W. Keller, S. A. Johnson, E. S. Brigham, E. H. Yonemoto, T. E. Mallouk, *J. Am. Chem. Soc*., **117**, 12879 (1995).
544. L. I. Trakhtenberg, G. N. Gerasimov, E. I. Grigor'ev, *Russ. J. Phys. Chem. (Engl. Trans.)*, **73**, 264 (1999).
545. F. Capasso, *Thin Solid Films*, **216**, 59 (1992).
546. J. H. Fendler, *Adv. Polym. Sci*., **113** (1994).
547. J. H. Fendler, F. C. Meldrum, *Adv. Mater*., **7**, 607 (1995).
548. E. R. Kleinfeld, G. S. Ferguson, *Sciences*, **265**, 370 (1994).
549. E. R. Kleinfeld, G. S. Ferguson, *Chem. Mater*., **7**, 2327 (1995).
550. E. R. Kleinfeld, G.S. Ferguson, *Mater. Res. Soc. Symp. Proc*., **369**, 697 (1995).
551. N. A. Kotov, I. Dekany, J. H. Fendler, *J.Phys. Chem*., **99**, 13065 (1995).
552. N. A. Kotov, I. Dekany, J. H. Fendler, *Adv. Mater*., **8**, 637 (1996).
553. N. A. Kotov, I. Dekany, J. H. Fendler, *Langmuir*, **10**, 3797 (1994).
554. S. W. Keller, H-N. Kirn, T. E. Mallouk, *J. Am. Chem. Soc*., **116**, 8817 (1994).
555. J. Schmitt, G. Decher, W. J. Dressik, S. L. Branduo, R. E. Geer, R. Shashidhal, J. M. Calvert, *Adv. Mater*., **9**, 61 (1997).
556. R. G. Freeman, K. C. Grabar, K. J. Allison, R. M. Bright, J. A. Davis, A. P. Guthrie, M. B. Hommer, M. A. Jackson, P. C. Smith, D. G. Walter, M. J. Natan, *Science*, **267**, 1629 (1995).
557. N. A. Kotov, T. Haraszti, L. Turi, G. Zavala, R. E. Greer, I. Dekany, J. H. Fendler, *J. Am. Chem. Soc*., **119**, 6821 (1997).
558. R. Lakes, *Nature*, **361**, 511 (1993).
559. A. Laschewsky, E. Wischerhoff, P. Bertrand, A. Delcorte, S. Denzinger, H. Ringsdorf, *Eur. Chem. J*., **3**, 28 (1997).
560. A. C. Fou, M. F. Rubner, *Macromolecules*, **28**, 7115 (1995).
561. Y. Lvov, K. Agira, I. Ichinose, T. Kunitake, *Langmuir*, **12**, 3038 (1996).
562. I. Ichinose, K. Fujiyoshi, S. Mizuki, Y. Lvov, T. Kunitake, *Chem. Lett*., 257 (1996).
563. D. Q. Li, M. Lmtt, M. R. Fitzsimmons, R. Synowicki, M. E. Hawley, G. W. Brown, *J. Am. Chem. Soc*., **120**, 8797 (1998).
564. D. Cochin, M. Passmann, G. Wilber, R. Zentel, E. Wischerhoff, A. Laschewsky, *Macromolecules*, **30**, 4775 (1997).
565. N. A. Kotov, S. Magonov, E. Tropsha, *Chem. Mater*., **10**, 886 (1998).

566. F. S. D'yachkovskii, L. A. Novokshonova, *Russ. Chem. Rev*., **53**, 117 (1984).
567. D. C. Lee, L. W. Jang, *J. Appl. Polym. Sci*., **68**, 1997 (1998).
568. P. B. Messersmith, F. Znidarsich, *Mater. Res. Soc. Symp. Proc*., **457**, 507 (1997).
569. H. G. Schild, *Prog. Polym. Sci*., **17**, 163 (1992).
570. M. E. Vol'pin, Yu. N. Novikov, N. D. Lapkina, V. I. Kasatochkin, Yu. T. Struchkov, M. E. Kazakov, R. A. Stukan, V. A. Povitskij, Yu. S. Karimov, A. V. Zvarikina, *J. Am. Chem. Soc*., **97**, 3366 (1975).
571. A. Furstner, ed., *Aktive Metals*, VCH, Weinheim, 1996.
572. V. L. Solozhenko, I. V. Arkhangel'skii, A. M. Gas'kov, Ya. A. Kalashnikova, M. V. Pletneva, *Russ. J. Phys. Chem. (Engl. Trans.)*, **57**, 2265 (1983).
573. V. A. Zhorin, N. I. Alekseev, I. N. Groznov, V. D. Kuznetsov, A. S. Bakman, V. G. Nagornyi, V. I. Goi'danskii, N. S. Enikolopyan, *Dokl. Chem. Technol., Dokl. Chem. (Engl. Trans.)*, **266**, 391 (1982).
574. J. J. Host, V. P. Dravid, *Mater. Res. Soc. Symp. Proc*., **457**, 225 (1997).
575. D. S. Wragg, G. B. Hix, R. E. Morris, *J. Am. Chem. Soc*., **120**, 6822 (1998).
576. J.-H. Choy, S.-Y. Kwak, J.-S. Park, Y.-J. Jeong, J. Portier, *J. Am. Chem. Soc*., **121**, 1399 (1999).
577. I. R. Radtchenko, G. B. Sukhorukov, N. Gaponik, A. Kornowski, A. L. Rogach, H. Möhwald, *Adv. Mater*., **13**, 1684 (2001).
578. Z. A. Peng, X. Peng, *J. Am. Chem. Soc*., **123**, 1389 (2001).
579. Y. Zhou, L. Hao, Y. Hu, Z. *Chen. Chem. Let*., 136 (2001).
580. M. Nath, C.N.R. Rao, *J. Am. Chem. Soc*., **123**, 4841 (2001).
581. J. Zeng, J. Yang, Y. Zhu, Y. Liu, Y. Qian, H. Zheng, *Chem. Commun*., 1332 (2001).
582. A. V. Volkov, M. A. Moskvina, A. E. Varfolomeev, A. L. Volynskii, N. F. Bakeev, *Polym. Sci*., **44**, 1690 (2002).
583. J. Yang, H. Lin, Q. He, L. Ling, C. Zhu, F. Bai, *Langmuir*, **17**, 5978 (2001).
584. Z. Qiao, Y. Xie, M. Chen, J. Xu, Y. Zhu, Y. Qian, *Chem. Phys. Lett*., **321**, 504 (2000).
585. F. Levy, ed., *Intercalated Layered Materials*, Reidel, Dodrecht, 1979.
586. B. DiBartolo (ed.), *Nanoparticles in Amorphous Solids and Their Nonlinear Properties, Advances and Applications, NATO ASI, Ser. B, Phys*., Plenum Press, New York, **399** (1994).
587. A. K. Atta, P. K. Biswas, D. Ganguli, in *Polymer and Other Advanced Materials. Emerging Technologies and Business Opportunities*, P. N. Prasad, J. E. Mark, T. J. Fai, eds., Plenum, New York, 1995.
588. L. Spanhel, E. Arpac, H. Schmidt, *J. Non-Cryst. Solids*., **147/148**, 657 (1992).
589. M. Zeiner, H. Minti, R. Reisfeld, H. Cohen, R Tenne, *Chem. Mater*., **9**, 2541 (1997).
590. A. V. Volkov, M. A. Moskvina, A. L. Volynskii, N. F. Bakeev, *Polym. Sci. (Engl. Trans.), A* **40**, 1441 (1998).
591. P. Mottner, T. Butz, A. Lerf, G. Ledezma, H. Knizinger, *J. Phys. Chem*., **99**, 8260 (1995).
592. P. Joensen, R. F. Frindt, S. R. Morrison, *Mater. Res. Bull*., **21**, 457 (1986).
593. M. A. Gee, R. F. Frindt, P. Joensen, S. R. Morrison, *Mater. Res. Bull*., **21**, 543 (1986).
594. S. G. Haup, D. R. Riley, J. Grassi, R.-K. Lo, J. Zhao, J.-P. Zhou, J. T. McDevitt, *J. Am. Chem. Soc*., **116**, 9979 (1994).
595. H.-L. Tsai, J. L. Schindler, C. R. Kannewurf, M. G. Kanatzidis, *Chem. Mater*., **9**, 875 (1997).
596. H.-L. Tsai, J. Heising, J. L. Schindler, C. R. Kannewurf, M. G. Kanatzidis, *Chem. Mater*., **9**, 879 (1997).
597. L. Wang, J. L. Schindler, J. A. Tomas, C. R. Kannewurf, M. G. Kanatzidis, *Chem. Mater*., **7**, 1753 (1995).
598. E. Ruiz-Hitzky, R. Jimenez, B. Casal, V. Manriquez, A. Santa Ana, G. Gonzalez, *Adv. Mater*., **5**, 738 (1993).

599. C. O. Oriakhi, R. L. Nafshun, M. M. Lerner, *Mater. Res. Bull*., **31**, 1513 (1996).
600. Y. Sun, E. Hao, X. Zhang, B. Yang, M. Gao, J. Shen, *Chem. Commun*., 2381 (1996).
601. V. L. Colvin, M. C. Schlamp, A. P. Alivisatos, *Nature (London)*, **370**, 354 (1994).
602. B. O. Dabbousi, M. G. Bawendi, O. Onitsuka, M. F. Rubner, *Appl. Phys. Lett*., **66**, 1316 (1995).
603. M. J. Ko, J. Plawsky, M. Biroboim, *J. Mater. Sci. Lett*., **17**, 917 (1998).
604. J. M. Yang, S. Y. Huang, S. Y. Liu, J. C. Shen, *J. Mater. Chem*., **7**, 131 (1997).
605. J. M. Yang, S. Y. Huang, S. Y. Liu, J. C. Shen, *Appl. Phys. Lett*., **69**, 377 (1996).
606. Y. Yang, J. Huang, B. Yang, S. Liu, J. Shen, *Synth. Met*., **91**, 347 (1997).
607. P. Bonneau, J. L. Mansot, J. Rouxel, *Mater. Res. Bull*., **28**, 757 (1993).
608. M. Potel, R. Chevrel, M. Sergent, J. C. Annici, M. Decroux, O. Fischer, *J. Solid State Chem*., **35**, 286 (1980).
609. J. H. Golden, F. J. DiSalvo, J.M.J. Frechet, *Chem. Mater*., **6**, 844 (1994); **7**, 232 (1995).
610. J. H. Golden, F. J. DiSalvo, J.M.J. Frechet, J. Silcox, M. Thomas, J. Elman, *Science*, **273**, 782 (1996).
611. B. Cheng, W. Q. Jiang, Y. R. Zhu, Z. Y. Chen, *Chem. Lett*., 935 (1999).
612. H-N. Cui, H-J. Zhang, S-Q. Xi, R. Wang, *J. Mater. Sci. Lett*., **17**, 913 (1998).
613. M. L. Bender, M. Komiyama, *Cyclodextrin Chemistry*, Springer, Berlin, 1978.
614. A. J. Bard, *Integrated Chemical Systems. A Chemical Approach to Nanotechnology*, Wiley, New York, 1994.
615. A. Ulman, *An Introduction to Ultrathin Organic Films from Langmuir-Blodgett to Self-Assembly*, Academic Press, New York, 1991.
616. R. H. Tredgold, R. A. Alien, P. Hodge, E. Khoshdel, *J. Phys. D, Appl. Phys*., **20**, 1385 (1987).
617. S. G. Yudin, S. P. Palto, V. A. Kravrichev, *Thin Solid Films*, **210/211**, 46 (1992).
618. V. L. Colvin, A. N. Goldstein, A. P. Alivisatos, *J. Am. Chem. Soc*., **114**, 5221 (1992).
619. G. Chumanov, K. Sokolov, B. M. Gregory, T. M. Cotton, *J. Phys. Chem*., **99**, 9466 (1995).
620. J. Yang, F. C. Meldrum, J. H. Fendler, *Phys. Chem*., **99**, 5500 (1995).
621. K. C. Yi, Z. Horvolgyi, J. H. Fendler, *Phys. Chem*., **98**, 3872 (1994).
622. S. Rajam, B. R. Heywood, J.B.A. Walker, S. Mann, R. J. Davey, J. D. Birchall, *J. Chem. Soc., Faraday Trans*., **87**, 727 (1991).
623. K. Tamura, H. Setsuda, M. Taniguchi, T. Nakamura, A. Yamagishi, *Chem. Lett*., 121 (1999).
624. H. S. Mansur, F. Grieser, R. S. Urquhart, D. N. Furlong, *J. Chem. Soc., Faraday Trans*., **91**, 3399 (1995).
625. J. Leioup, A. Ruadel-Teixier, A. Barraud, *Thin Solid Films*, **210/211**, 407 (1992).
626. F. C. Meldrum, N. A. Kotov, J. H. Fendler, *J. Chem. Soc., Faraday Trans*., **91**, 673 (1995).
627. F. C. Meldrum, N. A. Kotov, J. H. Fendler, *Langmuir*, **10**, 2035 (1994).
628. H. Jeong, B.-J. Lee, W. J. Cho, C.-S. Ha, *Polymer*, **41**, 5525 (2000).
629. K. S. Mayya, V. Patil, M. Sastry, *J. Chem. Soc., Faraday Trans*, **93**, 3377 (1997).
630. P. E. Laibinis, J. J. Hickman, M. S. Wrighton, G. M. Whitesides, *Science*, **245**, 845 (1989).
631. S. Schacht, Q. Huo, I. G. Voigt-Martin, G. D. Stucky, F. Schmth, *Science*, **273**, 768 (1996).
632. Y. Tian, C. Wu, J. H. Fendler, *J. Phys. Chem*., **98**, 4913 (1994).
633. X. K. Zao, S. Xu, J. H. Fendler, *Langmuir*, **7**, 250 (1991).
634. N. A. Kotov, F. C. Meldrum, C. Wu, J. H. Fendler, *J. Phys. Chem*., **98**, 2735 (1994).
635. F. C. Meldrum, N. A. Kotov, J. H. Fendler, *J. Phys. Chem*., **98**, 4506 (1994).
636. X. Peng, S. Guan, X. Chai, Y. Jiang, T. Li, *J. Phys. Chem*., **96**, 3170 (1992).
637. S. X. Ji, C. Y. Fan, F. Y. Ma, *Thin Solid Films*, **242**, 16 (1994).
638. J. K. Pike, H. Byrd, A. A. Morrone, D. R. Talham, *J. Am. Chem. Soc*., **115**, 8497 (1993).

639. F. N. Dultsev, L. L. Svechnikova, *Thin Solid Films*, **288**, 103 (1996).
640. F. N. Dul'tsev, L. L. Sveshnikova, *Russ. J. Struct. Chem. (Engl. Trans.)*, **38**, 803 (1997).
641. R. S. Urquhart, D. N. Furlong, T. Oegenbach, N. J. Geddes, F. Grieser, *Langmuir*, **11**, 1127 (1995).
642. Y. H. Park, B. I. Kim, Y. J. Kirn, *J. Appl. Polym. Sci*., **63**, 619 779 (1997).
643. M. A. Kalinina, V. V. Arslanov, V. D. Dozhikova, L. A. Tsar'kova, A. A. Rokhnyanskaya, in *The Chemistry of Surface and Nanotechnology (Abstracts of Reports of the First All-Russian Conference)*, Research Institute of Chemistry at St. Petersburg Technological University, St. Petersburg, 1999.
644. X. Peng, Y. Zhang, J. Yang, B. Zou, L. Xiao, T. Li, *J. Phys. Chem*., **96**, 3412 (1992).
645. Y. Zhang, Z. Xie, B. Hua, B. Mao, Y. Chen, Q. Li, Z. Tian, *Sci. China*, B **40**, 397 (1997).
646. Z. Liu, C. Zhao, M. Tang, S. Cai, *J. Phys. Chem*., **100**, 17337 (1996).
647. C.-X Zhao, J. Zhang, Z.-F. Liu, *Chem. Lett*., 473 (1997).
648. X. K. Zao, J. H. Fendler, *J. Phys. Chem*., **94**, 3384 (1990).
649. N. A. Kotov, M.E.D. Zaniquelli, F. C. Meldrum, J. H. Fendler, *Langmuir*, **9**, 3710 (1993).
650. S. H. Tolbert, P. Sieger, G. D. Stucky, S.M.J. Aubin, C-C. Wu, D. N. Hendrickson, *J. Am. Chem. Soc*., **119**, 8652 (1997).
651. M. Aiai, J. Ramos, C. Mingotaud, J. Amiell, P. Delhaes, A. Jaiswal, R. A. Singh, B. Singh, B. P. Singh, *Chem. Mater*., **10**, 728 (1998).
652. V. V. Arslanov, *Russ. Chem. Rev*., **63**, 1 (1994).
653. K. Yase, S. Schwiegk, G. Lieser, G. Wegner, *Thin Solid Films*, **210–211**, 22 (1992).
654. M. Rikukawa, M. F. Rubner, *Langmuir*, **10**, 519 (1994).
655. C. S. Winter, R. H. Tredgold, A. J. Vickers, E. Khoshdel, P. Hodge, *Thin Solid Films*, **134**, 49 (1985).
656. J. Nagel, U. Oertel, *Polymer*, **36**, 381 (1995).
657. Y.-S. Chen, Z.-K. Xu, B.-K. Xu, B.-K. Zhu, Y.-Y. Xu, *Chem. J. Chin. Univ*., **l8**, 973 (1997).
658. Z.-K. Xu, Y.-Y. Xu, M. Wang, *J. Appl. Polym. Sci*., **69**, 1403 (1998).
659. J. F. Liu, K. Z. Yang, Z. H. Lu, *J. Am. Chem. Soc*., **119**, 11061 (1997).
660. A. F. Diaz, J. F. Rubinson, H. B. Mark, *J Adv. Polym. Sci*., **84**, 11 (1988).
661. H. Shin, R. J. Collins, M. R. DeGuire, A. H. Heuer, C. N. Sukenik, *J. Mater. Res*., **10**, 692 (1995).
662. Y. Liu, A. Wang, R. Claus, *J. Phys. Chem., B* **101**, 1385 (1997).
663. E. Hao, L. Wang, J. Zhang, B. Yang, X. Zhang, J. Shen, *Chem. Lett*., 5 (1999).
664. T. Taniguchi, Y. Fukasawa, T. Mijashita, *J. Phys. Chem., B*, **103**, 1920 (1999).
665. N. Fukuda, M. Mitsuishi, A. Aoki, T. Mijashita, *J. Phys. Chem., B*, **106**, 7048 (2002).
666. A. Riul, Jr, D. S. Santos, Jr, K. Wohnrath, R. Di Tommazo, A. C. Carvalho, F. J. Fonseca, O. N. Oliveira Jr, D. M. Taylor, L.C.H. Mattoso, *Langmuir*, **18**, 239 (2002).
667. M. Ferreira, K. Wohnrath, R. M. Torresi, C.J.L. Constantino, R. F. Aroca, O. N. Oliveira Jr, J. A. Giacometti, *Langmuir*, **18**, 540 (2002).
668. A. Morneau, A. Manivannan, C. R. Cabrena, *Langmuir*, **10**, 3940 (1994).
669. T. Salditt, Q. An, A. Plech, C. Eschbaumer, U. S. Schubert, *Chem. Commun*., 2731 (1998).
670. T. Fujimoto, A. Fukuoka, J. Nakamura, M. Ichikawa, *Chem. Soc., Chem. Commun*., 845 (1989).
671. T. Fujimoto, A. Fukuoka, M. Ichikawa, *Chem. Mater*., **4**, 104 (1992).
672. S. P. Gubin, E. S. Soldatov, A. S. Trifonov, V. V. Khanin, *Inorg. Mater. (Engl. Trans.)*, **32**, 1265 (1996).
673. S. A. Yakovenko, S. P. Gubin, E. S. Soldatov, A. S. Trifonov, V. V. Khanin, G. B. Khomutov, *Inorg. Mater. (Engl. Trans.)*, **32**, 1272 (1996).

674. S. P. Gubin, V. V. Kolesov, E. S. Soldatov, A. S. Trifonov, S. G. Yudin, *Inorg. Mater. (Engl. Trans.)*, **33**, 1216 (1997).
675. S. A. Marakushev, *Geo-microbiology and Biochemistry of Gold*, Nauka, Moscow, 1991.
676. C. M. Niemeyer, *Angew. Chem. Int. Ed*., **40**, 4128 (2001).
677. G. I. Karavaiko, *Herald Russ. Acad. Sci. (Engl. Trans.)*, 72 (1985).
678. V. I. Karamushka, G. M. Gadd, T. G. Gruzina, Z. R. Ul'berg, N.V. Pertsov, *Colloid. J*., **60**, 775, 836 (1998).
679. O. Yamauchi, A. Odani, S. Hirota, *Bull. Chem. Soc. Jpn*., **74**, 1525 (2001).
680. J. T. Edsall, H. Gutfreund, *Biotermodynamics*, Willy, Chichester, UK, 1983.
681. J. Kostal, A. Mulchandani, W. Chen, *Macromolecules*, **34**, 2257 (2001).
682. H. Otsuka, Y. Akiyama, Y. Nagasaki, K. Kataoka, *J. Am. Chem. Soc*., **123**, 8226 (2001).
683. N. C. Seeman, *Nanoletters*, **1**, 22 (2001).
684. A. Eychmüller, *J. Phys. Chem., B*, **104**, 6514 (2000).
685. L. Addadi, S. Weiner, *Angew. Chem., Int. Ed. Engl*. **31**, 153 (1992).
686. S. Mann, J. Webb, R.J.P. Williams, *Biomineralization: Chemical and Biochemical Perspectives*, VCH, Weinheim. 1989.
687. F. C. Meldrum, B. R. Heywood, S. Mann, *Science*, **257**, 522 (1992).
688. I. Safarik, M. Safarikova, *Monats. Chem*., **133**, 737 (2002).
689. H. S. Joshi, Y. Tor, *Chem. Commun*., 549 (2001).
690. Y. Hitomi, C. E. Outten, T. V. O¢Halloran, *J. Am. Chem. Soc*., **123**, 8614 (2001).
691. G. Platt, C.-W. Chung, M. S. Searle, *Chem. Comm*., 1161 (2001).
692. O. Yamamoto, J. Sawai, *Bull. Chem. Soc. Jpn*., **74**, 1761 (2001).
693. Y. Zhou, W. Chen, K. Naka, Q. Ni, H. Yamane, Y. Chujo, *Chem. Commun*., 2518 (2001).
694. Y.-Z. Hu, S. Tsukiji, S. Shinkai, I. Hamachi, *Chem. Lett*., 517 (1999).
695. S. L. Woodhouse, L. M. Rendina, *Chem. Commun*., 2464 (2001).
696. J. J. Storhoff, A. A. Lazarides, R. C. Mucic, C. A. Mirkin, R. L. Letsinger, G. C. Schatz, *J. Am. Chem. Soc*., **122**, 4640 (2000).
697. Y. W. Cao, R. Jin, C. A. Mirkin, *J. Am. Chem. Soc*., **123**, 7961 (2001).
698 G. E. Brown Jr, V. E. Henrick, W. H. Casey, D. L. Dark, C. Eggleston, A. Felmy, D. W. Goodman, M. Gratzel, G. Maciel, M. I. McCarthy, K. H. Nealson, D. A. Sverjensky, M. F. Toney, J. M. Zachara, *Chem. Rev*., **99**, 77 (1999).
699. K. L. Taft, G. C. Papaefthymiou, S. L. Lippard, *Science*, **259**, 1302 (1993).
700. D. D. LeCloux, A. Barrios, T. J. Mizoguchi, S. P. Lippard, *J. Am. Chem. Soc*., **120**, 9001 (1998).
701. L. Que Jr. ed., *Metal Cluster in Proteins*, American Chemical Society, Washington, D.C., 1988.
702. J. E. Sheats, R. S. Czerauszewicz, G. C. Dismukes, A. L. Rheingold, V. Petraleas, G. Stubbe, W. H. Armstrong, R. H. Beer, S. J. Lippard, *J. Am. Chem. Soc*., **109**, 1435 (1987).
703. J. Reedjjk, ed., *Bioinorganic Catalysis*, Marcel Dekker, New York, 1993.
704. O. Joonen, A. Vessieres, I. S. Butler, *Acc. Chem. Res*., **26**, 361 (1993).
705. S. Yane, T. Inagaki, Y. Yamada, M. Kato, M. Yamasaki, T. Tsubomura, U. Sato, W. Mori, K. Yamaguchi, I. Kinoshita, *Chem. Lett*., 69 (1996).
706. D. Avnir, S. Braun, eds., *Biochemical Aspects of Sol-Gel Science and Technology*, Kluwer Academic, Boston, 1996.
707. D. Avnir, S. Braun, O. Lev, M. Ottolenghi, *Chem. Mater*., **61**, 605 (1994).
708. E.J.A. Pope, K. Braun, C. M. Peterson, *J. Sol-Gel Sci. Technol*., **8**, 635 (1997).
709. K. Kawakami, *Biotech. Technol*., **10**, 491 (1996).
710. P. Andebert, C. Demaille, C. Sanchez, *Chem. Mater*., **5**, 911 (1993).

711. F. Gao, Y. Tong, S. R. Schricker, B. M. Culbertson, *Polym. Adv. Technol*., **12**, 355 (2001).
712. D. Avnir, *Acc., Chem. Res*., **28**, 328 (1995).
713. O. Heichal-Segal, S. Rappoport, S. Braun, *Biotechnology*, **13**, 798 (1995).
714. J. E. Mark, *Heterog. Chem. Rev*., **3**, 307 (1996).
715. G. Falini, S. Fermani, M. Gazzano, A. Ripamondi, *J. Chem. Soc. Dalton Trans*. 3983 (2000).
716. M. S. Rao, I. S. Dubenko, S. Roy, N. Ali, B. C. Dave, *J. Am. Chem. Soc*., **123**, 1511 (2001).
717. T. K. Jain, I. Roy, K. De, A. Maitra, *J. Am. Chem. Soc.*, **120**, 11092 (1998).
718. Y. Levi-Kalisman, S. Raz, S. Weiner, L. Addadi, I. Sagi, *J. Chem. Soc. Dalton Trans*., 3977 (2000).
719. S. Braun, S. Rappoport, R. Zusman, D. Avnir, M. Ottolenghi, *Mater. Lett*., **10**, 1 (1990).
720. B. C. Dave, B. Dunn, J. S. Valentine, J. I. Zink, *Anal. Chem*., **66**, 1120A (1994).
721. O. Lev, Z. Wu, S. Bharathi, V. Glezer, A. Modestov, J. Gun, L. Rabinovich, S. Sampath, *Chem. Mater*., **9**, 2354 (1997).
722. J. I. Zink, J. S. Valentine, B. Dunn, *New J. Chem*., **18**, 1109 (1994).
723. R. Collino, J. Jherasse, P. Binder, F. Chaput, B-P. Boilot, Y. Levy, *J. Sol-Gel Sci. Technol*., **2**, 823 (1994).
724. D. Shabat, F. Grynszpan, S. Saphier, A. Turniansky, D. Avnir, E. Keinan, *Chem. Mater*., **9**, 2258 (1997).
725. A. Bronshtein, N. Aharonson, D. Avnir, A. Turniansky, M. Alstein, *Chem. Mater*., **9**, 2632 (1997).
726. J. F. Kennedy, J.M.S. Cabral, *Solid Phase Biochemistry*, vol. 66, Wiley, New York, 1983.
727. B. B. Lakshmi, C. J. Patrissi, C. R. Martin, *Chem. Mater*., **9**, 2544 (1997).
728. A. P. Alivisatos, *Science*, **289**, 736 (2000).
729. I. Gill, A. Ballesteros, *J. Am. Chem. Soc*., **120**, 8587 (1998).
730. M. Burow, N. Minoura, *Biochem. Biophys. Res. Commun*., **227**, 419 (1996).
731. K. Hirayama, M. Burow, Y. Morikawa, N. Minoura, *Chem. Lett*., **731**, (1998).
732. R. Makote, M. M. Collinson, *Chem. Mater*., **10**, 2440 (1998).
733. S. Mann, S. L. Burkett, S. A. Davis, C. E. Fowler, N. H. Mendelson, S. D. Sims, D. Walsh, N. T. Whilton, *Chem. Mater*., **9**, 2300 (1997).
734. G. A. Ozin, *Acc. Chem. Res*., **30**, 17 (1997).
735. S. A. Davis, S. L. Burkett, N. H. Mendelson, S. Mann, *Nature*, **385**, 420 (1997).
736. S. A. Davis, H. M. Patel, E. L. Mayes, N. H. Mendelson, G. Franco, S. Mann, *Chem. Mater*., **10**, 2516 (1998).
737. H. A. Pohl, in *Coherent Excitation in Biological Systems*, H. Frolich, F. Kremer, eds., Springer, Heidelberg, 1983.
738. S. Mann, *J. Chem. Soc., Dalton Trans*., 1 (1993).
739. T. Douglas, D.P.E. Dickson, S. Betteridge, J. Chamock, C. D. Garner, S. Mann, *Science*, **269**, 54 (1995).
740. C. T. Wan, K. A. Taulog, D. L. Chambers, G. T. Susi, in *Metallized Plastics*, vol. **2**, K. L. Mittal, eds., Plenum, New York, 1991.
741. B. S. Grishin, T. I. Pisarenko, G. I. Esen'kina, V. P. Tarasov, F. K. Khitrin, V. L. Erofeev, I. R. Markov, *Polym. Sci. (Engl. Trans.)*, A **34**, 91 (1992).
742. V. E. Zgaevskii, *Dokl. Chem. Technol., Dokl. Chem. (Engl. Trans.)*, **341**, 758 (1995); **363**, 42 (1998).
743. A. D. Pomogailo, V. S. Savost'yanov, G. I. Dzhardimalieva, A. V. Dubovitskii, A. N. Ponomarev, *Russ. Chem. Bull. (Engl. Trans.)*, 1096 (1995).
744. M. V. Shamurina, V. I. Roldugin, T. D. Pryamova, T. D. Vysotskii, *Colloid J. (Engl. Trans.)*, **56**, 450 (1994); **57**, 580 (1995).

745. X. Xu, G. Friedman, K. D. Humfeld, S. A. Majetich, S. A. Asher, *Adv. Mater*., **13**, 1681 (2001).
746. T. Ktapcinski, A. Galeski, M. Kruszewski, *J. Appl. Polym. Sci*., **58**, 1007 (1995).
747. I. L. Radtchenko, G. B. Sukhorukov, N. Gaponik, A. Kornowski, A. L. Rogach, H. Mohwald, *Adv. Mater*., **13**, 1684 (2001).
748. M. Pujiwara, T. Matsushita, K. Yamaguchi, T. Fueno, *Synth. Met*., **41–43**, 3267 (1991).
749. M. Fujiwara, W. Mori, K. Yamaguchi, *Mol. Cryst. Lig. Cryst*., **274**, 175 (1995).
750. R. Popielarz, C. K. Chiang, R. Nozaki, J. Obrzut, *Macromolecules*, **34**, 5910 (2001).
751. L. Wan g, L. X. Feng, S. L. Yang, *J. Appl. Polym. Sci*., **71**, 2087 (1999).
752. X. Cao, Y. Luo, L. Feng. J. Appl, *Polym. Sci*., **71**, 3412 (1999).
753. J. Ramos, A. Millan, F. Palacio, *Polymer*, **41**, 8461 (2000).
754. T. A. Ramadan, H. M. Moawad, *J. Appl. Polym. Sci*., **71**, 409 (1999).
755. Y. Osada, *Adv. Mater*., **3**, 107 (1991).
756. L. A. Shmeleva, L. N. Savina, N. I. Dyumovkin, V. V. Korolev, *Izv. Vyssh. Uchebn. Zaved., Khim. Khim. Tekhnol*., 38 **5**, 71 (1995).
757. V. V. Vysotskii, V. I. Raldugin, *Colloid J. (Engl. Transl.)*, **60**, 729 (1998).
758. Yu. N. Anisimov, L. P. Dobrova, A. Yu. Anisimov, *Russ. J. Appl. Chem. (Engl. Trans.)*, **71**, 790 (1998).
759. R. A. Andrievskii, A. M. Glezer, *Fiz. Met. Metalloved*., **88**, 50 (1999).
760. A. Bukowski, *Polimery*, **61**, 139 (1996).
761. X. Cai, C. Zhong, S. Zhang, H. Wand, *J. Mater. Sci. Lett*., **16**, 253 (1997).
762. T. Shiga, A. Okada, T. Kurauchi, *J. Appl. Polym. Sci*., **58**, 787 (1995).
763. T. Klapcinski, A. Galeski, M. Kryszewski, *J. Appl. Polym. Sci*., **58**, 1007 (1995).
764. C. J. Twomey, S. H. Chen, T. N. Blanton, A. Schmid, K. L. Marshall, *J. Polym. Sci., Part B, Polym. Phys*., **32**, 1687 (1994).
765. D. L. Leslie-Pelecky, R. D. Rieke, *Chem. Mater*., **8**, 1770 (1996).
766. A. G. Golubkov, N. R. Evrukov, *Plast.. Massy*, **3**, 22 (1998).
766. A. L. Buchachenko, *Russ. Chem. Rev*., **59**, 307 (1990).
767. M. M. Levitskii, A. L. Buchachenko, *Russ. Chem. Bull. (Engl. Trans.)*, 1432 (1997).
768. I. A. Akimov, I. Yu. Denisyuk, A. M. Meshkov, *Opt. Spektrosk*., **72**, 1026 (1992).
769. V. V. Sviridov, G. P. Shevchenko, E. M. Afanas'eva, A. N. Ponyavina, N. V. Loginova, *Colloid J. (Engl. Trans.)*, **58**, 390 (1996).
770. M. Moffit, A. Eisenberg, *Chem. Mater*., **7**, 1178 (1995).
771. M. Moffit, L. McMahon, V. Pessel, A. Eisenberg, *Chem. Mater*., **7**, 1185 (1995).
772. D. Duonghang, E. Borgarello, M. Gratzel, *J. Phys. Chem.*, **88**, 4006 (1984).
773. R. Rafaeloff, Y.-M. Tricot, F. Nome, P. Tundo, J. H. Fendler, *J. Phys. Chem.*, **89**, 1236 (1985).
774. L. L. Beecroft, C. K. Ober, *Chem. Mater*., **9**, 1302 (1997).
775. P. Chakraborty, *J. Mater. Sci*., **33**, 2235 (1998).
776. C. Liu, A. J. Bard, *J. Phys. Chem*., **93**, 3232 (1989).
777. D. E. Fogg, L. H. Radzilowski, B. O. Dabbousi, R. R. Schrock, E. L. Thomas, M. G. Bawendi, *Macromolecules*, **30**, 8433 (1997).
778. M. Herold, J. Gmeiner, C. Drummer, M. Schwoerer, *J. Mater. Sci*., **32**, 5709 (1997).
779. J. Serin, X. Schultze, A. Andronov, J.M.J. Frechet, *Macromolecules*, **35**, 5396 (2002).
780. L. D. Rampino, F. F. Nord, *J. Am. Chem. Soc*., **63**, 2745 (1941).
781. K. E. Kavanagh, F. F. Nord, *J. Am. Chem. Soc*., **65**, 2121 (1943).
782. G. Pacchioni, N. Rosch, *Acc. Chem. Res*., **28**, 390 (1995).
783. G. A. Martin, *Catal. Rev. Sci. Eng*., **30**, 519 (1988).

784. A. Henglein, *J. Phys. Chem*., **97**, 5457 (1993).
785. H. Weller, *Angew. Chem., Int. Ed. Engl*., **32**, 41 (1993).
786. A. D. Pomogailo, *Catalysis by Polymer-Immobilized Metal Complexes*, Gordon & Breach, Amsterdam, 1998.
787. T. Teranishi, N. Toshima, *J. Chem. Soc., Dalton Trans*., **20**, 2967 (1994).
788. T. Teranishi, K. Nakata, M. Miyake, N. Toshima, *Chem. Lett*., 277 (1996).
789. W.-Y. Wong, W.-T. Wong, *J. Organomet. Chem*., **513**, 27 (1996).
790. S. Bhaduri, K. Sharma, *Chem. Commun*., 207 (1996).
791. N. L. Pocard, D. C. Alsmeyer, R. L. McCreery, T. X. Neenan, M. R. Callstrom, *J. Am. Chem. Soc*., **114**, 769 (1992).
792. U. Schubert, *New J. Chem*., **18**, 1049 (1994).
793. N. Toshima, T. Takahashi, H. Hirai, *J. Macromol. Sci., A* **25**, 669 (1988).
794. K. I. Zamaraev, M. I. Khramov, V. N. Parmon, *Catal. Rev*., **36**, 617 (1994).
795. J. M. Stipkala, F. N. Castellano, T. A. Heimer, C. A. Kelly, K.J.T. Livi, G. J. Meyer, *Chem. Mater*., **9**, 2341 (1997).
796. M. Hara, T. Kondo, M. Komoda, S. Ikeda, K. Shinohara, A. Tanaka, J. N. Kondo, K. Domen, *Chem. Commun*., 357 (1998).
797. Y. Sakata, T. Yamamoto, T. Okazaki, H. Imamura, S. Tsuchiya, *Chem. Lett*., 1253 (1998).
798. M. Okumura, S. Tsubota, M. Iwamoto, M. Haruta, *Chem. Lett*., 315 (1998).
799. E. A. Trusova, M. V. Tsodikov, E. V. Slivinskii, G. C. Hemandes, O. V. Bukhtenko, T. N. Zhdanova, D. I. Kochubey, J. A. Navio, *Mendeleev Commun*., 102 (1998).
800. G. Jannes, V. Dubois, eds., *Chiral Reactions in Heterogeneous Catalysis*, Plenum Press, New York, 1995.
801. G. A. Somorjai, *Appl. Surface Sci*, **121/122**, 1 (1997).
802. A. D. Pomogailo, I. E. Uflyand, E. F. Vainshtein, *Russ. Chem. Rev*., **64**, 857 (1995).
803. S. K. Bhattacharya, R. R. Tummala, *J. Mater. Sci.: Mater. Electron*., **11**, 253 (2000).
804. H. Nagashima, A. Nakooka, Saito, M. Kato, T. Kanishi, K. Itoh, *Chem. Commun*., 377 (1992); *Chem. Lett*., 2153 (1993); *Organomet. News*, 12 (1992).
805. C. Guerret-Plecourt, Y. Le Bonar, A. Lolseau, H. Pascard, *Nature*, **372**, 761 (1994).
806. T. W. Ebbesen, H. Hiura, M. E. Bisher, M.M.J. Treacy, J. S. Shreevekeyer, R. C. Haushalter, *Adv. Mater*., **8**, 155 (1996).
807. J. Noolandi, A-C. Shi, *Macromol. Rap. Commun*., **17**, 471 (1996).
808. D. A. Tomalia, P. R. Dvornic, *The Polymeric Materials Encyclopedia*, vol. 3, CRC Press, Boca Raton, FL, 1996.
809. L. Wooley, C. J. Hawker, J. M. Frechet, *J. Chem. Soc. Perkin Trans*., **1**, 1059 (1991).
810. M. A. Hearshaw, J. R. Moss, *Chem. Commun.*, 1 (1999).
811. F. Zeng, S. C. Zimmerman, *Chem. Rev.*, **97**, 1681 (1997).
812. L. Balogh, D. A. Tomalia, *J. Am. Chem. Soc.*, **120**, 7355 (1998).
813. M. Zhao, L. Sun, R. M. Crooks, *J. Am. Chem. Soc*., **120**, 4877 (1998).

Index

Macromolecules Containing Metal and Metal-Like Elements,
Volume 7: Nanoscale Interactions of Metal-Containing Polymers,
edited by Alaa S. Abd-El-Aziz, Charles E. Carraher Jr., Charles U. Pittman Jr.,
and Martel Zeldin.